UNIV. OF MICHIGAN
FEB 12 1953
ENGINEERING LIBRARY

JOURNAL OF THE AERONAUTICAL SCIENCES

VOLUME 20 FEBRUARY, 1953 NUMBER 2

CONTENTS

On the Motion of a Tumbling Body.....A. M. O. SMITH 73
Slender-Body Theory—Review and Extension....MAC C. ADAMS AND W. R. SEARS 85
Penetration and Deflection of Jets Oblique to a General Stream...FREDRIC F. EHRICH 99
An Experimental Study of a Hypersonic Wind-Tunnel Diffuser.....
.....PETER P. WEGENER AND R. KENNETH LOBB 105
Analysis of Stiffened Curved Panels Under Shear and Compression.....
.....M. A. MELCON AND A. F. ENSRUD 111
Reverse-Flow and Variational Theorems for Lifting Surfaces in Nonstationary Compressible Flow.....A. H. FLAX 120
Differential Shear-Flow Analysis for Nonprismatic Semimonocoque Beams.....
.....WILLIAM B. KING AND WALTER R. GARRISON 127
Readers' Forum: "Some Remarks on 'A Solution of the Laminar Boundary-Layer Equations for a Compressible Fluid with Variable Properties, Including Dissociation,' " by M. Z. Krzywoblocki; "Some Remarks on the Effect of Flapping Hinge Offset on Rotor Blade Stall," by John R. Meyer, Jr., and G. Falabella, Jr.; "Approximate Solutions for the Detached Shock Problem," by S. F. Borg; "Influence Functions for Computing Lift and Rolling Moment of a Twisted Narrow Delta Wing," by Beverly Beane; "Energy Removal from a Supersonic Turbulent Boundary Layer," by John Joseph Martin; "Relation of Force, Acceleration, and Momentum for a Body Whose Mass Is Varying," by H. W. Sibert; "Further Comments on 'Turbulent Boundary-Layer Characteristics at Supersonic Speeds,' " by R. J. Monaghan; "On the Boundary-Layer Equations in Hypersonic Flow and Their Approximate Solutions," by Lester Lees; "On the Use of the Neutral Point as a Stability Parameter," by Judson R. Baron; "On Asymptotic Solutions for the Heat Transfer at Varying Wall Temperatures in a Laminar Boundary Layer with Hartree's Velocity Profiles," by H. Schuh; "Graphical Solution for 'Turbulent Boundary Layer in Compressible Fluids,' " by John Joseph Martin; "Additional Values of $C(k)$," by W. B. Brower and R. H. Lassen; "Comments on 'Two-Dimensional Airfoils at Moderate Hypersonic Velocities,' " by L. E. Flanagan, Jr.; "On the Transition Through a Weak Shock Front," by Paul Mandl.....136–152

Published by the

INSTITUTE OF THE AERONAUTICAL SCIENCES, INC.

JOURNAL OF THE AERONAUTICAL SCIENCES

Editor: HUGH L. DRYDEN, *Director, N.A.C.A.*

Associate Editor: ROBERT R. DEXTER *Managing Editor:* BERNEICE H. JARCK

Editorial Committee

Aerodynamics

Francis Clauser
Howard Emmons
Antonio Ferri
Alexander Flax
R. Paul Harrington
R. T. Jones
Carl Kaplan
H. W. Liepmann
C. C. Lin
H. F. Ludloff
Harold Luskin
John R. Markham
Clark B. Millikan
Shatswell Ober
W. Bailey Oswald
Allen E. Puckett
Elliott G. Reid
H. J. E. Reid
Russell Robinson
G. B. Schubauer
W. R. Sears
John Stack
Theodore von Kármán
Richard von Mises

Air Transport

Charles Froesch
J. A. Herlihy
R. D. Kelly
Otto E. Kirchner
Jerome Lederer
John C. Leslie
R. Dixon Speas

Flight Testing

W. K. Ebel
R. R. Gilruth
Melvin N. Gough
E. G. Stout

Structures and Materials

W. B. Bleakney
E. W. Conlon
L. H. Donnell
E. C. Hartmann
N. J. Hoff
Samuel Levy
E. E. Lundquist
Alfred S. Niles
W. Ramberg
E. Reissner
F. R. Shanley
H. W. Sibert
C. R. Strang
S. Timoshenko
H. S. Tsien
Chi-Teh Wang

Rotating Wing Aircraft

F. B. Gustafson
K. H. Hohenemser
Bartram Kelley
R. B. Maloy
Ralph McClarren
R. H. Miller
R. H. Prewitt
Igor I. Sikorsky

Vibration and Flutter

Lee Arnold
M. A. Biot
R. L. Bisplinghoff
William Bollay
Chieh-Chien Chang
I. E. Garrick
Martin Goland
J. P. Den Hartog

Aircraft Design

W. E. Beall
W. K. Ebel
Hall L. Hibbard
Richard Hutton
C. L. Johnson
A. A. Kartveli
C. J. McCarthy
Fred E. Weick
Robert J. Woods

Electronics in Aviation

K. C. Black
E. F. Herzog
David S. Little
D. K. Martin
George Rappaport
Paul Rosenberg
L. M. Sherer

Physiologic Problems

H. G. Armstrong
Louis H. Bauer
Robert J. Benford
Eugene Du Bois
W. Randolph Lovelace, II
Ross A. MacFarland

Fuels and Oils

D. P. Barnard
J. H. Doolittle
Graham Edgar
R. T. Goodwin
S. D. Heron
A. M. Rothrock

Flight Propulsion

George W. Brady
Frank W. Caldwell
L. S. Hobbs
E. E. Johnson
Joseph Keenan
R. P. Kroon
Hans Reissner
Abe Silverstein
C. Fayette Taylor
E. S. Taylor
P. Taylor
E. S. Thompson
H. S. Tsien

Instruments

Allan G. Binnie
J. R. Bradburn
Charles H. Colvin
C. S. Draper
S. G. Eskin
O. B. Esval
H. W. Holzapfel
W. L. Howland
George H. Purcell
C. F. Savage
O. Hugo Schuck
C. L. Seward, Jr.
L. D. Statham
R. C. Sylvander
D. K. Warner

Meteorology

C. F. Brooks
D. M. Little
E. J. Minser
F. W. Reichelderfer
H. C. Willett

SUBSCRIPTION RATES

JOURNAL OF THE AERONAUTICAL SCIENCES, Published Monthly.—United States and Possessions: 1 Year, $12.00; Single Copies, $1.50. Foreign Countries Including Canada (American Currency Rates): 1 Year, $13.00; Single Copies, $1.50.

AERONAUTICAL ENGINEERING REVIEW, Published Monthly.—United States and Possessions: 1 Year, $3.00; Single Copies, $0.50. Foreign Countries Including Canada (American Currency Rates): 1 Year, $3.50; Single Copies, $0.50.

Notices of change of address should be sent to the Institute at least 30 days prior to actual change of address.

Manuscripts for publication, proofs, and all correspondence should be addressed to the Editorial Office of the JOURNAL.

Correspondence regarding subscriptions may be addressed to Publication Office, 20th and Northampton Sts., Easton, Pa., or to the Editorial Office of the JOURNAL OF THE AERONAUTICAL SCIENCES, 2 East 64th Street, New York 21, New York.

Copyright, 1953, by the Institute of the Aeronautical Sciences, Inc.

Entered as Second Class Matter at the Post Office, Easton, Pa., May 1, 1937. Acceptance for mailing at a special rate of Postage provided for in the Act of August 24, 1912. Authorized April 29, 1937.

JOURNAL OF THE AERONAUTICAL SCIENCES

VOLUME 20 FEBRUARY, 1953 NUMBER 2

On the Motion of a Tumbling Body

A. M. O. SMITH*

Douglas Aircraft Company, Inc.

SUMMARY

The Douglas D-558 and D-558-2 research airplanes incorporated releasable nose sections to facilitate pilot escape in the case of an emergency. Because the free-nose sections did not have static stability, there was fear that the noses would fall with a steady tumbling type of motion.

Accordingly, an extensive investigation of the motion of the noses was initiated. In one phase of the work, small models dynamically similar to the full-scale noses were released in the N.A.C.A. 20-ft. Spin Tunnel to study free-fall characteristics. In these low Reynolds Number tests the noses did tumble. Later, in the high Reynolds Number tests on dimensionally similar models that were mounted to spin freely on a shaft, the models could not be made to autorotate. To explain the discrepancy, a modest investigation of the mechanics of tumbling was begun.

It was learned that the motion can be exceedingly complex. Factors that definitely produce a continuous net driving force per revolution are: (1) hysteresis effects on the lift coefficient, created by rotation; (2) Reynolds Number effects on the drag coefficient; (3) static net rotating moments characteristic of certain body shapes such as the anemometer; and (4) a coupling effect that enables rotational energy to be gained by an otherwise neutral body when allowed to tumble freely in space.

In addition, the following phenomena considerably influence the rotation and possibly contribute to the driving moment: (1) the effect of the shed vortex field on the moments of a rotating body; (2) spinning as with wings in the region, where the C_L-vs.-α curve has a negative slope; and (3) the Flettner rotor effect, which may sometimes occur if the body spins about a longitudinal axis.

In the light of the considerations presented herein, it can be seen that tumbling may be greatly influenced by Reynolds Number. In particular, it appears that bodies similar to the D-558 noses will tumble at a low rotational rate. However, means are pointed out by which tumbling can probably be prevented if so desired.

(I) NOMENCLATURE

C_D = drag coefficient

C_{D_π} = drag coefficient based on frontal area

$\bar{C}_{D_\pi}$ = drag coefficient averaged over a revolution,

$$\bar{C}_{D_\pi} = \frac{1}{2\pi}\int_0^{2\pi} C_{D_\pi}\, d\theta$$

C_L = lift coefficient

C_{L_π} = lift coefficient based on frontal area

C_m = moment coefficient

$\bar{C}_m$ = θ average of C_m over one revolution,

$$\bar{C}_m = \frac{1}{2\pi}\int_0^{2\pi} C_m\, d\theta$$

C_{m_π} = moment coefficient based on frontal area and length of body

$\bar{C}_{m_\pi}$ = θ average of C_{m_π} over one revolution,

$$\bar{C}_{m_\pi} = \frac{1}{2\pi}\int_0^{2\pi} C_{m_\pi}\, d\theta$$

$\Delta\bar{C}_{m_\pi}$ = average incremental moment coefficient

g = acceleration due to gravity

I = principal moment of inertia of the body with respect to axis perpendicular to plane of rotation.

l = length of body

M = Mach Number; also moment

q = dynamic pressure

R = Reynolds Number based on length

R_d = Reynolds Number based on diameter

S = reference area

t = time

V = velocity

W = weight

x, y, z = displacement in cartesian coordinates

α = angle of attack, for airfoils

θ = angle of attack, for bodies

ρ = mass density of air

ω = instantaneous angular velocity, rad. per sec.

$\bar{\omega}$ = angular velocity averaged over a revolution

(II) INTRODUCTION

As part of the Douglas D-558 high-speed airplane research project, an extensive investigation of the motion of a jettisonable nose was performed for the Navy Bureau of Aeronautics.† The work was for the purpose of determining the loads imposed by the nose on

Received April 7, 1952. Revised and received September 5, 1952.

* Supervisor, Design Research, El Segundo Plant.

† Submitted April 21, 1950, as Douglas Report ES 15379, Parts I through V. The present article is a revision of Part V.

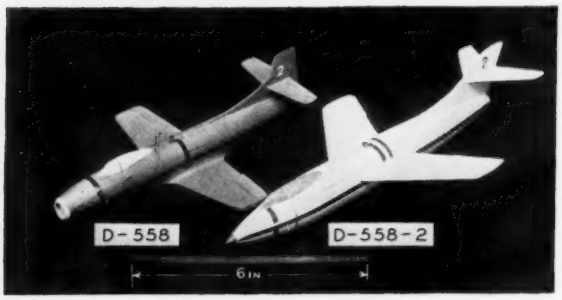

FIG. 1. 1/50-Scale dynamically similar models of the D-558 and D-558-2 airplanes showing the jettisonable nose sections.

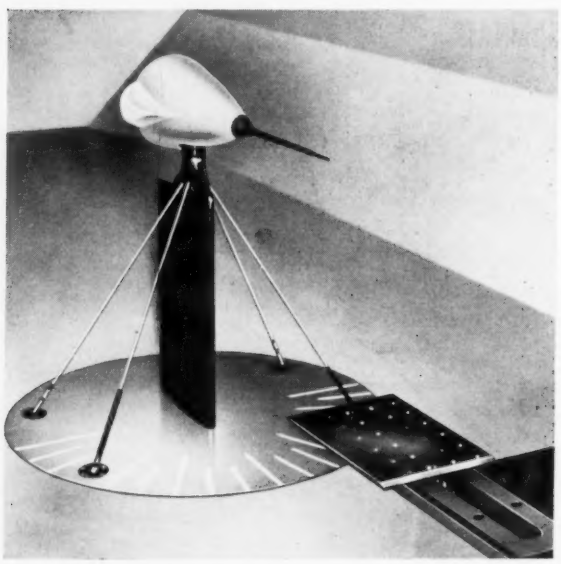

FIG. 2. The D-558-2 nose in the Southern California Cooperative Wind Tunnel.

a pilot riding within. Fig. 1, consisting of photographs of two balsa models dynamically similar to the D-558 and D-558-2 airplanes, illustrates the general appearance of the releasable noses.

Originally, in the research to determine loads imposed on the pilot by release of these noses, it was assumed that the noses would tumble. N.A.C.A. Spin Tunnel Tests on a free model[1] and 1/50-scale model tests in the Douglas El Segundo Wind Tunnel on a shaft-mounted model[2] substantiated the belief, for both types of tests did produce tumbling motion. However, the 1/6-scale models (Fig. 2) built for testing in the Southern California Cooperative Wind Tunnel would not autorotate about the fixed shaft even though bearing friction was low. Except for inevitable differences in the models due to construction inaccuracies, the main difference between the 1/50-scale models and the 1/6-scale models was size—that is, Reynolds Number. However, the instrumentation boom was on the large D-558-2 model but not on the small one. This boom is illustrated in Figs. 2 and 15.

Because of the unexpected discovery that the large model would not autorotate, studies were undertaken in order to learn whether rotation about a fixed axis might impose such restriction that the model would not autorotate and whether it would autorotate if allowed three or more degrees of freedom. In the process of the investigation several points of interest were brought to light. Since the literature on this subject is scarce, the findings are described herein to explain the results of the D-558 and D-558-2 nose-rotation tests and to assist others in treating the tumbling problem.

In this paper tumbling will be regarded as a free-body rotation, predominantly about an axis perpendicular to the air stream but not exclusively so, for a combination of motions may often be discerned. Rotation about a fixed axis will not be called tumbling because the axis is fixed, but instead it will be designated as autorotation.

(III) General Nature of Tumbling Motion

Consider the free body of Fig. 3, treated as if it were in equilibrium in a vertical wind tunnel, in order to eliminate considerations of translation as in free air. Because the body undergoes lift and drag fluctuations, its center of gravity obviously will travel in a closed path or orbit. Since the velocity of travel along this path is small, it can be assumed with only small error that the vector wind velocity over the body is not affected by the translatory motion and direction. Furthermore, it is assumed that the motion is predominantly in one plane. This plane of tumbling may gradually rotate because there are no forces to hold it fixed. However, such drift has only a minor effect on the development of the motion. N.A.C.A. motion-picture studies in the 20-Ft. Spin Tunnel indicate that fully developed tumbling of the D-558 and D-558-2 noses is substantially a motion in a vertical plane. Often the tumbling state is entered by means of a three-dimensional type of motion to be explained later. However, since the steady-state tumbling is a coplanar motion, explanations based on coplanar analyses should be adequate.

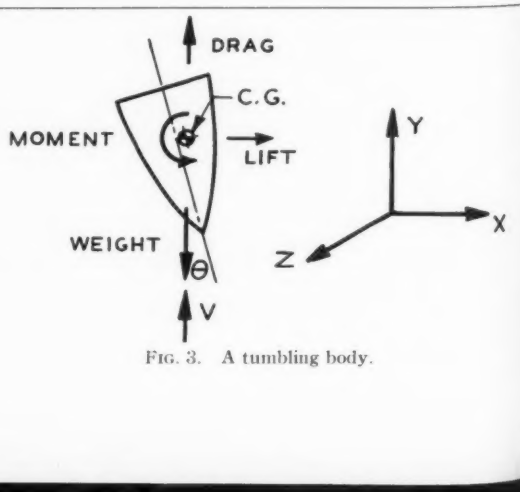

FIG. 3. A tumbling body.

Because the axis of rotation is assumed not to tilt and because there is negligible z motion, the equations of motion can be written as follows if it be understood that C_L, C_D, and C_m represent dynamic coefficients:

Lift:

$$\frac{W}{g}\frac{d^2x}{dt^2} = \frac{1}{2}\rho\, C_L\, SV^2 \tag{1}$$

Drag:

$$\frac{W}{g}\frac{d^2y}{dt^2} = \frac{1}{2}\rho\, C_D\, SV^2 - W \tag{2}$$

Moment:

$$I\frac{d^2\theta}{dt^2} = \frac{1}{2}\rho\, C_m\, SlV^2 \tag{3}$$

Because perturbation velocities for a body will usually be small, these three equations can be solved successively instead of simultaneously.

To solve them, the θ-vs.-time relation must first be found.

Let $\omega = d\theta/dt$. Then

$$\frac{d^2\theta}{dt^2} = \frac{d\omega}{dt} = \frac{d\omega}{d\theta}\frac{d\theta}{dt} = \omega\frac{d\omega}{d\theta}$$

and Eq. (3) can be integrated by means of the above substitution.

$$\frac{\omega^2}{2} = \frac{\rho SlV^2}{2I}\int_0^\theta C_m\, d\theta + \frac{{\omega_0}^2}{2}$$

or

$$\frac{d\theta}{dt} = \omega = \sqrt{\frac{\rho SlV^2}{I}\int_0^\theta C_m\, d\theta + {\omega_0}^2} \tag{4}$$

where ω_0 is the angular velocity when $\theta = 0$. On integrating again,

$$t = \int_0^\theta \frac{d\theta}{\sqrt{\frac{\rho SlV^2}{I}\int_0^\theta C_m\, d\theta + {\omega_0}^2}} + t_0 \tag{5}$$

Now with the time-θ relation established, x-θ and y-θ relations are determinable, since C_L and C_D are assumed to be known as functions of θ.

Consider Eq. (4). It shows that the resultant rotation is a function of the C_m-vs.-θ curve. (However, in general, this curve will vary with the angular velocity because of dynamic effects.) In steady tumbling or autorotation,

$$\int_0^{2\pi} C_m\, d\theta = 0$$

but for any value of θ except 2π, 4π, etc., the value of the integral is not equal to zero. Therefore, a steady-state rotation is one having a reference velocity ω_0 upon which is superimposed a fluctuating one. The amplitude of the fluctuations can be considerably changed, as is seen from the fact that the variable term in Eq. (4) is

$$\frac{\rho SlV^2}{I}\int_0^\theta C_m\, d\theta$$

For instance, note that increases in the moment of inertia will tend to reduce the fluctuations.

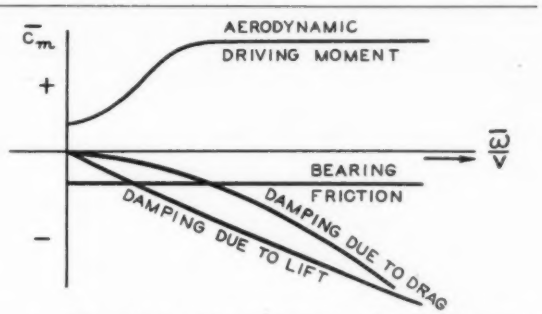

FIG. 4. Schematic breakdown of rotating forces acting on a rotating body.

A matter of great interest in considerations of tumbling motion is the effect of translational speed on the steady-state rate of rotation. Eq. (4) can hardly answer the problem because all it basically shows is that $\int_0^{2\pi} C_m\, d\theta$ must be zero if the rotation is to be steady—that is, periodic. Therefore, the prediction of steady-state rotational rates reduces to the problem of predicting the value of $\int_0^{2\pi} C_m\, d\theta$ as a function of ω/V, V, ρ, and M.

Since tumbling normally involves airflow separation, predictions of C_m as a function of θ are not likely to be accurate. However, if Reynolds Number effects and Mach Number effects are negligible, it appears that the steady-state value of ω is nearly proportional to V, regardless of density as will be shown.

The fundamental moments acting on a body are as shown schematically in Fig. 4, where mean values for a revolution are used. The case illustrated is that of a body mounted on a shaft. There may be a net static driving moment as for a windmill or anemometer. In addition, greater driving moments may develop when rotation occurs. Hysteresis in C_L-vs.-α curves is an example of such a force. If the rotation is about a fixed shaft, there is a bearing-friction damping moment of relatively constant magnitude. Also, there may be damping caused by lift and damping caused by drag. The damping caused by lift is the type treated in non-steady airfoil theory. Steady-state rotation occurs when mean driving moments just equal mean damping moments. If the slope of the net moment curve is negative, the rotation will be stable. An internal damper within the body is possible because fluctuating velocities exist from which energy can be absorbed. A piston in oil in a cylinder could absorb such energy.

For a given body, the net moment coefficient appears to be a function of ω/V. Reference 3 shows by potential-flow analysis that damping of an oscillating wing

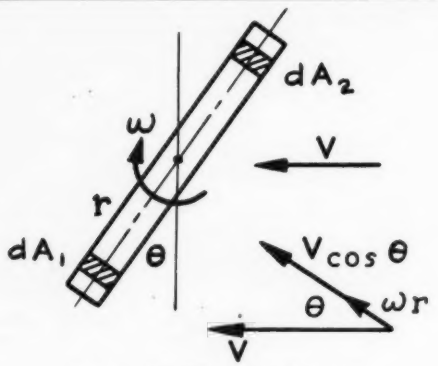

FIG. 5. Damping caused by drag.

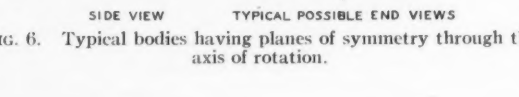

FIG. 6. Typical bodies having planes of symmetry through the axis of rotation.

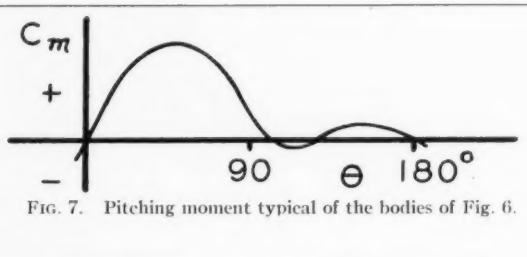

FIG. 7. Pitching moment typical of the bodies of Fig. 6.

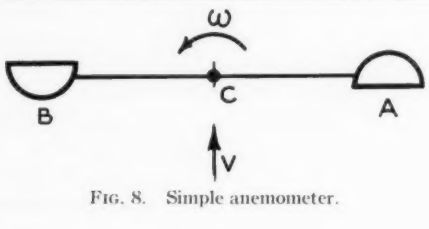

FIG. 8. Simple anemometer.

is a function of ω/V. By inference, a potential-flow analysis would reveal the same parameter for a rotating airfoil. This type of damping is derived from lift effects only. Damping created by drag effects is revealed by the following illustration: Consider the resisting torque of a circular cylinder of radius r_0 rotating about a transverse axis in a wind, as in Fig. 5.

According to well-known flow-resolution theorems, the effective relative velocity over the element dA_1, is V. $\cos\theta - \omega r$. The drag of this element is

$$dD_1 = 1/2\rho\ C_D\, dA_1 (V\cos\theta - \omega r)^2$$

Its torque is

$$dM_1 = 1/2\rho\ C_D\, dA_1\, r (V\cos\theta - \omega r)^2$$

The effective relative velocity at the same radius on the upstream end is $V\cos\theta + \omega r$. Then the net torque developed by these two elements is

$$dM = dM_2 - dM_1 = 2\rho r\ (\omega r)\ dA\, C_D V\cos\theta \quad (6)$$

In coefficient form,

$$dC_m = \frac{dM}{1/2\rho V^2 A r_0} = 4\,\frac{r}{r_0}\,\frac{dA}{A}\,C_D\cos\theta\left(\frac{\omega r}{V}\right) \quad (7)$$

Again ω/V steps forth as a parameter, determining the damping-moment coefficient. In the above illustration, C_D has been assumed to be independent of velocity.

Hysteresis in C_L-vs.-α curves constitutes one of the most powerful driving forces. When an airfoil, for example, is nearly at its steady-state stall, the boundary layer is thick as a result of flowing against adverse pressure gradients. However, if an airfoil is instantly increased from zero lift to a high angle of attack, the boundary layer at first remains as it was for zero lift. Consequently, no separation occurs immediately, even though the usual stall angle is far exceeded. Thus it is apparent that for a rotating body the condition of the boundary layer at any angle of attack is a function of the distance the fluid has traveled while the body is reaching that angle. The distance traveled by the fluid while a body changes its angular position by an amount α is $x = V\alpha/\omega$.

Therefore, it is probable that steady-state tumbling rates will usually be proportional to velocity regardless of air density. However, such a relation can be expected to break down if Reynolds Number effects or Mach Number effects become appreciable. Even without them, ω/V may not remain constant. Eq. (4) shows that the fluctuating velocity is affected by ρ and I. With very low values of I, for instance, the fluctuations in velocity may be very high. If I is very large, the rotation rate will be nearly constant. In view of the prior discussion of effects of angular velocity on the various moments, it becomes obvious that either moment-of-inertia changes or density changes can modify the net C_m-vs.-θ curve of a tumbling body and, consequently the average angular velocity.

(IV) Autorotations Explainable by Static Effects

Continuous autorotation of a body symmetrical about a plane through the axis of rotation, as in Fig. 6, cannot be explained by static data alone. This point is mentioned because literature on the tumbling of wings frequently implies that tumbling will develop if the wing becomes longitudinally unstable. This condition alone is insufficient, for instability merely gives the body an initial tendency to pitch away from normal flight attitudes.

Consider the bodies of Fig. 6 rotating about a point 0 on the plane of symmetry. With the wind blowing as

shown, the center of pressure is ahead of the point of rotation, and a turning moment will develop with the slightest displacement from $\theta = 0$. The pitching moment will be somewhat as in Fig. 7. If this indeed is the moment curve, net work proportional to $\int_0^{\pi} C_m \, d\theta$ is supplied by the rotation to 180°. However, the work derived from a clockwise rotation will be exactly equal and opposite to the work derived from a counterclockwise rotation. Therefore, no net work can be computed for such a body if static-moment-coefficient data alone are considered. Fore-and-aft shifts of the point of rotation greatly change the shape of the C_m-vs.-θ curve, but the antisymmetry will remain as long as the axis of rotation is on the plane of symmetry of the body.

The Anemometer

Nevertheless, there are cases of autorotation that can be explained by static data alone. One is the anemometer (Fig. 8). It utilizes the principle that a body has a lower drag coefficient when heading in one direction than when heading in the opposite direction. In Fig. 8, cup A has a higher drag coefficient than cup B. Therefore, a net torque is developed which is able to produce rotation.

It is also apparent from consideration of Fig. 8 that cup B could be removed and that rotation would still surely occur if the moment of inertia of the system were not too low. Furthermore, this type of torque differential between positions A and B will continue to exist for a single cup as the arm AC is shortened, until the centerline of the cup is on the very point of rotation C. When, finally, the axis of rotation is on the centerline, according to static considerations, the cup can produce no work because of symmetry.

The above discussion of the anemometer should make it clear that net torques can indeed be developed by symmetrical bodies of the type shown in Fig. 6. Such bodies will develop net driving moments if the axis of rotation is moved off the plane of symmetry as to 0′. This type of driving torque will be called the "anemometer-cup effect."

(V) Dynamic Effects Influencing Autorotation

The Lanchester Tourbillon

The Lanchester tourbillon is a fascinating toy windmill-like device that will be described here for the sake of completeness. Its motion is not a tumbling type, for its axis of rotation is parallel to the air stream like that of an ordinary windmill.

When given an initial spin in either direction, it will continue to rotate in that direction. When pointed directly into the wind, no static lift is possible because of symmetry (Fig. 10A). However, as soon as rotation occurs, the relative wind over a typical element A, Fig. 9 becomes as in Fig. 10B or 10C.

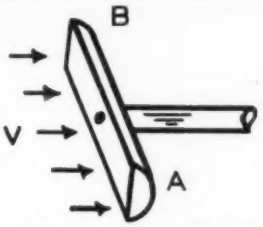

Fig. 9. Lanchester tourbillon.

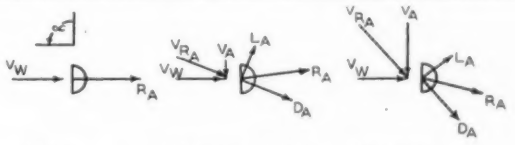

Fig. 10. Lanchester tourbillon at three rotational speeds.

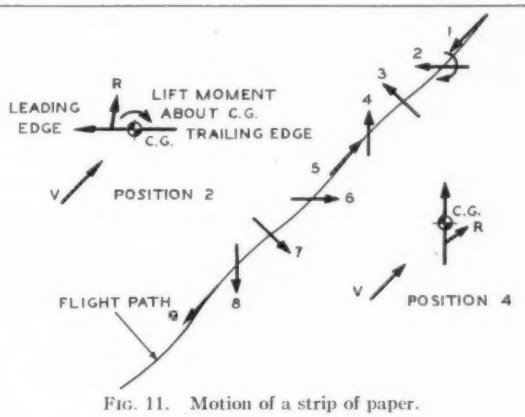

Fig. 11. Motion of a strip of paper.

Lift and drag vectors L_A and D_A are shown. If α is measured as shown, lift increases as α is reduced—that is, the slope of the lift curve is negative. When the lift and drag vectors are of such magnitude and direction that their resultant has a component in the direction of travel of the element, a driving force is developed. Fig. 10C shows the vector diagram for element A at a rotation rate above the autorotation limit. The lift and drag vectors are turned so greatly by the change in relative wind direction that the resultant force is in a direction opposing the motion. Consequently, autorotation of this nature can be predicted, given the necessary lift and drag data. From Fig. 10, it is apparent that R_A provides a force in the direction of motion if $L_A/D_A > V_A/V_W$. A flat spin is a rotation of this nature.

A Falling Strip of Paper

A flat strip of paper, having an aspect ratio of two or more will fall in about a 1:1 glide ratio, rotating as in Fig. 11. The motion can be explained very simply in the light of Fig. 11, which shows successive stages of the tumbling motion.

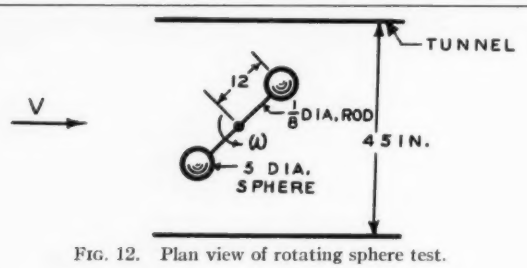

FIG. 12. Plan view of rotating sphere test.

Consider the forces on the strip when it is at position 2, shown to larger scale at the left in Fig. 11. It is at considerable angle of attack, exerting values of lift and drag that produce a resultant force R. If the center of gravity is behind the line of action of this resultant (25 per cent M.A.C. at low angles), a stalling couple is produced, tending to increase the angle. Rotation is rapid. Consequently, the boundary layer is thinner than for the steady state and the stall is delayed to higher values of C_L. At position 3, the strip probably is completely stalled. At position 4, it continues to be stalled. However, between positions 4 and 5, adhering flow over the trailing edge will be established. Reestablishment of unsaturated flow is delayed to angles below the static stall angle because the thick wake is a retarding influence. Hence, the downward lift impulse is less than the upward lift impulse. Moreover, the clockwise-rotation impulse is greater than the counterclockwise-rotation impulse, and the inertia of the paper carries it past the region of retarding impulse. The motion from 5 to 9 is essentially a repetition of that from 1 to 5. It can be concluded that this motion is characterized by the following features:

(1) The primary motive source is a hysteresis in the C_L-vs.-α curve.

(2) As a result a net upward lift is always developed, producing a finite gliding angle.

(3) Probably the center of gravity must be between 25 and 75 per cent M.A.C. Otherwise the net lift will produce a damping couple. See the detail diagram for position 2, Fig. 11.

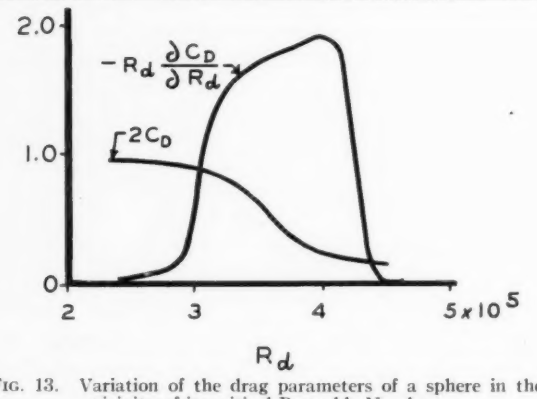

FIG. 13. Variation of the drag parameters of a sphere in the vicinity of its critical Reynolds Number.

(4) Damping moments appear to be a mixture of the lift and drag types.

Tumbling of tailless airplanes is a motion of this nature. Note that the fluctuating lift and drag forces will cause the center of gravity to follow a wavy path at a nonuniform velocity.

A Rotating Dumbbell

Autorotation of two 5-in. diameter balsa spheres (Fig. 12) was demonstrated in the Douglas El Segundo Wind Tunnel of 30- by 45-in. cross section. The assembly rotated on miniature ball bearings having extremely low friction. The rotation is explained as follows: The drag coefficient of a sphere is a function of Reynolds Number only, assuming the Mach Number to be low. At the sphere critical Reynolds Number, the drag coefficient decreases rapidly. The sphere moving upstream will then be at a higher Reynolds Number than the one moving downstream. Hence, if the drag coefficient decreases rapidly enough, the sphere moving upstream will have less drag than the sphere moving downstream. A criterion for such tendencies can be derived.

For one of the spheres, $D = (1/2)\rho S V^2 C_D$, where $C_D = f(R_d)$. For autorotation, drag must decrease as V increases or

$$\frac{dD}{dV} = \frac{1}{2}\rho S\left[2VC_D + V^2\frac{\partial C_D}{\partial V}\right] < 0$$

$$= \frac{1}{2}\rho S\left[2VC_D + V^2\frac{\partial C_D}{\partial R_d}\frac{dR_d}{dV}\right] < 0 \qquad (8)$$

Since $R_d = Vd/v$,

$$(d/dV)R_d = d/\nu = R_d/V$$

$$\frac{dD}{dV} = \frac{1}{2}\rho SV\left[2C_D + R_d\frac{\partial C_D}{\partial R_d}\right] \qquad (9)$$

For neutral stability

$$2C_D + R_d(\partial C_D/\partial R_d) = 0$$

or for autorotation

$$-R_d(\partial C_D/\partial R_d > 2C_D \qquad (10)$$

A typical plot of $R_d(\partial C_D/\partial R_d)$ is shown in Fig. 13. There is a considerable range of Reynolds Number over which autorotation might be expected. The original test observations as written by J. G. Brazier are quoted verbatim:

"The tunnel fan was started, and from dynamic pressures of zero inches of water to three and one-half inches of water (R_d = 296,000) the spheres would not autorotate. Any forced rotation was quickly damped out. At the lower dynamic pressures the spheres assumed a tandem attitude and oscillated with an amplitude of ±30°. Either sphere would remain in the upstream position. Between dynamic pressures of three and one-half and four inches of water the spheres were close to

being neutrally stable. After about one complete revolution either way, the rotation would damp out. At these dynamic pressures the spheres assumed a side-by-side attitude and oscillated with amplitudes of $\pm 15°$. At a dynamic pressure of four inches of water (R_d = 315,000), the spheres began to autorotate, the autorotation could be maintained in either direction. The motion was self-starting due to the initial oscillatory motion of the spheres. The rotational speed was approximately three cycles per second. The maximum dynamic pressure reached was approximately five inches of water (R_d = 353,000). The mounting of the spheres to the hub and the hub to the shaft was not rigid. After about one-half hour of running time the spheres were lost due to the failure of the vertical shaft just below the hub.

"Unfortunately, due to the loss of the model, the upper limit of the autorotation was not determined."

Consequently, a complete check of the theory was never made. However, the correlation of the start of the autorotation with sphere critical Reynolds Number was so good that there appears to be little doubt about the explanation of this type of autorotation. Sphere critical Reynolds number for this tunnel is about 375,000.

Shed Vortex Effects on Tumbling Motion

A tumbling body, especially a tumbling wing, develops lift of a cyclic nature. Therefore it will shed vortices of alternate right-hand and left-hand rotation. It is believed worth while to mention here that there may be a possibility of deriving a driving force from the downwash field created, depending on the value of ω/V. However, reference 3 indicates that an airfoil oscillating harmonically about its midpoint is affected not by the wake but only by the motions and accelerations with respect to the free stream. Therefore it is improbable that the wake will have any effect on an airfoil rotating at constant speed. Nevertheless, the question merits further investigation.

Effects of Change from Shaft Rotation to Free Tumbling

If the restraint to rotate about a fixed axis is eliminated, a completely free rotation occurs. On the shaft, only one degree of freedom is possible. But when free, as in a vertical spin tunnel or falling through the atmosphere, six degrees of freedom are available. In most cases observed, free tumbling appears to remain a motion in one plane, although the orientation of the plane may gradually change. Free motion in a plane then differs from rotation about a shaft, in that the center of gravity is free to travel up and down and back and forth.

Therefore a major question arises. Is it possible to obtain some sort of coupling or phase relationship during free rotation which will generate a driving moment that does not exist during pure shaft rotation?

The general problem is to find motions that make

$$\int_0^{2\pi} C_m \, d\theta > \int_0^{2\pi} C_m \, d\theta$$

(Free Rotation) (Shaft Rotation)

In the search for a driving mechanism, detailed knowledge of the free motion is desirable. A good starting point is to make calculations of the motion based on a C_m-θ curve antisymmetrical about the line $\theta = \pi$—that is, one having

$$\int_0^{2\pi} C_m \, d\theta = 0$$

Such can be supplied by either static or dynamic tests of a model supported on a shaft. If

$$\int_0^{2\pi} C_m \, d\theta = 0$$

the model will be rotating at a steady average rate. Then the motion can be examined to learn whether there is a net perturbation moment and, if so, what its sign is. If no perturbation moment is developed, the initial motion, of course, will continue unchanged because

$$\int_0^{2\pi} C_m \, d\theta = 0$$

Fig. 14 shows the lift, drag, and moment data used in calculating several free-motion orbits. Three c.g. positions were studied to show the effect of static stability on the motion. The curves in this figure represent static data. Dynamic values for lift and drag could have been used without trouble; but such use appeared to be a needless refinement, for differences between the static and dynamic values are small. For purposes of convenience, moment-coefficient values for the center of gravity at $0.676l$ were approximated by sinusoidal functions as follows:

$$\begin{aligned} C_{m_{cg.676}} &= 0.15 \sin 2\theta, \quad -90° \leqslant \theta \leqslant 90° \\ &= -0.075 \sin 4\theta, \quad 90° \leqslant \theta \leqslant 270° \end{aligned}$$

The values of $C_{m_{cg}}$ for the other c.g. positions were derived by conventional moment-transfer methods. The values can be considered consistent with the test results of Runs 55 and 56 of reference 5.

In making the calculations, the method of Section (III) was followed, using Eq. (4) rewritten as

$$\frac{d\theta}{dt} = \sqrt{\frac{\rho S l V^2}{I}} \sqrt{\int_0^{\theta} C_m \, d\theta + \frac{\omega_0^2}{\rho S l V^2 \, I}} \qquad (4a)$$

In addition to the three c.g. positions, the calculations covered five rotation rates:

$$\frac{\omega_0}{\sqrt{\rho S l V^2 / I}} = 0.008125, 0.0325, 0.13, 0.52, 2.08$$

Note that the values chosen increase in geometric progression. The calculations were made in this order: The θ-time relation was found; from it, the C_D-time re-

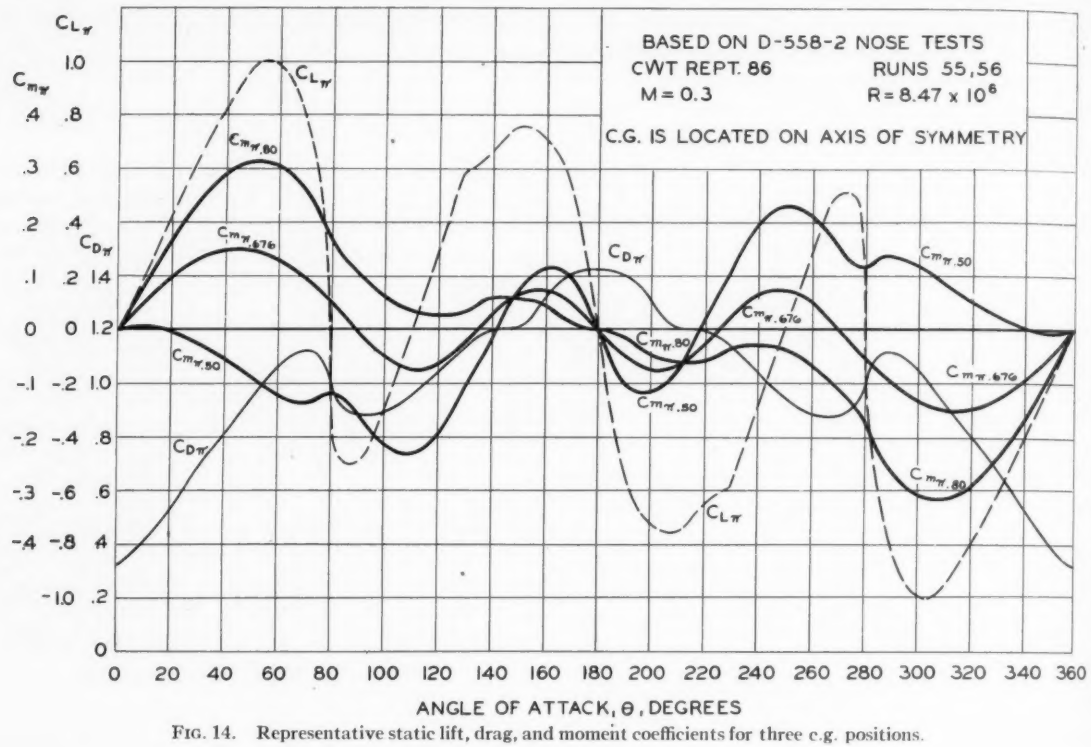

FIG. 14. Representative static lift, drag, and moment coefficients for three c.g. positions.

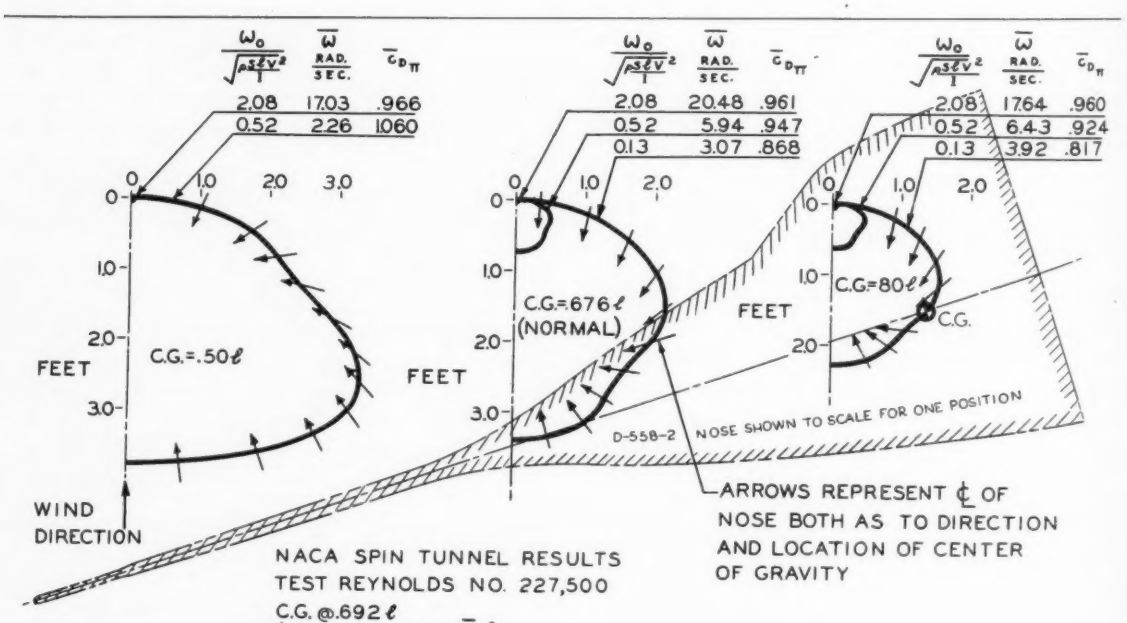

FIG. 15. Model D-558-2 nose. Calculated effect of position of center of gravity and tumbling rate on path of center of gravity while tumbling in a vertical wind tunnel. Conditions represent the full-scale nose falling at terminal velocity at 15,000 ft. Computed from data of Fig. 14 corresponding to R = 8.47 × 10⁶.

TABLE 1

Results of Orbit Studies at 15,000 ft.; D-558-2 Nose; Wt. = 775.5 Lbs.

C.G. Position	Rotation Parameter	Angular Drag Coefficient $\bar{C}_{D_\pi}$	Average Angular Velocity, Rad./sec.	Angular Velocity at $\theta = 0°$	Average Falling Velocity, Ft./Sec.	Average $\omega l/V$
0.50l	0.13	Rotation impossible				
	0.52	1.06	2.26	4.12	254	0.074
	2.08	0.996	17.03	17.27	266	0.533
0.676l	0.008125	0.586	1.73	0.101	342	0.042
	0.0325	0.746	2.39	0.359	303	0.066
	0.13	0.868	3.07	1.33	281	0.091
	0.52	0.947	5.94	5.10	269	0.184
	2.08	0.961	20.48	20.24	267	0.638
0.80l	0.13	0.817	3.92	1.26	290	0.113
	0.52	0.924	6.43	4.74	272	0.197
	2.08	0.960	17.64	18.63	267	0.550

TABLE 2

Values of $\overline{\Delta C}_{m_\pi} = \frac{1}{2\pi}\int_0^{2\pi} \Delta C_{m_\pi}\, d\theta$

Rotation Parameter	0.008125	0.0325	0.13	0.52	2.08
C.G. position					
0.5l			Will not rotate	−0.0021	−0.0007
0.676l	0.0061	0.0045	0.0033	0.0014	0.0004
0.80l	.....	....	0.0059	0.0031	0.0009

lation was found; and from them, the steady-state falling velocity was calculated. Computations apply to the full-scale D-558-2 nose at 15,000 ft. Because variations in c.g. position and $\omega_0/\sqrt{\rho S l V^2/I}$ both affect the C_D-time relationship, the steady-state falling velocity is not constant for the various cases. In other words $\bar{C}_{D_\pi}$, the mean drag coefficient varies.

Results of these calculations and the orbits of the center of gravity are shown in Table 1 and Fig. 15, respectively. At the lowest rate of rotation the orbits have considerable size; as the rate increases, they rapidly approach shaft rotation in nature. In Fig. 15 the arrows show the orientation of the nose as it moves around its orbit. It is in its highest position when pointing straight down—that is, when its drag is minimum.

The arrows are located to intersect the orbits at 0.50l, 0.676l, and 0.80l to provide better clues as to the position of the nose during its gyrations. N.A.C.A. test results at low Reynolds Number are tabulated in the figure.

The motions shown are based on static data in which

$$\int_0^{2\pi} C_m\, d\theta = 0$$

They have been computed upon the assumption that the translational velocities are so low that they produce a negligible effect on either the direction or magnitude of the true resultant velocity. The data of Table 1 were used as a first approximation in an iteration procedure for the purpose of learning the effect of using the true velocities and directions.

In the second approximation, the true velocity relative to the nose was computed by vectorial addition of the oribital velocity to the free-stream velocity. Then for the corrected angle of attack and velocity, an incremental moment coefficient ΔC_{m_π} at each θ position was obtained from the moment curves of Fig. 14. If the summation of the incremental values were positive, a incremental driving moment existed; if negative, a damping moment existed. The results of this study for each of the ten cases treated are presented in Table 2.

For the most stable case (c.g. at $x/l = 0.50$), $\overline{\Delta C}_{m_\pi}$ is negative. $\overline{\Delta C}_{m_\pi}$ is positive for the other two c.g. positions, although all the values are small. For example, at 15,000 ft., at the approximate terminal velocity of 186 m.p.h. with the center of gravity at 0.676l, the average angular acceleration $\ddot{\theta}$ is only 0.026 revolutions per sec. per sec., using $\overline{\Delta C}_{m_\pi} = 0.0033$. The analyses also showed that the changes in direction and magnitude of the relative-velocity vector were so slight that the original assumptions of independence of the x, y, and θ motions were exceedingly good.

The findings recorded in Table 2 are of considerable significance. *They show that the freedom of translation by itself can induce net moments, either driving or damping.* Therefore, tumbling may at times be possible even though static or dynamic data from shaft-supported models indicate otherwise.

An approximate physical picture of the origin of these dynamic driving moments can be given. Consider a model tumbling in equilibrium in a vertical wind tunnel. In the falling part of its orbit, its relative wind velocity is higher than the average value. If, during this period, the moments are in the direction of rotation, they are increased because of the additional velocity. In the other half of the orbit, the model is rising and the relative wind velocity is below the mean. In this phase, moments are resisting the rotation. However,

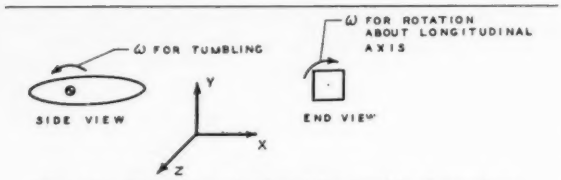

FIG. 16. Possible motion involving combined rotations.

FIG. 17. Transition of a nose from rocking motion to tumbling.

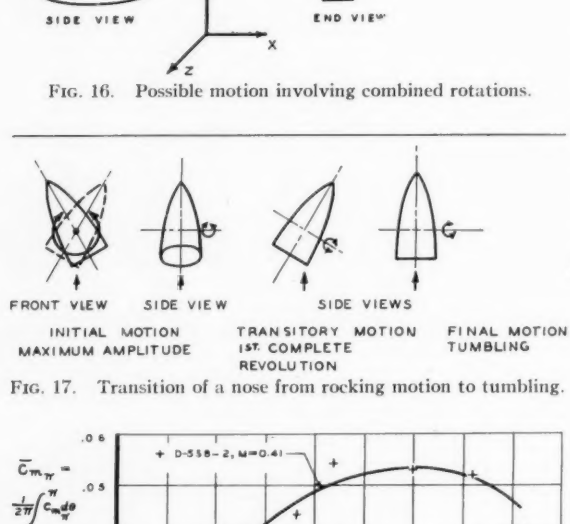

FIG. 18. Effect of $\bar{\omega}$ on net damping moment $^1/_6$-scale model results.

their resistance is reduced by the reduced relative wind. Therefore, a net driving moment for an entire cycle is created. A careful correlation of Figs. 14 and 15 will make these relations clear. In effect, the perturbation velocities distort the C_{m_π}-θ curve.

Other Possible Motions

Since free-tumbling motion has six degrees of freedom, there are undoubtedly numerous other possible motions of complex nature. For example, an elongated body tumbling end over and may also be subject to aerodynamic forces tending to rotate it about its longitudinal axis as in Fig. 16.

There are certain combinations of shape and Reynolds Number that will provide continuous rotation about the longitudinal axis. With such, a Flettner rotor effect may be developed which will give a turning moment about an axis parallel to the relative wind and through the center of gravity. Thus a rotation about all three axes may result. The general system of the several possible impressed aerodynamic forces can induce complex motions indeed, particularly when gyroscopic effects are added.

Motion pictures taken during the studies of reference 1 showed an interesting motion during the transition from rocking to steady-state tumbling. A nose model was released broadside to the airflow in the spin tunnel (Fig. 17). At first it floated around with a rocking motion. Gradually the amplitude built up. If the model had been supported on a horizontal shaft, the amplitude of rocking might possibly have increased until it went over "top dead center" and into continuous rotation. Instead, when the nose was within about 20° of pointing straight up, it appeared to fall to the side and keep on, instead of swinging back. In short, entry into the tumbling state was not made by motion in a vertical plane. The entry was first a build-up of rocking amplitude in a vertical plane until the first full revolution of tumbling was completed by rotation in a plane inclined about 45°. After the rotation was well established, the plane returned to vertical. One gained the impression that the model did not have enough kinetic energy to swing its weight right over "top dead center," so it got around the obstacle by tilting its plane of rotation to a position where not so much potential energy would be required. As a final steady motion was substantially in a vertical plane, the above transitory motion does not invalidate the assumptions of three degrees of freedom generally used in this report.

(VI) Analysis of the Motion of the D-558 and D-558-2 Noses

For elongated bodies roughly similar in shape to the D-558 and D-558-2 noses, the following effects appear to determine the tumbling motion: (a) the anemometer-cup effect, (b) the falling-strip-of-paper effect, (c) the rotating-dumbbell effect, (d) drag-type damping, and (e) the free-rotation effect.

The anemometer-cup effect exists because the models are not symmetrical fore and aft and because the center of gravity is not on the axis of symmetry. An idea of the magnitude of this effect can be obtained by examining the static $\bar{C}_{m_\pi}$ values obtained from the tests on the D-558 and D-558-2 noses (Figs. 18 and 19). In general, they are not equal to zero. The values shown on these two figures were obtained by planimeter from the moment data of reference 4 on models mounted as shown in Fig. 2.

For these bodies the falling-strip-of-paper effect should not be large because they are not primarily lifting bodies. This statement is borne out by examination of the C_L-vs.-θ data of reference 4, which shows, in general, no large increase in dynamic lift coefficient. However, the effect can definitely be seen. For example, see Fig. 22a of reference 4.

The rotating-dumbbell effect appears not to be a driving force at large scale. However, it evidently contributes the necessary driving moment for the small

$^1/_{50}$-scale nose tests of reference 2. Damping is probably nearly all of a drag type, for the reason that the bodies are poor lifting shapes.

The first four effects combine to produce the dynamic moment coefficient. Where dynamic test data are available, there is no need to consider the factors causing the resultant curve. Mean values of $\bar{C}_{m_\pi}$ for the two noses are shown as a function of both $\bar{\omega}$ and Mach Number in Figs. 18 and 19. Whereas the small $^1/_{50}$-scale noses would autorotate, the large noses definitely would not. In fact, the damping coefficients (Figs. 18 and 19) are high.

With this qualitative analysis of the motion of the two noses, we shall consider whether they are likely to tumble in full-scale flight. The known facts concerning them are listed below.

D-558 Nose

(a) N.A.C.A. $^1/_{14}$-scale model tumbled in a vertical spin tunnel. Test Reynolds Number $R = Vl/\nu = 255{,}000$.

(b) Douglas $^1/_{50}$-scale model rotated on fixed shaft below $R = 142{,}000$. Above this Reynolds Number, it would not rotate.

(c) Cooperative Wind Tunnel $^1/_6$-scale model did not rotate on a fixed shaft for Reynolds Number between 73,500 and 7,750,000. At the regular Cooperative Wind Tunnel test conditions ($R > 2.5 \times 10^6$), damping is high (Figs. 18 and 19).

D-558-2 Nose

(a) N.A.C.A. $^1/_{12}$-scale model tumbled in spin tunnel. Test Reynolds Number, $R = 120{,}000$. Model had no boom or pilot's enclosure.

(b) Douglas $^1/_{50}$-scale model rotated on a fixed shaft at all tunnel speeds, $R \leq 236{,}000$. Model had no nose boom.

(c) Cooperative Wind Tunnel $^1/_6$-scale model will not rotate on fixed shaft for Reynolds Numbers, R, between 812,000 and 8,500,000. Damping was extremely high (Figs. 18 and 19).

Since Reynolds Number effects were a likely explanation of the nonautorotating characteristics of the large models, several attempts were made in the Cooperative Wind Tunnel to induce autorotation of the D-558 nose by operation at the Reynolds Number of the smaller models. Because of the considerable difference in model size, the dynamic pressure became extremely low, as low as 0.1 lb. per sq.ft. Even with Reynolds Number the same as for the small models, the nose still refused to rotate. The probable reason it did not rotate is that bearing friction was then too high. At $q = 0.1$ lb per sq.ft. and $\bar{C}_{m_\pi} = 0.1$, the average moment for the D-558 nose is only 0.0044 ft.lb. or about the same as 2 Gm. acting at 1 ft. Even though the models had excellent bearings, their bearing friction was hardly negligible compared to 2 Gm.-ft. of moment.

The above facts seem to indicate that the N.A.C.A. and $^1/_{50}$-scale Douglas models rotated because they were in a Reynolds Number range favorable to the dumbbell type of autorotation. At $R_d > 2.5 \times 10^6$, the dumbbell type of driving force does not exist, and the hysteresis effect on lift is insufficient to produce rotation about a fixed shaft.

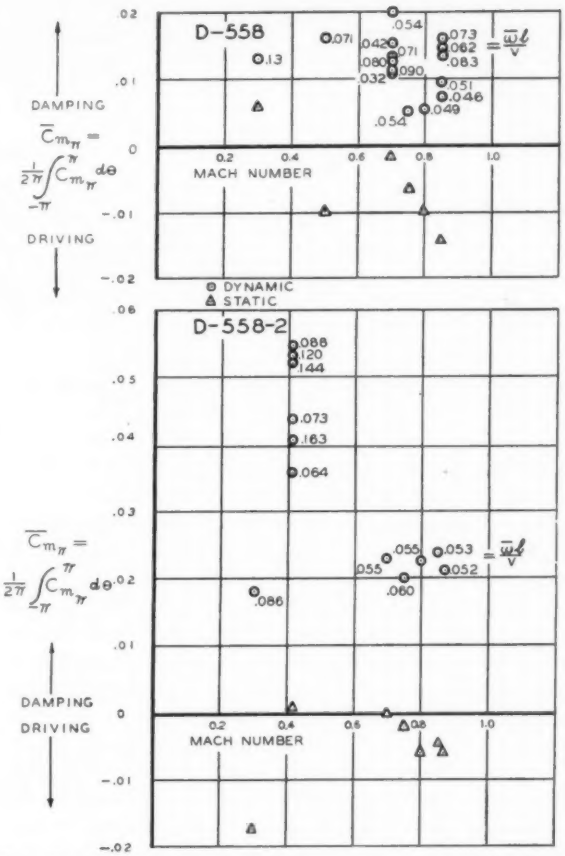

FIG. 19. Net damping or driving moment vs. Mach Number comparison of static and dynamic data. $^1/_6$-Scale model results.

Typical damping-moment data are presented in Figs. 18 and 19. The axes of rotation for these data were located as follows:

Model	Longitudinal Position	Vertical Position
D-558	$0.556l$	$0.021l$ above centerline
D-558-2	$0.676l$	$0.017l$ above centerline

In Fig. 19, where all available data points are plotted, the values at $M = 0.41$ for the D-558-2 nose are noticeably out of line. Checking failed to show any error in data reduction. One other explanation besides erroneous data appears possible. Consider a circular cylinder rotating about a transverse axis normal to the wind. The part moving downwind will be at a lower Mach Number than that moving upwind. For speeds either well below critical or well above critical, the curve of drag coefficient as a function of Mach Number will have nearly zero slope, dC_D/dM. However, at the critical Mach Number the drag coefficient rises rapidly. Therefore, the side of the cylinder moving downstream will have a much reduced drag coefficient and that moving upstream a much increased value. Therefore, resistance to rotation in the critical Mach Number range will be unusually high. Because of the long boom on the D-558-2 nose, differential Mach Numbers created by rotation will be appreciable. Now the critical Mach Number of

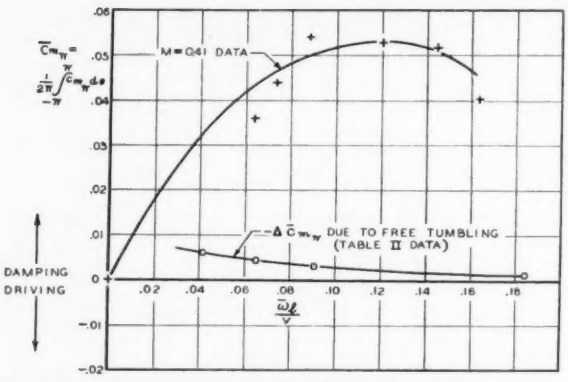

FIG. 20. Damping and incremental driving moments for the D-558-2 nose at approximately full-scale conditions.

a circular cylinder is just above 0.4. The test results showing high damping, exactly at the critical Mach Number of a cylinder, form a noteworthy coincidence, to say the least. This effect is just the reverse of the dumbbell effect developed at the critical Reynolds Number of a sphere or cylinder.

The remaining question is whether free rotation can develop sufficient driving moments to overcome the damping moments due to rotation. Since the data of Figs. 18 and 19 are at nearly full-scale conditions, they should account for all effects except that of free rotation. The effects of free rotation can best be analyzed by means of a plot of damping and driving moments versus $\bar{\omega}l/V$, as illustrated in Fig. 20 for the D-558-2 nose. If the incremental driving moment is greater than the damping moment, tumbling will occur. The plotted data show a distinct possibility of the occurrence of low-speed tumbling, even though the static net damping moment $\bar{C}_{m_\pi}$ is zero and the dumbbell effect on $\bar{C}_{m_\pi}$ has disappeared.

(VII) Conclusion

It is hoped that this article has clarified the nature of tumbling motions and has pointed out methods of predicting the occurrence of tumbling. In particular, this analysis shows that tumbling can probably be avoided by:

(1) Designing a neutral body shape whose net static moment, $\bar{C}_{m_\pi}$, is zero—that is, avoid the anemometer-cup effect.

(2) Operating above the sphere or cylinder critical Reynolds Number—that is, avoid the rotating-dumbbell effect.

(3) Properly locating the center of gravity fore and aft so that the incremental driving moment due to free rotation is zero or negative.

References

[1] Scher, Stanley H., *Wind Tunnel Investigation of the Stability of Jettisoned Nose Sections of the D-558 Airplane—Phases I and II*, N.A.C.A. Research Memorandum No. RM L7K10 (unclassified).

[2] Brazier, J. G., *Pilot Escape Study—Models D-558 and D-558-2; Part I—Low Speed Wind Tunnel Tests of 1/20-Scale Models Including Free Flight Tests*, Douglas Aircraft Company Report ES 15379.

[3] Durand, W. F., *Aerodynamic Theory*, 1st Ed., Vol. II, Division E V, Section 8; Julius Springer, Berlin, 1934.

[4] Brazier, J. G., *Pilot Escape Study—Models D-558 and D-558-2; Part II, High Speed Wind Tunnel Tests of 1/6 Scale Nose Section Models*, Douglas Aircraft Company Report ES 15379.

[5] *Report on High Speed Wind Tunnel Tests of 1/6 Scale Models of Jettisonable Nose Sections of the Douglas (El Segundo) D-558 and D-588-2 Airplanes*, Cooperative Wind Tunnel Report 86, May 17, 1949.

Bibliography

Tumbling

Dupleich, Paul, *Rotation in Free Fall of Rectangular Wings of Elongated Shape*, N.A.C.A. T.M. No. 1201, 1949.

Den Hartog, J. P., *Mechanical Vibration*, 2nd Ed., Chapt. VII; McGraw-Hill Book Company, Inc., New York, 1940.

Spinning

Bairstow, Leonard, *Applied Aerodynamics*, 2nd Ed., Chapt. V.; Longmans, Green and Company, New York, 1939.

Ober, Shatswell, *Some Experiments on Autorotation of an Airfoil*, N.A.C.A. T.N. No. 319, 1929.

Anemometers

Brevoort, M. J., and Joyner, U. T., *Experimental Investigation of the Robinson Type Cup Anemometer*, N.A.C.A. T.R. No. 513, 1935.

Slender-Body Theory—Review and Extension*

MAC C. ADAMS† AND W. R. SEARS‡
Cornell University

ABSTRACT

The approximate theory of flow about slender bodies and wings originated by Munk and Jones is reviewed. It is presented here in a form that emphasizes the relation to the source-sink methods of von Kármán and others. The extension to noncircular bodies is made for subsonic flow, paralleling Ward's extension for supersonic flow. The calculation of pressures and forces and the extension of the theory to unsteady flows are reviewed, and some discrepancies in the published literature are explained.

Finally, interpreting the Jones slender-wing result as the first term of an expansion in powers of a breadth parameter (e.g., aspect ratio), it is shown how a more accurate theory can be developed by carrying additional terms for both subsonic and supersonic speeds. This theory of not-so-slender wings is applied to some practical wing problems, including direct problems of flow past given wings and problems of wing design for minimum drag. The accuracy of the new results is assessed by comparison with linearized supersonic-airfoil theory for the special case of a flat delta wing.

(I) HISTORICAL INTRODUCTION

THE APPROXIMATE THEORY of the flow past slender bodies, elongated in the direction of flight, which is now generally known as "slender-body theory," was discovered by Munk[1] in 1924 and was applied by him to the calculation of the forces on airships in low-speed flight. Its extension to wings, which gave rise to a new branch of airfoil theory, was made in 1946 by Robert T. Jones.[2] Munk and Jones considered bodies and wings, respectively, flying at small angles of attack and, in view of the elongation in the flight direction, made the approximation that the flow pattern near the body in any transverse section is the same as in two-dimensional incompressible flow. Jones's important discovery was the method of applying this approximation to cases involving trailing-vortex sheets.

Tsien, in an important paper of 1938,[3] pointed out the remarkable fact that the Munk airship theory applies without modification to the flow about inclined, pointed projectiles at supersonic speeds. Subsequently, Jones made it clear in his paper that his slender-wing theory applied to both subsonic and supersonic flight, at least for pointed plan forms. To be sure, the meaning of "slender" is a bit different in the various speed régimes—namely, for any supersonic Mach Number, "slender" means that the body lies well within the Mach cone from the nose or apex. This, of course, is the reason for the limitation to pointed bodies and wings. It also leads to the conclusion that relatively blunt bodies and wings may qualify as "slender" at low supersonic speeds, while for very high supersonic (i.e., hypersonic) speeds the method must fail entirely for practical shapes. In the subsonic régime, it is easily verified that the word "slender" becomes less restrictive as the Mach Number increases from 0 toward 1, until at sonic flight speed all bodies and wings within a wide category become "slender" ones.

The well-known Prandtl-Glauert differential equation for the perturbation velocity potential in either subsonic or supersonic flight is

$$(1 - M^2)\phi_{xx} + \phi_{yy} + \phi_{zz} = 0 \qquad (1)$$

where x, y, and z are rectangular Cartesian coordinates, as in Fig. 1, the x-axis being aligned with the parallel stream far upstream, and where M denotes the stream Mach Number. The Munk-Jones approximation consists of neglecting the first term of Eq. (1) in comparison with the second and third. The statement at the end of the preceding paragraph means that, for a given wing or body, this term continually decreases, relative to the terms retained, as M increases from 0 toward 1. (Since ϕ_{xx} increases with increasing M for any given body, this conclusion is not so obvious as might at first appear, but it can easily be checked by means of the Prandtl-Glauert similarity rule.)

Robinson and Young[4,2] and later Heaslet, Lomax, and Spreiter[4] observed that the slender-wing theory of Jones yields reasonable and self-consistent results when applied to wings without thickness at $M = 1$. This conclusion, which might seem to follow immediately

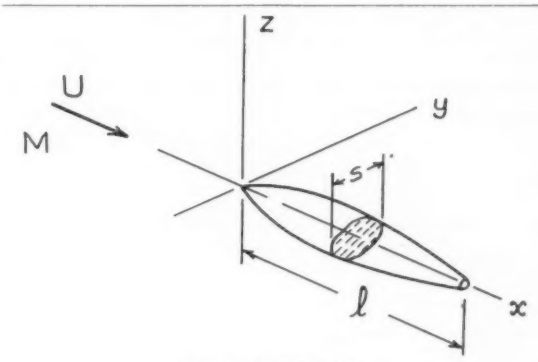

FIG. 1. Coordinates.

Presented at the Aerodynamics Session, Annual Summer Meeting, I.A.S., July 16–18, 1952.

* The authors wish to acknowledge the aid given them by their colleagues at the Graduate School of Aeronautical Engineering, especially Prof. N. Rott, and also by A. H. Flax and H. R. Lawrence, of the Cornell Aeronautical Laboratory, Inc. Part of the work reported here has received the financial support of the U.S. Air Force Research & Development Command.

† Research Assistant in Aeronautical Engineering.

‡ Director, Graduate School of Aeronautical Engineering.

from putting $M = 1$ in Eq. (1), is, in fact, somewhat surprising, since it is known that Eq. (1) itself is not generally valid in the transonic régime. The treatment of wings and bodies with thickness, for example, requires that Eq. (1) be discarded in favor of a different approximation in which a nonlinear term is retained.[5]

Thus the theory originated by Munk and Jones is seen to be almost unique within the category of small perturbation theories, in that it applies, at least to some cases, without modification throughout the whole spectrum of flying speeds from $M = 0$ to high supersonic (but not hypersonic) speeds. Furthermore, it is as simple and powerful as classical two-dimensional potential theory. Naturally, it has been widely exploited and extended. By means of conformal mapping, Spreiter extended the theory to wing-body combinations.[6] Applications to sweptback plan forms;[7, 11] rolling;[8, 9] yawing,[8] and pitching[8] wings; cruciform[10] and wing-body-tail[11] configurations; and other cases have also been made.

A particularly interesting extension has recently been made by Allen,[12] based on his experiments on extremely long inclined projectiles of circular cross section. Allen's experiments disclosed the presence of trailing vortices analogous to the von Kármán vortex street of two-dimensional viscous flow. This led Allen to the concept of utilizing viscous cross-flow fields in the Munk-Jones manner; the same idea has been successfully applied to low aspect ratio wings by Flax and Lawrence.[13] Finally, in unpublished work carried out at Langley Field, Clinton Brown and one of the present authors (Adams) have considered analytically the effects of flow separation from the leading edges of triangular slender wings. The resulting flow has been approximated by considering a pair of vortices near the wing's upper surface. Within the scope of slender-wing theory for triangular wings at supersonic speeds, it has been possible to determine the location of these vortices and their effect on lift, drag, and pressure distributions.

The agreement between experimental results and the predictions of the Munk-Jones theory is generally good, provided only that the limitations of slender shapes and small-perturbation flow are not violated.[13–15]

(II) Presentation of Slender-Body Theory

The slender-body theory, in its classical presentation, begins with the neglection of the term $(1 - M^2)\phi_{xx}$ in Eq. (1), leaving the approximate equation

$$\phi_{yy} + \phi_{zz} = 0 \tag{2}$$

The justification for this approximation is, at least intuitively, the slender elongated form of the wing or body under consideration. It seems clear that, since the geometrical properties of the body or wing vary only slowly in the x direction, the derivative ϕ_{xx}, which is the rate of change of the perturbation velocity component in the same direction, must also be small, at least in the close neighborhood of the body. This argument can be made more precise by introducing dimensionless coordinates ξ, η, and ζ as follows:

$$x = l\xi, \quad y = s\eta, \quad z = s\zeta \tag{3}$$

where l is a characteristic body dimension in the x direction, such as its overall length, and s is a characteristic width, such as maximum span of a wing or maximum diameter of a body of revolution (Fig. 1). Writing

$$\phi(x, y, z) = UlF(\xi, \eta, \zeta)$$

where U is the stream speed, one has, in place of Eq. (1),

$$(1 - M^2)\,(s^2/l^2)\,F_{\xi\xi} + F_{\eta\eta} + F_{\zeta\zeta} = 0 \tag{4}$$

In this form one can consider a family of wings or bodies differing from one another only in the value of the slenderness ratio s/l; it is more convenient to consider variations of Mach Number as well and to adopt as the slenderness parameter the number $(1 - M^2)\,(s^2/l^2)$. It is for sufficiently small values of this parameter that the first term can be neglected in Eq. (4), thus leading to Eq. (2). The fact that this neglection is restricted to the immediate neighborhood of the body will be made clearer later on in this paper.

Eq. (2) is exactly the equation for the velocity potential in two-dimensional incompressible flow; the conclusion to be drawn is, therefore, that the perturbation potential $\phi(x, y, z)$ has the form

$$\phi(x, y, z) = \varphi(y, z; x) + g(x) \tag{5}$$

where $\varphi(y, z; x)$ is a velocity potential for two-dimensional flow in a yz-plane, in which x appears only as a parameter introduced by the geometry of the cross section at x and $g(x)$ is any arbitrary function of x.*

All the cases considered by Munk and Jones—and, in fact, by all authors cited up to this point—fall into the category of *lifting cases*. These are cases in which the effects of incidence and camber alone are being calculated and the effects of thickness ignored, either because the wing under consideration has no thickness or because thickness effects do not affect the lift and are to be evaluated separately by a different method. They are, moreover, just the cases for which a knowledge of $g(x)$ in Eq. (5) is not needed, since this term makes only a uniform contribution to the pressure field at any x (in the small-perturbation approximation), which does not affect the lift distribution. In fact, in many of the technically interesting cases in this category it is clear that $g(x)$ is equal to zero because

* Since functions of the forms $yh(x)$, $zk(x)$, and $yzl(x)$ are also admissible in Eq. (5), $g(x)$ perhaps should stand for all such terms whose second derivatives with respect to y and with respect to z vanish. But actually terms of these forms do not appear, as will be shown later; hence, it is safe to consider $g(x)$ to be a function of x alone.

$\phi(x, y, z)$ must be antisymmetric with respect to the plane $z = 0$.

(III) Determination of $g(x)$

There are important problems, on the other hand, where $g(x)$ is different from zero and where a knowledge of this function is desirable for the calculation of pressure distribution and drag. It has not always been clear, in the literature of the slender-body approximation, why the Munk-Jones approximation represented by Eq. (2) seemed to fail in these problems. When the solution of Eq. (2) is written in the form of Eq. (5), it becomes evident that the failure is not so much a fault of the Munk-Jones approximation as it is due to one's inability to determine $g(x)$. One could determine this function by bringing in the additional boundary conditions $\phi = \phi_x = 0$ at large lateral distance from the wing or body—specifically, at an infinite distance if the flight speed is subsonic or at the nose Mach cone if the flight speed is supersonic. But solution (5) is invalid at such large distances.

Ward's Treatment of Pointed Bodies in Supersonic Flow

Light was shed on this dilemma by Ward[16] in his important and general discussion of the flow past slender, smooth, pointed bodies at supersonic speeds. Ward shows that the additional boundary condition can only be brought into the picture by returning, momentarily, to the complete potential equation, Eq. (1) or (4). He attacks the solution of this equation by use of Laplace transforms. Let

$$\mathfrak{L}[F(\xi, \eta, \zeta)] \equiv \bar{F}(p, \eta, \zeta) \equiv \int_0^\infty F(\xi, \eta, \zeta) e^{-p\xi}\, d\xi \quad (6)$$

Eq. (4) then becomes

$$\bar{F}_{\eta\eta} + \bar{F}_{\zeta\zeta} = m^2 k^2 p^2 \bar{F} \quad (7)$$

where m^2 denotes $M^2 - 1$, k denotes s/l, and use has been made of the boundary conditions

$$F(0, \eta, \zeta) = 0 = F_\xi(0, \eta, \zeta)$$

It might be pointed out here that these conditions are equivalent to putting $F = 0$ and $F_\xi = 0$ on the nose Mach cone, in view of the well-known nature of the supersonic small-perturbation equation—i.e., the "rule of forbidden signals."

Having thus introduced the important boundary condition at the Mach cone, Ward proceeds toward the slender-body approximation by expanding a general solution of Eq. (7) in a form appropriate for the region close to a slender body—i.e., for $mkr/\xi << 1$, where $r = \sqrt{\eta^2 + \zeta^2}$. [This technique is not reproduced here in detail because it is similar to that used immediately below and also in Section (VI.)] His result is, in the notation of Eq. (5),

$$g(x) = \frac{U}{2\pi}\left\{ S'(x) \ln \frac{m}{2} - \int_0^x S''(x') \ln (x - x')\, dx' \right\} \quad (8)$$

where $S(x)$ denotes the area of the body cross section at x and it is assumed that $S'(x)$ is continuous. The restriction to pointed-nose bodies requires that $S'(0) = 0$.

Thus, Ward has succeeded in applying the slender-body theory, in a unified and consistent manner, to smooth pointed bodies of arbitrary cross section, camber, and incidence in supersonic flight.*

* Some of Ward's conclusions were independently obtained by Graham.[41]

It is interesting to compare Ward's result with von Kármán's well-known ones[17] in the particular case of bodies of revolution. von Kármán's result for these bodies at zero incidence is

$$\phi(x, R) = -\frac{U}{2\pi}\int_0^{x - mR} S'(x') \frac{dx'}{\sqrt{(x - x')^2 - m^2R^2}} \quad (9)$$

$$\approx \frac{U}{2\pi}\left\{ S'(x) \ln R + S'(x) \ln \frac{m}{2} - \int_0^x S''(x') \ln (x - x')\, dx' \right\} \quad (10)$$

where R denotes the radius of the body at x—i.e., $\pi R^2 = S(x)$. But the first term in Eq. (10) is just $\varphi(y, z; x)$, the solution of the two-dimensional flow problem [Eq. (2)] for this particular case. Moreover, Lighthill[18] has shown that Eq. (10) is fully as accurate as the original differential equation, Eq. (1), so that this form is theoretically equivalent to Eq. (9). Thus, Ward's results include von Kármán's and are, for inclined bodies of revolution, equivalent to combining von Kármán's with Tsien's.

Actually, this combination was usually made by practical engineers—i.e., the slender-body approximation was used for the effect of angle of attack, but von Kármán's theory based on source-sink distribution was resorted to for the symmetrical flow component. It is one of the virtues of Ward's work that it unifies these seemingly different theories, besides extending the whole subject to a wider class of shapes.

Extension to Slender Bodies in Subsonic Flow

The same sort of analysis (for slender bodies of arbitrary cross section, camber, and incidence) can be carried out for subsonic speeds of flight. Again, one goes back to the complete Prandtl-Glauert equation, Eq. (4), but in this

case one transforms its terms in the Fourier, instead of Laplace, manner. Let

$$\mathfrak{F}[F(\xi, \eta, \zeta)] \equiv \tilde{F}(\omega, \eta, \zeta) \equiv \int_{-\infty}^{\infty} F(\xi, \eta, \zeta) e^{i\omega\xi}\, d\xi \tag{11}$$

Eq. (4) then becomes

$$\tilde{F}_{\eta\eta} + \tilde{F}_{\zeta\zeta} = \beta^2 k^2 \omega^2 \tilde{F} \tag{12}$$

where now β^2 denotes $1 - M^2$ and k denotes s/l as before. The following boundary conditions have been applied in obtaining Eq. (12):

$$F(\pm\infty, \eta, \zeta) = 0 = F_\xi(\pm\infty, \eta, \zeta)$$

From here on, the solution of this problem is practically the same as Ward's. A solution of Eq. (12) is

$$\tilde{F}(\omega, \eta, \zeta) = \sum_0^\infty K_n(\beta k|\omega| r)\, [A_n(\omega) \cos n\theta + B_n(\omega) \sin n\theta] \tag{13}$$

where the K_n are modified Bessel functions of the second kind and $\theta = \tan^{-1}(\zeta/\eta)$—i.e., r and θ are cylindrical coordinates in the ξ,η,ζ-space.

Since the correct boundary conditions far from the body have already been satisfied, one can now proceed to expand solution (13) in a form suitable for the region close to the body. The expansion formulas for the K_n's for small arguments are well-known;[19] if the leading term only is carried in each K_n, the result is

$$\tilde{F}(\omega, \eta, \zeta) \approx -A_0(\omega) \left[\ln\left(\frac{1}{2}\beta k|\omega| r\right) + \gamma \right] + \frac{1}{2} \sum_1^\infty (n-1)! \left(\frac{2}{\beta k}\right)^n \left[\frac{A_n(\omega)}{|\omega|^n} \frac{\cos n\theta}{r^n} + \frac{B_n(\omega)}{|\omega|^n} \frac{\sin n\theta}{r^n} \right] \tag{14}$$

where γ is Euler's constant ($\gamma = 0.57\ldots$). The Fourier transforms having served their purpose, one now returns to the variables ξ, η, and ζ by taking the inverse transform of each term; for the region near the body, then,

$$F(\xi, \eta, \zeta) \approx -a_0(\xi) \ln\left(\frac{1}{2}\beta k r\right) + \frac{1}{2}\int_0^\xi a_0'(\xi') \ln(\xi - \xi')\, d\xi' - \frac{1}{2}\int_\xi^1 a_0'(\xi') \ln(\xi' - \xi)\, d\xi' + \frac{1}{2} a_0(0) \ln \xi + \frac{1}{2} a_0(1) \ln(1 - \xi) + \sum_1^\infty \left[a_n(\xi) \frac{\cos n\theta}{r^n} + b_n(\xi) \frac{\sin n\theta}{r^n} \right] \tag{15}$$

where $a_0(\xi)$ is the inverse transform of $A_0(\omega)$. The new functions $a_n(\xi)$ and $b_n(\xi)$ are related to $A_n(\omega)$ $B_n(\omega)$ and remain arbitrary at this stage, to be determined by the boundary conditions at the body surface.

The function $a_0(\xi)$ is easily evaluated. From the boundary condition at the body surface, it follows that

$$\oint_C (\partial\phi/\partial\nu)\, d\tau = US'(x) \tag{16}$$

where the contour integral is taken around the body contour C in a cross section, ν is the normal to this contour, and S is the cross-sectional area. In terms of the coordinates ξ, η, and ζ, this condition becomes

$$\oint_{C'} (\partial F/\partial\nu)\, d\tau = (1/l^2) S'(\xi) \tag{17}$$

where now the normal ν and the element of arc length τ are both in the ξ,η,ζ-space and the contour integral is taken around the body contour C' in this space. Also, the cross-sectional area is now considered to be a function of the dimensionless variable ξ, rather than x, and $S'(\xi)$ denotes $dS/d\xi$. But $F(\xi, \eta, \zeta)$ in Eq. (15) has just the form of a plane incompressible-flow velocity potential, and the contour integral in Eq. (17) is proportional to the net flow of an incompressible fluid out of the contour C' in a plane-flow problem. Thus, it can be evaluated at any convenient contour enclosing C' and the ξ-axis, and its value is $-2\pi a_0(\xi)$. Hence,

$$-a_0(\xi) = (1/2\pi l^2) S'(\xi) \tag{18}$$

The first term and the summation in Eq. (15) are recognized as the two-dimensional potential function $\varphi(y, z; x)$ of Eq. (5). Therefore, introducing the result obtained in Eq. (18), one has for $g(x)$ the following result:

$$g(x) = \frac{U}{2\pi}\left[S'(x) \ln\frac{\beta}{2} - \frac{1}{2} S'(0) \ln x - \frac{1}{2} S'(l) \ln(l - x) - \frac{1}{2}\int_0^x S''(x') \ln(x - x')\, dx' + \frac{1}{2}\int_x^l S''(x') \ln(x' - x)\, dx' \right] \tag{19}$$*

Again it has been assumed that the body contour is smooth—i.e., that $S'(x)$ is continuous from bow to stern.

* Apparently this result has also been obtained by Heaslet and Lomax, since they mention it (without proof) in reference 20, where Ward's results, mentioned above, are obtained by a different procedure.

The first term in Eq. (15) represents, in the two-dimensional flow plane, a source at the axis; the summation consists of the contributions of doublets and higher degree singularities, all located at the axis. It is well known that, for any given contour C within a general class, this arrangement of singularities is not unique but is equivalent to a distribution of sources around the contour, for example. In practical problems it is likely that $\varphi(y, z; x)$ will actually be found by use of conformal mapping.

It is important to notice that the flow conditions at any station on a body in subsonic flow depend upon the whole body shape; this was to be expected and is confirmed by Eq. (19). In supersonic flow, of course, downstream effects are not felt upstream, so that Ward's $g(x)$ is integrated only from the body nose to the station under consideration. This difference between the two speed regimes makes an essential difference in the treatment of bodies that have blunt sterns; these are outside the scope of the subsonic theory given here but are not outside the scope of Ward's supersonic theory.

Just as Ward's results constituted, for bodies of revolution, a unification of von Kármán's and Tsien's, the result given here for subsonic flow is equivalent to a combination of subsonic source-sink theory with the Munk approximation for the cross-flow effect when applied to bodies of revolution. The source-sink theory gives[21, 22]

$$\phi(x, R) = -\frac{U}{4\pi}\int_0^l S'(x')\frac{dx'}{\sqrt{(x-x')^2+\beta^2R^2}} \tag{20}$$

$$\phi(x, R) \approx \frac{U}{2\pi}\left[S'(x)\ln R + S'(x)\ln\frac{\beta}{2} - \frac{1}{2}S'(0)\ln x - \frac{1}{2}S'(l)\ln(l-x) - \frac{1}{2}\int_0^x S''(x')\ln(x-x')\,dx' + \frac{1}{2}\int_x^l S''(x')\ln(x'-x)\,dx'\right] \tag{21}$$

Thus, the slender-body theory of Munk and Jones, when presented in the form of Eq. (5), clarifies the relationship between the familiar subsonic and supersonic versions of source-sink distribution theory for slender bodies of revolution. That is, a given body of revolution in subsonic axisymmetric flow has the same $\varphi(y, z; x)$ as in supersonic flow [namely, the first term in Eqs. (10) and (21)] but a different $g(x)$. As a matter of fact, this can also be deduced directly from the source-distribution integrals [as in Eq. (10)] and has already been noticed by some investigators.[23] The present study, together with Ward's, shows that this relationship extends to a much wider class of bodies.

Since $g(x)$ in both of the cases investigated above turns out to be a function of Mach Number M, it is not surprising that one cannot obtain it from Eq. (2), which (together with its boundary conditions) is independent of M.

(IV) Determination of Pressure and Forces

The pressure is calculated from $\phi(x, y, z)$ according to Bernoulli's equation. In view of the approximations of small-perturbation theory already made in Eq. (1), there is no purpose in using Bernoulli's equation in its exact form. For wings ("planar problems"), for example, the consistent approximation is

$$p - p_\infty = -\rho U\phi_x \tag{22}$$

On the other hand, as is well known by now, this is not a satisfactory approximation for slender bodies ("nonplanar problems"); a more accurate formula for these cases is, in wind coordinates,

$$p - p_\infty = -\rho[U\phi_x + (1/2)(\phi_y^2 + \phi_z^2)] \tag{23}$$

Moreover, Eq. (23) is consistent with the approximations of Eq. (1) and of the slender-body theory.[24, 25]

In any case, the velocity components are immediately available from Eq. (5)—viz., $\phi_y = \varphi_y$, $\phi_z = \varphi_z$—while ϕ_x is given by

$$\phi_x = (\partial\varphi/\partial x) + g'(x) \tag{24}$$

where $\partial\varphi/\partial x$ denotes the derivative of $\varphi(y, z; x)$ with respect to the parameter x.

Satisfactory agreement of slender-body results with either experiment or with the results of more exact theories depends upon the use of Eq. (23) instead of (22) in cases where bodies, as distinguished from wings alone, are involved. Many writers reached this conclusion, for example, by comparing the results of von Kármán's source-sink theory with those of nonlinear theory for right circular cones. The same matter is involved in the case of subsonic flow past slender ellipsoids of revolution presented in Fig. 2. The solid curves in this figure were calculated by Matthews[26] by use of exact incompressible-flow theory corrected for Mach Number by means of the extended Prandtl-Glauert rule (the Göthert rule). The dash-dot lines are the results of slender-body theory using Eq. (23), while the dotted curves are Matthews' results for the equivalent source-sink theory but using Eq. (22). It is seen that slender-body theory agrees satisfactorily with the more elegant method when the proper pressure formula is used; this is in contradiction to Matthews' conclusion.

Matthews' experimental results, also spotted in Fig. 2, are not in perfect agreement with theoretical ones. Presumably this is due to the rather large thick-

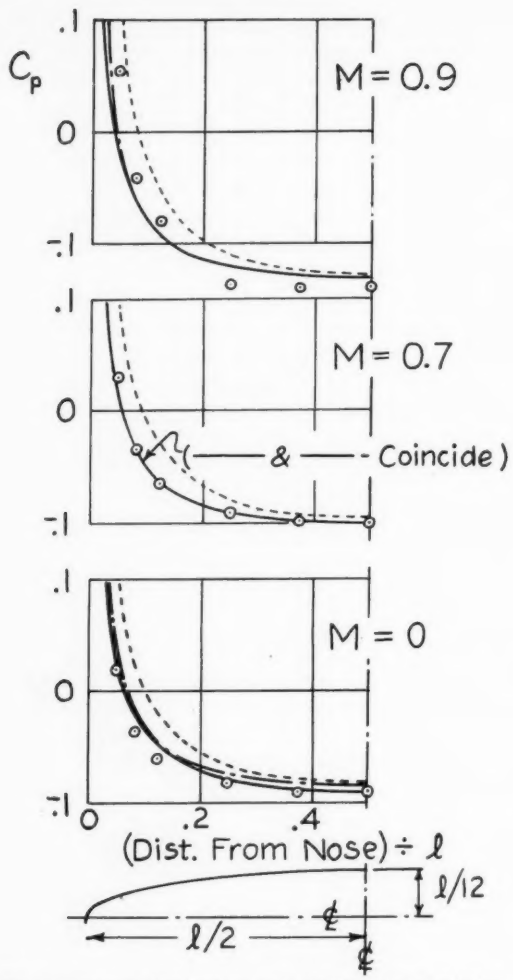

FIG. 2. Pressure distribution on 1:6 ellipsoid of revolution at zero incidence at various Mach Numbers. Solid curves: exact incompressible values corrected by extended Prandtl-Glauert rule. Dash-dot curves: slender-body theory using Eq. (23). Dotted curves: source-sink theory using Eq. (22). Circled points: Matthews' experiments.[26] Bottom: body contour.

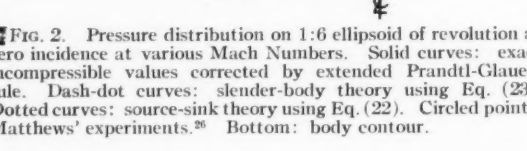

FIG. 3. Example of wing-body combination treated by Spreiter.[6]

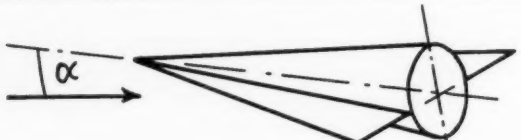

FIG. 4. Examples of configurations terminating in a baseplane.

ness ratio of the ellipsoid—viz., 1:6. Matthews finds better agreement for a 1:10 ellipsoid.

Lift

The distribution of the lift along the length of a body was calculated by Munk in his original paper[1] by considering the rate of increase of the transverse component of the fluid momentum (impulse) in a coordinate system at rest in the fluid. The same principle applies to wings and wing-body combinations, provided only that proper account is taken of the trailing vortices. The conclusion is always that the total transverse force (resultant of lift and side force) is vectorially equal to $(-U)$ times the impulse per unit x in the two-dimensional flow field at the rear end of the body:

$$\boldsymbol{R} = \rho U \oint_{C_1} \varphi \boldsymbol{\nu}\, d\tau \tag{25}$$

where C_1 is the contour of the wing, body, and trailing-wake configuration at the stern and $\boldsymbol{\nu}$ is the unit vector normal to this contour, directed out of the body, into the fluid.

Eq. (25) has an accuracy that may be surprising. It properly accounts for the effects of ϕ_y^2 and ϕ_z^2, as in Eq. (23), when they are needed. Thus, by neglecting ϕ_y^2 in a wing-body problem, Spreiter[6] found a discrepancy between Eq. (25) and the result of integrating pressures to determine lift. His error is a relatively obscure one, since it appears in the calculation of wing lift where ordinarily Eq. (22) is sufficient. But the configuration he studied (Fig. 3) involves components ϕ_y due to wing incidence, body incidence, and body divergence on the wing. Since the first two of these are antisymmetric with respect to the plane $z = 0$ while the third is symmetric, the quantity ϕ_y^2 contains an antisymmetric cross-product term, of the same order contemplated in Eq. (23), which contributes appreciably to the lift. That this error exactly accounts for Spreiter's lift deficiency mentioned above has been verified by Harold Mirels, at Cornell University. The same criticism of Spreiter's paper has independently been made by Miles.[27]

In those special cases where the wing trailing edge and body base lie entirely in one transverse plane, such as in Figs. 3 and 4, the total lift, according to Eq. (25), depends only on the configuration in this plane. More generally, chordwise lift loading at any station x on a wing, body, or combination thereof, which lies forward of every part of the wing's trailing edge, depends only on the geometry at x.

In many practical problems, however, it is necessary to calculate the loading and the lift on parts that are affected by trailing vortices. Frequently, the determination of the trailing-wake strength is a nontrivial problem. Consider first a wing of arbitrary twist $\alpha(x, y)$ lying close to the plane $z = 0$ (Fig. 5). The two-dimensional potential problem for a station such as *B-B* involves knowledge of the trailing-vortex distribu-

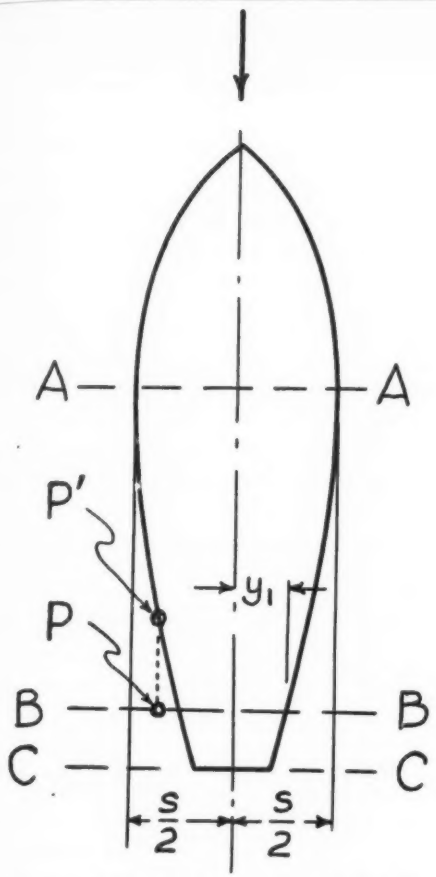

FIG. 5. Slender wing with curved trailing edge.

tion from all the wider sections farther forward. The boundary value problem for such a section is: To determine $\varphi(y, z; x)$ such that $\partial\varphi/\partial z = -U\alpha(x, y)$ for $-y_1 < y < y_1$, while φ along the strips $y_1 < |y| < s/2$ has the same values as at the trailing-edge points directly upstream—e.g., $\varphi(P) = \varphi(P')$ in Fig. 5. Thus, the solution at *B-B* involves knowledge of the solutions at upstream stations, and, in general, the values of φ at the trailing edge *C-C*, required in Eq. (25), depend upon the solutions of all these boundary-value problems for the stations between *A-A* and *C-C*. Fortunately, boundary-value problems of this type are not particularly difficult; however, it is difficult to reduce Eq. (25) for such cases to a more explicit form.

There is another class of problems where the trailing-vortex configuration is important—namely, problems involving bodies whose after parts contract downstream of the wing trailing edge, as in Fig. 6. Here the alteration of the trailing-vortex positions due to the body's convergence must be accounted for. The vortices must follow the stream lines of the flow around the body; in the present approximation they are displaced only radially, and this displacement may be calculated from the potential $\varphi(y, z; x)$ contributed by the body. In the problem illustrated in Fig. 6, for example, the radial velocity component is

$$\frac{\partial\phi}{\partial r} = \frac{\partial\varphi}{\partial r} = U\frac{dR^2}{dx}\frac{1}{r}$$

so that the radial displacement of a vortex originally at y_A (in Section *A-A*), when it arrives at *B-B*, is given by

$$y_B^2 - y_A^2 = \int_{x_A}^{x_B} \frac{dR^2}{dx}\,dx = R_B^2 - R_A^2 \qquad (26)$$

The lift on the portion of the body aft of the wing trailing edge is given by the difference between the values of the integral in Eq. (25) at the trailing edge and at the rear end of the body.

$$\Delta L_{AB} = \rho U \left(\oint_{B-B} \varphi\nu_z\,d\tau - \oint_{A-A} \varphi\nu_z\,d\tau\right) \qquad (27)$$

where ν_z denotes the vertical component of the outwardly directed unit normal vector $\boldsymbol{\nu}$.

Consider, for example, a case in which the body closes to a point at *B-B*. Eq. (27) becomes, upon introduction of Eq. (26),

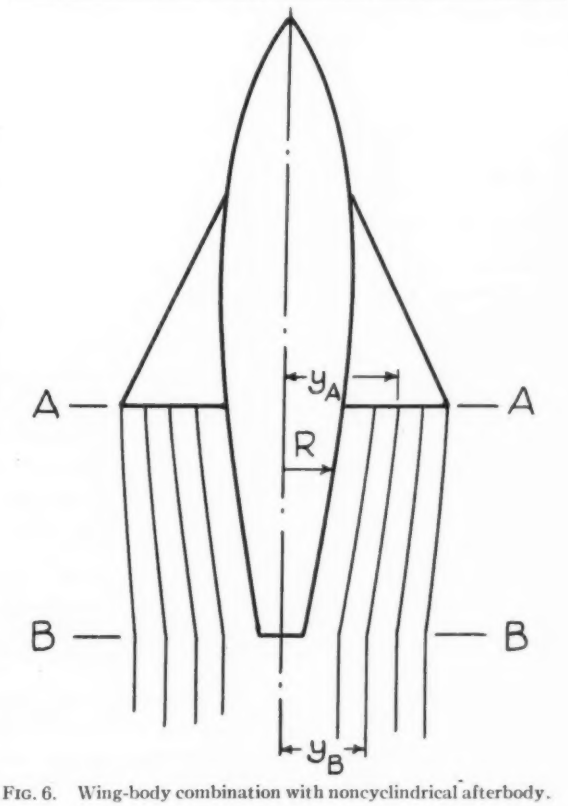

FIG. 6. Wing-body combination with noncylindrical afterbody.

$$\Delta L_{AB} = -\rho U \left[\int_{\substack{\text{body at} \\ A-A}} \varphi v_z \, d\tau + \int_{\substack{\text{wing at} \\ A-A}} (\varphi_{\text{top}} - \varphi_{\text{bottom}}) \left(1 - \frac{y}{\sqrt{y^2 - R_A^2}} \right) dy \right] \quad (28)$$

Obviously, this formula is based on the assumption that the vortex wake does not roll up and is not otherwise distorted or shifted before it reaches *B-B*. If the body is extremely long between *A-A* and *B-B*, this assumption may be unjustified. The motion of trailing vortices near cylindrical bodies of revolution has been studied by Lagerstrom and Graham.[28]

It is clear from Eq. (27) that, in the absence of rolling-up or other secondary effects, there is no lift on a cylindrical afterbody.

Drag

Ward has given a rather comprehensive discussion of the drag of slender bodies in *supersonic* flow in the paper mentioned above.[16] It may be useful to summarize his results here and to try to relate them to the familiar engineering concepts of wave drag and induced drag. Ward's result may be rearranged in the form

$$D = D_1 + D_2 + D_B \quad (29)$$

where

$$D_1 = -\frac{1}{4\pi} \rho l^2 \left\{ \int_0^l \int_0^l S''(x) S''(x') \ln |x - x'| \, dx \, dx' - 2S'(l) \int_0^l S''(x') \ln (l - x') dx' + [S'(l)]^2 \ln \frac{m}{2} \right\} \quad (30)$$

$$D_2 = -\frac{1}{2} \rho \oint_{C_1} \varphi \frac{\partial \varphi}{\partial \nu} \, d\tau \quad (31)$$

$$D_B = S(l) (p_\infty - p_B) \quad (32)$$

As before, C_1 denotes the contour of the body section at the stern, which, in the cases of wings and wing-body combinations, must include the trailing-vortex wake. Here p_B is the base pressure, so that D_B is the base drag, which presumably must be evaluated from experiment or viscous-fluid theory.

The first part of D_1 is recognized as von Kármán's famous result[17] for supersonic pointed bodies of revolution at zero incidence. Thus Ward has generalized this result, both for bodies not of revolution and for bodies where $S'(l)$ is not zero. Moreover, in D_2 he has included the contributions due to incidence and lift. It is interesting that the term $[S'(l)]^2 \ln (m/2)$ in D_1 is the only term affected by Mach Number within the supersonic régime.

In engineering terminology, D_1 is the *wave drag*, and D_2 might, in most cases, correctly be called the *induced drag*. The exceptions are, again, the cases where $S'(l)$ is not zero, for which $\varphi(y, z; l)$ includes a source term; for other cases, D_2 is just the kinetic energy produced in a unit cross-flow plane at the stern per second. For wings, D_2 includes the vortex drag and accounts correctly for the leading-edge suction. When the leading-edge drag discovered by Jones,[29] which occurs with rounded leading edges, is involved, it is correctly accounted for in D_2.

Ward has also derived an especially interesting form for drag at incidence: the drag is equal to its value at zero lift plus one-half the product of the lift and the angle measured from zero lift:

$$D = D_{L=0} + (1/2)\alpha L \quad (33)$$

The simplicity of this general result—and especially the absence of cross-product terms—seems remarkable.

In *subsonic* flow, the drag situation is even simpler, of course, since bodies are required to be closed at both ends and since there is no wave drag. The drag formula for this speed régime is simply

$$D = D_2 \quad (34)$$

where D_2 is defined in Eq. (31). Since the body closes at its stern, D_2 arises from the trailing wake and is truly *induced* drag. Again, the formula correctly accounts for leading-edge singularities.

(V) Application to Unsteady Flow

The original slender-body idea of Munk was actually to replace a steady three-dimensional flow by a non-steady two-dimensional one. Namely, fixing his attention upon a transverse lamina of fluid through which the body was flying, Munk noticed how the impulse of flow in this lamina changed with time because of the passage of the body through it. In this sense, it seems clear that unsteady three-dimensional problems do not require any essentially different treatment but only a simple extension of Munk's idea. Specifically, one may still treat the flow in any transverse plane as two-dimensional and incompressible, now applying boundary conditions that are not only local in terms of x but also in terms of t. Thus, the calculation of the potential distribution $\phi(x, y, z, t)$ is the same as in steady flow, and only the formulas for the pressure, and therefore the forces, are different.

The approximation involved becomes clearer if the differential equation for ϕ is written down. Two new terms must be added to Eq. (1)—viz.,

$$[1 - (U^2/a^2)]\phi_{xx} + \phi_{yy} + \phi_{zz} = (1/a^2)(\varphi_{tt} + 2U\phi_{xt}) \quad (35)$$

where a denotes the speed of sound and U is the undisturbed stream speed, both constants. The present approximation is to discard all of the terms in Eq. (35) except the last two on the left-hand side, whence, using a notation analogous to that of Eq. (5),

$$\left. \begin{aligned} \phi_{yy} + \phi_{zz} &= 0 \\ \phi(x, y, z, t) &= \varphi(y, z; x, t) + g(x, t) \end{aligned} \right\} \quad (36)$$

To evaluate this approximation, consider, for example, a problem involving sinusoidal motion for which it may be assumed that $\phi(x, y, z, t)$ is proportional to e^{int}; Eq. (35) becomes

$$-\frac{n^2}{a^2}\phi + 2i\frac{n}{a}M\phi_x + (M^2 - 1)\phi_{xx} = \phi_{yy} + \phi_{zz} \quad (37)$$

where M is the stream Mach Number. In terms of the variables $\xi = x/l$, $\eta = y/s$, and $\zeta = z/s$ introduced above [Eq. (4)] and writing κ for the usual "reduced frequency" nl/U, this is

$$\frac{s^2}{l^2}[-\kappa^2 M^2 F + 2i\kappa M^2 F_\xi + (M^2 - 1)F_{\xi\xi}] = F_{\eta\eta} + F_{\zeta\zeta} \quad (38)$$

where

$$\phi(x, y, z, t) = UlF(\xi, \eta, \zeta)e^{int}$$

Now, assuming $s << l$ as in slender-wing theory, one can see that the approximation represented by Eq. (36) is correct, provided only that neither M nor κ is large compared to 1. This is the correct approximation for many practical cases, such as flutter of low aspect ratio wings in any speed range below the hypersonic. Miles[30] has extended Ward's slender-body theory on this basis.

Recently, however, Lomax, Heaslet, and Fuller[31] have presented a different sort of slender-wing theory for unsteady flow—viz., they approximate to Eq. (35) by neglecting only the term ϕ_{xx}, but not $(-U^2/a^2)\phi_{xx}$ or the right-hand terms—i.e., they write

$$\phi_{tt} + 2U\phi_x + U^2\phi_{xx} = a^2(\phi_{yy} + \phi_{zz}) \quad (39)$$

This theory was subsequently criticized by Miles[32] as being inconsistent. Miles stated that the approximation of Eq. (36) should have been used. While Lomax, et al., do not explain why they have retained the left-hand terms in Eq. (39), a plausible reason may be advanced: They are interested in "indicial" problems—i.e., transients—rather than oscillations; it is well known that these require, in effect, adequate treatment of all values of κ in Eq. (38), including $\kappa >> 1$. Consequently, the approximation of Eq. (36) is unsatisfactory, and the first two left-hand terms in Eq. (38) must be retained. To be sure, the term $(s^2/l^2)(M^2 - 1)F_{\xi\xi}$ might well be dropped for any moderate M. But no harm is done and the order of approximation is not changed if a part of this small term—namely, $(s^2/l^2)M^2F_{\xi\xi}$—is retained; a considerable mathematical simplification results, for then, upon transformation to a coordinate system fixed with the stream, the velocity potential is found to satisfy the wave equation for two-dimensional motion—i.e.,

$$\phi_{tt} = a^2(\phi_{yy} + \phi_{zz}) \quad (40)$$

The result is an approximation quite analogous to Munk's and Jones's but employing the acoustic equation, Eq. (40), in place of the Laplace equation in transverse planes in a coordinate system at rest in the fluid. It appears from the analysis above that this will be more accurate at high frequencies and in transient problems.

Thus, it may be concluded that Lomax, et al., are justified in carrying certain time derivatives of ϕ and that they carried another "inconsistent" term to achieve a mathematical simplification. This term is small and has no significance to the order of approximation involved so long as the wing is slender.* It is interesting to note that Eq. (40) is the same as for small-perturbation hypersonic flow[33] past bodies and wings, the latter not necessarily in the slender-wing category.

(In a private communication, Dr. Miles has also pointed out an error in the application of this new theory to the transient motion of a delta wing in reference 31—viz., the increase of span with time in the spaced-fixed coordinate system was neglected in setting up the boundary-value problem for Eq. (40). This error does not, of course, affect our conclusions regarding the validity of the theory itself.)

(VI) Extension to "Not-So-Slender" Wings

It has already been noted in Section (III) how the slender-wing theory may be obtained by expanding the velocity potential of linearized theory in powers of a slenderness parameter [such as βk in Eqs. (12)–(15)] and retaining only the largest terms. An essential extension of the power of the slender-body theory seems to result if additional terms of this expansion are retained. The methods of Ward and the analogous methods for subsonic flow, both presented in Section (III), are appropriate for this purpose.

One further generalization of these methods is required, however, in order to make this idea useful. This is to distribute line singularities at various spanwise distances rather than only at the axis.

Subsonic Flow

This extension, which might be called the theory of "not-so-slender" wings, will now be outlined briefly for subsonic flow. In what follows, only planar problems are considered—i.e., wings having small incidence, camber, and thickness and lying nearly in the plane $z = 0$.

Once again, for subsonic flow, Fourier transforms are used, and the Prandtl-Glauert Eq. (4) is reduced to Eq. (12). A solution analogous to the first term of Eq. (13) but permitting the placement of singularities at arbitrary spanwise locations $\eta = \eta'$, say, is

$$\bar{F}(\omega, \eta, \zeta) = \bar{f}(\omega, \eta')K_0(\beta k|\omega|r') \quad (41)$$

where again K_0 is the Bessel function and now r' denotes $[\zeta^2 + (\eta - \eta')^2]^{1/2}$. In the ξ,η,ζ-space this is a line source of variable strength lying along the line

* It would *not* be correct, for example, to make the same approximation for a nonslender wing near $M = 1$.

$\eta = \eta'$, $\zeta = 0$. The strength of the line source is proportional to the inverse Fourier transform of $\bar{f}(\omega, \eta')$, say $f(\xi, \eta')$, and a distribution of such line sources in the ξ, η plane can be used to satisfy the boundary conditions of a symmetrical wing of small thickness at zero incidence. The velocity potential $\phi(x, y, z)$ is obtained by inversion of the Fourier transforms. In fact, this inversion leads immediately to the familiar surface integral over a source distribution of linearized subsonic wing theory.

To obtain the desired expansion in the width parameter $\beta s/l$, one must restrict the solution to the neighborhood of the wing and expand K_0 in Eq. (41) for small values of its argument—viz.,

$$K_0(\epsilon) = -\left(1 + \frac{\epsilon^2}{4}\right) \ln \frac{\epsilon}{2} - \gamma + (1 - \gamma)\frac{\epsilon^2}{4} + O(\epsilon^4 \ln \epsilon) \quad (42)$$

The perturbation potential $\phi(x, y, z)$ is therefore obtained, to terms of the desired order in the width parameter, by substituting Eq. (42) into (41), integrating over η', and inverting the transforms term-by-term. The relation between the arbitrary distribution function $f(\xi, \eta)$ and the surface boundary value is determined by investigating the behavior of the elementary solution (41) at the plane $z = 0$; the result is

$$f(\xi, \eta) = \mp (1/\pi)\phi_\xi(\xi, \eta, \pm 0) \quad (43)$$

i.e., f is proportional to the vertical velocity component at the wing surface. Thus, an expression for $\phi(x, y, z)$, correct to the second order, appropriate for thin symmetrical wings without incidence, is obtained. The surface boundary condition for this case is

$$\phi_z(x, y, \pm 0) = \pm U\sigma(x, y)$$

or

$$\phi_\xi(\xi, \eta, \pm 0) = \pm sU\sigma(\xi, \eta)$$

where σ denotes the local inclination of the wing surface in the x direction. The desired result, evaluated at the plane $z = 0$ in particular, is

$$\phi(\xi, \eta, 0) = \frac{sU}{\pi}\int \sigma(\xi, \eta') \ln|\eta - \eta'|\, d\eta' + U\frac{S'(\xi)}{2\pi l}\ln\frac{\beta k}{2} - \frac{U}{4\pi l}\left[\int_0^\xi S''(\xi')\ln(\xi - \xi')d\xi' - \int_\xi^1 S''(\xi')\ln(\xi' - \xi)\,d\xi'\right] + \beta^2 k^2 \frac{sU}{4\pi}\left[\frac{\partial^2}{\partial\xi^2}\int \sigma(\xi, \eta')(\eta - \eta')^2\left(1 - \ln\frac{\beta k|\eta - \eta'|}{2}\right)d\eta' + \frac{1}{2}\frac{\partial^3}{\partial\xi^3}\int_0^\xi \ln(\xi - \xi')\,d\xi'\int(\eta - \eta')^2\sigma(\xi', \eta')\,d\eta' - \frac{1}{2}\frac{\partial^3}{\partial\xi^3}\int_\xi^1 \ln(\xi' - \xi)d\xi'\int(\eta - \eta')^2\sigma(\xi', \eta')d\eta\right] \quad (44)$$

where all integrals with respect to η' are carried across the plan form.

The first four terms in this formula constitute the slender-wing approximation for the case in question and have their counterparts in the results of Section (III). The first term is $\varphi(y, z; x)$; the next three constitute $g(x)$. It has been assumed in Eq. (44) that $S'(0) = 0 = S'(l)$, as is appropriate for most practical cases, and that $S'(x)$ is continuous. The new theory provides the additional terms in Eq. (44).

The analogous treatment of lifting wings without thickness is easily accomplished by using a distribution of doublets in place of sources. The doublet solution is found in the usual way by differentiating the source potential, Eq. (41), with respect to z—i.e.,

$$\bar{F}(\omega, \eta, \zeta) = -\beta k|\omega|\frac{\zeta}{r'}\bar{h}(\omega, \eta')K_1(\beta k|\omega|r') \quad (45)$$

$\bar{h}(\omega, \eta')$ being arbitrary.

The corresponding potential is found by expanding K_1 for small argument, integrating over η', and inverting the transforms. In this case, the doublet strength $h(\xi, \eta)$ is proportional to the surface potential—viz.,

$$h(\xi, \eta) = \mp (1/\pi)\phi(\xi, \eta, \pm 0) \quad (46)$$

The surface boundary condition, however, ordinarily involves ϕ_z rather than ϕ—i.e.,

$$\phi_z(x, y, 0) = -U\alpha(x, y)$$

consequently, the integral expression for $\phi(x, y, z)$ must be differentiated, and an integral equation for $h(\xi, \eta)$ results:

$$U\alpha(\xi, \eta) = \frac{1}{s}\int h_{\eta'}(\xi, \eta')\frac{d\eta'}{\eta' - \eta} - \frac{\beta^2 k^2}{2s}\left[\left(-\frac{1}{2} + \ln\frac{\beta k}{2}\right)\frac{d}{d\xi}\int h_\xi(\xi, \eta')d\eta' + \frac{\partial}{\partial\xi}\int h_\xi(\xi, \eta')\ln|\eta - \eta'|\,d\eta' - \frac{1}{2}\frac{d^2}{d\xi^2}\int_0^\xi \ln(\xi - \xi')\,d\xi'\int h_{\xi'}(\xi', \eta')d\eta' + \frac{1}{2}\frac{d^2}{d\xi^2}\int_\xi^1 \ln(\xi' - \xi)d\xi'\int h_{\xi'}(\xi', \eta')\,d\eta'\right] \quad (47)$$

Here, the integrals with respect to η' must be carried across the wing plan form and also across the trailing-vortex

wake at stations farther aft than the position of maximum span. In this case the Jones theory is represented by the first integral alone, all the subsequent terms being provided by the new technique.

The procedure for solution of this integral equation for $h(\xi, \eta)$, which may seem rather formidable at this point, will be discussed immediately below after stating the analogous formulas for supersonic flow.

Supersonic Flow

The "not-so-slender" wing theory for the supersonic case is carried out exactly as described above, except that Laplace, instead of Fourier, transforms are used. This treatment has been outlined in reference 34. The results are:

(a) For symmetrical wings without incidence,

$$\phi(\xi, \eta, 0) = \frac{sU}{\pi}\int \sigma(\xi, \eta')\ln|\eta - \eta'|\, d\eta' + U\frac{S'(\xi)}{2\pi l}\ln\frac{mk}{2} - \frac{U}{2\pi l}\int_0^\xi S''(\xi')\ln(\xi - \xi')\, d\xi' - m^2k^2 \times$$

$$\frac{sU}{4\pi}\left[\frac{\partial^2}{\partial\xi^2}\int \sigma(\xi, \eta')(\eta - \eta')^2\left((1 - \ln\frac{mk|\eta - \eta'|}{2}\right)d\eta' + \frac{\partial^3}{\partial\xi^3}\int_0^\xi \ln(\xi - \xi')d\xi' \int (\eta - \eta')^2\sigma(\xi', \eta')d\eta'\right] \quad (48)$$

where it has been assumed that $S'(0) = 0$ and that $S'(x)$ is continuous.

(b) For lifting wings without thickness,

$$U\alpha(\xi, \eta) = \frac{1}{s}\int h_{\eta'}(\xi, \eta')\frac{d\eta'}{\eta' - \eta} + \frac{m^2k^2}{2s}\left[\left(-\frac{1}{2} + \ln\frac{mk}{2}\right)\frac{d}{d\xi}\int h_\xi(\xi, \eta')d\eta' + \frac{\partial}{\partial\xi}\int h_\xi(\xi, \eta')\ln|\eta - \eta'|d\eta' - \right.$$

$$\left.\frac{d^2}{d\xi^2}\int^\xi \ln(\xi - \xi')d\xi' \int h_{\xi'}(\xi', \eta')\, d\eta'\right] \quad (49)$$

Solution of the Integral Equations

As has already been mentioned, the customary "direct" problems of wing theory require that Eqs. (47) and (49) be solved as integral equations for $h(\xi, \eta)$. The difficulty of this mathematical problem disappears immediately when it is remembered that solutions to order β^2k^2 (or m^2k^2), only, are being sought. To clarify this, imagine the doublet distribution h to be written explicitly as

$$h = h^{(1)} + h^{(2)} \quad (50)$$

where $h^{(1)}$ is the doublet strength in Jones's slender-wing approximation, which is independent of βk, and $h^{(2)}$ includes the higher order terms, presumably of order β^2k^2 but the exact order need not be assumed here. Upon substitution of Eq. (50) into (47) and recalling that

$$\frac{1}{s}\int h_{\eta'^{(1)}}(\xi, \eta')\frac{d\eta'}{\eta' - \eta} = U\alpha(\xi, \eta) \quad (51)$$

(by definition of $h^{(1)}$), one has, in place of Eq. (47),

$$\left.\begin{aligned}\int h_{\eta'^{(2)}}(\xi, \eta')\frac{d\eta'}{\eta' - \eta} &= \beta^2k^2 \times (\text{functions of } h)\\ &\approx \beta^2k^2 \times (\text{functions of } h^{(1)})\end{aligned}\right\} \quad (52)$$

where terms of order higher than β^2k^2 have been neglected, as originally proposed.

Thus, in place of the formidable integral equations, Eqs. (47) and (49) for h, one has to solve only equations of the form of Eq. (52) for $h^{(2)}$. Fortunately, this form is one for which explicit solutions can immediately be written down. It is, in fact the same equation as occurs in Jones's theory and elsewhere in thin-airfoil theory.[36]

To date, this second-order theory has been applied to only a few practical cases. The results of these applications will now be presented briefly, and some features of the method will be pointed out.

Example 1: Flat Delta Wing

The flat delta wing at incidence, in the supersonic régime, presents an ideal problem on which to test the new theory, since for it, by virtue of its conical symmetry, results of the complete Prandtl-Glauert theory are available for comparison.[35] The calculation proceeds without difficulty, treating Eq. (49) in the manner sketched above. The significant results are summarized in Fig. 7, where the lift-curve slope divided by k, $C_L/\alpha k$ is plotted against the breadth parameter $mk/2$. When $mk/2 = 1$, the leading edge of the delta coincides with the tip Mach cone, and the wing surely cannot be considered slender. Jones's theory gives the value π for $C_L/\alpha k$ for all k.

Also spotted in Fig. 7 are experimental values taken from reference 14 and (one point) from reference 2. It may be concluded, on the basis of this test that inclusion of second-order terms in the breadth parameter provides an important improvement of Jones's theory over a considerable range of this parameter.

The present example is not well suited for a test of the improvement of pressure distribution afforded by the second-order theory, since all three theories give the same spanwise and chordwise distribution functions. In other words, a comparison of pressure distributions

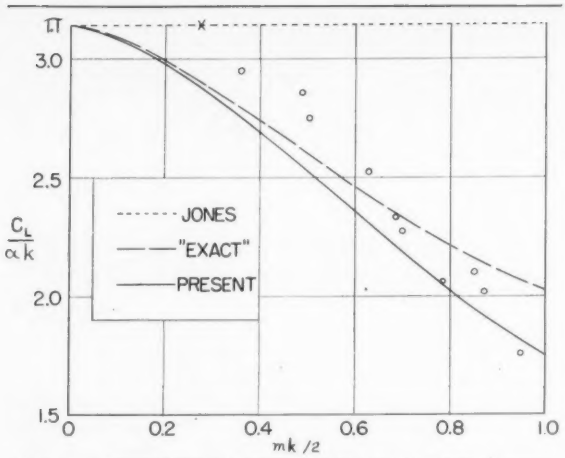

FIG. 7. Comparison of three theories for lift slope of supersonic delta wings. Experimental points (0) from reference 14 and (X) from reference 2.

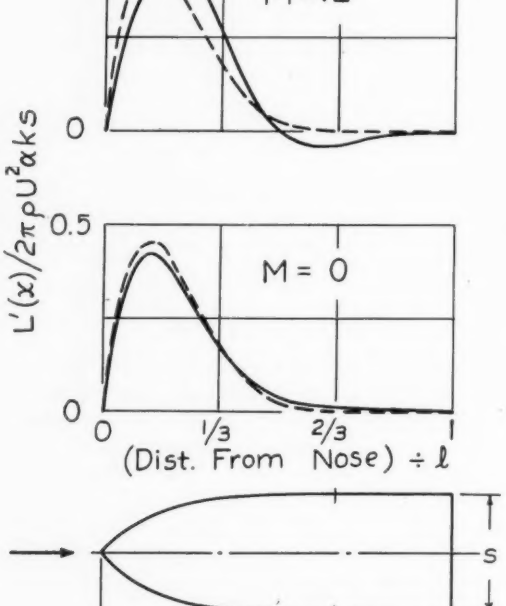

FIG. 8. Chordwise distribution of lift on the flat-plate wing sketched, at $M = \sqrt{2}$ (upper) and $M = 0$ (lower). $L'(x)$ denotes the lift loading. Solid line: present theory. Dash line: Jones's approximation.

at any point of the plan form leads only to the results plotted in Fig. 7; the pressures bear the same ratios to one another as $C_L/\alpha k$ for any given $mk/2$.

***Example 2* (*Fig. 8*)**

It is interesting to apply the new method to the case of a wing such as the flat-plate wing shown in Fig. 8, for which Jones's theory predicts no lift loading at stations aft of the maximum span for either subsonic or supersonic speed. For reasons to be explained later, the plan form of the wing selected for this example has continuous slope, curvature, and third derivative at the station of maximum width. The calculated chordwise lift loading is plotted in Fig. 8 for both subsonic and supersonic speeds.

***Example 3* (*Fig. 9*)**

A certain difficulty, apparently an essential one in some cases, arises in the application of the not-so-slender wing theory to wings whose chordwise lift loading according to Jones's theory is discontinuous or has discontinuous slope or curvature. This trouble arises in the last integrals in Eq. (47) or (49). The results in such cases exhibit infinite values of $h^{(2)}$ near such stations of discontinuity.* Naturally, for supersonic wings such discontinuities do not affect any parts of the plan form further forward, so that there is no difficulty in treating a wing (e.g., Example 1, above) whose Jones loading is discontinuous at the trailing edge.

To handle the after portions of the flat-plate wing of Fig. 9, however, requires a special technique, even in supersonic flow. One considers first a fictitious wing having the same plan form and the same incidence forward of maximum span but having its incidence $\alpha_f(x)$ adjusted along the x direction aft of station AB so as to render the Jones loading suitably continuous. For the flat wing of Fig. 9, for example, a suitable $\alpha_f(x)$ is quadratic in x aft of AB. Having solved this problem by the present second-order methods, one must proceed to correct the loading aft of AB for the presence of the fictitious incidence.

* Actually, this difficulty was introduced in the term-by-term inversion of the Fourier (or Laplace) transforms, above. In this step, smooth behavior of the functions was implied.

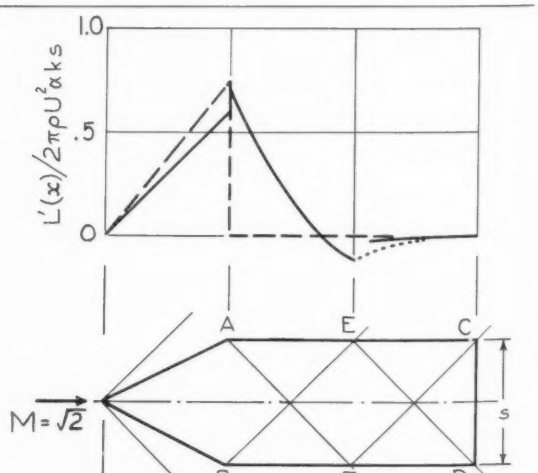

FIG. 9. Chordwise distribution of lift on the flat-plate wing sketched, at $M = \sqrt{2}$. (Designations of curves same as in Fig. 8). Dotted line: estimated fairing to asymptotic curve.

Let α, a constant, be the true incidence, and let $\alpha^{(1)}(x)$ denote $\alpha - \alpha_f(x)$. If $\phi^{(f)}$ is the potential calculated by the second-order theory for the fictitious wing, the correct potential for the original wing is

$$\phi(x, y, z) = \phi^{(f)} + \phi^{(1)} \tag{53}$$

where $\phi^{(1)}$ is the potential for the flow past the rectangular wing $ABCD$ with incidence $\alpha^{(1)}(x)$.

Now the calculation of $\phi^{(1)}$ is outside the scope of the second-order theory, but it lies within the category of cases treated easily by the complete Prandtl-Glauert theory. In fact, the incidence $\alpha^{(1)}(x)$ being a function of x only, a technique due to Rott[37] is especially suited for this calculation in the region ABEF, and the chordwise lift loading is obtained very simply. Fig. 9 shows the result of applying this method to a specific problem.

It may be remarked that the second-order results obtained for such "discontinuous" wings by direct use of Eq. (47) or (49), without benefit of the correction technique just outlined, are not without some significance in spite of their infinite behaviors at the discontinuities. Namely, they are asymptotically correct far downstream of the discontinuity (and upstream as well, for subsonic cases). In this statement, moreover, the word "far" must be interpreted with relation to the width, and for supersonic flow, as Stewartson has shown,[38] "far downstream" probably means the distance of only three or four Mach-wave reflections (Fig. 9). Thus the technique used here is analogous to Lighthill's technique[39] for slender bodies of revolution which are not smooth—i.e., whose meridian profiles exhibit discontinuous curvatures. In this spirit the corrected second-order curve in Fig. 9 has not been calculated aft of EF but has been faired roughly (dotted curve) toward the asymptotic second-order curve.

It is important to recognize that, although the second-order wing theory could not be used directly for the "discontinuous" wing, it nevertheless plays an essential part in reducing the problem from one that was intractable in Prandtl-Glauert theory to one that could be handled easily. Unfortunately, a comparable technique has not yet been worked out for subsonic cases, so that to date the theory of not-so-slender wings in subsonic flow is severely restricted in application.

Supersonic Wings of Minimum Drag

The present extended slender-wing theory permits the determination of wing configurations for minimum drag. In subsonic flow, as is well known, all wings with elliptic spanwise lift loading are minimum-drag wings for given lift and span. In supersonic flow, on the other hand, the phenomenon of wave drag appears, and the minimum-drag problem is more complex.

For the classical problem of the distribution of lift of a wing without thickness, to produce minimum drag, slender-wing theory gives the same result for supersonic as for subsonic flow, because wave drag is absent in the approximation. The second-order approximation introduced here brings in wave-drag terms, so that the minimum-drag problem yields information about the chordwise, as well as spanwise, loadings.

The drag for a supersonic wing without thickness can be obtained to second order by use of Eq. (49), taking account of the leading-edge suction. The result is

$$D = \pi\rho \int\int h_\eta(1, \eta) h(1, \eta') \frac{d\eta\, d\eta'}{\eta' - \eta} - \pi\rho m^2 k^2 \left\{ \frac{1}{2} \int\int h_\xi(1, \eta') h_\xi(1, \eta) \ln |\eta - \eta'| d\eta\, d\eta' + \right.$$
$$\left. \frac{1}{2} \int_0^1 \int_0^1 l'(\xi') l'(\xi) \ln |\xi - \xi'|\, d\xi\, d\xi' - l(1) \int_0^1 l'(\xi) \ln (1 - \xi) d\xi + \frac{1}{2} [l(1)]^2 \left(-\frac{1}{2} + \ln \frac{mk}{2} \right) \right\} \tag{54}$$

where $l(\xi)$ denotes $\int h_\xi(\xi, \eta) d\eta$, so that the chordwise lift loading is $-2\pi\rho U k l(\xi)$. Here again, the integrations with respect to η are carried across the wing and wake.

It is observed that there is an almost exact resemblance between the last three terms of this equation and Eq. (30) for the drag D_1 of slender bodies or slender wings with thickness. In this comparison the chordwise loading in one case and the slope of the cross-section area in the other case play the same role.

A few results that arise from a study of Eq. (54) can be mentioned briefly:

(a) For the case of a wing with the parameter $mk < 0.44$, Eq. (54) indicates that minimum drag is achieved for given lift, span, and chord when the spanwise loading is elliptic and the first-order (Jones) chordwise loading is also elliptic. This makes both induced and wave-drag minima, to second order. The drag in this case is given by

$$C_D = (C_L^2/\pi A) + (m^2 k^2/2)(C_L^2/\pi A) \tag{55}$$

where A denotes the aspect ratio, $s^2/(\text{area})$. Jones[40] seems to have arrived at this same result, although his methods were not disclosed.

For wings of higher aspect ratio, or $mk > 0.44$, the theory indicates that the chordwise loading should not be elliptic and that the wave drag can be reduced by maintaining a finite loading at the trailing edge. For example, a flat delta wing produces less drag than a wing with elliptic chordwise loading for $mk > 1.1$.

(b) For the special case of conical wings the minimum-drag wing is a flat plate. This is the same result as is well-known in slender-wing theory; the inclusion of second-order terms does not alter it.

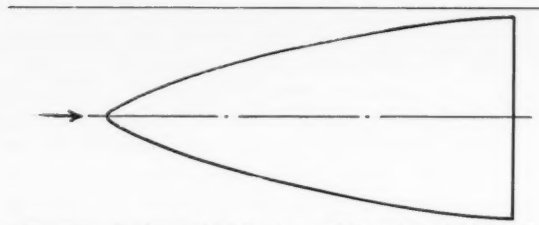

FIG. 10. A wing satisfying the conditions for minimum drag for given lift, span, and chord when $mk < 0.44$; viz., a flat plate having the plan form show.

(c) A simple example of a wing with elliptical distributions as discussed in (a) is a flat-plate wing having the same plan form as the meridian contour of von Kármán's famous ogive,[17] as sketched in Fig. 10.

REFERENCES

[1] Munk, Max M., *The Aerodynamic Forces on Airship Hulls* N.A.C.A. Report No. 184, 1924.

[2] Jones, Robert T., *Properties of Low-Aspect-Ratio Pointed Wings at Speeds Below and Above the Speed of Sound*, N.A.C.A. Report No. 835, 1946; also N.A.C.A. T.N. No. 1032, 1946.

[3] Tsien, Hsue-Shen, *Supersonic Flow over an Inclined Body of Revolution*, Journal of the Aeronautical Sciences, Vol. 5, pp. 480–483, 1938.

[4] Heaslet, Max. A., Lomax, Harvard, and Spreiter, John R., *Linearized Compressible-Flow Theory for Sonic Flight Speeds*, N.A.C.A. Report No. 956, 1950; also N.A.C.A. T.N. No. 1824, 1949.

[5] von Kármán, Theodore, *The Similarity Law of Transonic Flow*, Jour. Math. & Phys., Vol. 26, pp. 182–190, 1947.

[6] Spreiter, John R., *Aerodynamic Properties of Slender Wing-Body Combinations at Subsonic, Transonic, and Supersonic Speeds*, N.A.C.A. T.N. No. 1662, 1948.

[7] Lomax, Harvard, and Heaslet, Max. A., *Linearized Lifting-Surface Theory for Swept-Back Wings with Slender Plan Forms*, N.A.C.A. T.N. No. 1992, 1949.

[8] Ribner, Herbert S., *The Stability Derivatives of Low-Aspect-Ratio Wings at Subsonic and Supersonic Speeds*, N.A.C.A. T.N. No. 1423, 1947.

[9] Lomax, Harvard, and Heaslet, Max. A., *Damping-in-Roll Calculations for Slender Swept-Back Wings and Slender Wing-Body Combinations*, N.A.C.A. T.N. No. 1950, 1949.

[10] Spreiter, John R., *Aerodynamic Properties of Cruciform-Wing and Body Combinations at Subsonic, Transonic, and Supersonic Speeds*, N.A.C.A. T.N. No. 1897, 1949.

[11] Lomax, Harvard, and Byrd, Paul F., *Theoretical Aerodynamic Characteristics of a Family of Slender Wing-Tail Body Configurations*, N.A.C.A. T.N. No. 2554, 1951.

[12] Allen, H. Julian, *Pressure Distribution and Some Effects of Viscosity on Slender Inclined Bodies of Revolution*, N.A.C.A. T.N. No. 2044, 1950.

[13] Flax, A. H., and Lawrence, H. R., *The Aerodynamics of Low-Aspect-Ratio Wings and Wing-Body Combinations*, Proceedings, Third Anglo-American Aeronautical Conference, pp. 363–398, 1951.

[14] Ellis, Macon C., Jr., and Hasel, Lowell E., *Preliminary Investigation at Supersonic Speeds of Triangular and Sweptback Wings*, N.A.C.A. T.N. No. 1955, 1949.

[15] Vincenti, Walter G., *Comparison Between Theory and Experiment for Wings at Supersonic Speeds*, N.A.C.A. Report No. 1033, 1951; also N.A.C.A. T.N. No. 2100, 1950.

[16] Ward, G. N., *Supersonic Flow Past Slender Pointed Bodies*, Quart. Jour. Mech. & Appl. Math., Vol. 2, pp. 75–97, 1949.

[17] von Kármán, Th., *The Problem of Resistance in Compressible Fluids*, Atti del V Convegno della Fondazione Alessandro Volta, Rome, pp. 222–276, 1935.

[18] Lighthill, M. J., *Supersonic Flow Past Slender Bodies*, A.R.C. R. & M. No. 2003, 1945.

[19] Dwight, Herbert Bristol, *Tables of Integrals and Other Mathematical Data;* The Macmillan Company, New York, 1934.

[20] Heaslet, Max. A., and Lomax, Harvard, *Supersonic and Transonic Small-Perturbation Theory. Section D of Volume V of High-Speed Aerodynamics and Jet Propulsion*, to be published 1953 by Princeton University Press.

[21] Sauer, Robert, *Theoretische Einführung in die Gasdynamik*; Springer, Berlin, 1943; also Edwards, Ann Arbor, 1945, and (in English) 1947.

[22] Laitone, E. V., *The Subsonic Flow About a Body of Revolution*, Quart. Appl. Math., Vol. 5, pp. 227–231, pp. 1947.

[23] Rott, N., *Zür linearisierten Theorie von Rotationskörpern in kompressibler Strömung*, Habilitationschrift (unpub.), Eidg. Technische Hochschule, Zürich, 1947.

[24] Broderick, J. B., *Supersonic Flow Round Pointed Bodies of Revolution*, Quart. Jour. Mech. & App. Math., Vol. 2, pp. 98–120, 1949.

[25] Lighthill, M. J., *Methods for Predicting Phenomena in the High-Speed Flow of Gases*, Journal of the Aeronautical Science, Vol. 16, pp. 69–83, 1949.

[26] Matthews, C. W., *A Comparison of the Experimental Subsonic Pressure Distributions About Several Bodies of Revolution With Pressure Distributions Computed by Means of the Linearized Theory.* N.A.C.A. T.N. No. 2519, 1952.

[27] Miles, John W., *On Slender Wing-Body Theory*, Journal of the Aeronautical Sciences, Vol. 19, p. 140, 1952.

[28] Lagerstrom, P. A., and Graham, M. E., *Aerodynamic Interference in Supersonic Missiles*, Douglas Aircraft Company Rep. No. SM-13743, Santa Monica, 1950.

[29] Jones, Robert T., *Leading-Edge Singularities in Thin-Airfoil Theory*, Journal of the Aeronautical Sciences, Vol. 17, pp. 307–310, 1950.

[30] Miles, John W., *Slender Body Theory for Supersonic Unsteady, Flow*, Journal of the Aeronautical Sciences, Vol. 19, pp. 280–281 1952.

[31] Lomax, Harvard Heaslet, Max. A., and Fuller, Franklyn B., *Three-Dimensional Unsteady Lift Problems in High-Speed Flight—The Triangular Wing*, N.A.C.A. T.N. No. 2387, 1951.

[32] Miles, John W., Math. Reviews, Vol. 13, p. 181, 1952.

[33] Hayes, Wallace D., *On Hypersonic Similitude*, Quart. Appl. Math., Vol. 5, pp. 105–106, 1947.

[34] Adams, Mac C., and Sears, W. R., *On an Extension of Slender-Wing Theory*, Journal of the Aeronautical Sciences, Vol. 19, pp. 424–425, 1952.

[35] Stewart, H. J., *The Lift of a Delta Wing at Supersonic Speeds*, Quart. Appl. Math., Vol. 4, pp. 246–254, 1946.

[36] von Kármán, Th., and Burgers, J., *Aerodynamic Theory*, Vol. II (W. F. Durand, Ed.) Div. E, II, Sec. 9; Springer, Berlin, 1935.

[37] Rott, N., *On the Unsteady Motion of a Thin Rectangular Wing in Supersonic Flow*, Journal of the Aeronautical Sciences, Vol. 18, pp. 775–776, 1951.

[38] Stewartson, K., *Supersonic Flow over an Inclined Wing of Zero Aspect Ratio*, Proc. Cambridge Phil. Soc., Vol. 46, pp. 307–315, 1950.

[39] Lighthill, M. J., *Supersonic Flow Past Slender Bodies of Revolution the Slope of Whose Meridian Section is Discontinuous*, Quart. Jour. Mech. & Appl. Math., Vol. 1, pp. 90–102, 1948

[40] Jones, Robert T., *The Minimum Drag of Thin Wings in Frictionless Flow*, Journal of the Aeronautical Sciences, Vol. 18, pp. 75–81, 1951.

[41] Graham, Ernest W., *Pressure and Drag on Smooth Slender Bodies in Linearized Flow*, Douglas Aircraft Company Rep. No. SM-13417, Santa Monica, April 20, 1949.

[42] Robinson, A., and Young, A. D., *Note on the Application of the Linearized Theory for Compressible Flow to Transonic Speeds*, College of Aero., Cranfield, Rep. No. 2, January, 1947.

Penetration and Deflection of Jets Oblique to a General Stream

FREDRIC F. EHRICH*

Westinghouse Electric Corporation

SUMMARY

The dynamics of the entry of jets of fluid into a general stream at an oblique angle from slots and orifices is studied by means of a simplified two-dimensional potential flow analysis. The wake is approximated by an extensive area of dead fluid separated from the jet by a vortex sheet at uniform pressure. The jet is separated from the main stream by a stream line, and the jet velocity is restricted to one particular value so that there is no discontinuity across this stream line. Analysis using the conventional Helmholtz-Kirchhoff method leads to computations of the various relationships between the geometrical and velocity parameters. Calculations are also made of the shapes of jets in some common geometries.

An equivalent analysis is made of the situation in which the trailing edge of the jet does not separate from the downstream wall, and the results are compared to the analysis with separation.

The solution for the flow from a two-dimensional orifice is compared to experimental data for the roughly comparable case of flow from a circular orifice, and a qualitative agreement is shown.

The results have a possible utility in serving as a skeletal structure of a more complete analysis of the mixing process in combustion chambers and cooling films.

NOMENCLATURE

A', B', C', D', E', F'	= points in the jet
A, B, C	= points in the main stream
a	= width of the jet source
b	= offset of the jet source
c	= asymptotic width of the jet in the stream
F	= a function of ζ
h	= a distance in the ζ plane
q	= absolute value of the velocity at a point
$Q = \ln U/q + i\theta$	= logarithm of the conjugate hodograph plane
s	= distance along the vortex sheet
U	= velocity of the main stream
U_1	= velocity of the jet in the slot
x	= coordinate in the direction of the main stream
y	= coordinate in the direction perpendicular to the main stream
$z = x + iy$	= the physical plane
α	= angular direction of the forward side of the jet source
β	= angular direction of the rear side of the jet source
ϵ	= a small distance in the ζ plane
ζ	= the mapping half plane
θ	= angular direction of the velocity at a point
ϕ	= potential function
ψ	= stream function
$\omega = \phi + i\psi$	= complex potential plane

Received June 13, 1952.

* Mechanical Engineer, Development Section, Aviation Gas Turbine Division.

INTRODUCTION

OF SOME BASIC AND GENERAL INTEREST is an analytic description of the penetration and deflection of a jet of fluid entering a large body of fluid from an orifice set oblique to the direction of the main stream.

The complete problem is one in compressible, viscous, unsteady fluid flow in a complicated three-dimensional geometry. In order to make the problem amenable to analysis, it is necessary to restrict attention to some fluid dynamic aspects in a simplified geometry.

ANALYSIS

Making the usual assumptions of steady, incompressible two-dimensional potential flow reduces the problem to the schematic flow picture shown in Fig. 1a. It is assumed that the *densities and total pressures* of the jet stream and the main stream are *equal*. This last stipulation restricts our attention to the peculiar case where the boundary between the leading edge of the jet and the main stream is not a line of discontinuity but a stream line common to both flows with a continuous variation of velocity existing across that boundary.

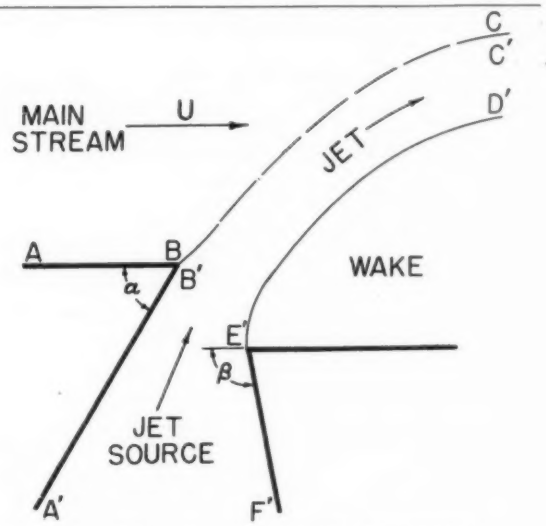

FIG. 1a. Schematic configuration (with separation).

A stream of fluid from an orifice formed by two oblique walls meets the main stream at a stagnation point BB' and forms a common stream line BC. The jet separates from the wall at point E', and a vortex sheet or free stream line $E'D'$ marks the boundary between the jet and an extensive wake assumed to be composed of still fluid. Since it is assumed that there is no motion in the wake, the pressure along the vortex sheet must be a constant, and, hence, the velocity must also be constant. A second possibility is the situation in which the downstream boundary of the jet does not separate from the wall as depicted in Fig. 1b. This, of course, involves an infinite velocity of the fluid in turning the sharp corner at E' but is probably approximately realizable in certain real flows.

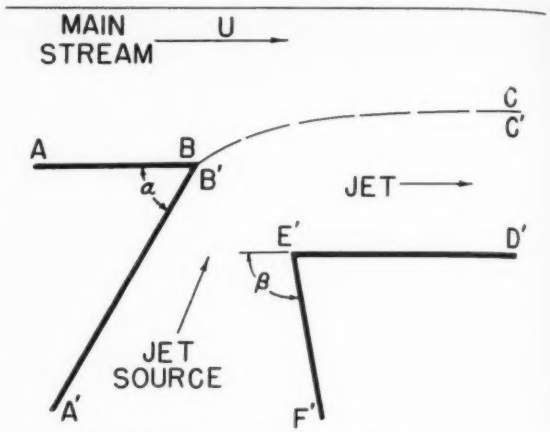

FIG. 1b. Schematic configuration (without separation).

The flows under consideration are bounded only by straight walls and constant-pressure vortex sheets and, hence, fit into the class of problems which can be treated by the Helmholtz-Kirchhoff method.[1] The analytic procedure consists of a series of conformal transformations which links the complex physical plane z to the complex potential plane ω. The degree of difficulty of the various transformations depends in general on the number of discontinuities in the flow—sources, sinks, doublets, stagnation points, points of infinite velocity, and points of separation. In order to reduce the number of points of discontinuity under consideration, two specializations of the generalized geometry will be considered. Firstly, a slot-type jet source with α equal to β will be studied to eliminate the zero velocity at the source of the jet $A'F'$. Also, an orifice-type jet source with α equal to zero can be considered, since the zero velocity at the joining point BB' is thus eliminated. These geometries are shown in the summary of transformation planes in Fig. 2.

Although the shape of the vortex-sheet boundary is not known in the physical plane, it can be drawn in the hodograph plane by virtue of the stipulation of constant velocity along it. With all the vortex sheets becoming arcs of circles and all straight boundaries transforming

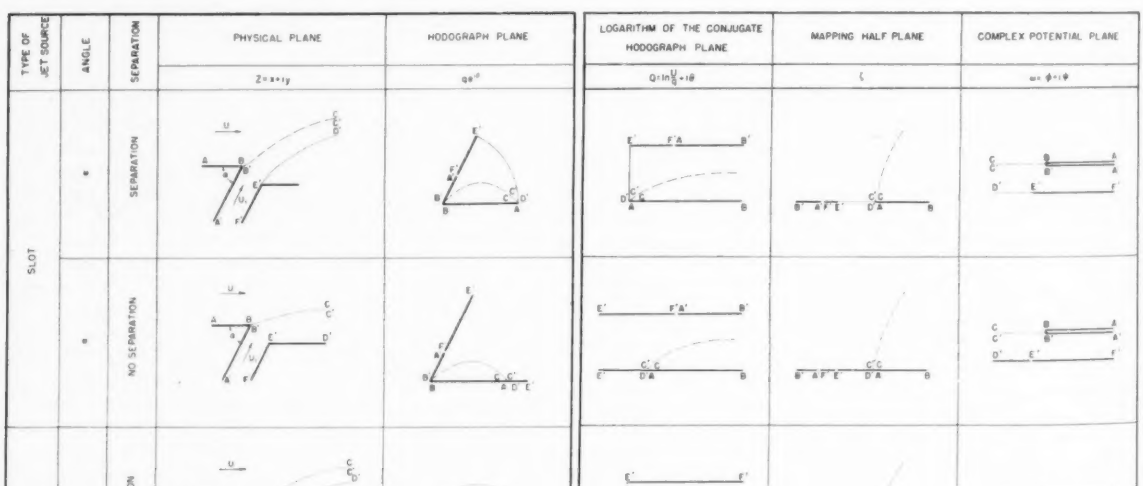

FIG. 2. The transformation planes.

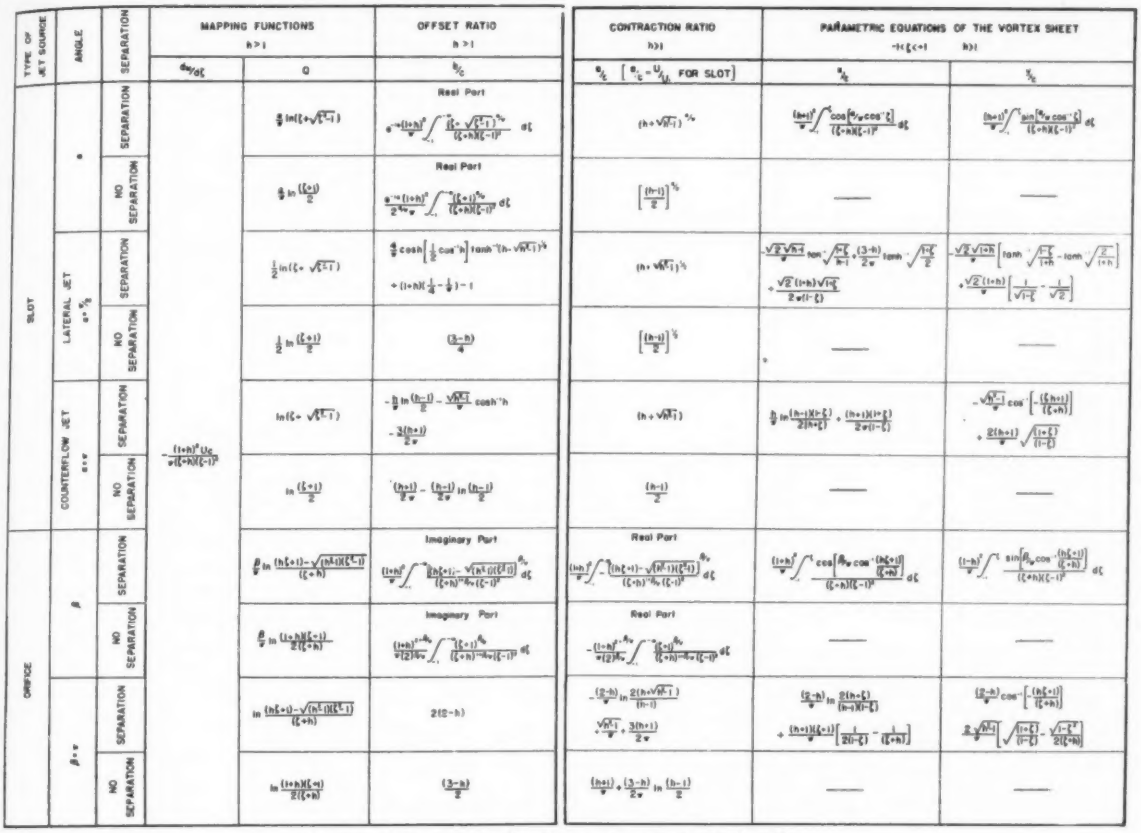

FIG. 3. The mapping functions and analytic relationships.

into radial lines, the boundaries of the flow are readily drawn in the hodograph plane as in Fig. 2. The conjugate of this plane is functionally related to the physical and potential planes, since

$$-d\omega/dz = qe^{-i\theta} \tag{1}$$

Taking the logarithm of the circle sector transforms the bounded area to a degenerate rectilinear polygon, since

$$Q = -\ln\left[(q/U)e^{-i\theta}\right] = \ln U/q + i\theta \tag{2}$$

The boundaries of constant velocity become vertical lines, and boundaries of constant inclination become horizontal lines as in Fig. 2.

The Schwarz-Christoffel transformation[2] permits this polygon to be transformed into the upper half of some new plane, ζ, giving the functional relationship

$$Q = Q(\zeta) \tag{3}$$

which is tabulated in Fig. 3. This function must be left in terms of a parameter h that indicates the relative location of the vertices of the polygon in the ζ plane and is a function of the relative orientation of the edges of the jet source in the physical plane.

The boundaries of the flow system may be drawn in the complex potential plane ω immediately, since all stream lines are horizontal lines by virtue of their constant stream function (as in Fig. 2). This plane may also be transformed directly into the ζ upper-half plane utilizing the Schwarz-Christoffel transformation. Because of the basic similarity of the configurations under consideration, they all give the same transforming function:

$$d\omega/d\zeta = -(1+h)^2 Uc/\pi(\zeta+h)(\zeta-1)^2 \tag{4}$$

The set of transformations given by Eqs. (1), (2), (3), and (4) completely determines the problem functionally and permits the calculation of various parameters.

CALCULATIONS

The shape of the vortex sheet may be found by virtue of the fact that the velocity is constant so that

$$ds = |dz| = |dz/d\omega||d\omega/d\zeta||d\zeta| = (1/U)|d\omega/d\zeta|d\zeta \tag{5}$$

and

$$dx = ds\cos\theta = [\text{real part } (e^Q)]ds \tag{6a}$$

$$dy = ds\sin\theta = [\text{imaginary part}(e^Q)]ds \tag{6b}$$

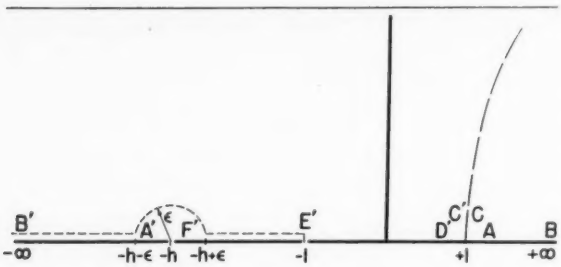

FIG. 4. Path of integration in the ζ plane.

Hence

$$x/c = -\int_{-1}^{\zeta} \frac{[\text{real part } (e^{Q})](1+h)^2 d\zeta}{\pi(\zeta+h)(\zeta-1)^2} \tag{7a}$$

$$y/c = -\int_{-1}^{\zeta} \frac{[\text{imaginary part } (e^{Q})](1+h)^2 d\zeta}{\pi(\zeta+h)(\zeta-1)^2} \tag{7b}$$

Eqs. (7a) and (7b) give a pair of parametric equations in ζ which determines the shape of the vortex sheet in terms of the constant h and are presented in Fig. 3 for the geometries in question.

A similar procedure, with some modification, is effective in evaluating the relative orientation of the edges of the orifice in terms of the parameter h. An integration in the physical plane from edge B' to E' is equivalent to an integration from B' to E' in the ζ plane. But an integration in the ζ plane along the real axis must avoid the pole at the point $A'F'$. This is most readily accomplished by the path shown in Fig. 4 where the integration is carried out along the real axis to a distance $(-h-\epsilon)$. Then the integration is calculated along a semicircle of radius ϵ from $(-h-\epsilon)$ to $(-h+\epsilon)$, from which point the integration can be carried out along the real axis. Thus,

$$\int_{B'}^{E'} dz/c = \int_{-\infty}^{-1} (dz/d\omega)(d\omega/d\zeta)d\zeta = \int_{-\infty}^{-1} \frac{e^{Q}(1+h)^2 d\zeta}{\pi(\zeta+h)(\zeta-1)^2} \tag{8a}$$

$$\int_{B'}^{E'} dz/c = \lim_{\epsilon \to 0}\left[\int_{-\infty}^{-h-\epsilon} F(\zeta)d\zeta + \int_{\pi}^{0} F(\epsilon e^{i\theta} - h)d(\epsilon e^{i\theta}) + \int_{-h+\epsilon}^{-1} F(\zeta)d\zeta\right] \tag{8b}$$

The complex quantity given by this equation may be split into two geometry ratios, a/c and b/c, which indicate the width of the orifice and the offset of the rear edge from the horizontal plane of the forward edge of the orifice. For the case of the slot-type jet source, part of this calculation is unnecessary since continuity requires that

$$Uc = U_1 a \tag{9}$$

so that a/c is more easily calculated from Eqs. (2) and (3) such that

$$\ln U/U_1 + i\alpha = Q(-h) \tag{10}$$

Although the problems have been set up for generalized values of α and β, the pertinent integrals cannot be integrated for the general case. They can be solved only if α and β are rational fractions of π. But for practical purposes, the integrations can be carried out only for $\alpha = \pi$, $\alpha = \pi/2$, and $\beta = \pi$, utilizing partial fraction reductions. (The cases $\alpha = 0$ and $\beta = 0$ are trivial.) Fig. 3 summarizes the pertinent analytic relationships, and Figs. 5, 6, 7, and 8 show plots of the geometry and velocity parameters for the various configurations under consideration. It must be realized that only *one particular* velocity ratio corresponds to any set of specific values of the geometry ratios, and this velocity ratio is governed by the criterion of smooth entry—i.e., it is the only velocity such that the total pressure of the jet is equal to the total pressure of the main stream.

Figs. 9, 10, and 11 show typical plots of the shape of the jet from various types of orifices. The leading edge of the jet or the stream line common to both the jet flow and the main flow is not readily calculable, but its shape is easily and accurately sketched from the knowledge of its asymptotic behavior. The stream line must bisect the corner at BB' because of the symmetric nature of a stagnation point. Also, the jet quickly reaches an asymptotic width of value c, which quantity has entered the calculations of the other geometric parameters.

CONCLUSIONS

Although the analysis is severely limited in its applicability because of the extreme nature of the simplifying assumptions, certain general conclusions may be ascertained.

The concept of smooth entry of a jet with no discontinuity in velocity across the stream line common to the jet and the main stream is of extreme significance in certain applications. A film introduced at such a velocity would have little tendency to mix with the main stream and, hence, would be extremely effective as an insulating layer. Similarly, if mixing is desired, as in the case of the introduction of secondary air into a combustor, such velocities must be avoided.

Fig. 11 includes a curve from an empirical formula deduced by Callaghan and Ruggeri[3] from extensive measurements on heated air jets from circular orifices perpendicular to the main stream. Their formula, reduced to the nomenclature of this paper and specialized for the assumptions under consideration, gives

$$y/a = 1.91[(x + a/2)/a]^{0.303} \tag{11}$$

Of course, this is only a qualitative comparison, since the circular jet is by no means directly equivalent to the two-dimensional jet under consideration, especially since it in no way approximates the extensive wake that has been assumed.

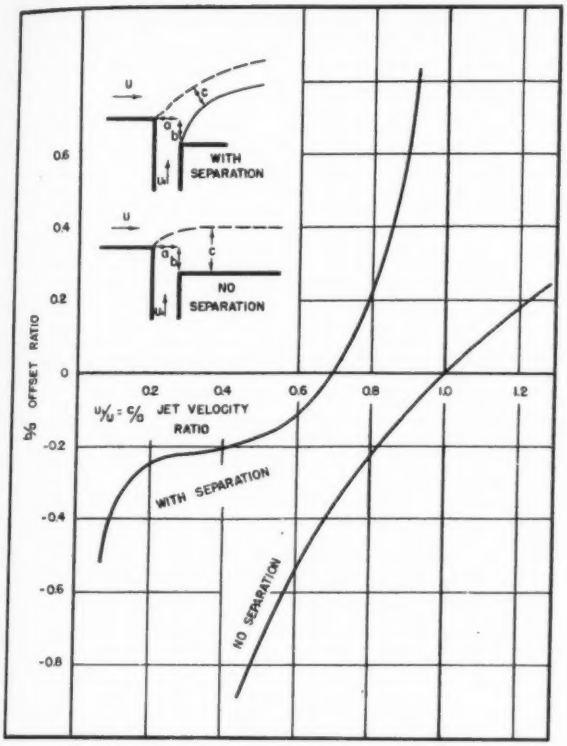

FIG. 5. Smooth entry velocity for a lateral jet.

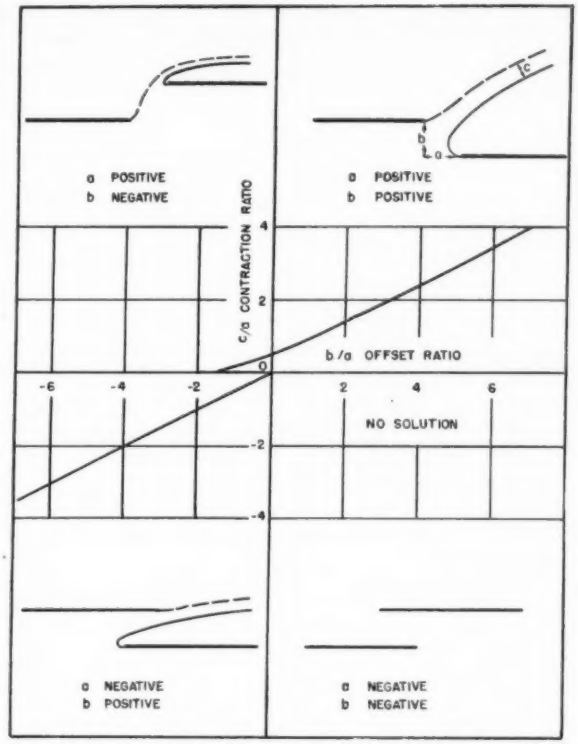

FIG. 7. Contraction ratio from an orifice (with separation).

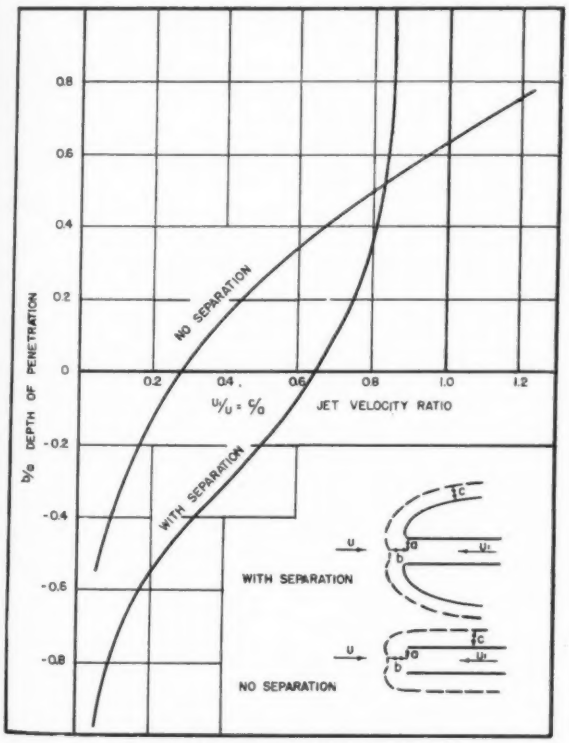

FIG. 6. Depth of penetration for a counterflow jet.

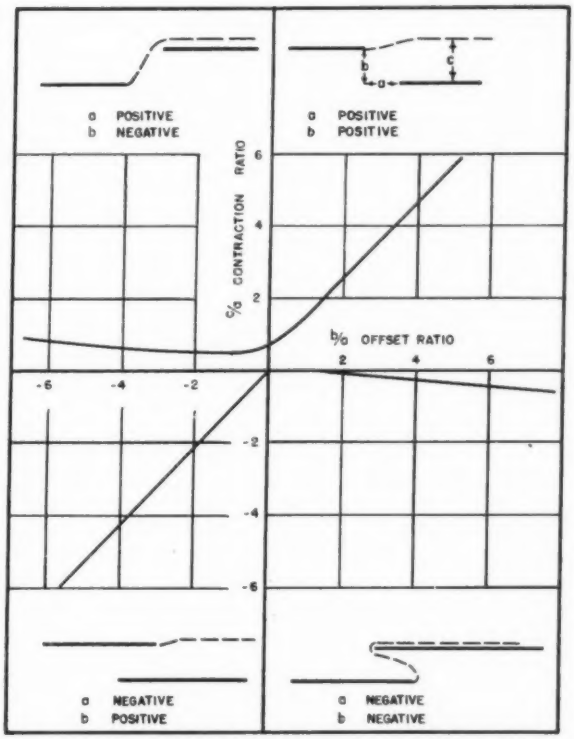

FIG. 8. Contraction ratio from an orifice (without separation).

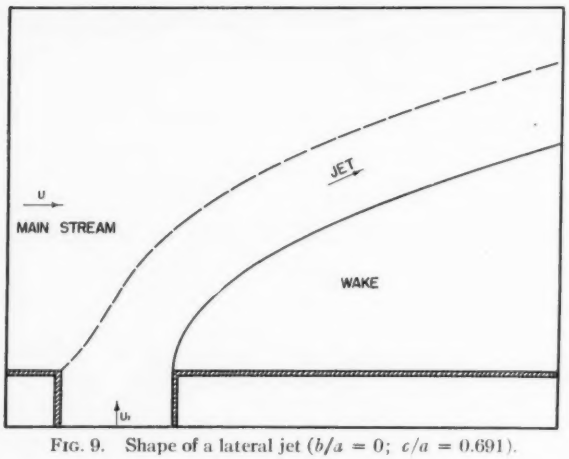

FIG. 9. Shape of a lateral jet ($b/a = 0$; $c/a = 0.691$).

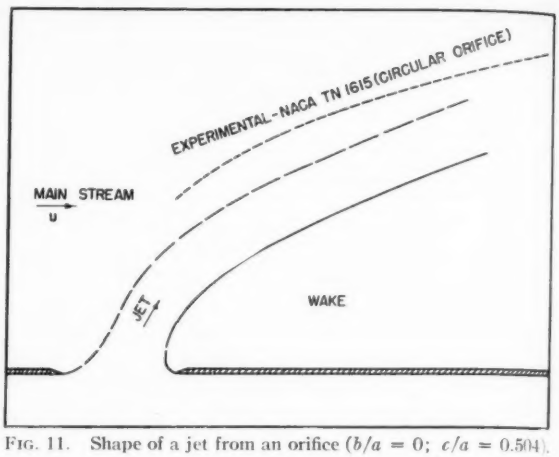

FIG. 11. Shape of a jet from an orifice ($b/a = 0$; $c/a = 0.504$).

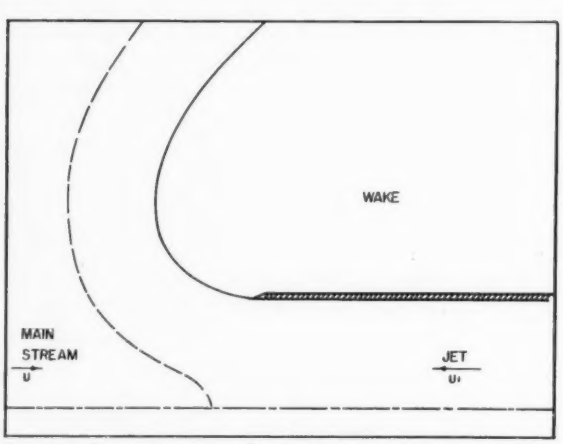

FIG. 10. Shape of a counterflow jet ($b/a = 0.358$; $c/a = 0.800$).

Probably no other solutions of the type discussed in this paper are obtainable in terms of elementary functions. Solutions for general values of α and β are probably available by numerical integrations but are of a difficult nature because of the presence of the undetermined constant h. As yet, the author is unaware of an effective procedure for the inclusion of the parameters of variable viscosity, unequal densities, and jet velocities other than the particular values studied here.

REFERENCES

[1] Milne-Thomson, L. M., *Theoretical Hydrodynamics*, 2nd Ed., pp. 269 ff.; The Macmillan Company, London, 1934.

[2] Churchill, R. V., *Complex Variables and Applications*, 1st Ed., pp. 171 ff.; McGraw-Hill Book Company, Inc., New York, 1948.

[3] Callaghan, E. E., and Ruggeri, R. S., *Investigation of the Penetration of an Air Jet Directed Perpendicularly to an Air Stream*, N.A.C.A. T.N. No. 1615, p. 6, June, 1948.

An Experimental Study of a Hypersonic Wind-Tunnel Diffuser*

PETER P. WEGENER† AND R. KENNETH LOBB‡

U.S. Naval Ordnance Laboratory, White Oak

ABSTRACT

Results of a variable-area diffuser investigation in the continuous 12- by 12-cm. Naval Ordnance Laboratory Hypersonic Tunnel No. 4 are presented. A brief introduction discusses previous supersonic diffuser work. The diffuser investigated and the experimental technique are then described. The results show that air condensation in the test section at high Mach Numbers has only a minor effect on diffuser performance. Data on overall pressure ratios for starting and maintaining hypersonic flow for a number of diffuser configurations are presented. The test Mach Numbers range from 5.9 to 9.6. From these data, a diffuser with a single-peaked throat and a three-degree plane wall divergence aft of the throat was selected as most practical. The pressure recovered by this optimum diffuser varies, depending on Mach Number, from 1.8 to 2.3 times that recovered by a pitot (or impact) tube operated at the test-section Mach Number. Data on pressure-distribution measurements throughout the nozzle and diffuser, spark schlieren photographs of diffuser flow, and data on Reynolds Number effects are also given. Finally, these data are compared with those of other investigators and with one-dimensional theory.

INTRODUCTION

A MAJOR COMPONENT OF supersonic wind tunnel working sections is the diffuser that decelerates the flow from supersonic to low subsonic speeds. A review of this problem is given by Ferri.[1] Diffusers do not operate free of losses, and their performance is characterized by indicating their overall pressure ratios (p_0/p_e, see Fig. 1) or pressure recovery. This is sufficient because the air leaving the diffuser has practically wind-tunnel supply temperature. A low overall pressure ratio or high pressure recovery is then desirable for wind-tunnel power-plant operation. This operating pressure ratio is different for different types of diffuser and test-section configurations. It is also a function of test-section Mach and Reynolds Numbers.

Many supersonic wind tunnels have diffusers designed primarily on the basis of subsonic experience, resulting in high overall pressure ratios.[2] Diffuser end pressure in these cases is below test-section pitot pressure. (A pitot tube decelerates the flow through a normal shock and a subsequent isentropic compression.) This lower recovery is due to the fact that, aside from a normal shock, viscosity effects in the diffuser introduce additional losses, thus lowering the end pressure. Since a diffuser employing a system of oblique shocks should have a better pressure recovery than one with a single normal shock, efforts were made to improve supersonic wind tunnels along these lines. This method had already proved successful in ram-jet diffusers. Variable-area diffusers whose throats can be closed after flow has been established were of interest here because of their higher pressure recovery.

To the authors' knowledge, the first supersonic tunnel diffusers giving end pressures higher than pitot pressure were discussed by Kurzweg[3] and Neumann and Lustwerk.[4] Diggins (N.O.L., unpublished) extended Kurzweg's work up to a Mach Number of 4.9. The first hypersonic diffuser was investigated by Bertram.[5] His tests were carried out in the 11-in. Hypersonic Wind Tunnel of the N.A.C.A.'s Langley Laboratory at a Mach Number of 6.9. End pressures up to 2.1 times pitot pressure were achieved by him. The present

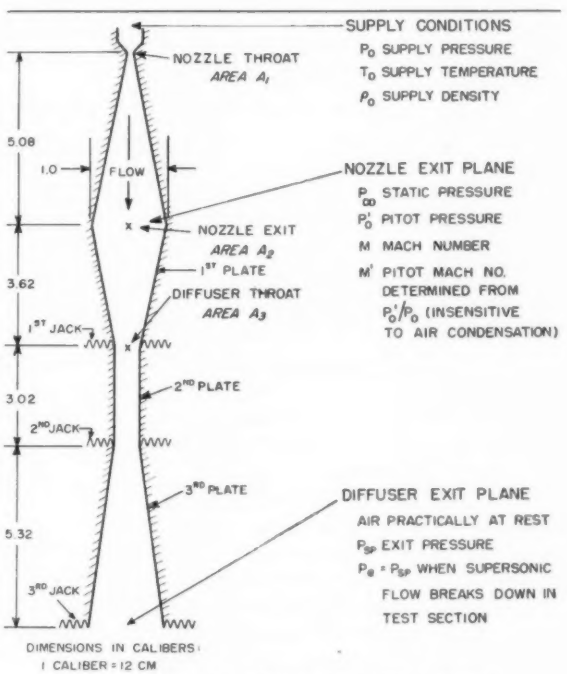

FIG. 1. Nozzle and diffuser dimensions, notation.

Received September 8, 1952.

* The work reported was jointly sponsored by the U.S. Naval Bureau of Ordnance and the U.S. Air Force Flight Research Laboratory in connection with the Gas Dynamics Facility of the Arnold Engineering Development Center, Tullahoma, Tenn., represented by R. Smelt. The assistance of H. Staab during the tests is gratefully acknowledged.

† Deputy Chief, Aerophysics Division.

‡ Chief, Hypersonic Branch.

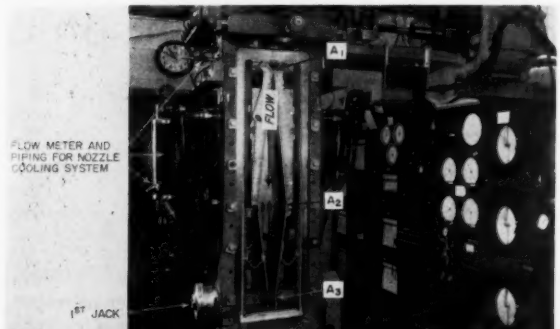

FIG. 2. Working section of the N.O.L. Hypersonic Tunnel No. 4.

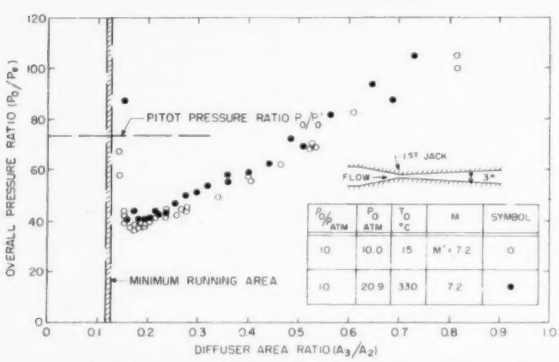

FIG. 3. Overall pressure ratios with and without air condensation.

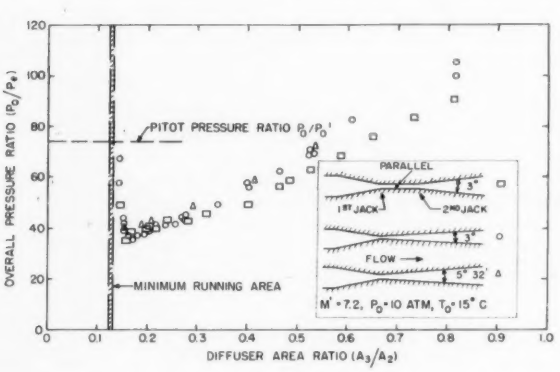

FIG. 4. Overall pressure ratios for three diffuser configurations.

investigation with a variable-area diffuser covers a Mach Number range from 5.9 to 9.6.

The overall pressure ratio needed for starting supersonic flow is important because it alone determines the maximum performance requirements for the power plant. At the present time little is known on this subject.[6–8] Starting requirements were also investigated and the results are presented.

Finally, it is interesting to note that, although the open jet diffuser type is amenable to theoretical treatment,[9] the closed jet diffuser of interest here cannot yet be treated by a unified theory. This is because the variation of pressure and shearing stress along the solid walls must be included in the analysis. Such a calculation would require presently unavailable knowledge of turbulent boundary-layer characteristics in coverging and diverging channels and an understanding of shock-wave boundary-layer interaction.

Wind-Tunnel and Experimental Method

The continuous N.O.L. 12- by 12-cm. hypersonic tunnel[10] operates from a 3,000 lbs. per sq.in. supply of dried air. Pressure-regulating valves control the supply pressure of the tunnel in the range from 1 to 30 atmospheres. Electric heaters control the supply temperature of the tunnel in the range from room temperature to above 500°C. Heating of the air is needed if air condensation in the test section is to be avoided. A steel wedge-type nozzle with a built-in cooling system to maintain nozzle wall temperature at a low value during high-temperature operation expands the air to a desired Mach Number in the range from 5 to 10 (see Fig. 2). The Mach Number distribution in a traverse across the exit plane of this wedge nozzle, exclusive of the boundary layer, is uniform to within $\pm 0.01M$ at $M = 7.2$, the Mach Number for which most of the data are shown.

Each diffuser wall has three plates, the first of which is linked directly to the nozzle end. Because of the high Mach Number in the test section, the shock angle caused by the flow deflection at this point is small, and long models can be used without having the conventional parallel wall test section. Three pairs of jacks control the motion of the three plates with respect to the working section wall. Sliding gaskets of Silicone rubber stripping fastened to the diffuser plates seal the diffuser in all positions. A flexible compartment seal between the first plates and the outside tunnel walls keeps the air behind these plates at near test-section pressure. The diffuser can be operated electrically during the run from fully opened to fully closed position. The diffuser throat opening is recorded to within 0.005 in. Steel sidewalls with pressure taps along the centerline or walls with 1-in. thick circular commercial plate-glass windows enclose the diffuser. Photographs are taken with a spark light source of $^1/_2$-microsec. duration.

The diffuser leads into a 12-in. pipe connecting the tunnel to vacuum pumps. Since the high-pressure air supply lasts for hours and the vacuum pump capacity exceeds tunnel requirements, tunnel operation is continuous. Arbitrarily chosen overall pressure ratios can be established to the order of 1 per cent accuracy.

To determine operating conditions, supersonic flow was established with a high pressure ratio. (Pressure ratios of the order 10^4 are available.) The diffuser throat was then closed to a point where supersonic flow broke down in the test section. After this minimum throat area had been established, minimum overall pressure ratios were measured for all diffuser throat areas larger than the minimum area. The overall pressure ratio (p_0/p_e) at the moment of "breakdown" of supersonic flow in the test section was noted. Flow breakdown was determined by any of three methods, which yield identical results: visual observation of the flow in the test section with the schlieren system, change of noise, and change of test section static and pitot pressure.

Minimum starting diffuser throat areas and minimum overall starting pressure ratios were determined in a similar manner.

Operating Requirements

If a supersonic tunnel is operated from a reservoir of dry air at room temperature and pressure at $M > 4.8$, a fraction of the air will condense at, or shortly after reaching, its saturation point in the nozzle.[10, 11] Such air condensation affects the commonly measured flow parameters differently. In particular, static pressure is extremely sensitive and pitot pressure nearly insensitive to the presence of condensed air in the flow. Fig. 3 shows overall pressure ratios for one diffuser configuration and nozzle-area ratio. In one test the air was not heated and air condensation occurred. In the other test the air was preheated above the supply temperature needed to keep the thermodynamic state of the air outside the condensation region during the entire expansion process. (To minimize Reynolds Number effects in this comparison, the supply density was kept the same for both the high and low T_0.) It can be seen that overall pressure ratios in the case with air condensation are somewhat lower than in the heated case free of such condensation. This is to be expected since the actual flow Mach Number is higher in the "hot" case. However, the difference is small enough for engineering purposes to state that diffuser performance is nearly insensitive to air condensation as previously found for the performance of the pitot tube.[10] The following tests (except the sensitive static pressure measurements and checks on starting) were therefore made without preheating the air, and the Mach Numbers indicated as M' are to be taken as those derived from the insensitive pitot measurements with the aid of a flow table. This procedure (of running the tunnel with cold air) makes it possible to photograph and observe the flow without the danger of cracking glass windows because of the heat. It also speeds up testing.

The pressure recovery of the diffuser in terms of pitot pressure over the range of Mach Numbers tested was generally of the same order. A detailed investigation was therefore carried out at the optimum Mach Number 7.2 only.

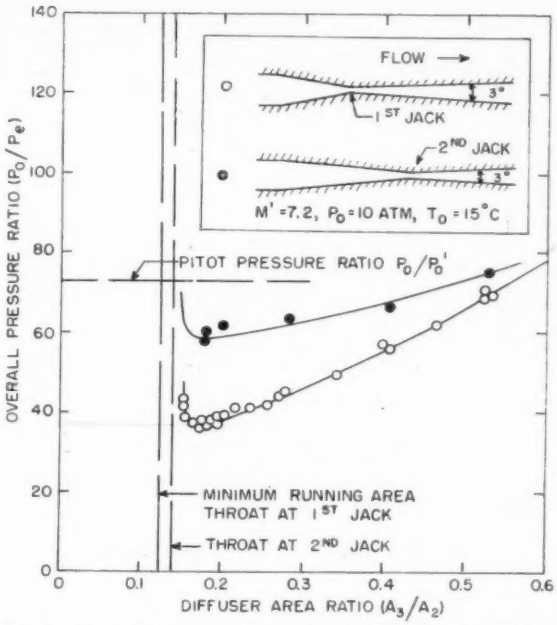

FIG. 5. Overall pressure ratios for two diffuser throat positions.

Overall pressure ratios as functions of diffuser-area ratio for three different diffuser configurations are given in Fig. 4. The Reynolds Number, based on tunnel width, for the comparable condition of no air condensation (Fig. 3) is 3,500,000. It can be noted that the case of parallel second diffuser plates[5] requires the lowest pressure ratio for large throat openings. No improvement is obtained when the angle between the second plates is increased from parallel to 1° to allow for boundary-layer growth. Diffuser performance is also practically unaffected if the angle between the third plates is increased from 3° to 14° and presumably flow separation takes place between the last plates. Fig. 5 gives a comparison of the pressure ratio for two different throat locations corresponding to the first and second jack position. It can be seen that the first throat position gives a better pressure recovery. It is assumed that in the second case the advantage of an increased number of shock reflections is more than offset by the increased friction along the longer duct.

A reduction of supply pressure increases the viscous effects at the diffuser throat. If the supply pressure is lowered, the minimum throat opening must be increased to accommodate the thicker boundary layer as shown in Fig. 6. It was also found that for a given diffuser throat an increase in supply pressure resulted in a decreased overall pressure ratio.

Fig. 7 gives a set of spark schlieren photographs taken with the configuration of a single peaked throat and subsequent 3° wall divergence. Pressure-ratio data corresponding to the conditions photographed in Fig. 7 are shown in Figs. 3 and 4.

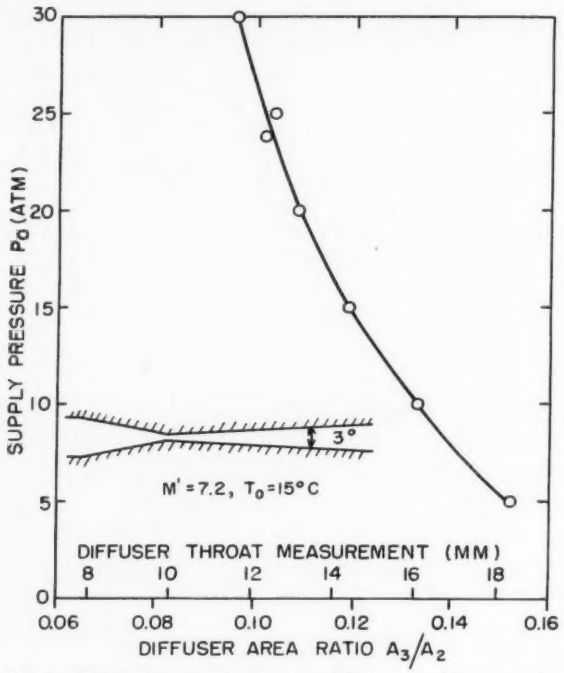

FIG. 6. Effect of supply pressure on minimum running area ratio.

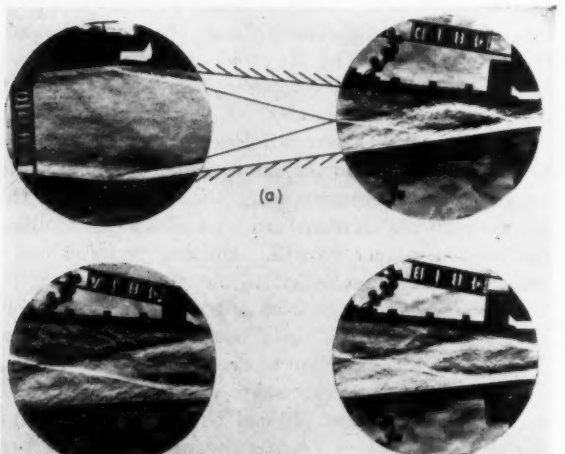

FIG. 7. Spark schlieren photographs of diffuser flow; M' = 7.2, p_0 = 30 Atm., T_0 = 15°C. (a) Test section and converging diffuser plates, A_3/A_2 = 0.20 (optimum); (b) converging diffuser plates, A_3/A_2 = 0.60; (c) converging diffuser plates, A_3/A_2 = 0.40.

In the photographs it may be noted that the boundary layers along the test section and diffuser walls are turbulent. This was confirmed by detailed pressure and temperature measurements in the layers with T_0 high enough to avoid air condensation.

Finally, Fig. 8 gives pressure distribution measurements taken along the sidewall centerline. These measurements were carried out with the supply air heated to T_0 = 320°, 30°C. higher than is needed to avoid air condensation throughout.

Diffuser data for the same configuration taken at other Mach Numbers as check points are presented in the collection of all available results in Figs. 12 and 13.

Using the data given above, we may postulate the following diffusion process: The oblique shocks emanating from the junction of first diffuser plates with the nozzle exit and their single reflection slightly ahead of the throat cause the significant increase in pressure. The Mach Number at the throat outside the large area taken up by boundary layers is still rather high (in the case of M = 7.2 in the test section it is of the order 4 to 5). Further diffusion from the throat to the end of the diffuser is relatively inefficient; in fact, it is about equal to that obtained in any diverging pipe with an entrance Mach Number of about that at the diffuser throat. Aft of the throat (see Fig. 8), transition to subsonic flow takes place through an oscillating shock system. Noise measurements at this point show a predominant frequency of the order of 5,000 cycles per sec. for a diffuser setting giving optimum pressure recovery. This frequency is a function of diffuser throat area, decreasing to about 1,000 cycles per sec. if the diffuser throat is wide open. Parallel second diffuser plates apparently contribute little to the stabilization of this shock system.[12]

Aside from structural reasons, it is desirable to eliminate the parallel section, because at M = 1 the product of density and velocity shows a maximum and, consequently, the heat transfer from the flow to the tunnel walls is maximized. This is important because of the high stagnation temperatures involved, resulting in the possible need for diffuser cooling systems in addition to nozzle cooling. This heat transfer was sufficient to cause glass cracks near the diffuser throat during heated runs.

In a further series of tests with cone cylinder, sphere and missile models, and supports in the test section, it

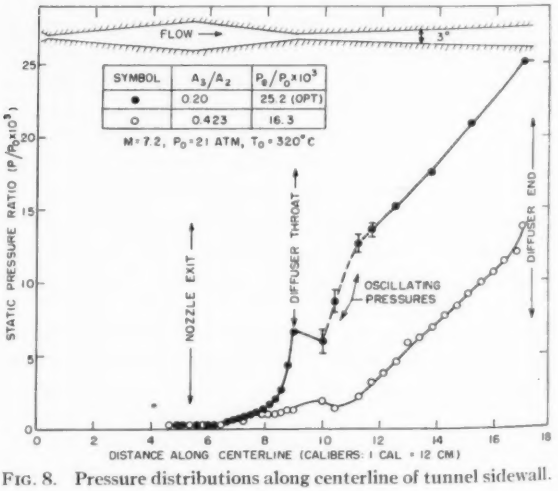

FIG. 8. Pressure distributions along centerline of tunnel sidewall.

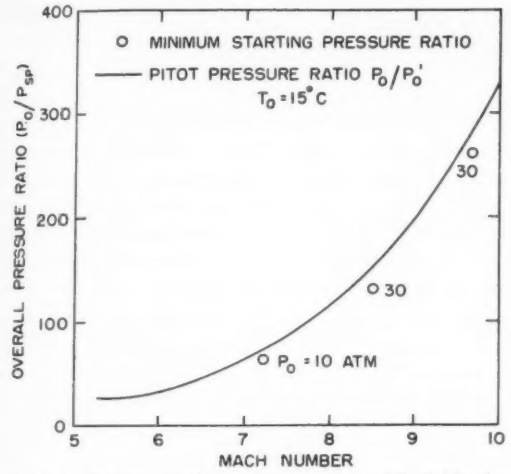

FIG. 9. Minimum starting pressure ratio vs. Mach Number.

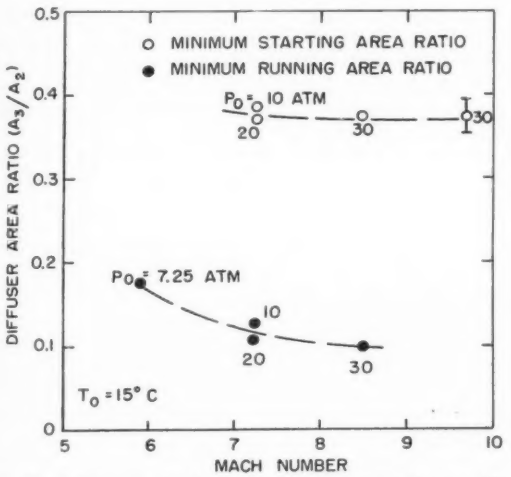

FIG. 10. Minimum starting and running area ratios vs. Mach Number.

was found that, aside from an increased minimum diffuser throat area, overall pressure ratios were little changed.[5] Apparently, the favorable additional oblique shock system introduced by the model counteracted the detrimental viscous effects due to surface friction and wake.

STARTING REQUIREMENTS

Minimum pressure ratios and minimum area ratios to start the tunnel are shown in Figs. 9 and 10. It can be seen that, although the minimum starting area is appreciably larger than the minimum operating area, it is about one-third smaller than that predicted by one-dimensional theory.[1] If the diffuser throat is larger than the minimum needed to establish supersonic flow, the starting pressure ratios are nearly equal to those given previously for operation. The minimum starting pressure ratio is somewhat lower than the pitot pressure ratio for the test-section Mach Number, and it is considerably below the pressure ratios previously anticipated by hypersonic wind-tunnel designers. This result is important because it may eliminate costly additions to hypersonic tunnel power plants for the momentary attainment of extremely high pressure ratios. An effect of the rapidity with which flow was established could not be found. A distinction was made between a "slow" and a "fast" start. In the case of the "slow" start, the overall pressure ratio was slowly increased, while the tunnel operated subsonically. The pressure ratio at which steady supersonic flow occurred in the test section was noted. For the "fast" start, the starting pressure ratio was established within 1/500 sec. by means of the fast-acting valve. No change in this ratio could be found with respect to the previous test. During the starting process, a supersonic jet detached itself from one nozzle wall and passed into the diffuser as shown in Fig. 11. Only for sufficient pressure ratio did this jet spread to the full width of the nozzle. Neither the diffuser configuration nor the presence of models had an appreciable effect on starting requirements.

COMPARISONS AND CONCLUSIONS

The present results are compared with data from other diffusers in Fig. 12. A general increase of pressure recovery with Mach Number in terms of pitot pressure can be noticed. The drop at the highest Mach

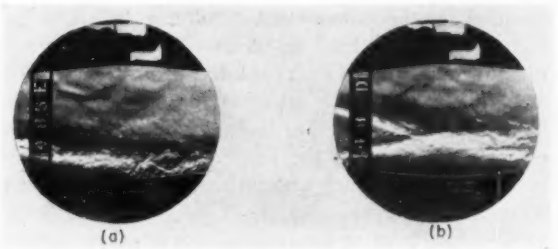

FIG. 11. Schlieren photographs of jet in test section before complete starting of tunnel; p_0 = 10 atm., T_0 = 25°C. (a) p_0/p_{sp} = 60.8 and (b) p_0/p_{sp} = 62.8. (Starting pressure ratio p_0/p_{sp} = 64.4; M' = 7.2.)

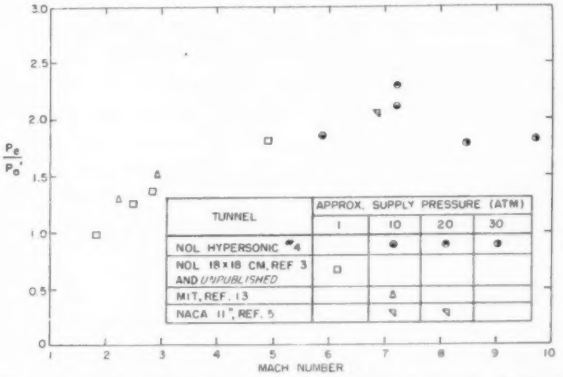

FIG. 12. Comparison of pressure recovery in terms of pitot pressure for several closed jet tunnels.

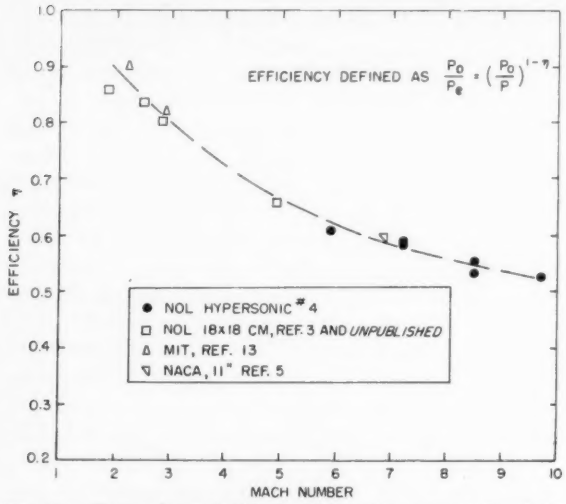
EFFICIENCY DEFINED AS $\frac{P_0}{P_e} = \left(\frac{P_0}{P}\right)^{1-\eta}$
EFFICIENCY η
MACH NUMBER
NOL HYPERSONIC # 4
NOL 18x18 CM, REF. 3 AND UNPUBLISHED
MIT, REF. 13
NACA, 11" REF. 5

FIG. 13. Comparison of diffuser efficiency for several closed jet tunnels.

Numbers might be avoided by optimizing the length of the first diffuser plates. In fact, a special configuration would be needed for every Mach and Reynolds Number to attain the best performance. However, for practical reasons, a diffuser with a fixed first plate length is desirable. Its shape would then be selected to be reasonably efficient in a whole range of Mach Numbers and have maximum efficiency at either the highest Mach Number or at some other critical point dictated by the power-plant requirements. Although recovery appears high in terms of pitot pressure, it must be remembered that the latter drops to low values at high Mach Numbers (at $M = 10$, $p_0'/p_0 = 3/1{,}000$). This is illustrated in Fig. 13 by a plot of diffuser efficiency as defined on the figure. Again the available results of other tunnels are given, and all data appear to lie on a single curve.

No tunnel starting data suitable for direct comparison could be found in the literature.

Finally, the following may be stated: A simple, single peaked throat, variable-area diffuser with plane walls was found to work as well or better than more complicated configurations in the range of Mach Numbers 5.9 to 9.6. In this range of Mach Numbers the pressure recovery of this diffuser was better than that of a pitot tube operated at the same Mach Number. It was found that the essential part of the pressure recovery takes place up to the throat and that viscous effects play an important role in this process. Since neither the parallel plates nor the angle of the diverging section had any significant effect on the pressure recovery, it is concluded that the diffuser section after the throat may be kept short. This minimizes the total heat transfer to the wall for high-temperature operation of hypersonic tunnels. It was also found that hypersonic tunnels may be started at pressure ratios about equal to the pitot pressure ratio, thus making additional starting devices unnecessary. The minimum diffuser throat area at which the shock system could be "swallowed" and supersonic flow could be established was only two-thirds of that predicted by one-dimensional theory in spite of the viscous effects present. Apparently, an oblique shock system is immediately built up during the starting process. The presence of models and supports increased the minimum diffuser throat somewhat but did not materially affect overall pressure ratios.

REFERENCES

[1] Ferri, A., *Elements of Aerodynamics of Supersonic Flows*, Chapt. 9, The Macmillan Company, New York, 1949.

[2] Liepmann, H. W., and Puckett, A. E., *Introduction to Aerodynamics of a Compressible Fluid*, pp. 82–85, GALCIT Aeronautical Series; John Wiley & Sons, Inc., New York, 1947.

[3] Kurzweg, H. H., *A Few Aspects of Future Supersonic Wind-Tunnel Design and Test Techniques*, U.S. Naval Ordnance Laboratory, NOLR 1133, June 29, 1949.

[4] Neumann, E. P., and Lustwerk, F., *Supersonic Diffusers for Wind Tunnels*, Journal of Applied Mechanics, Vol. 16, No. 2, June, 1949.

[5] Bertram, M. H., *Investigation of the Pressure-Ratio Requirements of the Langley 11-inch Hypersonic Tunnel with a Variable-Geometry Diffuser*, N.A.C.A. R.M. L50I13, October 6, 1950, declassified, N.A.C.A. Change in Classification Form No. 750, March 21, 1952.

[6] Eggink, H., *Stroemungsaufbau und Druckrueckgewinnung in Ueberschallkanaelen*, Forschungsbericht No. 1756, ZWB 1943. English translation by the University of Michigan: *Flow Structure and Pressure Recovery in Supersonic Tunnels*, ATI 3570, CGD 808.

[7] Diggins, J. L., *Diffuser Investigation in a Supersonic Wind Tunnel*, U.S. Naval Ordnance Laboratory NAVORD Report 1570, January 3, 1951.

[8] Bull, G. V., *Starting Processes in an Intermittent Supersonic Wind Tunnel*, Institute of Aerophysics, University of Toronto, UTIA Report No. 12, February, 1951.

[9] Hermann, R., *Diffuser Efficiency of Free-Jet Supersonic Wind-Tunnels at Variable Test Chamber Pressure*, Journal of the Aeronautical Sciences, Vol. 19, No. 6, p. 375, June, 1952.

[10] Wegener, P., *Summary of Recent Experimental Investigations in the N.O.L. Hyperballistics Wind Tunnel*, Journal of the Aeronautical Science, Vol. 18, No. 10, p. 665, October, 1951.

[11] Wegener, P., Reed, S., Stollenwerk, E., and Lundquist, G., *Air Condensation in Hypersonic Flow*, Jour. of Appl. Phys., Vol. 22, No. 8, August, 1951.

[12] Kantrowitz, A., *The Formation and Stability of Normal Shock Waves in Channel Flows*, N.A.C.A. T.N. No. 1225, March, 1947.

[13] Neumann, E. P., and Lustwerk, F., *High Efficiency Supersonic Diffusers*, Journal of the Aeronautical Science, Vol. 18, No. 6, p. 369, June, 1951.

Analysis of Stiffened Curved Panels Under Shear and Compression

M. A. MELCON* AND A. F. ENSRUD†

Lockheed Aircraft Corporation

SUMMARY

This paper presents a method of analysis for curved panels reinforced by longitudinal stiffeners subjected to shear and compression. New formulas have been derived for the critical buckling stress of curved panels in shear and for the various effects of the diagonal tension field in the postbuckling state of the sheet. These latter effects are expressed by fictitious compressive stresses in the stiffeners which are then combined by an interaction equation with the compression stresses due to the external loading. In addition, a formula is given for the ultimate shear strength of the sheet. The method proposed in this paper has been compared with available experimental data, and satisfactory agreement is found. The method has been put in a form that requires the solution of certain mathematical relations and a minimum of chart reading and, hence, is readily adaptable to IBM or other high-speed computing techniques. A sample interaction diagram is included showing how the results of this method may be presented for practical application.

INTRODUCTION

IN SPITE OF GREAT ADVANCEMENTS in the design of aircraft structures, the analysis of stiffened shells still presents a challenging problem. The difficulty arises mainly from the fact that no practical mathematical treatment of the stress pattern in the postbuckling state has been developed as yet. Therefore, for the time being, the designer has to be satisfied with semi-empirical solutions that show sufficient agreement with test results.

Based on a study of the available literature giving theoretical and experimental data pertaining to this subject, a method has been developed for the prediction of the ultimate strength of sheet and longitudinal stiffeners in a curved panel.

NOTATION

A_{st} = stiffener area
a = ring spacing
b = stiffener spacing
C_r = rivet factor, ratio of net to gross area of web
F_c' = allowable compression stress for stiffener alone; F_c' is the lower of either the column allowable (use a fixity of 2 for stiffeners continuous across rings) or the crippling cutoff of the stiffener
F_c = allowable compression stress for stiffener plus effective skin
f_c' = effective compression stress in stiffener due to diagonal tension
f_c'' = a measure of stiffener bending stiffness required to break up shell into panels
f_c = applied compression stress based on stiffener area plus effective width of skin
f_{c_0} = applied compression stress based on stiffener area plus total area of skin
F_s = Allowable gross area shear stress for web failure.
F_{so} = basic allowable gross area shear stress (for homogeneous diagonal tension field at 45°)
F_s' = critical buckling shear stress for shell
F_s'' = critical buckling shear stress for flat panel
$F_{scr.}$ = $F_s' + F_s''$ = critical buckling shear stress for curved panel
F_{su} = ultimate shear stress of the material
f_s = applied gross area shear stress
f_{sDT} = part of applied shear stress carried in diagonal tension
F_{tu} = ultimate tensile stress of the material
I_{st} = moment of inertia of stiffener about centroidal axis parallel to the tangent of the skin contour
J_{st} = torsional stiffness factor: for open sections, $J = A_{st}t_{st}^2/3$; for closed sections $J = 4A^2t_{st}/p$, where A is the enclosed area and p is the perimeter
S = shell parameter
R = radius of curvature of panel
t = thickness of web
t_{st} = thickness of stiffener
ν = a factor reflecting the various effects of the diagonal tension field on the stiffener
η = a factor indicating the intensity of diagonal tension in web
λ = a factor reducing the critical shear stress under combined loading

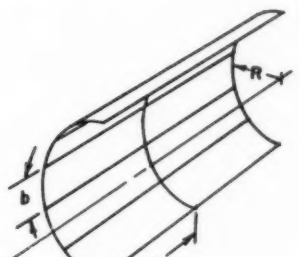

FIGURE 1.
TYPICAL SHELL STRUCTURE

Presented at the Structures Session, Twentieth Meeting, I.A.S., January 28–February 1, 1952, New York. Revised and received August 27, 1952.

* Group Engineer, Structural Methods and Dynamics.
† Structures Engineer.

Method of Analysis

A semimonocoque shell reinforced by rings and longitudinal stiffeners (Fig. 1) may fail in three ways: (1) failure of stiffeners, (2) failure of sheet, and (3) failure of rings. If several components fail simultaneously, the type of failure is usually referred to as general instability. It is assumed that the attachments between skin and supporting members will not shear or pop and thus reduce the ultimate load carrying capacity of the structure.

The following deliberations are limited to an investigation of the first two types of failure. The results of this investigation are then checked against the test data of specimens that failed by buckling of stiffeners or tearing of the skin. Formulas derived in this paper apply specifically only to thin-walled shells of circular cross section with constant values for shear flow, stiffener area, stiffener spacing, and sheet thickness. Adaptations for variation in these items are easily made.

The proposed method may be outlined as follows:

The critical buckling stress of a curved panel is given as the sum of the strength of the shell and that of the panel. If the applied shear stress is below the critical shell-buckling stress, no longitudinal stiffeners are required. On the other hand, it is obvious that the stiffeners must have a certain amount of bending stiffness in order to subdivide the shell into panels. As soon as the applied shear exceeds the critical buckling stress for a curved panel, a rather complex interaction between sheet and supporting members is started. The mathematical treatment becomes extremely involved, if not impossible.

At the start, the shell between the rings bows outward like a barrel. With increasing shear flow, the radial components of the diagonal tension field will pull the stringers inward. In addition, a nonlinear relationship between the applied torque and the compressive stress in the stiffeners can be observed. Failure usually occurs from an individual buckle in the shell forcing the stiffener out of its original location, thus bringing about its collapse by an intricate beam-column action.

Critical Shear Buckling Stress

A simplified expression has been derived for the critical buckling stress of a curved panel. For a flat panel the critical buckling stress may be expressed by

$$F_s'' = KE(t/b)^2 \tag{1}$$

where the magnitude of the coefficient K depends on the material, the degree of edge restraint, and the aspect ratio of the panel. For aluminum alloys and standard construction, this value is taken equal to 5.25 irrespective of aspect ratio. The variation in panel length is taken care of in the term that reflects the effect of curvature. The critical buckling stress of the curved panel may be expressed by

$$F_{s_{cr.}} = KE(t/b)^2$$

where in this case $K = 5.25 + (\pi/4)(b/a)^2 S^{3/4}$ and $S = a^2/Rt$ denotes the shell parameter. This formula for the critical buckling stress of a curved panel may be transformed to the form

$$F_{s_{cr.}} = F_s' + F_s'' \tag{2}$$

where

$$F_s' = (\pi/4\sqrt[4]{S})(Et/R)$$
$$F_s'' = 5.25E(t/b)^2$$

Postbuckling Behavior of a Shear Panel

With the introduction of thin sheet construction for aircraft structure, engineers began to accept the new idea that the buckling of structural components did not necessarily indicate failure. Since that time, a great deal has been written on the postbuckling behavior of structures. Of foremost importance in the study of this subject, is the theory of the incomplete diagonal tension field.

The stress pattern in a flat sheet subjected to shear forces beyond its buckling strength is known as diagonal tension. A rigorous formulation of the transition from the unbuckled state to Wagner's[7] ideal diagonal tension field has not yet been accomplished. Semiempirical formulas developed by Kuhn[8] are most widely used.

When the stress in a plane web starts to exceed its initial buckling strength, the applied shear forces are gradually taken by a combined truss action of the web and stiffeners. The sheet acts more and more like a diagonal, while the stiffeners take the place of uprights. There is a tendency for a buckle to form from corner to corner of the panel, provided this pattern is compatible with the deformation of the stiffeners supporting the edges of the panel.

The various methods proposed for the analysis of flat panels in the postbuckling state differ in the assumption of magnitude of compression stress the sheet is able to sustain in its buckled shape. Additional complications arise when the panel is curved. The diagonal tension in the sheet tends to reduce its curvature in the direction of the wrinkles. This action induces nonuniform radial loads on the longitudinal stiffeners.

Analysis of Longitudinal Stiffeners

The longitudinal stiffeners in a reinforced shell perform three functions: (1) They subdivide the shell into panels; (2) they sustain axial and radial loads induced by the tension field; and (3) they sustain directly applied axial loads. As long as the shell stiffened by rings only is able to sustain the applied shear flow without buckling, no stiffeners are required for the purpose of reducing the panel size. With increasing shear flow, it usually becomes more desirable to raise the initial buckling stress by the addition of longitudinal stiffeners than by thickening of the shell. The required bending stiffness of the stiffeners which will raise the initial

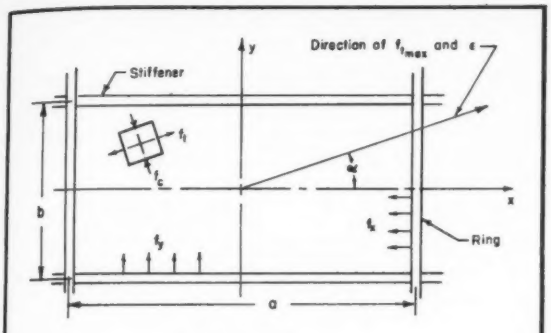

FIGURE 2.

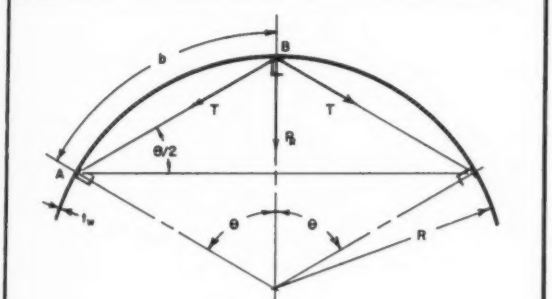

FIGURE 3.

buckling stress to the full value of shell plus panel may be determined according to Seydel's[10] formula for the critical shear stress of flat orthotropic plates,

$$F_{s_{cr.}} = (32/ta^2)\sqrt[4]{D_1D_2^3}$$

where

$$D_1 = D$$
$$D_2 = EI_{st}/b$$
$$D = Et^3/12(1-\mu^2)$$

Setting this expression equal to F_s'' and eliminating on both sides, there follows the expression for the portion of the moment of inertia, ΔI_{st}, of the stiffener required to divide the shell into panels,

$$\Delta I_{st} = (bt^3/5)(a/b)^{3/2}$$

As mentioned previously, this requirement will be transformed into a fictitious compression stress indicating the portion of the stiffener strength needed for effective subdivision into panels. It is assumed that the ratio of the stiffener moment of inertia required for this purpose to its total moment of inertia may be taken equal to the ratio of an additional area to the total area of the stiffener. The following relation for the fictitious compression stress f_c'' is established:

$$f_c''A_{st} = F_c'\Delta A_{st}$$

Then,

$$f_c'' = F_c'\frac{\Delta A_{st}}{A_{st}} = F_c'\frac{\Delta I_{st}}{I_{st}}$$

where $F_c' = \pi^2EI_{st}/a^2A_{st}$ reflects the column strength of the stiffener. Combining and solving these equations gives

$$f_c'' = F_s''(at/A_{st})\sqrt[3]{0.053b/a} \qquad (3)$$

This equation indicates that heavy skin and wide ring spacing require strong stiffeners in order to avoid excessive values of f_c''. However, this portion of the total effective compression stress in the stiffener in most structures is usually small.

The effects of the diagonal tension field on the stiffeners in a buckled shell are rather complex. The axial load build-up in the longitudinal stiffeners caused by the diagonal tension (Fig. 2) is given by

$$P = (f_s - F_{s_{cr.}})bt\cot\alpha$$

In addition, there are radial components of the diagonal tension field which produce bending moments in the stiffeners. The pull per running inch (Fig. 3) exerted by the tension field along this chord line is

$$T = (f_s - F_{s_{cr.}})t\tan\alpha$$

and the radial load per running inch is

$$P_R = Tb/R = (f_s - F_{s_{cr.}})bt(\tan\alpha/R)$$

The unknown angle α may be found by trial and error. However, this standard approach to the analysis of longitudinal stiffeners does not agree with tests for many reasons, and, hence, a different approach to the problem was chosen.

Fig. 4 pictures a stiffened shell subjected to torsion. Assuming a diagonal tension field of 45° and no bending in the stiffeners, the induced compression stress in the stiffeners is given by

$$f_c' = (f_s - F_{s_{cr.}})(bt/A_{st}) \qquad (4)$$

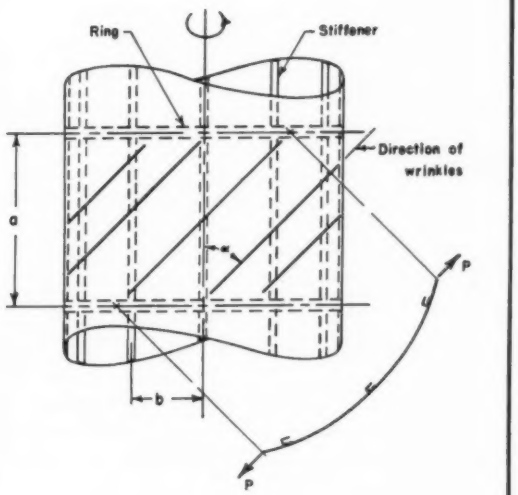

FIGURE 4.

The actual angle of the tension field is usually smaller than 45°; in addition, there is a pull P along the direction of the wrinkles which forces the stringers toward the center of the cylinder. It can be seen from Fig. 4 that the pull P has a greater effect on stringers of smaller flexibility, because the shell support in this case starts at a later state. Furthermore, it is obvious that this effect is increased with sharper curvature. These, in addition to other considerations, led to the determination of the empirical factor ν, which was introduced into Eq. (4) to give a fictitious compression stress that is a measure of required stiffener strength to sustain the effects of diagonal tension. Eq. (4) then transforms into

$$f_c' = \nu(f_s - F_{s_{cr.}})(bt/A_{st}) \tag{5}$$

where

$$\nu = 1 + (a/R)\sqrt[4]{(I_{st}/J_{st})(t/b)}$$

This formula gives satisfactory results for shells with $R \leqslant 100$ in. The total effective or fictitious compression stress for which the stiffener must be designed becomes, then,

$f_c' + f_c''$ = total effective compression stress in stiffener

The allowable stress to be used for determining the strength of the stiffener is F_c', which is the lower of the column allowable (using a fixity of 2 for stiffeners that are continuous across rings) or the crippling cutoff for the stiffener alone. Allowables determined from tests on the stiffener by itself may often be unsuitable for this analysis, since the stiffener may fail in a mode not possible for a stiffener that is attached to the shell. Table A summarizes the effective compression stress to be used at different values of f_s when the panel is subjected to shear alone.

TABLE A

f_c' and f_c'' When Panel Is Subjected to Shear Only

f_c'	f_c''
$f_c' = 0$, when $f_s < F_{s_{cr.}}$	$f_c'' = 0$, when $f_s < F_s'$
$f_c' = \dfrac{\nu(f_s - F_{s_{cr.}})bt}{A_{st}}$, when $f_s \geqslant F_{s_{cr.}}$	$f_c'' = \left(\dfrac{f_s - F_s'}{F_s''}\right)\left(\dfrac{F_s''at}{A_{st}}\right) \times \sqrt[3]{\dfrac{0.053b}{a}}$, when $F_s' \leqslant f_s < F_{s_{cr.}}$
	$f_c'' = \dfrac{F_s''at}{A_{st}} \sqrt[3]{\dfrac{0.053b}{a}}$, when $f_s \geqslant F_{s_{cr.}}$

If, in addition to shear, the panel is also subjected to direct compression, the effects of shear on the stiffener are combined by an interaction equation with the effects of the direct compression. The only exception to the method as previously outlined for determining the effects of shear on the stiffener is that the critical shear buckling stresses, in this case, must be reduced because of the effects of compression. There are well-known interaction equations that give the initial buckling of panels under combined loadings. However, for the purpose at hand, these equations are not satisfactory, since they will not properly account for the amount of the shear being carried in diagonal tension nor will the angle of diagonal tension be the same as when the sheet buckled under shear alone. In other words, it would be conservative to assume that, after buckling occurs in combined shear and compression, any additional shear is carried in the same manner as if the buckling were due to shear alone. If linear interaction were assumed for initial buckling in compression and shear, the following equation may be written:

$$(f_s/F_{s_{cr.}}) + (f_{c_0}/F_{c_{cr.}}) = 1$$

Then the shear stress at which the panel buckles becomes

$$f_s = \frac{1}{1 + (f_{c_0}/f_s)(F_{s_{cr.}}/F_{c_{cr.}})} F_{s_{cr.}}$$

Based on this reasoning, a factor λ was arbitrarily selected to reflect the reduction in the critical shear buckling stress due to compression,

$$\lambda = \sqrt[4]{1/[1 + (f_{c_0}/f_s)]} \tag{6}$$

where f_{c_0} is the applied compression stress based on stiffener area plus total area of skin.

The prediction of stiffener failure due to the combined action of shear and direct compression is based upon the following interaction equation:

$$\left(\frac{f_c' + f_c''}{F_c'}\right)^{1.125} + \left(\frac{f_c}{F_c}\right)^{1.125} = 1 \tag{7}$$

where f_c is the direct compression stress based on stiffener area plus effective width of skin and F_c is the allowable compression stress based on the same area. In other words, the ratio f_c/F_c is the ratio of the applied compression load to the allowable compression load of the stiffener plus skin. Table B summarizes the effective compression stress to be used at different values of f_s when the panel is subjected to shear and compression. For $\lambda = 1$, Table B is identical with Table A.

TABLE B

f_c' and f_c'' When Panel Is Subjected to Shear and Compression

f_c'	f_c''
$f_c' = 0$, when $f_s < \lambda F_{s_{cr.}}$	$f_c'' = 0$, when $f_s < \lambda F_s'$
$f_c' = \dfrac{\nu(f_s - \lambda F_{s_{cr.}})bt}{A_{st}}$, when $f_s \geqslant \lambda F_{s_{cr.}}$	$= \left(\dfrac{f_s - \lambda F_s'}{F_s''}\right)\left(\dfrac{\lambda F_s''at}{A_{st}}\right) \times \sqrt[3]{\dfrac{0.053b}{a}}$, when $\lambda F_s' \leqslant f_s < \lambda F_{s_{cr.}}$
	$f_c'' = \dfrac{\lambda F_s''at}{A_{st}} \sqrt[3]{\dfrac{0.053b}{a}}$, when $f_s \geqslant \lambda F_{s_{cr.}}$

Little test data could be found for shells reinforced by stiffeners with closed section. Whether the factor ν still applies in this case could therefore not be substantiated by comparison with test data. The only

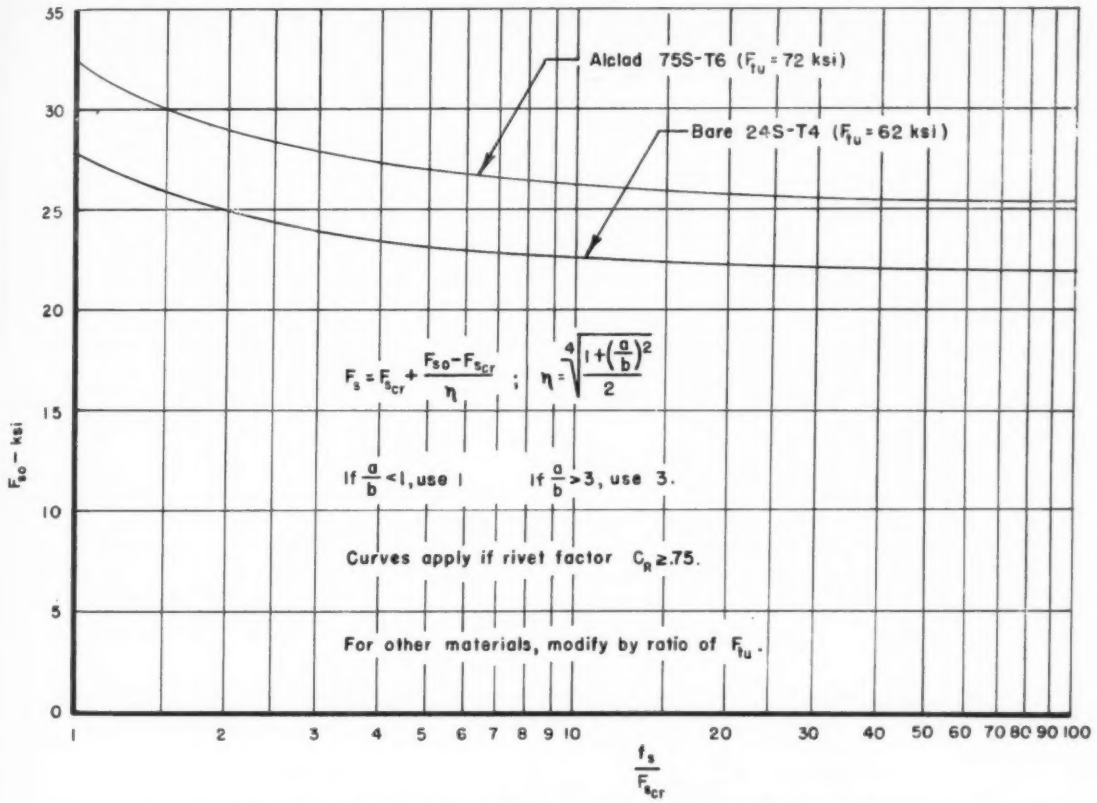
Alclad 75S-T6 (F_{tu} = 72 ksi)
Bare 24S-T4 (F_{tu} = 62 ksi)
$F_s = F_{s_{cr}} + \frac{F_{so} - F_{s_{cr}}}{\eta}$; $\eta = \sqrt[4]{\frac{1+\left(\frac{a}{b}\right)^2}{2}}$
If $\frac{a}{b} < 1$, use 1 If $\frac{a}{b} > 3$, use 3.
Curves apply if rivet factor $C_R \geq .75$.
For other materials, modify by ratio of F_{tu}.
F_{so} - ksi
$\frac{f_s}{F_{s_{cr}}}$

FIGURE 5 - ULTIMATE ALLOWABLE GROSS AREA SHEAR STRESS.

two specimens that had closed stiffeners failed by tearing of the web.

Analysis of Shear Web

The formulas for the allowable gross area shear stress presented here are based on the assumption that the net area of the sheet is equal to, or greater than, 75 per cent of its gross area. In the unbuckled condition of the web, the maximum tension stress in the sheet is equal to the shear stress. For aluminum alloys, the ultimate tensile strength is approximately 1.67 times the ultimate shear strength of the material. This indicates a marginal tension capacity of 67 per cent. In the ideal tension field, where the compression strength of the sheet is assumed equal to zero, the maximum tension of the sheet is equal to twice the shear stress. This indicates that in the homogeneous tension field the sheet cannot develop the ultimate shear strength of the material. The curve of Fig. 5, giving the basic allowable shear stress F_{so}, takes account of this. However, a correction is also needed to provide for an angle α different from 45° and for wrinkles forming from corner to corner of the panel. This correction is reflected by the empirical factor

$$\eta = \sqrt[4]{[1 + (a/b)^2]/2}$$

if $a/b < 1$, use 1; if $a/b > 3$, use 3. The ultimate allowable gross area web stress is, therefore,

$$F_s = F_{s_{cr.}} + [(F_{so} - F_{s_{cr.}})/\eta] \tag{9}$$

where F_{so} is obtained from Fig. 5.

The curves of Fig. 5 are similar to the lower curves of reference 11, Fig. 9. The curves of this reference were modified so that for $f_s/F_{s_{cr.}} = 1$ the basic allowable shear stress becomes $F_{so} = 0.75F_{su}$. This correction is made so that net area shear stress will never exceed F_{su}.

In exceptional cases where the net area of the sheet is less than 75 per cent of the gross area, an additional check is recommended. The circular interaction for combined tension and shear is given by the formula

$$\left[\frac{f_s}{C_R F_{su}}\right]^2 + \left[\frac{\eta(f_s - F_{s_{cr.}})}{C_R F_{tu}}\right]^2 = 1 \tag{10}$$

where C_R denotes the rivet factor.

If compression is superimposed on the shear stress in the panel, the initial buckling stress is again multiplied by the factor λ in both Eqs. (9) and (10).

Analysis of Attachments

At either end of the sheet or at splices, the load in the sheet must be transferred by rivets or fasteners to other

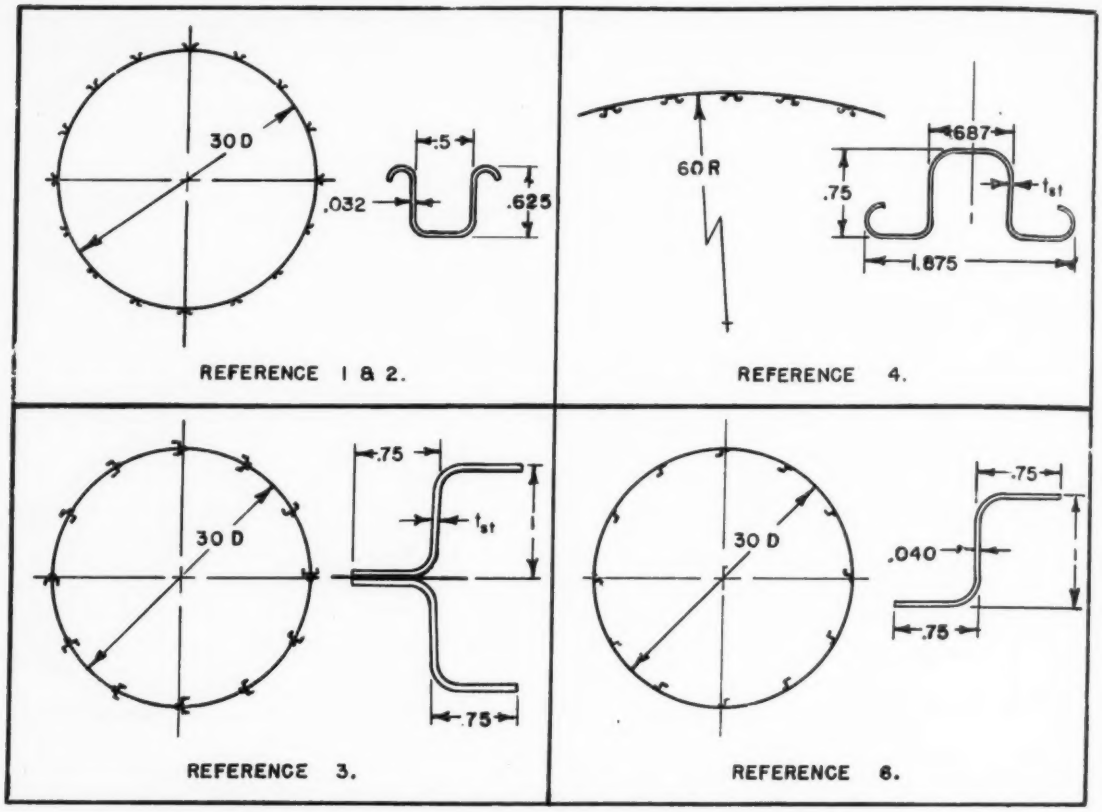

FIGURE 6 - TYPES OF SPECIMENS TESTED

parts of the structure. The shear load for which each fastener should be checked is given by

$$P = qp\sqrt{1 + \left[\frac{\eta(f_s - F_{s_{cr.}})}{f_s}\right]^2} \qquad (11)$$

where p = pitch of fasteners and q = shear flow in sheet. Again, reduce $F_{s_{cr.}}$ by the factor λ if compression is present.

Comparison with Test Data

The substantiation for the methods proposed herein are based upon the test work performed by the N.A.C.A.[3,6], the Aluminum Company of America,[1,2] Douglas Aircraft Company, Inc.,[4] and the National Bureau of Standards.[5] A sum total of 54 test specimens has been analyzed in this investigation. Fig. 6 shows the general configurations of the types of specimens tested. As can be observed, some of the specimens are complete cylinders stiffened with longitudinal stiffeners and rings, while others are portions of cylinders. The radius of specimens varied from 15 to 60 in.; skin gage, from 0.020 to 0.051; and the factor ν had a range on the specimens examined from approximately 1.10 to 3.

Critical Buckling Shear Stress

Table 1 gives a comparison of the critical buckling shear stress computed by the method of this paper, by the method of reference 9, and observed test values. Twenty-six panels were checked. Test values averaged 2.0 per cent higher than predicted by the proposed method and 5.8 per cent higher than by the method of reference 9. Figure 7 shows graphically the relationship between test and predicted values. There is no significant difference between the predictions of the two methods. The advantage of the proposed method lies in the fact that the buckling stress of the curved panel is expressed explicitly in terms of parameters of the panel and that reference to charts is not required.

Panels Subjected to Shear Only (Stiffener Failures)

A total of 24 specimens that were subjected to shear only failed in the stiffener. Fig. 8 shows the relationship between the shear strength predicted by the method of this paper and test shear strength. Including all specimens, the average conservatism of the prediction is 7.8 per cent. The results from specimen 2 of reference 2 and specimen 10 of reference 4 were overly conservative. In the first case the stiffener apparently

TABLE 1

Comparison of Initial Buckling Stress Computed by $F_{scr.} = F_s' + F_s''$ by Method of Reference 9 and Observed Test Values. Panels Subjected to Shear Only

		Initial Buckling Stress			Ratio of Test to Predicted	
Reference	Specimen	Proposed method, $F_{scr.} = F_s' + F_s''$	Method of ref. 9	Observed by test	Proposed method	Method of ref. 9
1	14	2,869	2,840	2,950	1.028	1.039
	20	2,844	2,750	2,870	1.009	1.044
	21	3,455	3,230	4,120	1.192	1.276
2	2	3,018	3,160	3,460	1.146	1.095
	5	4,128	3,730	4,130	1.000	1.107
	8	4,854	4,480	4,660	0.960	1.040
	11	5,442	5,400	5,160	0.948	0.956
	3	4,245	4,790	4,720	1.112	0.985
	6	5,580	5,700	6,040	1.082	1.060
	9	5,755	5,480	5,840	1.015	1.066
	12	6,710	6,120	7,150	1.066	1.168
3	1	3,318	2,950	3,200	0.964	1.085
	2	4,897	4,580	5,000	1.021	1.092
	3	3,643	3,480	3,700	1.016	1.063
	4	4,908	4,600	4,800	0.978	1.043
	5	6,317	6,700	6,400	1.013	0.955
	6	8,383	8,360	8,500	1.014	1.017
	7	7,115	6,530	6,700	0.942	1.026
	8	8,508	8,640	8,800	1.034	1.019
	9	3,939	3,940	3,040	0.774	0.773
	10	2,326	2,350	2,380	1.023	1.014
	11	7,552	7,110	7,900	1.046	1.111
	12	6,472	6,170	7,270	1.123	1.179
4	8	1,480	1,470			
	28	1,212	1,230			
	27	1,480	1,460			
	32	2,200	2,200			
	16	1,212	1,230			
	3	1,480	1,460			
	10	2,200	2,200			
5	20a	14,420	12,780	12,200*	0.846	0.955
	30a	12,258	10,850	13,150	1.073	1.212
6	1	3,418	3,280	3,700	1.083	1.128

*This observed test value is probably low because of some initial condition, since identical panels with larger radii buckled at a higher stress.

developed a fixity of 4 instead of 2 as determined from the compression stresses read in the strain gages, and in the second case the test is questioned, since this specimen was one of a family of specimens and the test results were incompatible with the rest. If these two specimens are excluded, the average conservatism becomes 5.8 per cent.

Panels Subjected to Shear Only (No Stiffener Failures)

As a negative check of the method for predicting stiffener failures, 15 specimens that did not fail in the stiffener were analyzed for stiffener failure. The purpose of this was to determine to what extent stiffener failures would be predicted by the proposed method when they did not actually occur in the test panel. Fig. 9 is a graph of predicted shear stress vs. test shear stress and indicates that for most of the specimens the test stress is lower than the predicted stress. This is as it should be, since these panels did not fail in the stiffener.

Those panels that had a test stress close to the predicted stress based on stiffener failure failed by popping of the rivets, and it is questionable whether the panels would have carried much more stress had the rivets not failed.

Panels Subjected to Combined Shear and Compression (Stiffener Failures)

A total of 15 specimens subjected to shear and compression were analyzed. Fig. 10 shows the interaction between effective compression in stiffener due to shear and the direct compression for the test specimens analyzed.

The results indicate an average conservatism for the method of prediction of 5.0 per cent. The test result from one specimen from reference 4 with a high conservatism was considered to be questionable, since it was not compatible with other tests in the same series of specimens. If this specimen is neglected, the average conservatism drops to 3.8 per cent. The actual conservatism in an interaction diagram between shear flow in skin and compression load on stiffener would be less than the above value, since the conservatism enters into only that portion of the shear flow supported by the stiffeners.

Panels Subjected to Shear Only (Web Failures)

Nine specimens failed in the web. Fig. 11 shows a graph of test stress vs. predicted stress for web failure. The results indicate that the method is conservative by an average of 0.3 per cent. There is reason to question

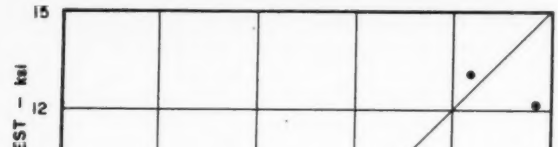

FIGURE 7. - INITIAL SHEAR BUCKLING STRESS IN CURVED PANELS.

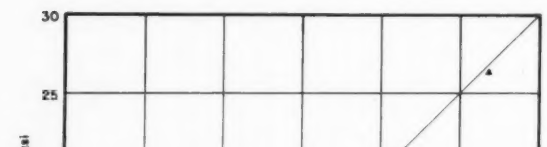

FIG 8 - SHEAR STRESS AT FAILURE vs PREDICTED SHEAR STRESS FOR PANELS WITH STIFFENER FAILURES. PANELS SUBJECTED TO SHEAR ONLY.

the results from three of the specimens. Specimens 20a and 30a of reference 5 failed by tearing the sheet in the end panels and was precipitated by shearing of rivets connecting stringers to jig. In testing specimen 1 of reference 3, the loading jig bound, and the applied torque was actually about 10 per cent greater than the test gage indicated. If these three specimens were omitted, the average conservatism becomes 4.0 per cent.

Typical Application

A typical application to which this method of analysis may be applied is the determination of allowable strengths for a fuselage shell structure. The following is an outline of the procedure for constructing an interaction curve of combined shear and compression on a curved panel. An example of such curves is shown in Fig. 12.

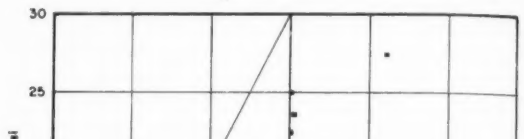

FIG 9 - SHEAR STRESS AT FAILURE vs PREDICTED SHEAR STRESS FOR PANELS WITHOUT STIFFENER FAILURES. PANELS SUBJECTED TO SHEAR ONLY.

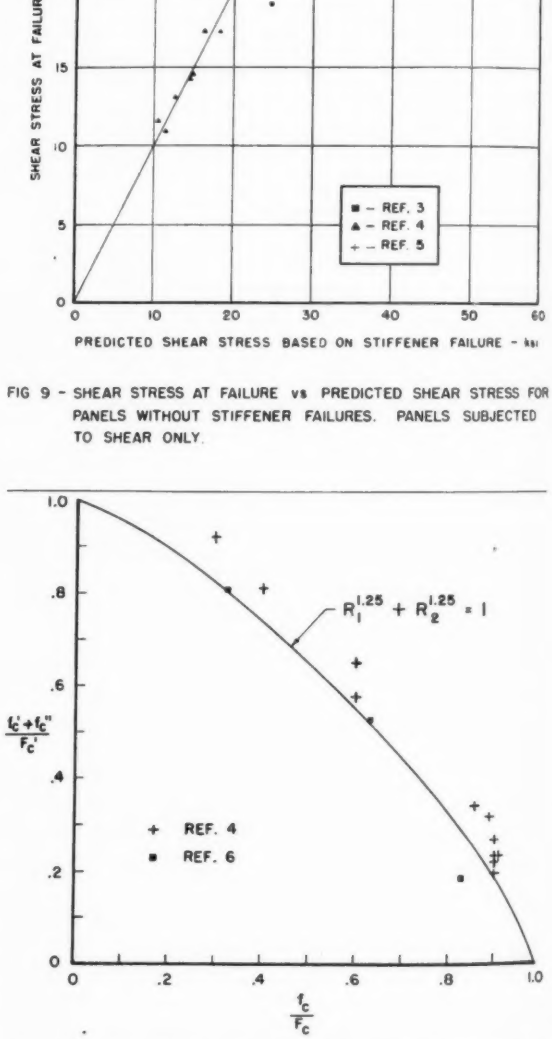

FIGURE 10 - INTERACTION OF COMPRESSION DUE TO SHEAR AND DIRECT COMPRESSION FOR PANELS WITH STIFFENER FAILURES. PANELS SUBJECTED TO SHEAR AND COMPRESSION.

Interaction for Stiffener Failure

(1) The ring spacing, stiffener spacing, stiffener section, skin gage, and the radius of the panel are known; hence, the factor ν may be calculated.

(2) Determine F_c' and F_c. These may be calculated by standard procedures. The allowable compression strength of a panel is often determined as a load per stiffener and skin rather than as a stress on stiffener plus effective skin. For the rest of this example, it will be assumed that P is the allowable compression load and p is the applied compression load.

(3) Assume a value for p.

(4) For the assumed value p, assume several values of f_s and obtain corresponding values of λ from Eq. (6). [λ involves f_{cg}, which is determined by $p/(A_{st} + bt)$.]

(5) From Table B, determine f_c' and f_c'' for assumed values of f_s and corresponding values λ.

(6) Determine value of f_s which makes

$$\left(\frac{f_c' + f_c''}{F_c'}\right)^{1.25} = 1 - \left(\frac{p}{P}\right)^{1.25}$$

(7) This value of f_s times t is then the shear flow that may be applied with the compression load p. Repeat this procedure for other values of p to complete the interaction for stiffener failure.

Interaction of Web Failure

The effect of compression on the ultimate shear strength of the web is small, since its only influence is to reduce the critical buckling shear stress, $F_{s_{cr.}}$, by the factor λ. The web failure curve with the effect of compression included may be obtained as follows:

(1) Compute η.

(2) Perform steps 3 and 4 under section above.

(3) Determine the value of f_s such that $f_s = F_s$, where F_s is given by Eq. (9). It should be noted that in these determinations $F_{s_{cr.}}$ must be multiplied by the factor λ. If the rivet factor $C_R < 0.75$, then an additional check must be made in accordance with Eq. (10). The value f_s times t is then the shear flow that will produce web failure.

The envelope of the stiffener failure curve and web failure curve forms the complete interaction curve for the panel. In plotting the curves, it is recommended that $p = 0$ be the first point investigated, since in this case λ is always equal to one and the trial-and-error solution involved in steps 4, 5, and 6 of the section above is eliminated. Once the value of f_s at $p = 0$ has been determined, it is possible to make a close first approximation as to what f_s will be at other values of p, and again labor of trial and error will be greatly reduced.

Conclusions

(1) Simplified formulas for the calculation of critical shear buckling stress of curved panels have been derived. Test values averaged 2.0 per cent higher than predicted values.

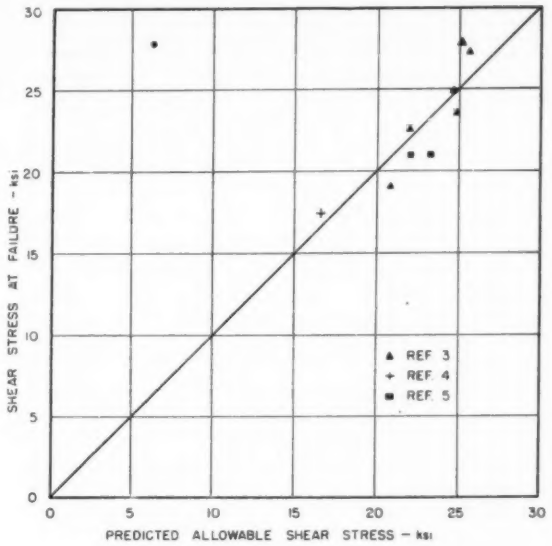

FIGURE 11. - SHEAR STRESS AT FAILURE vs PREDICTED ALLOWABLE SHEAR STRESS FOR PANELS WITH WEB FAILURES. PANELS SUBJECTED TO SHEAR ONLY.

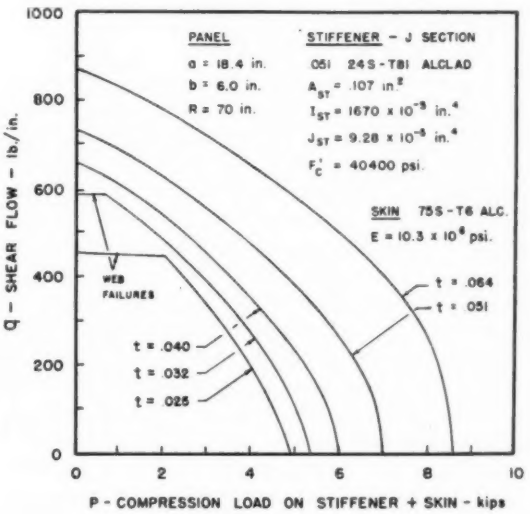

FIGURE 12. - EXAMPLE OF INTERACTION CURVES OF COMBINED SHEAR AND COMPRESSION ON CURVED PANELS.

(2) A method has been determined for predicting the ultimate strength of a stiffened curved panel subjected to shear. The average prediction is approximately 6 per cent conservative for longitudinal stiffener failure and 4 per cent conservative for web failure.

(3) A method has been determined for predicting the ultimate strength of a stiffened curved panel subjected to combined shear and compression. The average prediction is slightly less than 3.8 per cent conservative for longitudinal stiffener failure.

(*Concluded on page 126*)

Reverse-Flow and Variational Theorems for Lifting Surfaces in Nonstationary Compressible Flow

A. H. FLAX*

Cornell Aeronautical Laboratory, Inc.

SUMMARY

A reverse-flow theorem for compressible nonsteady flow, valid within the limits of linearized theory, is derived. This theorem gives a general class of relations between linearized solutions for lifting surfaces in direct and reverse flow. Based on the same considerations used to establish the theorem, an adjoint variational principle, which may be useful in approximate solutions of nonsteady lifting surface problems, is obtained. To illustrate the uses of the reverse-flow theorem, it is applied to the determination of relations between aerodynamic coefficients in direct and reverse flow and to the obtaining of influence functions for total lift, pitching moment, and rolling moment for a wing oscillating with arbitrary motion and surface deformation, in terms of the pressure distributions for simpler cases in reverse flow.

INTRODUCTION

REVERSE-FLOW THEOREMS for various cases of steady flow, valid within the limits of linearized theory, have been presented by von Kármán,[1] Hayes,[2] the author,[3] Munk,[4] Harmon,[5] and Brown.[6] The most general forms of these theorems have been given by Ursell and Ward[7] and by the author[8] using different methods of attack. It has been found that the general form of the theorem may be extended to nonstationary flows as well. The proof of this result for incompressible flow has been given previously, but the more general proof for compressible flow, both subsonic and supersonic, was left for the present paper. The derivation is completely analogous to that given for nonsteady incompressible flow, but due account must be taken of the fact that the velocity potential for compressible nonsteady flow satisfies a form of the wave equation rather than Laplace's equation. For convenience, the case of harmonic time variation will be considered. Other cases of variation in time follow from the result for harmonic motion by a direct application of the Fourier integral theorem.[9] Since the results obtained will be valid for all frequencies for which the linearized-flow equations themselves are valid, it follows that the results will also be valid for any time dependent motion of the airfoil which possesses a Fourier integral transform in the time variable. The unit step and unit impulse motions of the airfoil are, of course, among such motions, as are most others of practical interest.

Received February, 1952. Revised and received October 23, 1952.

* Head, Aerodynamic Research Department.

The results obtained will be seen to bear a certain formal relation to Helmholtz's reciprocal theorems in the theory of acoustics.[12] In the case where the airfoil is at rest with respect to the fluid, the classical Helmholtz theorems are, of course, directly applicable, but this case is of little interest in aerodynamics.

MATHEMATICAL FORMULATION

A nonstationary compressible inviscid flow to the usual linear approximation is characterized by the well-known wave equation in a moving coordinate system,[11]

$$\nabla^2\phi - \frac{1}{a_0^2}\left(\frac{\partial}{\partial t} + U_0\frac{\partial}{\partial x}\right)^2\phi = 0 \qquad (1)$$

where ϕ is the usual velocity potential, such that the perturbation velocity components along the x, y, and z axis (u, v, and w, respectively) are given by

$$u = \frac{\partial\phi}{\partial x}, \qquad v = \frac{\partial\phi}{\partial y}, \qquad w = \frac{\partial\phi}{\partial z}$$

a_0 is the velocity of sound in the free stream, and U_0 is the free-stream velocity along the x axis. The axes are shown in Fig. 1. The flow is irrotational and, in particular, $\partial u/\partial z - \partial w/\partial x = 0$. The pressure at any point (to within an arbitrary additive function of time) is, according to the linearized Bernoulli equation,

$$\pi = P/\rho_0 = U_0 u + (\partial\phi/\partial t) \qquad (2)$$

where ρ_0 is the free-stream density and P is the pressure at any point. It may readily be seen that $u = (\partial\phi/\partial x)$ and $\partial\phi/\partial t$ satisfy Eq. (1) by simply differentiating Eq.

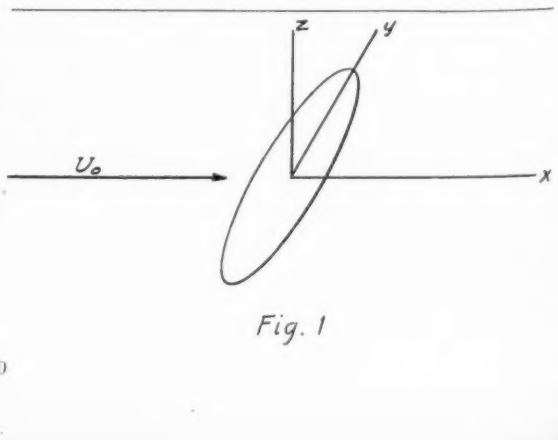

Fig. 1

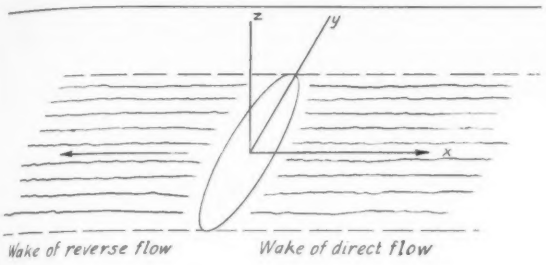

Fig. 2

(1) with respect to either x or t. Thus, π also satisfies Eq. (1).

The specified motion of the boundary of the lifting surface lying approximately in the plane $z = 0$ is given for harmonic oscillation by

$$z = z(x, y, t) = z_0(x, y)e^{i\omega t} \tag{3}$$

The boundary condition for the flow is

$$\frac{\partial \phi_0}{\partial z} = w_0 = U_0 \frac{\partial z_0}{\partial x} + i\omega z_0 \tag{4}$$

where $\phi = \phi_0(x, y, z)e^{i\omega t}$ and $w = w_0(x, y, z)i\omega t$. It is, of course, necessary to admit complex values of ϕ_0 and w_0 to take care of the phase differences that may exist. Over that part of the plane $z = 0$ occupied by the lifting surface, there is a pressure discontinuity, $\Delta\pi$, between the upper and lower surfaces, but everywhere else in the fluid $\Delta\pi$ must be zero. At the trailing edge, the Kutta condition requires that $\Delta\pi = 0$, in order that π go smoothly into its value in the wake.

Now if there be considered a flow over the same plan form with the direction of the free-stream velocity U_0 reversed, oscillating at the same frequency, there will be associated with this flow functions, $\bar{\phi}$ and $\bar{\pi}$, which have properties and imposed conditions similar to those of ϕ and π. For the reverse flow case, however, the wake trails from what was in the first case the leading edge, the Kutta conditions being applied there. It should be noted in each case that, across the plane $z = 0$, $\Delta\phi$ and Δu differ from zero only on the wing and on the respective wakes. The wakes in the two cases are illustrated in Fig. 2. In each case, there is a singularity in u and π of the type $1/\sqrt{d}$ at the leading edge, d being the distance from the edge.[6–8]

If the directions of positive x, y, and z and positive perturbation velocity $\bar{u}$, $\bar{v}$, $\bar{w}$ are held the same in the reverse flow case for convenience, the equation satisfied by the velocity potential $\bar{\phi}$ is

$$\nabla^2\bar{\phi} - \frac{1}{a_0^2}\left(\frac{\partial}{\partial t} - U_0\frac{\partial}{\partial x}\right)^2\bar{\phi} = 0 \tag{5}$$

The pressure is given by

$$\bar{\pi} = \bar{P}/\rho_0 = -U_0\bar{u} + (\partial\bar{\phi}/\partial t) \quad \ldots\ldots (6)$$

$\bar{\pi}$ also satisfies Eq. (5)

The expressions for π and $\bar{\pi}$ may be specialized to harmonic motion to give

$$\pi = U_0 u + i\omega\phi \tag{7}$$

$$\bar{\pi} = -U_0\bar{u} + i\omega\bar{\phi} \tag{8}$$

Similarly, Eqs. (1) and (5) may be written for the case of harmonic motion

$$\nabla^2\phi - M^2\frac{\partial^2\phi}{\partial x^2} - 2i\frac{\omega}{a_0}M\frac{\partial\phi}{\partial x} + \frac{\omega^2}{a_0^2}\phi = 0 \tag{9}$$

$$\nabla^2\phi - M^2\frac{\partial^2\bar{\phi}}{\partial x^2} + 2i\frac{\omega}{a_0}M\frac{\partial\bar{\phi}}{\partial x} + \frac{\pi^2}{a_0^2}\bar{\phi} = 0 \tag{10}$$

where $M = U_0/a_0$ is the free-stream Mach Number. It is of interest to note that the two partial differential equations are adjoint in the usual sense, thus further illustrating the fact, already brought out for the integral equations of lifting surfaces in steady flow,[8] that reverse flows satisfy adjoint equations.

Consider the volume integral

$$I_0 = \int_v\int\int\left[\bar{\pi}\left(\nabla^2\phi - M^2\frac{\partial^2\phi}{\partial x^2} - 2i\frac{\omega}{a_0}M\frac{\partial\phi}{\partial x} + \frac{\omega^2}{a_0^2}\phi\right) - \phi\left(\nabla^2\bar{\pi}^2 - M^2\frac{\partial^2\bar{\pi}}{\partial x^2} + 2i\frac{\omega}{a_0}M\frac{\partial\bar{\pi}}{\partial x} + \frac{\omega^2}{a_0^2}\bar{\pi}\right)\right]dv \tag{11}$$

where v, the volume of integration, is taken to be all space outside the wing. It should be noted that Eqs. (1) and (5) are satisfied by ϕ and $\bar{\phi}$ everywhere outside the lifting surface except in the respective wakes and that, as x approaches $+\infty$ in the wake of the direct flow, $\bar{\phi}$ and $\bar{\pi}$ go to zero, while as x approaches $-\infty$ in the wake of the reverse flow, ϕ and π go to zero. Further, at the leading edge, where the derivatives of ϕ are singular, $\bar{\pi}$ is zero because of the Kutta condition in the reverse flow and, similarly, for π and $\bar{\phi}$. Thus, a simple extension of Green's theorem may be applied to the volume integral, using as the fluid boundary, the plane $z = 0$, from $x = -\infty$ to $x = +\infty$.

It will be convenient to consider the terms of the integral I_0 in pairs of corresponding terms from the first and second parentheses. The first pair of terms gives

$$I_1 = \int\int_V\int (\bar{\pi}\nabla^2\phi - \phi\nabla^2\bar{\pi})dv \tag{12}$$

Green's theorem may be applied directly to I_1 to give

$$I_1 = \int\int_{A+,\,A-} \bar{\pi}\frac{\partial\phi}{\partial n}\,dS - \int\int_{A+,\,A-} \phi\frac{\partial\bar{\pi}}{\partial n}\,dS \tag{13}$$

where the area of integration A is the entire plane $z = 0$ from $x = -\infty$ to $x = +\infty$ and from $y = -\infty$ to $y = +\infty$. The subscript $+$ denotes the positive side of the plane, while the subscript $-$ denotes the negative side. The n direction is positive for the outward normal of the bounding plane. Because of the antisymmetry of the lift problem,

$$\left.\begin{gathered}\left(\frac{\partial\phi}{\partial n}\right)_+ = \frac{\partial\phi}{\partial z};\quad \left(\frac{\partial\phi}{\partial n}\right)_- = -\frac{\partial\phi}{\partial z} \\ \phi_+ = -\phi_-;\quad \pi_+ = -\pi_-\end{gathered}\right\} \tag{14}$$

Thus,

$$I_1 = \int\int_A \bar{\pi}\,\frac{\partial\phi}{\partial z}\,dS - \int\int_A \phi\,\frac{\partial\bar{\pi}}{\partial z}\,dS \tag{15}$$

where only values on the $+$ side of the plane $z = 0$ need now be considered, but P and π may be taken, in surface integrals over the plane $z = 0$, to represent the difference in pressure between upper and lower surface.

The second pair of terms from the two parentheses in I_0 gives

$$I_2 = -M^2\int\int\int\left(\bar{\pi}\,\frac{\partial^2\phi}{\partial x^2} - \phi\,\frac{\partial^2\bar{\pi}}{\partial x^2}\right)dv \tag{16}$$

This may be written

$$I_2 = -M^2\int\int\int_V \frac{\partial}{\partial x}\left(\bar{\pi}\,\frac{\partial\phi}{\partial x} - \phi\,\frac{\partial\bar{\pi}}{\partial x}\right)dv \tag{17}$$

Carrying out the integration with respect to x gives a surface integral,

$$I_2 = M^2\int\int_A\left(\bar{\pi}\,\frac{\partial\phi}{\partial x} - \phi\,\frac{\partial\bar{\pi}}{\partial x}\right)\cos(n\cdot x)\,dS \tag{18}$$

The direction cosine of the angle between the n direction (in this case, the z direction) and x is zero, so that $I_2 = 0$.

The third such pair of terms in I_0 gives

$$I_3 = -2i\,\frac{\omega}{a_0}\,M\int\int\int_V\left(\bar{\pi}\,\frac{\partial\phi}{\partial x} + \phi\,\frac{\partial\bar{\pi}}{\partial x}\right)dv \tag{19}$$

which may be written

$$I_3 = -2i\,\frac{\omega}{a_0}\,M\int\int\int_V \frac{\partial}{\partial x}\,(\bar{\pi}\phi)\,dv \tag{20}$$

Performing the integration on x gives

$$I_3 = 2i\,\frac{\omega}{a_0}\,M\int\int_A (\bar{\pi}\phi)\cos(n\cdot x)\,dS \tag{21}$$

which is zero, since $\cos(n\cdot x) = 0$ as for I_2.

The remaining pair of terms in I_0 gives

$$I_4 = \frac{\omega^2}{a_0^2}\int\int\int_V (\bar{\pi}\phi - \phi\bar{\pi})\,dv \tag{22}$$

which is identically zero.

I_0 is equal to the sum of I_1, I_2, I_3, and I_4. It has been shown that I_2, I_3, and I_4 are zero, so that $I_0 = I_1 \ldots I_0$ however, is clearly also zero, since ϕ and $\bar{\pi}$ satisfy wave equations of the forms Eqs. (1) and (5), respectively. Thus, $I_1 = 0$ or

$$\int\int_A \bar{\pi}\frac{\partial\phi}{\partial z}\,dS - \int\int_A \phi\,\frac{\partial\bar{\pi}}{\partial z}\,dS = 0 \tag{23}$$

To put this result in a more symmetrical form, it is expedient to write, from Eq. (8),

$$\frac{\partial\bar{\pi}}{\partial z} = -U_0\frac{\partial\bar{u}}{\partial z} + i\omega\,\frac{\partial\bar{\phi}}{\partial z} \tag{24}$$

From the irrotationality condition,

$$\partial\bar{u}/\partial z = \partial\bar{w}/\partial x$$

Also, by definition,

$$\bar{w} = \partial\bar{\phi}/\partial z;\quad w = \partial\phi/\partial z$$

Then,

$$\partial\bar{\pi}/\partial z = -U_0(\partial\bar{w}/\partial x) + i\omega\bar{w} \tag{25}$$

Substituting this result into Eq. (23) gives

$$\int\int_A \bar{\pi}\,w\,dS - \int\int_A \phi\left(-U_0\frac{\partial\bar{w}}{\partial x} + i\omega\bar{w}\right)dS = 0 \tag{26}$$

The first term of the second integral may be integrated by parts on x, and since at $x = -\infty$, $\phi = 0$, while at $x = +\infty$, $\bar{w} = 0$, there results

$$U_0\int\int_A \phi\,\frac{\partial\bar{w}}{\partial x}\,dS = -U_0\int\int_A \frac{\partial\phi}{\partial x}\,\bar{w}\,dS = -U_0\int\int_A u\bar{w}\,dS \tag{27}$$

Substituting Eq. (27) into Eq. (26),

$$\int\int_A \bar{\pi}w\,dS - \int\int_A (U_0u + i\omega\phi)\bar{w}\,dS \tag{28}$$

But according to Eq. (7), the term in parentheses in the second integral is simply π, so that

$$\int\int \bar{\pi}\,w\,dS - \int\int \pi\bar{w}\,dS = 0$$

or

$$\int\int \bar{\pi}\,w\,dS = \int\int \pi\bar{w}\,dS \tag{29}$$

where the integrations are over the wing plan form only, since π and $\bar{\pi}$ are zero over the remainder of the plane $z = 0$.

This is the desired reverse-flow relation for compressible nonsteady flow. In the case of steady flow ($w = 0$), Eq. (29) reduces to the theorems of Ursell and Ward[7] and the author,[8]

$$\int\int u\bar{w} = \int\int \bar{u}w \tag{30}$$

The Variational Principle

As in the case of steady flow, the foregoing considerations may also be applied to the derivation of an adjoint variational principle, which provides a convenient basis for the approximate solution of lifting-surface problems. The type of variational problem considered is one in which solutions satisfying the partial differential equation exactly but not the boundary conditions are employed. This is the common case in lifting-surface problems and is typified by the methods that involved building up a solution from distributions of sources, doublets, and elementary horseshoe vortices. Thus, consider

$$\delta H = \delta \int\int_A \left[(w\bar{\pi} + \bar{w}\pi) - \frac{1}{2}\left(\bar{\pi}\frac{\partial\phi}{\partial n} + \pi\frac{\partial\bar{\phi}}{\partial n} \right) \right] dS \tag{31}$$

where δ is the usual symbol for variation according to the calculus of variations and w and $\bar{w}$ are the specified arbitrary boundary conditions for $\partial\phi/\partial n$ and $\partial\bar{\phi}/\partial n$, respectively, on the wing plan form. The two problems, one in direct flow and the other in reverse flow, are independent, and, accordingly, variations with respect to $\delta\phi$ and $\delta\bar{\phi}$ or $\delta\pi$ and $\delta\bar{\pi}$ are independent. The variations are arbitrary over the class of flows that satisfy the Kutta condition for direct and reverse flows, give finite downwash over the airfoil, and satisfy the differential equations, Eqs. (1) and (5). The variation of H may be written

$$\delta H = \int\int_A \left[(w\delta\bar{\pi} + \bar{w}\delta\pi) - \frac{1}{2}\left(\delta\bar{\pi}\frac{\partial\phi}{\partial n} + \delta\pi\frac{\partial\bar{\phi}}{\partial n} + \bar{\pi}\frac{\partial\delta\phi}{\partial n} + \pi\frac{\partial\delta\bar{\phi}}{\partial n} \right) \right] dS \tag{32}$$

Returning to the derivation of Eq. (29), it will be observed that the only requirements on ϕ, π, $\bar{\phi}$, and $\bar{\pi}$ related to their satisfying the appropriate wave equation for moving coordinates; no requirements as to boundary condition were imposed. Thus, Eq. (29) may be applied to the last two terms of Eq. (32) to give

$$\left.\begin{aligned} \int\int_A \bar{\pi}\frac{\partial\delta\phi}{\partial n}\,dS &= \int\int_A \delta\pi\frac{\partial\bar{\phi}}{\partial n}\,dS \\ \int\int_A \pi\frac{\partial\delta\bar{\phi}}{\partial n}\,dS &= \int\int_A \delta\bar{\pi}\frac{\partial\phi}{\partial n}\,dS \end{aligned}\right\} \tag{33}$$

Substituting Eq. (33) into (32),

$$\delta H = \int\int_A \left[\left(w - \frac{\partial\phi}{\partial n} \right)\delta\bar{\pi} + \left(\bar{w} - \frac{\partial\bar{\phi}}{\partial n} \right)\delta\pi \right] dS \tag{34}$$

In the vicinity of the correct solution, ϕ and $\bar{\phi}$ corresponding to w and $\bar{w}$, respectively,

$$w = \partial\phi/\partial n; \quad \bar{w} = \partial\bar{\phi}/\partial n \tag{35}$$

so that

$$\delta H = \delta \int_A\int \left[(w\bar{\pi} + \bar{w}\pi) - \frac{1}{2}\left(\bar{\pi}\frac{\partial\phi}{\partial n} + \pi\frac{\partial\bar{\phi}}{\partial n} \right) \right] ds = 0 \tag{36}$$

which is the variational theorem for this case. The variational method for approximate solution of nonsteady lifting-surface problems may be applied in the same manner as for steady-flow problems, by application of a Rayleigh-Ritz type of procedure. This has been more completely discussed in a previous paper on the steady-flow case.[8] Further extensions of these ideas have been developed; it is possible to choose the variation functions $\bar{\pi}$ corresponding approximately to such $\bar{w}$'s as will make the total lift, total pitching moment, total rolling moment, etc., approximately stationary. The details of such procedures will be discussed in a later paper.

It is also possible to derive a variational principle in which $\delta\phi$, $\delta\pi$, $\delta\bar{\phi}$, and $\delta\bar{\pi}$ do not satisfy the partial differential equations but rather, the boundary conditions. At present, these appear to be of less interest in lifting-surface problems.

Applications of the Reverse-Flow Theorem

Applications of the reverse-flow theorem for nonstationary flow are similar to those for stationary flow which have been given in detail in several papers. First, they may be used to establish relations between the aerodynamic coefficients for a wing in direct and reverse flow. These are of interest in the case where one of the solutions is already known or more easily obtained than the other. Second, and perhaps more important, influence functions for total lift, pitching moment, and rolling moment are easily obtained in terms of the pressure distributions over the wing in reverse flow with certain simple prescribed boundary conditions. These are analogous to the generalized Munk formulas already given for steady flow;[8] they are so called because, in the limiting case of two-dimensional incompressible flow, they reduce to Munk's integral formulas for the total lift and moment on an airfoil with an arbitrary distribution of local angle of attack. The cases of two-dimensional flow, lifting-line approximations, or wings having a spanwise axis of symmetry are of particular interest, since, in these cases, a reversal of flow direction gives a flow around essentially the same wing. Thus, it is not necessary to consider a separate reverse-flow problem at all. A few specific applications will be illustrated below. These will serve to illustrate the manner in which the general theorem may be applied.

(1) *Relations Between Lifts Due to Vertical Motion*

Let

$$\left.\begin{aligned} z_1/c &= (h/c)e^{i\omega t} \\ \bar{z}_1/c &= (h/c)e^{i\omega t} \end{aligned}\right\} \tag{37}$$

corresponding to vertical motion of the surface, where c is any representative dimension of the plan form. By Eq. (4),

$$\left.\begin{aligned} w_1 &= i\omega c(h/c)e^{i\omega t} \\ \bar{w}_1 &= i\omega c(h/c)e^{i\omega t} \end{aligned}\right\} \tag{38}$$

Applying the general theorem, Eq. (29), it may be noted that since w and $\bar{w}$ are equal and constant, they may be taken out from under the integrals and canceled, leaving the integrals of the pressure over the surface equal. Thus, for vertical motion, the lifts in direct and reverse flow are equal. In all that follows, lifts upward are defined as positive.

(2) *Relation Between Lifts and Pitching Moments for Pitching Rotation*

For the case when the wing is rotating about the axis $x = 0$ (actually, the choice of origin is arbitrary) in both the direct and reverse flows, a more complex relation is obtained. Let

$$\left.\begin{aligned} z_2 &= xe^{i\omega t} \\ w_2 &= (U_0 + i\omega x)e^{i\omega t} \end{aligned}\right\} \tag{39}$$

and let

$$\left.\begin{aligned} \bar{z}_2 &= -xe^{i\omega t} \\ \bar{w} &= [-U_0(\partial \bar{z}_0/\partial x) + i\omega z_0]e^{i\omega t} \end{aligned}\right\} \tag{40}$$

or

$$\bar{w}_2 = (U_0 - i\omega x)e^{i\omega t} \tag{41}$$

Applying the general theorem,

$$\int\int P_2\left(1 - i\frac{\omega c}{U_0}\frac{x}{c}\right)dS = \int\int \bar{P}_2\left(1 + i\frac{\omega c}{U_0}\frac{x}{c}\right)dS$$

The integrals of P_2 and $\bar{P}_2$ over the surface are simply the lifts L_2 and $\bar{L}_2$, respectively, and, also,

$$\left.\begin{aligned} \int\int P_2(-x/c)dS &= M_2/c \\ \int\int \bar{P}_2(x/c)dS &= \bar{M}_2/c \end{aligned}\right\} \tag{42}$$

where a positive moment is defined as nose-up for either direct or reverse flow. Finally, then,

$$L_2 + i\frac{\omega c}{U_0}\frac{M_2}{c} = \bar{L}_2 + i\frac{\omega c}{U_0}\frac{\bar{M}_2}{c} \tag{43}$$

If, for instance, the axis of x is along the quarter-chord position for a rectangular wing in direct flow, it is along the three-quarter-chord position in the reverse flow, and Eq. (42) provides a relation between the lifts and moments for oscillating rotations around these positions.

(3) *Cross Relation Between Lifts and Pitching Moment for Pitching Rotation and Vertical Translation*

Let the two cases considered be w_1 and P_1 of 1 and $\bar{w}_2$ and $\bar{P}_2$ of 2. Applying the general theorem for $\theta_0 = h/c = 1$,

$$\int\int P_1\left(1 - i\frac{\omega c}{U_0}\frac{x}{c}\right)dS = \int\int \bar{P}_2 i\frac{\omega c}{U_0}\,dS$$

or using the previous definition of lift and moment,

$$L_1 + i\frac{\omega c}{U_0}\frac{M_1}{c} = i\frac{\omega c}{U_0}\bar{L}_2 \tag{44}$$

where L_1 is the lift and M_1 the moment about the axis $x = 0$ for vertical translation of the wing in direct flow and where $\bar{L}_2$ is the lift of the wing rotating about the axis $x = 0$ in reverse flow. For a two-dimensional wing or one having a spanwise axis of symmetry (such as a rectangular wing), this provides a relation between the lifts and moments of the wing for two different motions with the same flow direction.

(4) *Relation Between Rolling Moments of Wings Oscillating in Roll*

Let

$$\left.\begin{aligned} z_3 &= aye^{i\omega t} \\ \bar{z}_3 &= aye^{i\omega t} \end{aligned}\right\} \tag{45}$$

$$\begin{aligned} w_3 &= i\omega aye^{i\omega} \\ \bar{w}_3 &= i\omega aye^{i\omega t} \end{aligned}$$

Applying the general theorem,

$$\int\int P_3 y\,dS = \int\int \bar{P}_3 y\,dS \tag{46}$$

But $\int\int P_3 y\,dS$ is the rolling moment in direct flow and $\int\int \bar{P}_3 y\,dS$ is the rolling moment in reverse flow, so that the rolling moments due to oscillation in roll are equal.

(5) *Influence Function for Lift*

The total lift for a plan form executing any oscillatory motion whatever may easily be obtained in terms of the pressure distribution of the plan form in reverse flow executing vertical translational oscillations only.

Let

$$\left.\begin{aligned} \bar{z}_1/c &= e^{i\omega t} \\ \bar{w}_1 &= i\omega c\, e^{i\omega t} \end{aligned}\right\} \tag{47}$$

where again c is some representative dimension and

$$\left.\begin{aligned} z/c &= (z_0/c)(x, y)e^{i\omega t} \\ w &= U_0(\partial z_0/\partial x) + i\omega c(z_0/c) \end{aligned}\right\} \tag{48}$$

To $\bar{w}_1$ corresponds the presumably known pressure distribution $\bar{P}_1$, while to w corresponds the unknown distribution P.

Applying the general theorem,

$$\int\int\left(\frac{\partial z_0}{\partial x}+U\,\frac{\omega c}{U_0}\,\frac{z_0}{c}\right)\bar{P}_1\,dS=\frac{i\omega c}{U_0}\int\int P\,dS$$

then,

$$L=\int\int P\,dS=\frac{U_0}{i\omega c}\int\int\left(\frac{\partial z_0}{\partial x}+\frac{i\omega c}{U_0}\,\frac{z_0}{c}\right)\bar{P}_1\,dS \tag{49}$$

gives the total lift for the wing in direct flow with arbitrary z_0.

It is of interest to compare this last result with a formula given by Schwartz[12] for the total lift on a two-dimensional oscillating airfoil oscillating with arbitrary $w(x)$. In the present notation, Schwartz[13] gives for the pressure distribution on a two-dimensional wing oscillating in vertical translation in incompressible flow

$$P_1=\rho U_0^2e^{i\omega t}\left[(1+T)i\,\frac{\omega c}{U_0}\sqrt{\frac{1-x}{1+x}}+2\left(\frac{i\omega c}{U_0}\right)^2\sqrt{1-x^2}\right] \tag{50}$$

where T is a function of $\omega c/U_0$ only.

For a reversal of flow direction, this becomes

$$\bar{P}_1=\rho U_0^2e^{i\omega t}\left[(1+T)\,\frac{\omega c}{U_0}\sqrt{\frac{1+x}{1-x}}+2\left(\frac{i\omega c}{U_0}\right)^2\sqrt{1-x^2}\right] \tag{51}$$

Substituting this result into Eq. (49), there is obtained, for the lift on an airfoil with arbitrary $w(x,t)=w_0(x)e^{i\omega t}$,

$$L=\frac{U_0}{i\omega c}\int\frac{w(x,t)}{U_0}\,\rho U_0^2\left[(1+T)\,\frac{i\omega c}{U_0}\sqrt{\frac{1+x}{1-x}}+2\left(\frac{i\omega c}{U_0}\right)^2\sqrt{1-x^2}\right]dx$$

or

$$L=2\rho U_0\int w(x,t)\left[\frac{(1+T)}{2}\sqrt{\frac{1+x}{1-x}}+\frac{i\omega c}{U_0}\sqrt{1-x^2}\right]dx \tag{52}$$

This is just the result obtained by Schwartz as a result of rather lengthy calculation.

---

(6) *Influence Function for Pitching Moment*

An influence function for the pitching moment on a wing performing oscillations with arbitrary $w_0(x,\ y)$ may also be obtained in terms of a combination of simple solutions for the wing in reverse flow. Let

$$\bar{z}=-xe^{i\omega t}+(U_0/i\omega)e^{i\omega t} \tag{53}$$

Then

$$\bar{w}=-U_0e^{i\omega t}+i\omega xe^{i\omega t}+U_0e^{i\omega t}$$

or

$$\bar{w}=-i\omega xe^{i\omega t}$$

It may be seen from Eq. (53) that the pressure distribution $\bar{P}$ corresponds to the superposition of the reverse-flow solutions for the wing oscillating in rotation about the axis $x=0$ and for the wing translating vertically with amplitude $U_0/i\omega$. Applying the general theorem,

$$\frac{i\omega c}{U_0}\int\int P\cdot\left(-\frac{x}{c}\right)dS=\int\int\bar{P}_1\,\frac{w}{U_0}\,dS$$

or

$$\frac{M}{c}=\frac{U_0}{i\omega c}\int\int\bar{P}_1\,\frac{w}{U_0}\,dS \tag{54}$$

which gives the desired result for pitching moment about the axis $x=0$. The formula given by Schwartz for pitching moment in the two-dimensional incompressible case has been checked by Eq. (54).

(7) *Influence Function for Rolling Moment*

The influence function for the total rolling moment on a wing oscillating with arbitrary $w_0(x,\ y)$ is also readily obtained in terms of the pressure distribution on the wing in reverse flow oscillating in roll. Let

$$\left.\begin{aligned}\bar{z}&=ye^{i\omega t}\\ \text{or}\qquad\bar{w}&=i\omega ye^{i\omega t}\end{aligned}\right\} \tag{55}$$

with pressure distribution $\bar{P}_1$ presumed known, and $w=w_0(x,\ y)e^{i\omega t}$ with pressure distribution P presumed unknown.

Applying the general theorem,

$$\frac{i\omega}{U_0}\int\int Py\,dS=\int\int\bar{P}\,\frac{w}{U_0}\,dS$$

or

$$\frac{1}{c}\int\int P_y\,dS = \frac{U_0}{i\omega c}\int\int \bar{P}_w\,dS \qquad (56)$$

The integral on the left side is the rolling moment that gives the required result.

Conclusions

A general relation between linearized solutions of lifting-surface problems in direct and reverse flow has been established for compressible nonsteady flows. This relation is a direct extension of that already known for steady-flow solutions. On the basis of the analysis leading to this result, an adjoint variational principle, also the counterpart of one already known for steady flows, has been established. This may be useful in the approximate solution of lifting-surface problems in nonsteady flow. Several applications of the general theorem to problems in nonstationary wing theory have been given. These included determination of relations between certain aerodynamic coefficients for plan forms in direct and reverse flow and establishment of influence functions for total lift, pitching moment, and rolling moment for wings oscillating with arbitrary motion and deformation of the plan form. The influence functions were found to be certain simple solutions for the plan form in reverse flow.

References

[1] von Kármán, Th., *Supersonic Aerodynamics—Principles and Applications*, Journal of the Aeronautical Sciences, Vol. 14, No. 6, pp. 373–409, July, 1947.

[2] Hayes, W. D., *Linearized Supersonic Flow*, North American Aviation, Inc., Report No. AL-222, June 18, 1947.

[3] Flax, A. H., *Relations Between the Characteristics of a Wing and Its Reverse in Supersonic Flow*, Journal of the Aeronautical Sciences, Vol. 16, No. 8, pp. 496–504, August, 1949.

[4] Munk, M. M., *The Reversal Theorem of Linearized Supersonic Airfoil Theory*, Journal of Applied Physics, Vol. 21, No. 2, pp. 159–161, February, 1950.

[5] Harmon, S., *Theoretical Relations Between the Stability Derivatives of a Wing in Direct and in Reverse Supersonic Flow*, N.A.C.A. T.N. No. 1943, September, 1949.

[6] Brown, C. E., *The Reversibility Theorem for Thin Airfoils in Subsonic and Supersonic Flow*, N.A.C.A. T.N. No. 1944, September 1949.

[7] Ursell, F., and Ward, G. N., *On Some General Theorems in the Linearized Theory of Compressible Flow*, Quarterly Journal of Mechanics & Applied Mathematics, Vol. III, Part 3, pp. 326–348, September, 1950.

[8] Flax, A. H., *General Reverse Flow and Variational Theorems in Lifting-Surface Theory*, Journal of the Aeronautical Sciences, Vol. 19, No. 6, pp. 361–374, June 1952.

[9] Webster, A. G., *Partial Differential Equations of Mathematical Physics*, p. 219; G. E. Steckert & Company, 1933.

[10] Rayleigh, Lord, *Theory of Sound*, Vol. II, pp. 145–147; Dover Publications, Inc., 1945.

[11] Reissner, E., *On the General Theory of Thin Airfoils for Non-Uniform Motion*, N.A.C.A. T.N. No. 946, August, 1944.

[12] Schwartz, L., *Berechnung der Druckverteilung einer harmonish sich verformenden Tragfläche in ebener Strömung*, Luftfahrtforschung, Vol. 17, pp. 379–386, 1940.

[13] Söhngen, H., Schwartz, L., and Dietze, F., Three Papers from Conference on "Wing and Tail Surface Oscillations," Munich, March 6–8, 1941. Also, N.A.C.M. T.M. No. 1306, August, 1951.

Analysis of Stiffened Curved Panels Under Shear and Compression

(*Concluded from page 119*)

References

[1] Moore, R. L., and Wescoat, C., *Torsion Tests of Stiffened Circular Cylinders*, N.A.C.A. Advanced Restricted Report No. 4 E 31, 1944.

[2] Clark, J. W., and Moore, R. L., *Torsion Tests of Aluminum Alloy Stiffened Circular Cylinders*, Unpublished Alcoa Report No. 12-50-15-A, 1951.

[3] Kuhn, Paul, and Peterson, James P., *A Summary of Diagonal Tension*, N.A.C.A. T.N. No. 2662, 1952. (N.A.C.A. T.N. No. 1481, 1947, *Diagonal Tension in Curved Webs.*)

[4] Anderson, P. N., *Combined Compression and Shear in Skin and Stiffener Combinations*. Douglas Aircraft Company Report No. 3021, 1941.

[5] Goodman, Stanley, *Tests of Reinforced Curved Sheet in Shear*, National Bureau of Standards Lab. No. 64180 PRI, 1949.

[6] Peterson, James P., *Experimental Investigation of Stiffened Circular Cylinders Subjected to Combined Torsion and Compression*, N.A.C.A. T.N. No. 2188, 1950.

[7] Wagner, Herbert, *Flat Sheet Metal Girders with Very Thin Metal Web*, N.A.C.A. T.M. No. 606, 1931.

[8] Kuhn, Paul, and Peterson, James P., *Strength Analysis of Stiffened Beam Webs*, N.A.C.A. T.N. No. 1364, 1947.

[9] Batdorf, S. B., *A Simplified Method of Elastic Stability Analysis for Thin Cylindrical Shells*, N.A.C.A. Report No. 874, 1947.

[10] Seydel, E., *The Critical Shear Load of Rectangular Plates*, N.A.C.A. T.M. No. 705, 1933.

[11] Levin, L. R., and Sandler, C. W., Jr., *Strength Analysis of Stiffened Thick Beam Webs*, N.A.C.A. T.N. No. 1820, 1949.

Differential Shear-Flow Analysis for Nonprismatic Semimonocoque Beams

WILLIAM B. KING* AND WALTER R. GARRISON†

Boeing Airplane Company

SUMMARY

This paper gives the derivation of a method for obtaining the shear-flow distribution in a nonprismatic semimonocoque beam with nonlinear axial-load variations due to externally applied loads. This method is based on the actual rates of change of segment axial loads at a particular station rather than the average rate of change of segment axial loads between two reasonably separated stations. The particular application presented is for a wing; however, the method is applicable to any semimonocoque structure. It also has special adaptations for many loading conditions at each station.

The shear-flow distribution may be determined for each component of the loading condition such as torsion and beam and chord shear and moment. The location of the shear center may be determined if the shear flow due to pure torsion is desired.

This method of analysis is adaptable to International Business Machine operations. The IBM calculations may be performed on machines such as the relatively slow 602 A Multiplier or the faster Card Program Sequence Calculator. The time required by IBM to calculate and check the shear center and unit shear flows and determine, for ten complete loading conditions, the resultant shears for a 20-segment station is approximately 30 min.

The results obtained by using the method presented in this paper on two beams, one with straight surfaces and one with curved surfaces, are compared with those obtained by VQ/I and the "Unit Method of Beam Analysis."[1]

SYMBOLS

a	=	segment area
A	=	total section area
c.g.	=	center of gravity
C_1	=	$1/(I_X I_Z - I_{XZ}^2)$
C_2	=	$C_1 I_{XZ}$
C_3	=	$C_1 I_X$
C_4	=	$C_1 I_Z$
E	=	modulus of elasticity
f	=	axial stress due to bending
G	=	shear modulus
h_X	=	chordwise coordinate with respect to l.r.a.
h_Z	=	beamwise coordinate with respect to l.r.a.
I_X, I_Z	=	moments of inertia about X and Z axes, respectively
I_{XZ}	=	product of inertia
l.r.a.	=	load reference axis
Δl	=	periphery of the skin or spar web between two adjacent stiffeners
M_X, M_Z	=	bending moments about the X and Z axes, respectively
n	=	segment number (counting clockwise)
N	=	total number of segments in a particular section
P	=	segment axial load
ΔP	=	difference in segment axial loads at two adjacent sections
q	=	corrected shear flow
q_o	=	correcting shear flow
q_u	=	uncorrected shear flow
Q	=	first moment of area
s	=	twice the sweep area enclosed by the skin or spar web ℄ between two adjacent stiffeners and the section c.g.
s.c.	=	shear center
S	=	twice the section enclosed area = Σ_s
t	=	skin or spar web thickness
$T_{\text{l.r.a.}}$	=	torsion moment about Y axis through the l.r.a.
$T_{\text{s.c.}}$	=	torsion moment about Y axis through the s.c.
V_X, V_Z	=	shear loads parallel to X and Z axes, respectively
w.b.p.	=	wing beam plane
w.c.p.	=	wing chord plane
x	=	segment c.g. chordwise coordinate with respect to the section c.g.
$x_{\text{s.c.}}$	=	s.c. chordwise coordinate with respect to the section c.g.
$\bar{x}$	=	section c.g. chordwise coordinate with respect to w.b.p.
X	=	horizontal axis (chordwise)
y	=	section spanwise coordinate with respect to the wing tip
Δy	=	spanwise distance between two stations
Y	=	horizontal axis (spanwise)
z	=	segment c.g. beamwise coordinate with respect to the section c.g.
z_{n} ℄	=	skin ℄ beamwise coordinate at segment n with respect to the section c.g.
$z_{\text{s.c.}}$	=	s.c. beamwise coordinate with respect to the section c.g.
$\bar{z}$	=	section c.g. beamwise coordinate with respect to w.c.p.
Z	=	vertical axis (beamwise)
δ	=	shearing strain
$( )'$	=	d/dy
$\stackrel{s}{=}$	=	should equal

Subscripts V_X, V_Z, M_X, M_Z, and T refer to segment axial loads or shear flow, which are results of the indicated loading condition.

Received March 26, 1952. Revised and received September 19, 1952.

* Senior Group Engineer, Stress Unit, Seattle Division.

† Stress Analyst, Stress Unit, Seattle Division.

INTRODUCTION

THE CONFIGURATIONS OF AIRPLANES designed today are vastly different from the configurations of those designed a few years ago. The presently designed semimonocoque types of airplanes have developed from those with wings of constant thickness ratios with unmachined stringers and skin to those with wings of varying thickness ratios, machine-tapered skins and stringers, and tapered stringer spacing. Combinations

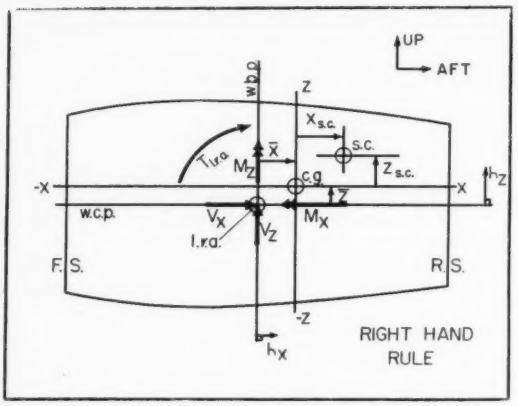

FIG. 1. Sign convention and coordinate system (loads and directions positive as shown).

of these variables result in nonlinear segment axial-load variations and consequently ever changing shear-flow distributions. It has been realized for some time that the assumptions upon which the classical prismatic beam theory ($q = VQ/I$) is based are seldom fulfilled. A second method, "Unit Method of Beam Analysis," was developed to account for taper in the beam, thus allowing a more accurate determination of the shear flow. This method is based on the difference in axial loads at two adjacent stations, and the accuracy of the resulting shear flow depends upon how closely the segment axial loads between these two stations approach a linear variation. Should a wing with a relatively long span be designed in such a manner that the segment axial-load variations are nonlinear, an excessively large number of sections must be analyzed in order to obtain sufficient accuracy for a shear-flow analysis.

The method of shear-flow analysis developed in this paper is based on the rate of change of segment axial load at a particular station and accounts for the actual rates of change of segment areas, segment coordinates, and section properties. The accuracy of this method is dependent upon the accuracy of the means by which the axial stress distribution is determined. For a beam with no abrupt changes in continuity or unusual end-fixity conditions, the normal procedure of determining elastic bending stresses will be sufficiently accurate. Should a beam have abrupt changes (such as sweep-back, cutouts, or unusual end-fixity conditions), this method or any method of analysis will be accurate only to the extent of the capabilities of the engineer to determine the effectiveness of the structural material. Abrupt changes may be accounted for in the analysis by using effective segment areas in place of the actual segment areas.

The assumptions upon which this method is based are similar to those used in most practical methods of shear-flow analysis. The material is assumed to obey Hookes' Law, the moments of inertia of the individual segments about their own c.g.'s are assumed negligible, and the segment areas are assumed concentrated at their centers of gravity. The load derivative is taken with respect to the Y component of the segment load.

An interesting comparison is made in an example problem worked by two presently accepted methods of shear-flow analysis and the method presented by this paper. The two methods for comparison are the VQ/I method and the "Unit Method of Beam Analysis."

The basic principle of the following development is simple. Primarily, it consists of setting up the equation for the segment axial load and obtaining its rate of change with respect to the span by taking the first derivative of that equation. At a first glance it may appear to be a long and laborious method. Actually, the man-hours expended by engineering personnel in using this method may be short in view of the fact that it is adaptable to IBM operations. If the basic section properties used in the bending stress analysis are calculated by IBM, the only additional items required to obtain the shear-flow analysis are $\Delta l/t$, $(a)'$, $(h_X)'$ and $(h_Z)'$. The values of $\Delta l/t$ are required only if the shear center is desired. In all widely used methods of shear-flow analysis which determine the shear center, the values of $\Delta l/t$ are required. The remainder of the additional items will be discussed in later paragraphs.

Equations for the Rate of Change of Segment Axial Load

Let axes X and Z of Fig. 1 be any two perpendicular axes through the section c.g.

With the sign convention shown in Fig. 1, the elastic bending stress at any point whose coordinates with respect to the c.g. are x and z is

$$f = \frac{[I_{XZ}M_X - I_X M_Z]x + [I_{XZ}M_Z - I_Z M_X]z}{I_X I_Z - I_{XZ}^2} \quad (1)$$

This equation may be rewritten as

$$f = M_X[C_2 x - C_4 z] + M_Z[C_2 z - C_3 x] \quad (2)$$

where

$$C_1 = 1/[I_X I_Z - I_{XZ}^2] \quad (3)$$
$$C_2 = C_1 I_{XZ} \quad (4)$$
$$C_3 = C_1 I_X \quad (5)$$
$$C_4 = C_1 I_Z \quad (6)$$

The segment axial load then is

$$P = fa = M_X a[C_2 x - C_4 z] + M_Z a[C_2 z - C_3 x] \quad (7)$$

The rate of change of P with respect to y is obtained by taking the derivative of Eq. (7) with respect to y,

$$\begin{aligned}(P)' &= M_X a(C_2 x - C_4 z)' + [C_2 x - C_4 z]\,(M_X a)' + \\ &\quad M_Z a(C_2 z - C_3 x)' + [C_2 z - C_3 x]\,(M_Z a)' \\ &= M_X a[C_2(x)' + x(C_2)' - C_4(z)' - z(C_4)'] + \\ &\quad [C_2 x - C_4 z]\,[a(M_X)' + M_X(a)'] + \\ &\quad M_Z a[C_2(z)' + z(C_2)' - C_3(x)' - x(C_3)'] + \\ &\quad [C_2 z - C_3 x]\,[a(M_Z)' + M_Z(a)'] \quad (8)\end{aligned}$$

By combining terms, Eq. (8) results in

$$(P)' = [a(x)' + x(a)']^* [C_2M_X - C_3M_Z]^\phi + [a(z)' + z(a)']^* [C_2M_Z - C_4M_X]^\phi + [ax]^* [C_2(M_X)' - C_3(M_Z)' + M_X(C_2)' - M_Z(C_3)']^\phi + [az]^* [C_2(M_Z)' - C_4(M_X)' + M_Z(C_2)' - M_X(C_4)']^\phi \quad (9)$$

It should be noted that in Eq. (9) the first term (*) of each of the four multiplications is a function of the segment, whereas the second term (ϕ) is a function of the section.

The $(P)'$ derived is the change in shear flow between adjacent segments. The value obtained for a segment from Eq. (9) indicates an instantaneous change in load at segment c.g. The change is actually a gradual change between the c.g.'s of adjacent segments if the skin is effective in bending.

Often it is desirable to know the breakdown of a particular shear value—i.e., the values of the component parts due to each of the beam and chord shears and moments, and torsion. Therefore, the development of this method of analysis will deal with shear flows due to each of the above components.

Eq. (9) may be broken down into four equations, each dealing with a $(P)'$ due to a single loading condition of shear or moment. Since

$$\left.\begin{aligned}(M_X)' &= V_Z\\ (M_Z)' &= V_X\end{aligned}\right\} \quad (10)$$

the following may be written:

$$(P_{V_X})' = aV_X[C_2z - C_3x] \quad (11)$$

$$(P_{V_Z})' = aV_Z[C_2x - C_4z] \quad (12)$$

$$(P_{M_X})' = [a(x)' + x(a)']\, C_2M_X - [a(z)' + z(a)']\, C_4M_X + axM_X(C_2)' - azM_X(C_4)' \quad (13)$$

$$(P_{M_Z})' = [a(z)' + z(a)']\, C_2M_Z - [a(x)' + x(a)']\, C_3M_Z + azM_Z(C_2)' - axM_Z(C_3)' \quad (14)$$

Eqs. (11), (12), (13), and (14) deal with the $(P)'$ of an individual segment. It may be noted that three basic items are involved: (a) area, (b) coordinates, and (c) loads. The section properties, of course, are functions of segment areas and coordinates. The area is assumed to be concentrated at the c.g. of the combined stringer area and the area of the skin acting with that stringer in bending. The most convenient way of obtaining $(a)'$ is by plotting area vs. y for each segment and by graphically determining the slopes at any section. Before obtaining the rates of change of the coordinates of a segment and the section properties of a section, the coordinates must be defined. In the derivations to follow, a wing will be used as an example. The equations may be modified to suit any beam, such as a fuselage.

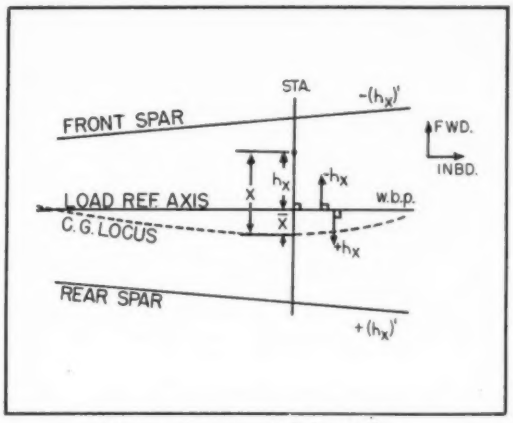

FIG. 2. Plan view, left-hand wing.

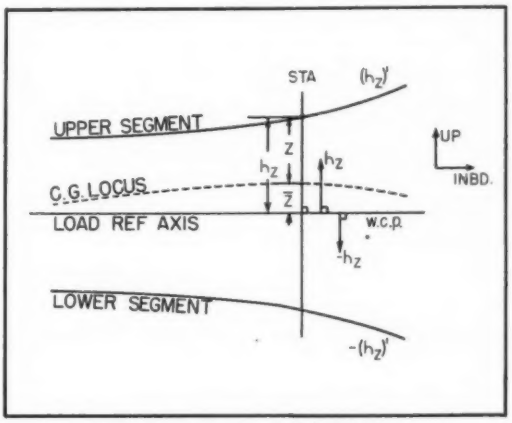

FIG. 3. Rear view, left-hand wing.

To obtain the correct relationship between section properties, such as $(x)'$, $(z)'$, and $(a)'$, at different sections all coordinates should be referred to three basic perpendicular planes. Figs. 2 and 3 illustrate the coordinate system assumed. The horizontal plane will be taken as the w.c.p. The spanwise vertical plane will be taken as the w.b.p., which is perpendicular to the w.c.p. and through the l.r.a.

The l.r.a. shown in Fig. 2 is the axis about which the torsions are computed. The bending sections are taken perpendicular to this axis. Normally, the load axis is chosen as one that is midway between the spars and in the w.c.p. The chordwise vertical plane will be taken at the tip perpendicular to the l.r.a.

To correspond with the coordinate planes set up in Figs. 2 and 3, properties that increase positively going inboard will have a positive rate of change with respect to y.

From Fig. 2 the horizontal coordinate of a segment may be expressed as

$$x = h_X - \bar{x} \quad (15)$$

Thus, it can be written that

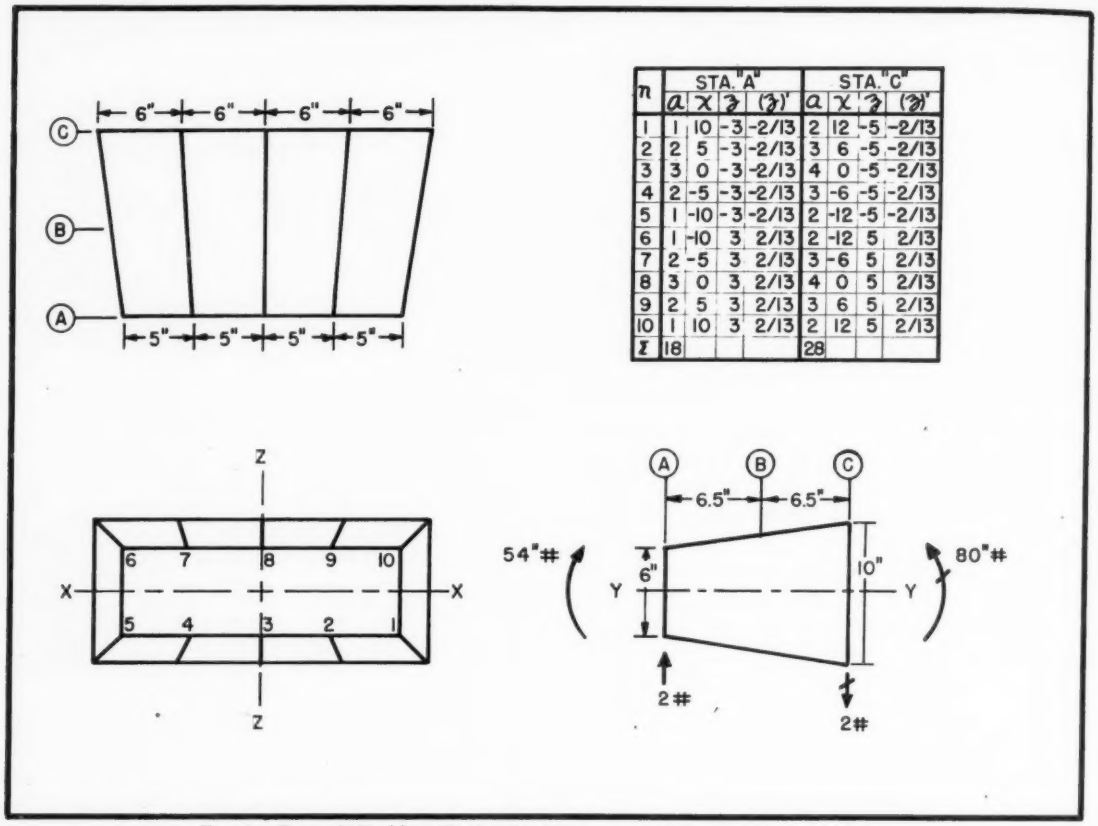

n	STA. "A"				STA. "C"			
	a	x	z	(z)'	a	x	z	(z)'
1	1	10	-3	-2/13	2	12	-5	-2/13
2	2	5	-3	-2/13	3	6	-5	-2/13
3	3	0	-3	-2/13	4	0	-5	-2/13
4	2	-5	-3	-2/13	3	-6	-5	-2/13
5	1	-10	-3	-2/13	2	-12	-5	-2/13
6	1	-10	3	2/13	2	-12	5	2/13
7	2	-5	3	2/13	3	-6	5	2/13
8	3	0	3	2/13	4	0	5	2/13
9	2	5	3	2/13	3	6	5	2/13
10	1	10	3	2/13	2	12	5	2/13
Σ	18				28			

FIG. 4. Example Problem No. 1: sketch, areas, coordinates, slopes, and loads.

$$(x)' = (h_X)' - (\bar{x})' \tag{16}$$

where

$$\bar{x} = \sum[ah_X]/A \tag{17}$$

Therefore,

$$(x)' = (h_X)' - \frac{A[\sum a(h_X)' + \sum h_X(a)'] - [\sum ah_X]\,(A)'}{A^2} \tag{18}$$

Similarly, from Fig. 3, $(z)'$ may be written as

$$(z)' = (h_Z)' - \frac{A[\sum a(h_Z)' + \sum h_Z(a)'] - [\sum ah_Z]\,(A)'}{A^2} \tag{19}$$

Spanwise plots of h_X and h_Z for each segment may be used to determine $(h_X)'$ and $(h_Z)'$ at any section.

For most airplane wings, the moments of inertia of the individual segments about their own c.g.'s are comparatively negligible. In this paper they are neglected. On that basis, the moments of inertia and the product of inertia are

$$I_Z = \sum(ax^2) \tag{20}$$
$$I_X = \sum(az^2) \tag{21}$$
$$I_{XZ} = \sum(axz) \tag{22}$$

and their rates of change are

$$(I_Z)' = 2\sum[ax(x)'] + \sum[x^2\,(a)'] \tag{23}$$
$$(I_X)' = 2\sum[az(z)'] + \sum[z^2\,(a)'] \tag{24}$$
$$(I_{XZ})' = \sum[ax(z)'] + \sum[az(x)'] + \sum[xz(a)'] \tag{25}$$

The rates of change of the section coefficients C_1, C_2, C_3, and C_4 are then determined. From Eqs. (3), (4), (5), and (6),

$$(C_1)' = -\frac{(I_XI_Z - I_{XZ}^2)'}{[I_XI_Z - I_{XZ}^2]^2} = -\frac{I_X(I_Z)' + I_Z(I_X)' - 2I_{XZ}\,(I_{XZ})'}{[I_XI_Z - I_{XZ}^2]^2} \tag{26}$$

$$(C_2)' = C_1(I_{XZ})' + I_{XZ}(C_1)' \tag{27}$$

$$(C_3)' = C_1(I_X)' + I_X(C_1)' \tag{28}$$

$$(C_4)' = C_1(I_Z)' + I_Z(C_1)' \tag{29}$$

The above derivatives may now be used in Eqs. (11), (12), (13), and (14) to determine $(P)'$.

Equations for Section Shear-Flow Distribution

In view of the fact that the shear flows are to be computed for each of the loading conditions (shear, moment, and torsion) it will be necessary to determine the location of the s.c. The s.c. is immaterial as far as the final net q is concerned; however, it is the only

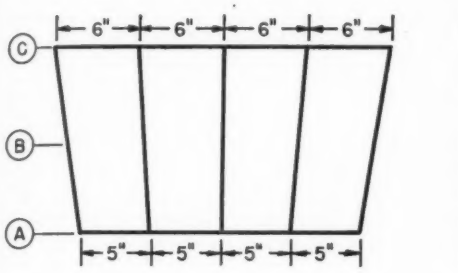

n	STA. "A"				STA. "B"				STA. "C"			
	a	x	z	(z)'	a	x	z	(z)'	a	x	z	(z)'
1	1	10	-3	0	3/2	11	-7/2	-2/13	2	12	-5	-3/13
2	2	5	-3	0	5/2	11/2	-7/2	-2/13	3	6	-5	-3/13
3	3	0	-3	0	7/2	0	-7/2	-2/13	4	0	-5	-3/13
4	2	-5	-3	0	5/2	-11/2	-7/2	-2/13	3	-6	-5	-3/13
5	1	-10	-3	0	3/2	-11	-7/2	-2/13	2	-12	-5	-3/13
6	1	-10	3	0	3/2	-11	7/2	2/13	2	-12	5	3/13
7	2	-5	3	0	5/2	-11/2	7/2	2/13	3	-6	5	3/13
8	3	0	3	0	7/2	0	7/2	2/13	4	0	5	3/13
9	2	5	3	0	5/2	11/2	7/2	2/13	3	6	5	3/13
10	1	10	3	0	3/2	11	7/2	2/13	2	12	5	3/13
Σ	18				23				28			

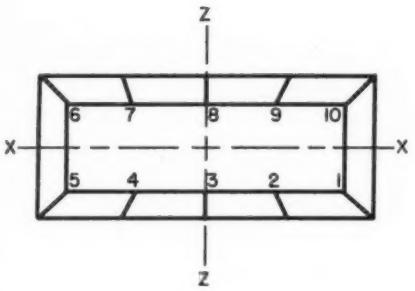

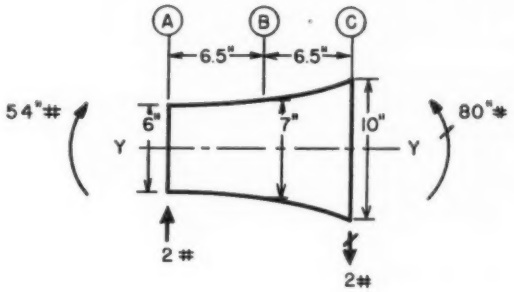

FIG. 5. Example Problem No. 2: sketch, areas, coordinates, slopes, and loads.

point about which the true torsion and, consequently, q_T may be computed. Should the engineer desire to have a net shear-flow distribution rather than a breakdown as indicated above, the location of the s.c. need not be determined; any reference point (such as the c.g.) may be used, and the equations of equilibrium should be written about this point.

Having obtained $(P)'$ for each segment of a section for each of the shear and moment loads, the section shear-flow distributions for each of the loading conditions may then be obtained.

Shear-Flow Distribution Due to V_Z

Assume the shear flow at any point in the periphery of the section to be zero. For example, assume the rear spar of the structure to be cut so that it can transfer no shear between the rear spar upper and lower chords. With this assumption, start at the rear spar just below the cut and sum, in a clockwise direction, the $(P)'$ for each segment. The resulting uncorrected shear flow is

$$q_u = \sum(P_{VZ})' \qquad \text{[Ref. Eq. (12)]} \qquad (30)$$

It will be clockwise at any point at which q_u is positive and counterclockwise at any point at which q_u is negative. As a numerical check, after summing clockwise, q_u should be equal to zero at the cut. The sum of the forces in the vertical direction should equal the applied V_Z. The sum of the horizontal forces should equal zero. That is,

$$\sum[q_u \, \Delta z] \stackrel{?}{=} V_Z \qquad (31)$$

$$\sum[q_u \, \Delta x] \stackrel{?}{=} 0 \qquad (32)$$

where

$$\Delta z = z_{n+1} - z_n \qquad (33)$$

$$\Delta x = x_{n+1} - x_n \qquad (34)$$

The total shearing strain around the section perimeter due to q_u is

$$\delta \sim \Sigma[q_u \Delta l/t] \qquad (35)$$

If the section is to deflect without twisting this strain must be balanced by an applied correcting shear flow q_0, where

$$q_0 = -\Sigma[q_u \Delta l/t]/\Sigma[\Delta l/t] \qquad (36)$$

The resulting corrected shear flow is

$$q_{VZ} = q_u + q_0 \qquad (37)$$

Since q_{VZ} deflects the section without twisting, the resultant must pass through the s.c. For the horizontal location of the s.c., take moments about the Y axis through the c.g. This may be written as

TABLE 1

Example Problem No. 1: Station "A" Using Differential Shear Flow Analysis

n	a	$\bar{y}$	$\bar{x}$	$\bar{y}^2$	f	P	$(a)'$	$(\bar{y})'$	$a\bar{y}$	$a(\bar{y})'$	$\bar{y}(a)'$	$[\Delta(P)'\bar{y}]$	$[\Delta(P)'\bar{x}]$	$(P)'$	q_u	$\bar{y}_n\bar{x}_{n+1}$	$\bar{x}_n\bar{y}_{n+1}$	$2A$	q
COL	1	2	3	4	5	6	7	8	9	10	11	12	13	14	15	16	17	18	19
REF.	♦	♦	♦	②²	Δ	①⑤	♦	♦	①②	①⑧	②⑦	Δ	Δ	⑫+⑬	Δ	②ₙ③ₙ₊₁	③ₙ②ₙ₊₁	⑯−⑰	Δ
UNIT	IN²	IN.	IN.	IN.²	#/IN.²	#	IN.		IN.³	IN.²	IN.²	#/IN.	#/IN.	#/IN.	#/IN.	IN.²	IN.²	IN.²	#/IN.
1	1	-3	10	9	1	1	1/13	-2/13	-3	-2/13	-3/13	5/39	-114/1053	21/1053	21/1053	-15	-30	15	59/702
2	2	-3	5	9	1	2	1/13	-2/13	-6	-4/13	-3/13	7/39	-228/1053	-39/1053	-18/1053	0	-15	15	33/702
3	3	-3	0	9	1	3	1/13	-2/13	-9	-6/13	-3/13	9/39	-342/1053	-99/1053	-117/1053	15	0	15	-33/702
4	2	-3	-5	9	1	2	1/13	-2/13	-6	-4/13	-3/13	7/39	-228/1053	-39/1053	-156/1053	30	15	15	-59/702
5	1	-3	-10	9	1	1	1/13	-2/13	-3	-2/13	-3/13	5/39	-114/1053	21/1053	-135/1053	30	-30	60	-45/702
6	1	3	-10	9	-1	-1	1/13	2/13	3	2/13	3/13	-5/39	114/1053	-21/1053	-156/1053	-15	-30	15	-59/702
7	2	3	-5	9	-1	-2	1/13	2/13	6	4/13	3/13	-7/39	228/1053	39/1053	-117/1053	0	-15	15	-33/702
8	3	3	0	9	-1	-3	1/13	2/13	9	6/13	3/13	-9/39	342/1053	99/1053	-18/1053	15	0	15	33/702
9	2	3	5	9	-1	-2	1/13	2/13	6	4/13	3/13	-7/39	228/1053	39/1053	21/1053	30	15	15	59/702
10	1	3	10	9	-1	-1	1/13	2/13	3	2/13	3/13	-5/39	114/1053	-21/1053	0	30	-30	60	45/702
Σ	18																	240	

♦ REF. FIG. 4

Δ SEE DETAILS BELOW

⑤ $= -M_X\bar{y}/I_X = -[54/162]\bar{y} = -②/3$ EQ.(1)

WHERE $M_X = 54$ IN.# ; $I_X = \Sigma[a\bar{y}^2] = 162$ IN.⁴ EQ.(21)

⑫ $= [a(\bar{y})' + \bar{y}(a)'][-M_X/I_X] = -[⑩+⑪]/3$

⑬ $= [a\bar{y}][-(M_X)'/I_X + M_X(I_X)'/I_X^2]$
$= [⑨][38/1053]$

WHERE $(M_X)' = V_Z = 2$# EQ.(10)

$(I_X)' = 2\Sigma[a\bar{y}(\bar{y})'] + \Sigma[\bar{y}^2(a)']$
$= 2\Sigma[⑨⑧] + \Sigma[④⑦]$
$= 306/13$ IN.³ EQ. (24)

⑮ = LINE Σ⑭

⑲ $= q_u + q_0 =$ ⑮ $+ 5/78$

WHERE $q_0 = \Sigma[-q_u\Delta\bar{x}]/S$
$= \Sigma[-$⑮⑱$]/\Sigma$⑱
$= 5/78$ #/IN. EQ.(59)

VERTICAL SHEAR CHECK

$\Sigma[-P(\bar{y})'] + \Sigma[q_u\Delta\bar{y}] \overset{S}{=} V_Z$

$-\Sigma$⑥⑧ $+\Sigma[②_{n+1} - ②_n][⑮] \overset{S}{=} 2$

$36/13 + [-135/1053][3] + 3] \overset{S}{=} 2$

$36/13 - 10/13 \overset{S}{=} 2$

$26/13 = 2$

$$V_Z x_{s.c.} = -q_0 S - \Sigma[q_u s] \tag{38}$$

Therefore

$$x_{s.c.} = -[q_0 S + \Sigma[q_u s]]/V_Z \tag{39}$$

where

$$s = z_{n}x_{n+1} - x_n z_{n+1} \tag{40}$$

Shear-Flow Distribution Due to V_X

The derivation of the shear-flow distribution due to V_X follows the line of reasoning employed for the shear-flow distribution due to V_Z. The resulting equations are

$$q_u = \Sigma(P_{VX})' \quad [\text{Ref. Eq. (11)}] \tag{41}$$
$$[q_u]_N \overset{s}{=} 0 \tag{42}$$
$$\Sigma[q_u\Delta x] \overset{s}{=} V_X \tag{43}$$
$$\Sigma[q_u\Delta z] \overset{s}{=} 0 \tag{44}$$
$$q_0 = -\Sigma[q_u\Delta l/t]/\Sigma[\Delta l/t] \tag{45}$$
$$q_{VX} = q_u + q_0 \tag{46}$$
$$z_{s.c.} = [q_0 S + \Sigma[q_u s]]/V_X \tag{47}$$

Shear-Flow Distribution Due to M_Z

The uncorrected shear flow due to M is similar to that due to V. That is,

$$q_u = \Sigma(P_{Mz})' \quad [\text{Ref. Eq. (14)}] \tag{48}$$
$$[q_u]_N \overset{s}{=} 0 \tag{49}$$

The equilibrium numerical checks at this point for M, however, are different from those for V. Should the segments not be perpendicular to the plane of the section, the segment axial loads due to bending moments will produce X and Z components. Therefore, as a check, one may use the following equations:

$$\Sigma[q_u\Delta x] \overset{s}{=} \Sigma[P_{MZ}(h_X)'] \tag{50}$$
$$\Sigma[q_u\Delta z] \overset{s}{=} \Sigma[P_{MZ}(h_Z)'] \tag{51}$$

The correcting shear flow is determined by equating the moment about the Y axis of q_u, the X and Z components of P_{Mz}, and q_0 to zero. That is,

$$\Sigma[P_{MZ}z(h_X)'] - \Sigma[P_{MZ}x(h_Z)'] - \Sigma[q_u s] - q_0 S = 0 \tag{52}$$

Therefore,

$$q_0 = \frac{\Sigma[P_{MZ}z(h_X)'] - \Sigma[P_{MZ}x(h_Z)'] - \Sigma[q_u s]}{S} \tag{53}$$

TABLE 2
Example Problem No. 1: Station "B" Using VQ/I Shear Flow Analysis

n	a	y	ay	f	P	$(y)'$	Q	q_u	x	$y_n x_{n+1}$	$x_n y_{n+1}$	Δ	q
COL.	1	2	3	4	5	6	7	8	9	10	11	12	13
REF.	†	†	① ②	Δ	① ④	†	Σ③	Δ	†	②$_n$ ⑨$_{n+1}$	⑨$_n$ ②$_{n+1}$	⑩ − ⑪	Δ
UNITS	IN.^{2}	IN.	IN.^{3}	#/IN.^{2}	#		IN.^{3}	#/IN.	IN.	IN.^{2}	IN.^{2} •	IN.^{2}	#/IN.
1	3/2	-4	-6	67/92	201/184	-2/13	-6	-1035/110032	11	-22	-44	22	5865/220064
2	5/2	-4	-10	67/92	335/184	-2/13	-16	-2760/110032	11/2	0	-22	22	2415/220064
3	7/2	-4	-14	67/92	469/184	-2/13	-30	-5175/110032	0	22	0	22	-2415/220064
4	5/2	-4	-10	67/92	335/184	-2/13	-40	-6900/110032	-11/2	44	22	22	-5865/220064
5	3/2	-4	-6	67/92	201/184	-2/13	-46	-7935/110032	-11	44	-44	88	-7935/220064
6	3/2	4	6	-67/92	-201/184	2/13	-40	-6900/110032	-11	-22	-44	22	-5865/220064
7	5/2	4	10	-67/92	-335/184	2/13	-30	-5175/110032	-11/2	0	-22	22	-2415/220064
8	7/2	4	14	-67/92	-469/184	2/13	-16	-2760/110032	0	22	0	22	2415/220064
9	5/2	4	10	-67/92	-335/184	2/13	-6	-1035/110032	11/2	44	22	22	5865/220064
10	3/2	4	6	-67/92	-201/184	2/13	0	0	11	44	-44	88	7935/220064
Σ	23											352	

† REF. FIG. 4

Δ SEE DETAILS BELOW

④ = $-M_X y / I_X = -[67/368]y = -67/368$ ② EQ.(1)
WHERE $M_X = 54 + 2[13/2] = 67$ IN.#
$I_X = \Sigma[a y^2] = 368$ IN.^{4} EQ.(21)

⑧ = $-VQ/I_X = 345Q/[598][368] = 345$ ⑦ $/220064$ #/IN
WHERE $V = V_Z - \Sigma[-P(y)'] = 2 - 1541/598 = -345/598$#

⑬ = $q_u + q_0 =$ ⑧ $+7935/220064$
WHERE $q_0 = \Sigma[-q_u \Delta]/S$
$= \Sigma[-$ ⑧ ⑫ $]/\Sigma$ ⑫
$= 698280/[55016][352]$
$= 7935/220064$ #/IN.

VERTICAL SHEAR CHECK

$\Sigma[-P(y)'] + \Sigma[q_u \Delta y] \overset{S}{=} V_Z$ EQ.(31) & (58)
$1541/598 - [7935][8]/110032 \overset{S}{=} 2$
$2 = 2$

The resulting corrected shear flow is

$$q_{MZ} = q_u + q_0 \tag{54}$$

Shear-Flow Distribution Due to M_X

The equations for shear-flow distribution due to M_X are similar to those for M_Z. They are as follows:

$$q_u = \sum(P_{MX})' \quad [\text{Ref. Eq. (13)}] \tag{55}$$
$$[q_u]_X \overset{S}{=} 0 \tag{56}$$
$$\sum[q_u \Delta x] \overset{S}{=} \sum[P_{MX}(h_X)'] \tag{57}$$
$$\sum[q_u \Delta z] \overset{S}{=} \sum[P_{MX}(h_Z)'] \tag{58}$$

$$q_0 = \frac{\sum[P_{MX} z (h_X)'] - \sum[P_{MX} x (h_Z)'] - \sum(q_u s)}{S} \tag{59}$$

$$q_{MX} = q_u + q_0 \tag{60}$$

Shear-Flow Distribution Due to $T_{s.c.}$

Normally, torsions are computed about l.r.a. as a matter of convenience. To obtain the torsion about the s.c., the beam and chord shears must be transferred to the s.c. and the resulting torsion added to $T_{l.r.a.}$. For this transfer the following equation may be written:

$$T_{s.c.} = T_{l.r.a.} + V_Z[\bar{x} + x_{s.c.}] - V_X[\bar{z} + z_{s.c.}] \tag{61}$$

The torsional shear flow is a constant value for the entire periphery of the section and is

$$q_T = T_{s.c.}/S \tag{62}$$

Net Shear-Flow Distribution

The net shear-flow distribution is the algebraic sum of the individual shear-flow distributions due to each of the beam and chord shear and moment, and torsion.

$$q = q_{VZ} + q_{VX} + q_{MZ} + q_{MX} + q_T \tag{63}$$

Unit Shear-Flow Distributions

Since the design conditions on a wing are often numerous, it is desirable to compute unit shear-flow distributions for each section analyzed rather than to carry the complete analysis through for each of the design conditions. The magnitude of the unit values, V_Z, V_X, M_Z, M_X, and $T_{s.c.}$ will depend upon the size of the structure analyzed. The shear-flow distributions for any particular design condition may then be obtained by multiplying the unit shear flows by their appropriate shears, moments, and torsion.

TABLE 3
Example Problem No. 1: Station "C" Using Unit Method of Beam Analysis

n	a	γ	χ	f	P_A	$(\gamma)'$	$\gamma_n \chi_{n+1}$	$\chi_n \gamma_{n+1}$	Δ	a	γ	χ	f	P_C	$(\gamma)'$	$\gamma_n \chi_{n+1}$	$\chi_n \gamma_{n+1}$	Δ	ΔP	$\Delta P/\Delta Y$	q_v	q
COL	1	2	3	4	5	6	7	8	9	10	11	12	13	14	15	16	17	18	19	20	21	22
REF.	♦	♦	♦	Δ	Δ	♦	②ₙ③ₙ₊₁	③ₙ②ₙ₊₁	Δ	♦	♦	♦	Δ	⑩⑬	♦	⑪ₙ⑫ₙ₊₁	⑫ₙ⑪ₙ₊₁	⑯-⑰	⑭-⑤	⑲/13	Δ	Δ
UNIT	IN.²	IN.	IN.	#/IN.²	#	•	IN.²	IN.²	IN.²	IN.²	IN.	IN.	#/IN.²	#		IN.²	IN.²	IN.²	#	#/IN.	#/IN.	#/IN.
1	1	-3	10	1	1	-2/13	-15	-30	15	2	-5	12	4/7	8/7	-2/13	-30	-60	30	1/7	1/91	1/91	9/182
2	2	-3	5	1	2	-2/13	0	-15	15	3	-5	6	4/7	12/7	-2/13	0	-30	30	-2/7	-2/91	-1/91	5/182
3	3	-3	0	1	3	-2/13	15	0	15	4	-5	0	4/7	16/7	-2/13	30	0	30	-5/7	-5/91	-6/91	-5/182
4	2	-3	-5	1	2	-2/13	30	15	15	3	-5	-6	4/7	12/7	-2/13	60	30	30	-2/7	-2/91	-8/91	-9/182
5	1	-3	-10	1	1	-2/13	30	-30	60	2	-5	-12	4/7	8/7	-2/13	60	-60	120	1/7	1/91	-7/91	-7/182
6	1	3	-10	-1	-1	2/13	-15	-30	15	2	5	-12	-4/7	-8/7	2/13	-30	-60	30	-1/7	-1/91	-8/91	-9/182
7	2	3	-5	-1	-2	2/13	0	-15	15	3	5	-6	-4/7	-12/7	2/13	0	-30	30	2/7	2/91	-6/91	-5/182
8	3	3	0	-1	-3	2/13	15	0	15	4	5	0	-4/7	-16/7	2/13	30	0	30	5/7	5/91	-1/91	5/182
9	2	3	5	-1	-2	2/13	30	15	15	3	5	6	-4/7	-12/7	2/13	60	30	30	2/7	2/91	1/91	9/182
10	1	3	10	-1	-1	2/13	30	-30	60	2	5	12	-4/7	-8/7	2/13	60	-60	120	-1/7	-1/91	0	7/182
Σ	18								240	28								480				
	STATION "A"									STATION "C"												STA. "C"

♦ REF. FIG. 4

Δ SEE DETAILS BELOW

④ = $-M_X \gamma / I_X$ = $-$ ②/3
WHERE M_X = 54 IN#
$I_X = \Sigma[a\gamma^2] = 162$ IN.⁴

⑤ = ① ④

⑨ = ⑦ − ⑧

⑬ = $-M_X \gamma / I_X$ = -4 ⑪ /35
WHERE M_X = 80 IN.#
$I_X = \Sigma[a\gamma^2] = 700$ IN.⁴

㉑ = LINE Σ⑳

㉒ = $q_a + q_o$
= ㉑ + 7/182
WHERE
$q_o = -\Sigma[q_a \Delta] / \Sigma \Delta$
= 7/182 #/IN

VERTICAL SHEAR CHECK:

$\Sigma[-P_C(\gamma)'] + \Sigma[q_a \Delta \gamma] \doteq V_z$

Σ ⑭ ⑮ + Σ{㉑ (⑪ₙ₊₁ − ⑪ₙ)} ≐ 2

154/91 ≠ 2 VERT. SHEAR DOES NOT CHECK

EXAMPLE PROBLEMS

Discussion

Two example shear-flow problems are shown. For each problem the shear-flow values are computed at three adjacent stations by the Differential method, by the Unit Beam method, and by VQ/I. It should be noted that for reasons of simplicity the problems chosen are tapered beams with rectangular cross sections. The example problems are presented merely to indicate that a difference can exist in the calculated values for shear flows obtained by the several methods noted above. The problems are not intended to be representative of any actual design. To illustrate the effects of surface curvature, the only difference in the two problems is in a side view. Problem No. 1 has straight upper and lower surfaces, whereas Problem No. 2 has curved upper and lower surfaces. The shear-flow values have been computed using fractions in order to show the checks on the summation of vertical forces. The shear-flow values shown in Table 4 are given in decimal form for comparative purposes.

Normally, for a wing, one chooses stations to check bending stresses and shear flows that are spaced spanwise approximately the same distance as exists between spars. In the example problems, however, stations "A" and "C" are spaced slightly less than two-thirds of the interspar distance. An additional intermediate station is also included to show that the Unit Beam method, when calculated on the basis of the difference in end loads between stations "A" and "C" but applied at a station midway between the two, will give results that closer approximate the more accurate values obtained at that mid-station by the Differential method. It may appear at first glance that the only additional information needed to obtain good results with the Unit Beam method are the sweep areas, s, at a station midway between the two for which the segment axial loads are computed. This is true in the example problems because the sections are symmetrical about the X and Z axes. In actual design this is seldom true; therefore, the section properties, bending loads, etc., must be calculated in order to determine what portions of the external shear and torsion are carried by the slopes of the segments.

TABLE 4
Comparison of Shear Flows for the Example Problems

SEG. n	EXAMPLE PROBLEM NO. 1								
	STATION "A"			STATION "B"			STATION "C"		
	DIFFERENTIAL SHR. FLOW	UNIT BEAM SHEAR FLOW	VQ/I SHEAR FLOW	DIFFERENTIAL SHR. FLOW	UNIT BEAM SHEAR FLOW	VQ/I SHEAR FLOW	DIFFERENTIAL SHR. FLOW	UNIT BEAM SHEAR FLOW	VQ/I SHEAR FLOW
REF.	FIGS. 4&6	FIG. 4	FIG. 4	FIG. 4	FIG. 4	FIGS. 4&7	FIG 4	FIGS. 4&8	FIG. 4
UNITS	#/IN	#/IN	#/IN.	#/IN.	#/IN.	#/IN.	#/IN.	#/IN.	#/IN.
1	.0841	.0495	.0499	.0461	.0495	.0267	.0290	.0495	.0165
2	.0470	.0275	.0214	.0256	.0275	.0110	.0160	.0275	.0066
3	-.0470	-.0275	-.0214	-.0256	-.0275	-.0110	-.0160	-.0275	-.0066
4	-.0841	-.0495	-.0499	-.0461	-.0495	-.0267	-.0290	-.0495	-.0165
5	-.0641	-.0385	-.0641	-.0361	-.0385	-.0361	-.0231	-.0385	-.0231
6	-.0841	-.0495	-.0499	-.0461	-.0495	-.0267	-.0290	-.0495	-.0165
7	-.0470	-.0275	-.0214	-.0256	-.0275	-.0110	-.0160	-.0275	-.0066
8	.0470	.0275	.0214	.0256	.0275	.0110	.0160	.0275	.0066
9	.0841	.0495	.0499	.0461	.0495	.0267	.0290	.0495	.0165
10	.0641	.0385	.0641	.0361	.0385	.0361	.0231	.0385	.0231
Σ OF SECT. VERT. SHR.	2.00 #	2.31 #	2.00 #	2.00 #	1.96 #	2.00 #	2.00 #	1.69 #	2.00 #

SEG. n	EXAMPLE PROBLEM NO. 2								
	STATION "A"			STATION "B"			STATION "C"		
	DIFFERENTIAL SHR. FLOW	UNIT BEAM SHEAR FLOW	VQ/I SHEAR FLOW	DIFFERENTIAL SHR FLOW	UNIT BEAM SHEAR FLOW	VQ/I SHEAR FLOW	DIFFERENTIAL SHR. FLOW	UNIT BEAM SHEAR FLOW	VQ/I SHEAR FLOW
REF.	FIG. 5	FIG. 5	FIG. 5	FIG. 5	FIG. 5	FIG. 5	FIG. 5	FIG. 5	FIG 5
UNITS	#/IN	#/IN.	#/IN.	#/IN.	#/IN.	#/IN.	#/IN.	#/IN.	#/IN.
1	-.0954	.0495	-.1296	.0722	.0495	.0499	.0730	.0495	.0604
2	-.0299	.0275	-.0556	.0372	.0275	.0205	.0336	.0275	.0242
3	.0299	-.0275	.0556	-.0372	-.0275	-.0205	-.0336	-.0275	-.0242
4	.0954	-.0495	.1296	-.0722	-.0495	-.0499	-.0730	-.0495	-.0604
5	.1667	-.0385	.1667	-.0675	-.0385	-.0675	-.0846	-.0385	-.0846
6	.0954	-.0495	.1296	-.0722	-.0495	-.0499	-.0730	-.0495	-.0604
7	.0299	-.0275	.0556	-.0372	-.0275	-.0205	-.0336	-.0275	-.0242
8	-.0299	.0275	-.0556	.0372	.0275	.0205	.0336	.0275	.0242
9	-.0954	.0495	-.1296	.0722	.0495	.0499	.0730	.0495	.0604
10	-.1667	.0385	-.1667	.0675	.0385	.0675	.0846	.0385	.0846
Σ OF SECT. VERT. SHR.	2.00#	-.46#	2.00#	2.00#	2.41#	2.00#	2.00#	2.92#	2.00#

CONCLUSIONS

The selection of a method for determining shear flows of sufficient accuracy for practical design of a semimonocoque beam depends upon a number of variables. No attempt is made in this paper to describe the limits of the parameters which determine whether or not the Unit Beam method, or any other similar method, gives sufficiently accurate results. The Unit Beam method, considering the classical bending stress assumptions noted in the introduction, gives accurate results if the segment axial load variations are linear. Under the same assumptions, the Differential method gives accurate shear-flow results for beams with linear or nonlinear variations in segment axial load. The VQ/I method gives accurate results only for prismatic beams.

In the design of the wing for a large intercontinental bomber now in production, a comparison of the shear-flow values obtained by the Unit Beam method and the Differential method was made. For the same number of stations analyzed, spar shear differences of as much as 30 per cent were noted. The wing configuration was such that, had the Unit Beam method alone been considered, errors of at least one gage in shear material would have resulted. Accuracy obtained by the Unit Beam method comparable to that obtained by the Differential method would have required that approximately twice as many stations be analyzed. With the use of IBM calculating machines, the engineering man-hours required would have been greater had the Unit Beam method been used.

The Differential method provides an expedient tool in the preparation of a unit-load analysis, which is desirable if a large number of loading conditions require investigation.

REFERENCE

[1] Shanley, F. R., and Cozzone, F. P., *Unit Method of Beam Analysis*, Journal of the Aeronautical Sciences, Vol. 8, No. 6, p. 246, April, 1941.

Readers' Forum

BRIEF REPORTS of investigations in the aeronautical sciences and discussions of papers published in the JOURNAL are presented in this special department. Publication will be completed as soon as possible after receipt of the material. The Editorial Committee does not hold itself responsible for the opinions expressed by the correspondents. Contributions should not exceed 800 words in length.

Some Remarks on "A Solution of the Laminar Boundary-Layer Equations for a Compressible Fluid with Variable Properties, Including Dissociation"[1]

M. Z. Krzywoblocki
Professor of Aerodynamics, University of Illinois, Urbana, Ill.
October 6, 1952

TO UNDERSTAND THOROUGHLY the interesting and highly elaborated results presented by Moore,[1] it seems that some remarks might be in order. These are: (a) As the fundamental equations, the Navier-Stokes equations are assumed. This means that the analysis refers to that domain of flow in which those equations are valid. As is well known, there is today a highly controversial question up to which altitude those equations are valid. Although the calculations were performed up to $M = 20$, they may be not necessarily valid in the régime of rarefied and highly rarefied gases for the simple reason that no one knows, as yet, which fundamental equations should be used correctly in those régimes. Certainly, the results may be correct in the hypersonic flow in a gas of a higher density. (b) The author ignored the second equation of motion (momentum). This means that the Prandtl hypothesis was applied—i.e., the boundary layer is extremely thin, and the vertical velocity component and the pressure gradient in the vertical direction can be neglected. As is well known, in the hypersonic flow in a rarefied gas the boundary layer is thick, the vertical velocity component and the pressure gradient in the vertical direction cannot be neglected, and the second equation of motion must be preserved. This is another hint that the calculation refers rather to a hypersonic flow in a gas of higher density. (c) The third remark refers to purely formal transformation of a system of partial differential equations into a system of ordinary differential equations. In general, such a transformation is impossible in a one-to-one correspondence. It was shown in the past by the author of the present note that in the transformation from x, y, to x, z, the Jacobian of the transformation vanishes, which clearly means that the transformation cannot be one-to-one. Thus, automatically the uniqueness of the solution cannot be proved. Although the applied transformation may give a solution, it cannot give the unique solution. The next remark refers to the neglecting of terms containing x. Again, in general, *a priori*, one is not allowed to neglect the terms containing x, since they may be of large magnitude. One should not diminish the degree of determination of the class of functions, which are supposed to give a solution of the differential system in question, by neglecting *a priori* some terms in the original nonlinear differential systems.

If one neglects them *a priori*, one should show *a posteriori* that his step was justified. In his work Mr. Moore assumes *a priori* that the velocity and temperature pattern depend only upon z. This may be a sufficiently strong point that the terms containing x may be neglected, although no proof is presented. But the dependence on z only seems to indicate strongly that the calculation refers to a particular case—namely, to a parabolic distribution of velocity and all the other functions. The question arises by itself: "Which are those cases (altitudes, density relations, etc.) in which one is allowed to assume such a pattern?"

REFERENCE

[1] Moore, L. L., Journal of the Aeronautical Sciences, Vol. 19, No. 8, pp. 505–518, August, 1952.

Some Remarks on the Effect of Flapping Hinge Offset on Rotor Blade Stall

John R. Meyer, Jr., and G. Falabella, Jr.
Massachusetts Institute of Technology, Cambridge, Mass.
October 7, 1952

IN A READERS' FORUM ITEM in the JOURNAL OF THE AERONAUTICAL SCIENCES, July, 1952, Chawla presented a preliminary investigation of the effect of introducing a flapping hinge offset on rotor blade stall. It was concluded that, in the helicopter régime of flight and with normal values of blade mass constant ($\gamma = 12$), the stall condition at the retreating blade tip is not materially improved by hinge offsets up to 20 per cent of the blade radius.

The authors have recently completed a study[1] concerning the above effect. It should be pointed out that Chawla's result, although correct for the conditions that he imposed, is misleading, since an alternate treatment of the theory yields entirely different results.

Whenever a first harmonic aerodynamic loading is produced on a rotor element, a hub moment proportional to this harmonic loading times its distance to the center of rotation must result. Therefore, if the hub moment is forced to zero either by employing a zero offset hinge or by cyclic feathering of an offset or rigid rotor, then the first harmonic aerodynamic loading must also go to zero or disappear. The result is to sacrifice the possibility of obtaining a variation in angle of attack which would postpone or eliminate stall in the reverse flow region. Chawla has chosen θ_1 so as to produce a zero hub moment and, therefore, eliminates at the outset any chance of revealing the overall effect of flapping hinge offset on the stall of the retreating blade tip. In addition, he has not included a sufficient variation in blade mass constant. If the cyclic pitch condition is not imposed and a hub moment is accepted, it will be found that the flapping hinge offset is aerodynamically significant for proper combinations of offset and blade mass constant.

The local blade angle-of-attack variation with azimuth is naturally determined by the loading distribution and the flapping motion required for equilibrium about the flapping hinge. The

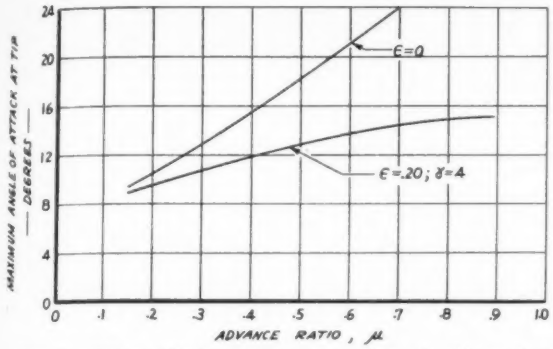

FIG. 1. Effect of blade mass constant and flapping hinge offset on the stall of retreating blade tip, no cyclic pitch, blade loading $(C_t/\sigma) = .10$

experimental results given in reference 2 indicate that a pronounced decrease in the maximum angle of attack is experienced by the blade tip at all advance ratios for the rotor tested. The theoretical approach given in reference 1 verifies these experimental results to a close approximation.

As an example of the effect of offset hinge taken from reference 1, the combination of an offset of 20 per cent and a blade mass constant of 4 results in the following characteristics at an advance ratio of 0.60:

(1) A concentration of aerodynamic loading at $\psi \approx 140°$.

(2) First harmonic flapping coefficients of $a_1 = 5.7°$ and $b_1 = -5.0°$.

(3) A maximum blade tip angle of attack of 14°.

(4) Tip path plane approximately horizontal with shaft axis inclined forward 5.5°.

(5) No sacrifice in lift.

A theoretical comparison of maximum angles of attack over a large range of advanced ratios between rotors of zero and 20 per cent offset is given in Fig. 1 as further indication of offset effect.

The question of possible full-scale rotor application of the offset rotor of course can only be answered after the investigation and evaluation of such unknowns as propulsive force characteristics, weight penalties, vibration, controllability, and stability.

REFERENCES

[1] Meyer, J. R., Jr., and Falabella, G., Jr., *Effect of Blade Mass Constant and Flapping Hinge Offset on the Maximum Blade Angle of Attack at High Advance Ratios*," Proceedings of the Eighth Annual Forum of the American Helicopter Society, May, 1952.

[2] Meyer, J. R., Jr., and Falabella, G., Jr., *An Investigation of the Experimental Aerodynamic Loading on a Model Helicopter Rotor Blade*," M.I.T. Report for N.A.C.A. NAw-5983, February, 1952.

Approximate Solutions for the Detached Shock Problem*

S. F. Borg
Stevens Institute of Technology, Hoboken, N.J.
September 4, 1952

GUDERLEY[1] POINTED OUT the essential simplification obtained by considering the hodograph plane for the transonic detached shock flow about a wedge. Vincenti and Wagoner[2, 3] solved the problem using relaxation methods. The present note describes a rapid procedure for obtaining approximate values of the stream function. These values may then be used either as the first values of a relaxation solution or, depending upon the accuracy desired, directly for transforming back to the physical plane

Using the notation of reference 3 except that unbarred letters are used throughout, the problem requires finding a function ψ which satisfies the equation

$$(\partial^2\psi/\partial\eta^2) - 2\eta(\partial^2\psi/\partial\theta^2) = 0 \qquad (1)$$

in the region OBEAO, Fig. 1, subject to the boundary conditions shown.

For constant values of η, Eq. (1) becomes, under suitably transformed coordinates, Laplace's equation. Hence, in narrow strips adjacent to η = constant, the equation of the field will be approximately satisfied by potential functions. In particular, the boundary conditions may also be satisfied or approximated by means of a potential doublet pair reflected about axis OB. We must now distinguish between two regions.

(I)—REGION CBEA

In this region, by using doublets, we may satisfy (a) the differential equation in the strip η = constant; (b) the boundary condition along AE; and (c) the boundary condition along CB.

It is possible, based upon physical reasoning, to determine beforehand approximate doublet locations (η_0, θ_0), $(\eta_0, 2\theta_w - \theta)$. However, in view of the similarity of the stream pattern for various values of θ_w and because of the form of the dependence of the stream pattern upon η_0, it would be preferable to proceed as follows: Determine η_0 for the case $\theta_w = 1.6$ (which is solved in reference 3) so that good agreement is obtained for the stream-line numbers. For other values of θ_w use the same values of η_0. θ_0 will vary corresponding to the change in θ_w.

(II)—REGION OCAO

In this region, the differential equation and the boundary condition along OC are satisfied. However, the dual requirement along OA

$$\left.\begin{aligned}\psi &= 0\\ \partial\psi/\partial\eta &= 0\end{aligned}\right\} \qquad (2)$$

cannot be satisfied by the simple doublet pair. It is possible, however, to approximate the required boundary conditions in any one of several different ways. For example:

(A) We can satisfy $\partial\psi/\partial\eta = 0$ and can locate the doublets so that (a) $\psi = 0$ occurs for small values of θ; (b) on physical grounds $\psi_{max.}$ will occur at $\theta_w/2$ for values of $-\eta$ somewhat greater than -1. We may locate the doublets in such a way as to obtain $\psi_{max.}$ at the estimated value of θ.

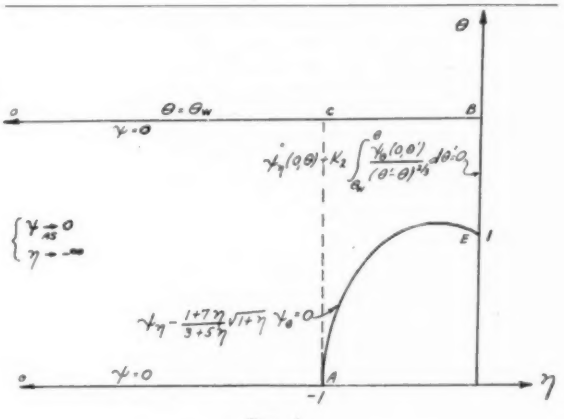

FIG. 1.

* This work was done while the writer was a Research Engineer at Grumman Aircraft Engineering Corporation, Bethpage, L.I., N.Y.

TABLE 1 $\theta_w = 1.6$

θ	$\gamma = -.025$		$\gamma = -.20$		$\gamma = -.50$		$\gamma = -.80$		$\gamma = -1.0$		$\gamma = -1.2$	
	THIS METHOD	REF. 3	THIS METHOD	REF. 3	THIS METHOD	REF. 3	THIS METHOD	REF. 3	THIS METHOD	REF. 3	THIS METHOD	REF. 3
1.5	299		585	389	400	394	313	329				
1.4	654		1168	875	825	811	653	662	151	197	72	98
1.3	1124		1930	1585	1268	1268	981	997				
1.25	1458											
1.20	1940		3070	2879	1745	1755	1285	1312	277	352	141	176
1.15	2595		3775	3567								
1.125	3115	3168										
1.10	3780	3805	4860	4862	2210	2196	1538	1552				
1.075	4660	4666										
1.068	5220	5228										
1.05	6020	5909										
1.0375	7050	6751										
1.028	8150	7833										
SHOCK	9830	9339	5600	5810	2365	2313	1638	1633				
.9									439	428	220	
.8									420	407	234	220
.7									401	389		
.6									358	321	226	187
.5									271	267		
.4									147	211	147	132

TABLE 2 $\theta_w = 4.2$

θ	$\gamma = 0$		$\gamma = -.2$		$\gamma = -.4$		$\gamma = -.5$		$\gamma = -.6$		$\gamma = -1.0$	
	THIS METHOD	V. & W.	THIS METHOD	V. & W.	THIS METHOD	V. & W.	THIS METHOD	V. & W.	THIS METHOD	V. & W.	THIS METHOD	V. & W.
3.8	30	39			55	113						
3.4	79	83			123	236						
3.0	147	134			214	383						
2.6	247	204			346	568						
2.4	315	253	381	623	436	689			489	657	440	452
2.2	402	314	486	760	554	837			587	788	523	525
2.0	518	397	630	950	715	1023			743	945	619	604
1.8	686	518	842	1218	948	1277			955	1148	725	690
1.6	946	716	1150	1602	1305	1626	1298	1522	1247	1407	953	771
1.4	1422	1089	1817	2270	1911	2152	1811	1950	1649	1742	938	885
1.2			3359	3670	2998	3005	2551	2548	2126	2150	1000	896
1.15	3127	2671										
1.125	3525	3093										
1.100	4040	3663	5297	5180								
1.075	4733	4467										
1.050	5710	5606										
1.0375	6390	6497										
1.0733			6147	5760								
1.0844					3855	3690						
1.0807							3303	3000				
1.0119									2380	2400	887	525
.8											703	357
.6											476	209
.4												

(B) We can assume additional pairs of doublets symmetrically disposed with respect to $\theta = \theta_w$, in order that the required boundary condition may be more closely approximated.

It should be noted that for $\eta < -1$ the relaxation procedure is simple to apply, and, in addition, the values of ψ are relatively small and vary regularly. Hence, if desired, a relaxation solution may be obtained for ψ values in this region, using values along $\eta = -1$ as the base.

The procedure in solving the problem is as follows: Starting at the strip $\eta = -0.5$, locate the doublets as in (I) above. Compute ψ. Do the same for adjacent strips, matching the values of ψ from strip to strip at some point as determined for the case $\theta_w = 1.6$. The values at $\eta = 0$ are obtained by noting that, for $\eta = 0$, $\partial\psi/\partial\eta$ = constant.

The tables show representative values of ψ obtained in this way to the same scale as in Vincenti's work. Values for $\theta_w = 1.6$ are from reference 3. Values for $\theta_w = 4.2$ were kindly supplied by the N.A.C.A.

Extension to Finite Wedges at $M > 1$

The above work suggests the possibility of obtaining usable approximate solutions for wedges with detached shocks in the supersonic (as against transonic) range. The streamline pattern in the hodograph plane can be approximated by means of suitable potential functions. Having the approximate stream-line pattern the effects of compressibility and rotation can be included very simply. A solution based upon this idea is shown in Fig. 2. It corresponds to a 90° wedge in a field of $M = 1.5$. The figure shows the shock wave, sonic line, and wedge face. Also shown are density ratios and pressure ratios at various points.

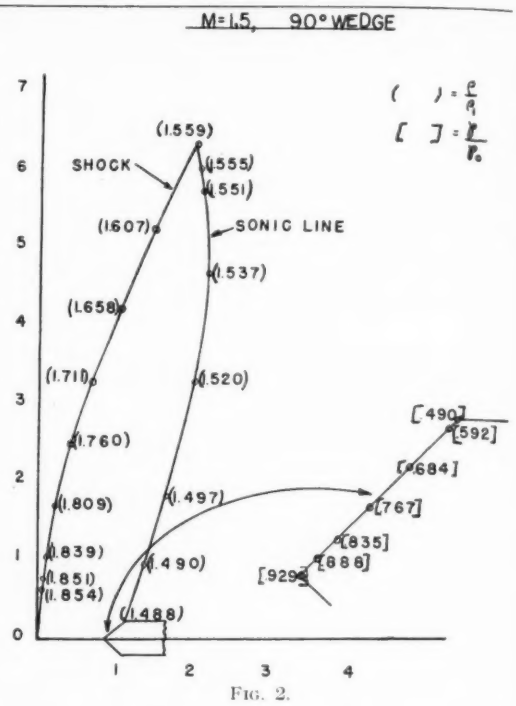

FIG. 2.

References

[1] Guderley, G., *Considerations of the Structure of Mixed Subsonic-Supersonic Flow Patterns*, Wright Field Technical Report No. F-TR-2168-ND, October, 1947.

[2] Vincenti, W. G., and Wagoner, C. B., *Transonic Flow Past a Wedge Profile with Detached Bow Wave—General Analytic Method and Final Calculated Results*, N.A.C.A. T.N. No. 2339, 1951.

[3] Vincenti, W. G., and Wagoner, C. B., *Transonic Flow Past a Wedge Profile with Detached Bow Wave—Details of Analysis*, N.A.C.A. T.N. No. 2588, 1951.

Influence Functions for Computing Lift and Rolling Moment of a Twisted Narrow Delta Wing

Beverly Beane

Aerodynamicist, Douglas Aircraft Company, Inc., Santa Monica Division, Santa Monica, Calif.

October 21, 1952

RECENT INVESTIGATIONS OF AERODYNAMIC RECIPROCITY CONCEPTS (e.g., reference 1) have indicated several general integral theorems for computing the linearized aerodynamic characteristics of wings in nonuniform downwash fields. These theorems state that the total lift and rolling moment on any wing plan form in a spanwise-varying downwash field may be written as the integral over the span of the product of the local angle of attack and an influence function that, for the lift case, is simply the span loading $[\bar{F}(y)]$ for the same plan form at constant angle of attack in reverse flow and, for the rolling case, is the span loading $[\bar{R}(y)]$ for the same plan form rolling with constant angular velocity in reverse flow. That is,

$$L = \int_{-s}^{+s} \bar{F}(y)\alpha(y)\,dy \qquad (1)$$

$$RM = \int_{-s}^{+s} \bar{R}(y)\alpha(y)\,dy \qquad (2)$$

The products $\bar{F}(y)\alpha(y)$ and $\bar{R}(y)\alpha(y)$ cannot be used for computing load or moment distributions for the forward wing.

In this note, approximate solutions are developed for the span loadings, $\bar{F}(y)$ and $\bar{R}(y)$, at supersonic speeds for a flat reverse delta wing with subsonic trailing edges. These solutions, together with the reciprocity theorems, provide a convenient method for computing the total lift or rolling moment on a narrow forward delta wing having arbitrary spanwise geometric or apparent twist. The latter results from wing-wing or wing-body interference. For such problems, the downwash can usually be considered to vary only along the span.

The following solutions are based on nonviscous linearized supersonic thin-wing theory. The wings are assumed to be unyawed. The rolling moment is computed with respect to the wing centerline.

A) Span Loading for Reverse Delta Wing at Constant Angle of Attack, α

The solution to this problem is known for two cases. The first occurs when the tip Mach cones are coincident with the trailing edge of the wing. In this case the span loading is triangular and is given by

$$\frac{1}{qS}\frac{\Delta L}{\Delta(y/s)} = \frac{4\alpha}{\beta}\,d\left(1 - \left|\frac{y}{s}\right|\right) \tag{3}$$

(S is the wing area, q is the dynamic pressure, s is the semispan, y is the spanwise coordinate measured from the wing centerline, β is the Mach Number parameter $\sqrt{M^2 - 1}$, and d is the edge parameter $\beta \tan \delta$, where δ is the semivertex angle of the trailing edge. In Eq. (3), d is equal to unity and need not be written explicitly; it is included for later convenience.) The second case is the slender wing theory result ($d = 0$). Here, the spanwise loading is elliptic and independent of Mach Number.[3]

$$\frac{1}{qS}\frac{\Delta L}{\Delta(y/s)} = \frac{4\alpha}{\beta}\,d\sqrt{1 - \left(\frac{y}{s}\right)^2} \tag{4}$$

For the intermediate cases, $0 < d < 1$, partial load distributions may be found by applying the reciprocity concepts in the reverse of their customary usage. That is, the loading at a station near the tip of the reverse wing is the same as the exact "strip" solution for the lift due to the corresponding deflected chordwise element of the forward wing. This solution was derived in reference 4 for a flat delta wing with subsonic leading edges as

$$\frac{1}{qS}\frac{\Delta L}{\Delta(y/s)} = \frac{4\alpha}{\beta}\sqrt{d}\left(1 - \left|\frac{y}{s}\right|\right) \tag{5}$$

Eq. (5) is valid at any spanwise station outboard of that at which the tip Mach cone first intersects the opposite edge—i.e., $|y/s| \geq (1 - d)/(1 + d)$. At the limit $|y/s| = (1 - d)/(1 + d)$, Eqs. (4) and (5) give identical results. In addition, Morikawa[5] has shown that the lift due to the central strip of a delta wing is independent of Mach Number. Therefore, at the wing centerline,

$$\left.\frac{1}{qS}\frac{\Delta L}{\Delta(y/s)}\right]_{y/s\,=\,0} = \frac{4\alpha}{\beta}\,d \tag{6}$$

(B) Span Loading for Reverse Delta Wing Rolling with Constant Angular Velocity, p

Similar solutions can be found for the rolling reverse delta wing. The slender wing theory result ($d = 0$) is[6]

$$\frac{1}{(2s)Sq}\frac{\Delta L}{\Delta(y/s)} = \frac{1}{\beta}\frac{p}{V}\,d\,\frac{y}{s}\sqrt{1 - \left(\frac{y}{s}\right)^2} \tag{7}$$

When the tip Mach cones lie along the trailing edge of the wing ($d = 1$), the loading is[7]

$$\frac{1}{(2s)Sq}\frac{\Delta L}{\Delta(y/s)} = \frac{2}{\beta}\frac{p}{V}\,d\,\frac{y}{s}\left(1 - \left|\frac{y}{s}\right|\right) \tag{8}$$

For intermediate values ($0 < d < 1$), the correct loading on the outer part of the wing is the same as the exact solution for the rolling moment due to the corresponding deflected (at angle p/V) chordwise strip of the forward delta wing. This result is found by the method of Evvard[8] to be

$$\frac{1}{(2s)Sq}\frac{\Delta L}{\Delta(y/s)} = \frac{1}{2\beta}\frac{p}{V}\frac{1}{\sqrt{d}}\left(1 - \left|\frac{y}{s}\right|\right)\times \left[(3d + 1)\left(\frac{y}{s}\right) \mp (1 - d)\right] \tag{9}$$

when $|y/s| \geq (1 - d)/(1 + d)$. [The sign of the last term of Eq. (9) must be opposite to the sign of y/s.] At $|y/s| = (1 - d)/(1 + d)$, the loadings computed by Eq. (9) and Eq. (7) are equal. Furthermore, it is known that the lift at the centerline of the reverse wing (or the rolling moment due to deflecting the central strip of the forward wing) is zero,

$$\left.\frac{1}{(2s)Sq}\frac{\Delta L}{\Delta(y/s)}\right]_{y/s\,=\,0} = 0 \tag{10}$$

The span-loading parameters,

$$F\left(\frac{y}{s}\right) = \frac{1}{\alpha d}\frac{\beta}{qS}\frac{\Delta L}{\Delta(y/s)}$$

from Eqs. (3)–(6) for the constant angle of attack wing, and

$$R\left(\frac{y}{s}\right) = \frac{1}{(p/V)d}\frac{\beta}{(2s)Sq}\frac{\Delta L}{\Delta(y/s)}$$

from Eqs. (7)–(10) for the rolling wing, are plotted in Figs. 1 and 2, respectively. These curves suggested that a reasonable approximation for the loading of the inner sections of the reverse delta wing would be obtained from slender wing theory. That is, in the region $0 \leq |y/s| \leq (1 - d)/(1 + d)$, the loading is assumed to be given by Eq. (4) for the wing at constant angle of attack and by Eq. (7) for the wing that is rolling with constant rate of roll. In the region $(1 - d)/(1 + d) \leq |y/s| \leq 1$, the loading is given correctly by Eq. (5) or (9).

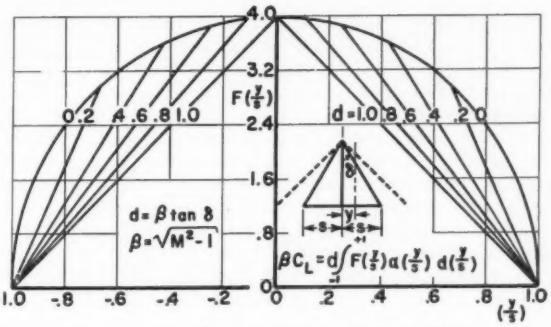

FIG. 1. Lift influence function for delta wings.

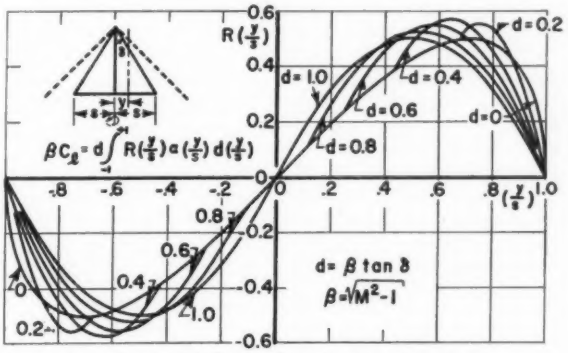

FIG. 2. Roll influence function for delta wings.

Since the reverse wing span loadings, if correct, are also influence functions for computing total lift or moment on forward delta wings, the reliability of the assumed loadings was checked by using the analytical formulation of the curves in Figs. 1 and 2 to compute the lift and rolling moment coefficients for some forward delta wings for which exact solutions are known. In the lift case, comparisons were made for delta wings having constant angle of attack[2] and linear symmetric twist.[9] The assumed lift influence function led to total lifts that were lower than the true ones by less than 2 per cent. In the rolling moment case, comparisons were made for a delta aileron and for the damping in roll of a plane delta wing. These calculations employed the roll influence function from Fig. 2, where, for any d, the influence function inboard of the station $|y/s| = (1 - d)/(1 + d)$ is approximated by the slender wing result. The solution obtained by this method for the delta aileron problem was the exact result reported in reference 10, $\beta C_l = \alpha(2/3)d$. This means that there is the same total area under any one of the curves in Fig. 2, and the amount of area is correct. For the second example, damping in roll of a plane delta wing, the present method yields an analytical expression different from the exact result;[11] yet the numerical difference between the two solutions is less than can be determined with four-decimal-place accuracy. This agreement is probably due to the fact that the local angle of attack of this wing is relatively small over the inner part of the span where the solution is approximate and is larger over the outer span where the influence function is exact.

From these examples, it is concluded that, for any Mach Number, slender wing theory gives a good approximation for the span loading on a reverse delta wing inboard of the spanwise station at which the tip Mach cones first intersect the trailing edge. Outboard of this station, exact loadings are known. These solutions are useful in reducing the complexity of many problems involving the calculation of lift or rolling moment on forward delta wings in nonuniform flow fields.

References

[1] Heaslet, M. A., and Spreiter, J. R., *Reciprocity Relations in Aerodynamics*, N.A.C.A. T.N. No. 2700, May, 1952.

[2] Puckett, A. E., and Stewart, H. J., *Aerodynamic Performance of Delta Wings at Supersonic Speeds*, Journal of the Aeronautical Sciences, Vol. 14, No. 10, p. 567, October, 1947.

[3] Jones, R. T., *Properties of Low-Aspect-Ratio Pointed Wings at Speeds Below and Above the Speed of Sound*, N.A.C.A. Report No. 835, 1946.

[4] Graham, M. E., *Some Linearized Computations of Supersonic Wing-Tail Interference*, Douglas Report SM-13430, December, 1948.

[5] Morikawa, G., *Conical Potential Solutions in Linearized Supersonic Flow* (to be published).

[6] Ribner, H. S., *The Stability Derivatives of Low-Aspect-Ratio Triangular Wings at Subsonic and Supersonic Speeds*, N.A.C.A. T.N. No. 1423, 1947.

[7] Lagerstrom, P. A., and Graham, M. E., *Some Aerodynamic Formulas in Linearized Supersonic Theory for Damping in Roll and Effect of Twist for Trapezoidal Wings*, Douglas Report SM-13200, March, 1948.

[8] Evvard, J. C., *Distribution of Wave Drag and Lift in the Vicinity of Wing Tips at Supersonic Speeds*, N.A.C.A. T.N. No. 1382, July, 1947.

[9] Goodman, T. P., *The Lift Distribution on a Delta Wing with Linear Symmetric Twist*, Cornell Aeronautical Laboratory CM-524, February, 1949 (revised May, 1949).

[10] Bleviss, Z. O., *Some Roll Characteristics of Plane and Cruciform Delta Ailerons and Wings in Supersonic Flow*, Douglas Report SM-13431, June, 1949.

[11] Brown, C. E., and Adams, M. C., *Damping in Pitch and Roll of Triangular Wings at Supersonic Speeds*, N.A.C.A. Report No. 892, 1948.

Energy Removal from a Supersonic Turbulent Boundary Layer

John Joseph Martin

Research Engineer, Aerophysics Laboratory, North American Aviation, Inc., Downey, Calif.

October 6, 1952

THE SUPERSONIC BOUNDARY LAYER is apparently a convenient source of thermal energy for use within aircraft propelled at high velocities. Before considerable time is spent determining a suitable means for utilizing this energy, an analysis to determine the desirability of such a utilization should be carried out.

Let the system being analyzed be represented by a section of a flat plate of 1 sq.ft., the restrictions being that the section's distance from the leading edge be sufficient so that the dimension of the 1 sq.ft. in the direction of flow is small and that one side of the plate is "inside" and the other "outside." These conditions are imposed so that the skin-friction and heat-transfer coefficients ($c_{f\infty}$ and h) will be essentially constant over the 1 sq.ft. and so that the high temperature on one side of the plate may be used on the other. Assume, also, that the following constants obtain for air:

Molecular weight: $m = 29.0$ lbs.$_m$/mole
Gas constant: $R = 1{,}544$ ft.lbs.$_F$/mole °R.
Isobaric specific heat: $c_p = 0.24$ B.t.u./lb.$_m$ °R.
Specific heat ratio: $\gamma = 1.40$
Mechanical equivalent of heat: $J = 778.2$ ft.lbs.$_F$/B.t.u.
Acceleration due to gravity: $g = 32.2$ ft./sec.^{2}

In addition, the following relations are used:

Speed of sound: $a_\infty^2 = \gamma g R T_\infty/m$
Drag force: $D_f = c_{f\infty}\rho_\infty u_\infty^2/2g$
Drag power: $P = u_\infty D_f/J$
Heat transferred: $q = h(T_{\text{ins.}} - T_w)$
Temperature ratio: $\theta_x = T_x/T_\infty$
Insulated wall temperature ratio: $\theta_{\text{ins.}} = 1 + (1/2) \times (\gamma - 1)M_\infty^2$

The primary requirement in this analysis is a set of values for $c_{f\infty}$ and h which is consistent with variation of θ_w. Such a consistent system is available in reference 1 and is, in fact, the basis of this note. If the assumption is made that the only net work that must be done in propelling the plate is the difference $(P - \eta q)$, then there is a basis for comparison of various pairs of power requirement and heat flux. Making this assumption is the same as saying that a percentage (η, which may correspond to a heat engine overall efficiency) of the heat extracted from the boundary layer is useful in some way in driving the plate and that this energy is available at the temperature θ_w.

The power required is

$$P = u_\infty D_f/J = (c_{f\infty}\rho_\infty u_\infty T_\infty/2)\,(\gamma R M_\infty^2/Jm)$$

The heat flux is

$$q = h(T_{\text{ins.}} - T_w) = (c_{f\infty}\rho_\infty u_\infty T_\infty/2)\,(\theta_{\text{ins.}} - \theta_w)c_p$$

since, according to reference 2, $c_{H\infty} = h/\rho_\infty u_\infty c_p = c_{f\infty}/2$.* Hence, if η is a heat engine efficiency, the net work is

$$(P - \eta q) = \Phi_{\theta w} = (c_{f\infty}\rho_\infty u_\infty T_\infty/2)[(\gamma R M_\infty^2/Jm) - \eta c_p(\theta_{\text{ins.}} - \theta_w)]$$

or, since $\theta_{\text{ins.}} = 1 + [1/2(\gamma - 1)M_\infty^2]$,

$$\Phi_{\theta w} = (c_{f\infty}\rho_\infty u_\infty T_\infty/2)[1/2(\gamma - 1)M_\infty^2(2 - \eta) + \eta(\theta_w - 1)]\,c_p$$

in which $c_{f\infty} = c_{f\infty}(\theta_w, R_\infty)$.

For $M_\infty = 5.0$, $R_\infty = 10^7$, and various values of θ_w and η, Fig. 1 shows the variation of $\Phi_{\theta w}/\Phi_{\theta\text{ins.}}$. For values $0 \leqslant \eta \leqslant 0.4$ (approximately), the net work apparently increases with decreasing θ_w, so that heat extraction from the boundary layer is undesirable. For $0.4 \leqslant \eta \leqslant 1.0$, the net work is decreasing with de-

* A more accurate value of $c_{H\infty}$ is given by Van Driest as $c_{f\infty}/2Pr^{2/3}$. In Fig. 1, $Pr = 1$ was chosen for convenience; if $Pr \neq 1$, a modified efficiency is given by $\eta' = Pr^{2/3}\eta$.

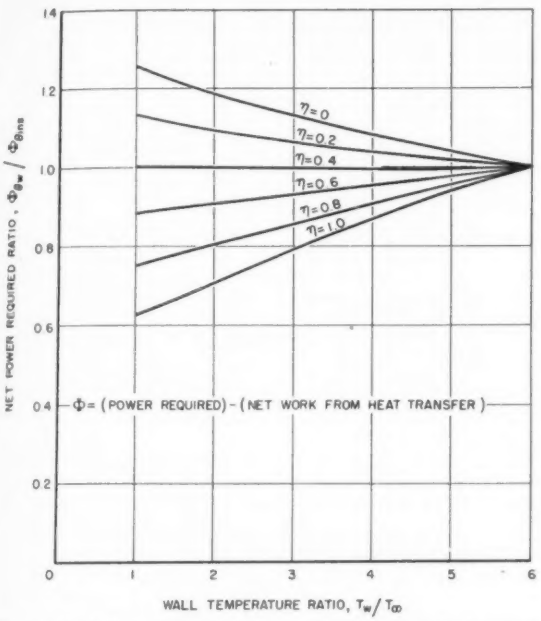

FIG. 1. Variation of dimensionless net power required versus wall temperature ratio with parametric heat engine efficiency.

creasing θ_w so that heat extraction seems desirable. However, the fact that most stationary heat engines have overall efficiencies less than 0.4 means that, generally, heat extraction from a supersonic *turbulent* boundary layer is an inefficient process.

REFERENCES

[1] Van Driest, E. R., *Turbulent Boundary Layer in Compressible Fluids*, Journal of the Aeronautical Sciences, Vol. 18, No. 3, p. 145, March, 1951.

[2] Van Driest, E. R., *Calculation of the Stability of the Laminar Boundary Layer in a Compressible Fluid on a Flat Plate with Heat Transfer*, North American Aviation, Inc., Aerophysics Laboratory Report AL-1334, September 3, 1951.

Relation of Force, Acceleration, and Momentum for a Body Whose Mass Is Varying

H. W. Sibert
Professor of Aeronautical Engineering, University of Colorado, Boulder, Colo.

October 2, 1952

SUMMARY

It is the belief of many engineers that the relation force $= d(MV)/dt$ is fundamental for both constant and variable mass, while the relation force $= Ma$ is true only for constant mass. It is shown that the latter equation is fundamental for both constant and variable mass while the former equation is valid for variable mass only when the added mass is initially at rest or the discarded mass is finally at rest.

EQUATIONS

EXPERIMENTS HAVE DEMONSTRATED that

$$F_{res.} = Ma \qquad \text{(constant } M\text{)} \tag{1}$$

where M is the mass of a body, a is its acceleration, and $F_{res.}$ is the resultant force acting on the body. If V is the speed of the body,

$$F_{res.} = M(dV/dt) = d(MV)/dt \qquad \text{(constant } M\text{)} \tag{2}$$

Since a jet airplane or missile has a high rate of fuel consumption, its mass cannot be considered to be constant. Hence, the designer must know whether formulas that have been derived for constant mass can also be applied to a body of varying mass. In particular, can either or both of Eqs. (1) and (2) be applied to a body whose mass is varying rapidly?

To avoid the use of vectors, all forces and velocities will be assumed to be parallel. Let the body be picking up mass, let all velocities be measured relative to the ground, and let

M = mass of the body at any time t
V = velocity of the body at time t
v = initial velocity at time t of the mass that is being picked up
$F_{ext.}$ = external force acting on the body at time t, exclusive of any force due to jet action

During an infinitesimal length of time from t to $t + \Delta t$, the mass picked up is $(dM/dt)\Delta t$, and its increase in momentum is $(V - v) \times (dM/dt)\Delta t$. During time Δt, the increase in momentum of mass M is $M\Delta V$. Since impulse equals change in momentum,

$$F_{ext.}\Delta t = M\Delta V + (V - v)(dM/dt)\Delta t \tag{3}$$

Dividing by Δt and then letting $\Delta t \to 0$,

$$F_{ext.} = M(dV/dt) + (V - v)dM/dt \tag{4}$$

Eq. (4) is given in reference 1.

Note that $M(dV/dt)$ is the rate of change of momentum of the instantaneous mass while $(V - v)dM/dt$ is the rate of change of momentum of the added mass. Hence, Eq. (4) becomes

$F_{ext.}$ = rate of change of momentum of instantaneous mass + rate of change of momentum of added mass (5)

At first it might be thought that Eqs. (2) and (5) are identical. This is not true because

$$d(MV)/dt = M(dV/dt) + V(dM/dt)$$

and, hence, Eq. (4) becomes

$$F_{ext.} = d(MV)/dt - v(dM/dt) \tag{6}$$

Thus Eq. (2) is valid only when the mass picked up is initially at rest and $F_{res.} = F_{ext.}$.

The mass being picked up by the body at time t exerts on the body a jet force $F_{jet} = (V - v)dM/dt$ that acts in a direction opposite to V. Hence, from Eq. (4),

$$F_{ext.} = M(dV/dt) + F_{jet} \tag{7}$$

Eq. (7) can be written

$$F_{res.} = M(dV/dt) \tag{8}$$

with $F_{res.} = F_{ext.} - F_{jet}$. Hence, Eq. (1) is also valid for a body of variable mass, provided $F_{res.} = F_{ext.} - F_{jet}$.

By a similar analysis it can be shown that Eqs. (4) through (8) also hold when the body is discarding mass. Moreover, these equations will also be valid when the forces and velocities are not parallel, provided each velocity and force in them is written as a vector.

CONCLUDING REMARKS

It is the belief of many engineers that Eq. (2) is fundamental for both constant and variable mass, while Eq. (1) is true only for constant mass. They have justified the use of Eq. (1) for variable mass on the basis that for most aircraft the rate of change of mass is small compared with the mass at any instant and, hence, the effect of the change in mass is negligible. It has been shown above that Eq. (1) is fundamental for both constant and variable mass provided the resultant force includes any jet force on the body while Eq. (2) is valid for variable mass only when the added mass is initially at rest or the discarded mass is finally at rest. This last condition is not met in jet airplanes or rockets, because the jet speed relative to the aircraft is always larger than the speed

of the aircraft and, hence, the jet is not at rest relative to the ground. It should be noted, however, that the resultant force is equal to the rate of change of the momentum for both constant and variable mass provided that the resultant force does not include any jet force and the rate of change of momentum is calculated separately for the instantaneous mass and the added (or discarded) mass [see Eq. (5)].

Reference

[1] Timoshenko, S., and Young, D. H., *Advanced Dynamics*, p. 114; McGraw-Hill Book Company, Inc., New York, 1948.

Further Comments on "Turbulent Boundary-Layer Characteristics at Supersonic Speeds"

R. J. Monaghan*
Royal Aircraft Establishment, Farnborough, Hants., England
September 29, 1952

In a contribution[1] to the Readers' Forum in the May, 1952, issue of the Journal, Luther presented a simple interpolation formula based on Wilson's equation[2] for turbulent skin friction in compressible flow, under zero heat-transfer conditions.

An equally simple formula can be obtained if we write Wilson's equation in the form

$$\frac{0.242\ \Phi}{C_{F_w}^{1/2}} = \log_{10}(R_w C_{F_w}) \tag{1}$$

where

$$\Phi = \sin^{-1}\sqrt{\sigma}/\sqrt{\sigma}$$

with $\sigma = M^2/(M^2 + 5)$ if $\gamma = 1.4$; subscript w denotes that density and viscosity are to be evaluated at wall (plate surface) temperature, and it is assumed that $\mu \propto T^{0.768}$.

By comparison of Eq. (1) with the corresponding incompressible flow formula

$$0.242/C_{F_i}^{1/2} = \log_{10}(R_i C_{F_i}) \tag{2}$$

we see that

$$\left.\begin{aligned} C_{F_i} &= C_{F_w}/\Phi^2 \\ R_i &= R_w\Phi^2 \end{aligned}\right\} \quad \text{when} \tag{3}$$

Eqs. (3) can then be applied to the more convenient Blasius or Prandtl-Schlichting formulas for mean skin friction in incompressible flow to obtain corresponding formulas for compressible flow. Thus, if we take

$$C_{F_i} = 0.46(\log_{10}R_i)^{-2.6} \tag{4}$$

and apply Eqs. (3), we obtain

$$C_{F_w} = 0.46\ \Phi^2(\log_{10}R_w\Phi^2)^{-2.6} \tag{5}$$

which gives results in close agreement with those from Eq. (1) and is more simple in application.

Wilson's analysis[2] starts by assuming the shearing stress relation to be of incompressible flow form and by allowing for variations in the mean density obtains expressions for velocity profile and then for skin friction in compressible flow. If, however, we start by assuming that the log law velocity distribution

$$u/u_\tau = C_1 + C_2 \log yu_\tau/\nu_w \tag{6}$$

where $u_\tau^2 = \tau_0/\rho_w$ and C_1, C_2 are the constants found valid in incompressible flow, will be valid in compressible flow, with or without heat transfer, provided density and viscosity are evaluated at wall temperature, and if we assume a temperature distribution of the form

$$T/T_w = 1 + B(u/u_1) - A^2(u/u_1)^2 \tag{7}$$

then by substitution in the momentum equation and by the comparison already described, we obtain[3]

$$\left.\begin{aligned} C_{F_i} &= C_{F_w} \\ R_i &= R_w(T_1/T_w) \end{aligned}\right\} \quad \text{when} \tag{8}$$

where T_1 is free-stream static temperature.

Applying Eqs. (8) to Eq. (4), we obtain

$$C_{F_w} = 0.46\ [\log_{10}R_w(T_1/T_w)]^{-2.6} \tag{9}$$

which gives equally as good agreement with experimental results as Wilson's equation [Eq. (1) or (5)] gives under zero heat-transfer conditions. It also gives results within 10 per cent of the values given by an extension of Wilson's analysis to include heat-transfer conditions for Mach Numbers up to 4 and for values of T_{H1}/T_w between 0.5 and 2.0, with $R = 10^7$ (T_{H1} is free-stream stagnation temperature).

The reason for this agreement is presumably to be found in the fact that the velocity profiles as given by Wilson's analysis[2] are forced by boundary conditions to agree with the log law profile [Eq. (6)] in the inner portion of the layer, which region is of major importance when evaluating the momentum integral.

Note that the "compressibility parameter" in Eq. (9) is the ratio T_1/T_w. Thus, if the formula were valid, the skin friction in a high-speed flow under zero heat-transfer conditions should be the same as that in a low-speed flow with heat transfer from plate to stream for the same value of T_1/T_w. A partial check of this was obtained by an analysis[4] of the skin-friction and heat-transfer coefficients obtained from subsonic flow tests in pipes with high heat-transfer rates[5] when a good correlation was obtained on the basis of Eqs. (8).

On the other hand, recent measurements at the R.A.E. of the boundary layers on a flat plate at $M = 2.43$ and 2.82 under heat-transfer conditions ($T_w = 373°$K., $T_{H1} = 237°$K., 276.5°K.) have shown no variation of skin-friction coefficient from its zero heat-transfer value at the same Mach Number. These results (unpublished M.O.S. reports) were obtained from pitot traverses, but heat-transfer rates were measured directly and showed a variation somewhat as given by Eqs. (8).

Finally, the analysis of reference 3 also gave

$$H/H_i = (T_w/T_1) + [(\gamma - 1)/2]M_1^2 \tag{10}$$

for the variation of the ratio (H) of displacement thickness to momentum thickness with Mach Number and heat transfer, and this formula has given good agreement with our experimental results to date (with and without heat transfer) if H_i is taken to be 1.3 and if the second term on the right-hand side is multiplied by the cube root of Prandtl Number—i.e.,

$$H = 1.3\{(T_w/T_1) + Pr^{1/3}[(\gamma - 1)/2]M_1^2\} \tag{10a}$$

(The original analysis[3] was for $Pr = 1$, and it can be argued that a logical extension to other values would include the factor $Pr^{1/3}$.)

References

[1] Luther, M. L., *Comments on "Turbulent Boundary Layer Characteristics . . . ,"* Readers' Forum, Journal of the Aeronautical Sciences, Vol. 19, No. 5, p. 357, May, 1952.

[2] Wilson, R. E., *Turbulent Boundary-Layer Characteristics at Supersonic Speeds—Theory and Experiment*, Journal of the Aeronautical Sciences, Vol. 17, No. 9, p. 585, September, 1950.

[3] Monaghan, R. J., and Johnson, J. E., *The Measurement of Heat Transfer and Skin Friction at Supersonic Speeds, Part II*, British A.R.C. Current Paper No. 64, 1952.

[4] Monaghan, R. J., *Comparison Between Experimental Measurements and a Suggested Formula for the Variation of Turbulent Skin Friction in Compressible Flow*, British A.R.C. Current Paper No. 45, 1951.

[5] Humble, L. V., Lowdermilk, W. H., and Desmon, L. G., *Measurements of Average Heat Transfer and Friction Coefficients for Subsonic Flow of Air in Smooth Tubes at High Surface and Fluid Temperatures*, N.A.C.A. Report No. 1020, 1951.

* The writer is indebted to the Chief Scientist, Ministry of Supply, for permission to publish this note.

On the Boundary-Layer Equations in Hypersonic Flow and Their Approximate Solutions†

Lester Lees
Department of Aeronautical Engineering, Princeton University, Princeton, N.J.
October 2, 1952

Summary

Analytical solutions of the Prandtl boundary-layer equations are obtained for the problem of the "strong" interaction between the leading-edge shock and the viscous layer over a flat plate at hypersonic velocities. As the Mach Number increases and the interaction region spreads downstream over the plate, the local skin-friction coefficient increases rapidly over its conventional value. The local heat-transfer coefficient at first remains practically unaffected but then also begins to increase with Mach Number.

List of Symbols

Free-stream quantities are denoted by the subscript ∞, while the subscript w denotes quantities evaluated at the surface and the subscript δ denotes quantities evaluated at the outer edge of the viscous layer.

- x^*, y^* = coordinates parallel and normal to surface, respectively, with origin at leading edge of plate
- u^*, v^* = components of velocity parallel and normal to surface, respectively
- p^* = pressure
- ρ^* = density
- T^* = absolute temperature
- μ^* = viscosity
- ν^* = kinematic viscosity, μ^*/ρ^*
- γ = ratio of specific heats, C_p/C_v
- δ = thickness of viscous layer
- L = characteristic length
- M_∞ = free-stream Mach Number
- Re_{x^*} = Reynolds Number based on free-stream quantities
- p = $p^*/p_\infty{}^*$
- ρ = $\rho^*/\rho_\infty{}^*$, etc.
- x, y = x^*/L, y^*/δ

Discussion

In a recent note, Shen[1] shows that the Prandtl boundary-layer equations are valid even for the interaction between the leading-edge shock and the viscous layer over an insulated flat plate or wedge at hypersonic velocities, provided that $(\delta/x^*)^2 << 1$. However, the argument leading to the statement that the static pressure variation across the layer is of order $1/M_\infty{}^2$, and is therefore negligible, seems inconclusive. This argument is based on the postulate that $\rho \sim 1/T \sim 1/M_\infty{}^2$, in spite of the fact that T is certainly not of order $M_\infty{}^2$ near the outer edge of the viscous layer or near the surface for the case of heat transfer. Thus a few important statements must be added to Shen's discussion.

From the y-momentum and continuity equations, $p_y \sim y^3$ near the surface, and the contribution of this region to the pressure variation across the layer is negligible, as expected. Near the outer edge,

$$p_y = -\gamma M_\infty{}^2(\delta \cdot \rho u v_{x^*} + \rho v v_y) + \text{viscous terms} \approx -\gamma M_\infty{}^2(\delta/x^*)^2$$

where the subscript denotes differentiation with respect to the indicated variable. But the energy equation shows that $\partial T/\partial y \sim M_\infty{}^2$, so that the thickness of the outer zone in which $\rho = 0(1)$ is of order $1/M_\infty{}^2$. Therefore the contribution of this zone to the pressure variation across the layer is of order $(\delta/x^*)^2$ and is negligible when $(\delta/x^*)^2 << 1$. In the interior of the layer $\rho \sim 1/M_\infty{}^2$; thus Shen's argument is completed.

Once it is established that the pressure variation across the viscous layer is negligible when $(\delta/x^*)^2 << 1$, the problem of the interaction of shock and viscous layer over a flat plate for large values of $M_\infty{}^3/\sqrt{Re_{x^*}} = \chi$ treated by Shen[2] and by Li and Nagamatsu[3] can be considerably simplified. By solving the von Kármán momentum integral equation approximately for an insulated surface, these investigators find that $\delta \sim x^{3/4}$ and $p \sim x^{-1/2}$ for $\chi >> 1$. But this result can be obtained directly by means of an order of magnitude consideration. Flows with large χ are characterized by the fact that the pressure gradient $\partial p^*/\partial x^*$ and the viscous stress term $(\partial/\partial y^*)\,[\mu^*(\partial u^*/\partial y^*)]$ are of the same order. At the outer edge of the viscous layer the oblique shock relation

$$\frac{\partial p}{\partial x^*} = \gamma(\gamma+1)M_\infty{}^2 \frac{d\delta}{dx^*}\frac{d^2\delta}{dx^{*2}}$$

holds approximately; therefore,

$$M_\infty{}^2 \frac{\delta^2}{(x^*)^3}\; p_\infty{}^* \sim \mu\mu_\infty{}^* \frac{u_\infty{}^*}{\delta^2}$$

or

$$\delta = \delta_0 C^{1/4} \frac{\sqrt{M_\infty}}{(u_\infty{}^*/\nu_\infty{}^*)^{1/4}}(x^*)^{3/4} \tag{1}$$

and

$$p = p_0 \chi \tag{2}$$

where $\chi = \sqrt{C}\,\chi$ and C is the constant in the linear viscosity-temperature relation $\mu = CT$; δ_0 is a constant, and $p_0 = (9/32)\gamma(\gamma+1)\delta_0{}^2$.‡

In reference 3 it is also shown that the Pohlhausen parameter λ determining the shape of the velocity profile $u/u_\delta = (y, \lambda)$ is approximately constant for $\chi >> 1$. This result, together with the relations (1) and (2), suggests that "exact" solutions of the boundary-layer equations can be obtained directly for both insulated and noninsulated surfaces, without resorting to the approximate Pohlhausen method. The asymptotic series solution for $u(x, y)$, for example, is of the form

$$\frac{u}{u_\delta}(x,y) = u_0(\sigma) + \frac{1}{\chi}u_1(\sigma) + \ldots$$

where $\sigma = y^*/(x^*)^{3/4}$ and $u_0(\sigma)$, $u_1(\sigma)$, etc.; each satisfies an ordinary second-order differential equation. In the "von Mises coordinates" x,ψ along and normal to the stream lines, the x-momentum equation is

$$uu_x = u(\rho u u_\psi)_\psi - \frac{1}{\gamma M_\infty{}^2}\frac{p_x}{p}T \tag{3}$$

and the energy equation is

$$T_x = \frac{\gamma-1}{\gamma}\frac{p_x}{p}T + (\gamma-1)M_\infty{}^2 p u(u_\psi)^2 + p(uT_\psi)_\psi \tag{4}$$

Here $\psi = \psi^*/\sqrt{\nu_\infty{}^* u_\infty{}^* LC}$, while $\rho u^* = \partial\psi^*/\partial y^*$ and $\rho v^* = -\partial\psi^*/\partial x^*$. By employing Eq. (2) for the pressure and introducing the nondimensional stream function $\zeta \sim (\psi/\sqrt{p})\,(1/\sqrt{x})$, or

$$\zeta = \frac{1}{\sqrt{2}}\left(\frac{u_\infty{}^*}{\nu_\infty{}^*}\right)^{1/4}\frac{L^{1/4}}{C^{1/4}p_0{}^{1/2}}\frac{1}{M_\infty{}^{3/2}}\frac{\psi}{x^{1/4}}$$

the momentum equation [Eq. (3)] is reduced to the following equation for u_0:

† This work was supported by the U.S.A.F., Air Research and Development Command, under Contract No. AF-33(038)-250.

‡ In references 2 and 3, the slope of the outer edge of the viscous layer $d\delta/dx^*$ is regarded as identical with the oblique shock angle θ_s, so that

$$p = \frac{2\gamma}{\gamma+1}M_\infty{}^2\left(\frac{d\delta}{dx^*}\right)^2$$

But this statement is inconsistent with the fact that $v_\delta = d\delta/dx^*$ by the continuity equation, whereas $\theta_s = [(\gamma+1)/2]v$ when $M_\infty{}^2 >> 1$, according to the oblique shock relations. In the present note the approximate boundary condition

$$p = \frac{\gamma}{2}(\gamma+1)M_\infty{}^2 v^2 = \frac{\gamma}{2}(\gamma+1)M_\infty{}^2\left(\frac{d\delta}{dx^*}\right)^2$$

is employed instead.

$$\zeta u_0 \frac{du_0}{d\zeta} + 2u_0 \frac{d}{d\zeta}\left(u_0 \frac{du_0}{d\zeta}\right) + \frac{2}{\gamma M_0^2} T_0 = 0 \qquad (5)$$

where the term xuu_x is dropped because it is of order $(\delta/x^*)^2$ compared to the other terms ($u_\delta^* \approx u_\infty^*$ for $M_\infty >> 1$). The energy equation is

$$2x \frac{\partial T_0}{\partial x} + \frac{\gamma - 1}{\gamma} T_0 = (\gamma - 1) M_\infty^2 u_0 \left(\frac{du_0}{d\zeta}\right)^2 + \frac{d}{d\zeta}\left(u_0 \frac{dT_0}{d\zeta}\right) + \frac{\zeta}{2} \frac{dT_0}{d\zeta} \qquad (6)$$

Similar equations are obtained for u_1, T_1, etc., but they will not be given here.

(a) Insulated Surface

For a Prandtl Number of unity and zero surface heat transfer, Crocco found that

$$T = 1 + [(\gamma - 1)/2] M_\infty^2 (1 - u^2)$$

Therefore, when $M_\infty >> 1$, Eq. (5) becomes

$$\zeta u_0 \frac{du_0}{d\zeta} + 2u_0 \frac{d}{d\zeta}\left(u_0 \frac{du_0}{d\zeta}\right) + \frac{\gamma - 1}{\gamma}(1 - u_0^2) = 0 \qquad (7)$$

and this equation is exactly the Falkner-Skan differential equation[4] for the low-speed laminar boundary layer with $u_\delta \sim x^m$. If the coordinate η_i defined by the relation $d\zeta/d\eta_i = u_0$ is introduced, then Eq. (7) takes the more familiar form

$$2 \frac{d^3\zeta}{d\eta_i^3} + \zeta \frac{d^2\zeta}{d\eta_i^2} + \beta\left[1 - \left(\frac{d\zeta}{d\eta_i}\right)^2\right] = 0$$

where

$$\beta = 2m/(m + 1) = (\gamma - 1)/\gamma$$

In other words, $u_0(\zeta)$ is the same known function of ζ as in the Falkner-Skan case with $\beta = (\gamma - 1)/\gamma$. (For air, $(\gamma - 1)/\gamma = 0.286$.) The corresponding actual distance from the surface is found by means of the simple quadrature

$$y^* = \int_0^{\eta_i} \frac{d\zeta}{d\eta_i} d\eta_i \Big/ \left(\frac{d\zeta}{d\psi}\frac{d\psi}{dy^*}\right) \qquad (8)$$

or

$$\frac{y^*}{x^*}(Re_{x^*})^{1/4} = \frac{4}{3} C^{1/4} M_\infty^{1/2} \frac{(\gamma - 1)}{\sqrt{\gamma(\gamma + 1)}} \frac{1}{\delta_0} \int_0^{\eta_i} (1 - u_0^2) d\eta_i \qquad (8a)$$

where

$$\delta_0 = \frac{2}{\sqrt{3}} \frac{\sqrt{\gamma - 1}}{[\gamma(\gamma + 1)]^{1/4}} \left[\delta^* \sqrt{\frac{u_\infty^*}{\nu_\infty^* x^*}} + \delta^{**} \sqrt{\frac{u_\infty^*}{\nu_\infty^* x^*}}\right]^{1/2}$$

and the quantity in brackets is the sum of the displacement and momentum thickness for the Falkner-Skan profile with $\beta = (\gamma - 1)/\gamma$. (The necessary values are given by Pretsch.[5])

The expression for the local skin-friction coefficient for large $\bar{\chi}$ is given by

$$c_{f_0} = \frac{2\mu_w^*}{\rho_\infty^* u_\infty^*} \left(\frac{du_0}{d\eta_i}\right)_w \left(\frac{d\eta_i}{dy^*}\right)_w$$

or

$$c_{f_0} = \left[\frac{3}{4}\sqrt{\gamma(\gamma + 1)}\,\delta_0\right] \left(\frac{du_0}{d\eta_i}\right)_w C^{3/4} \frac{M_\infty^{3/2}}{(Re_{x^*})^{1/4}} \frac{1}{\sqrt{Re_{x^*}}} \qquad (9)$$

If $\mu \sim T^m$, then

$$C = \left(\frac{T_w^*}{T_\infty^*}\right)^{m-1} = \left(\frac{\gamma - 1}{2}\right)^{m-1} M_\infty^{2m-2}$$

for an insulated surface. Thus

$$c_{f_0} \sim \frac{M_\infty^{(3/2)m}}{(Re_{x^*})^{1/4}} \cdot \frac{1}{\sqrt{Re_{x^*}}}$$

$$\delta \sim \frac{M_\infty^{m/2} (x^*)^{3/4}}{(u_\infty^*/\nu_\infty^*)^{1/4}}$$

These results agree with those obtained in reference 3, but for various reasons that will not be discussed here the numerical constants are different. (See footnote, for example.) These results can also be obtained as a special application of the Stewartson transformation.[6]

(b) Heat Transfer

In free flight the surface temperature is much lower than the equilibrium temperature, and T_0 is approximately equal to $[(\gamma - 1)/2] M_\infty^2 u(1 - u)$ in the interior of the viscous layer for a Prandtl Number of unity. The maximum value of the term $(2/\gamma M_\infty^2) T_0$ in Eq. (5) is $(\gamma - 1)/4\gamma$, which is small. (For air, $(\gamma - 1)/4\gamma = 0.071$.) Therefore, $u_0(\zeta)$ approximately satisfies the differential equation

$$\frac{\zeta}{2} \frac{du_0}{d\zeta} + \frac{d}{d\zeta}\left(u_0 \frac{du_0}{d\zeta}\right) = 0$$

and is therefore approximately equivalent to the Blasius velocity distribution in the ζ-coordinate. More precisely,

$$u_0(\zeta) = u_B(\zeta) + \Delta u(\zeta)$$

$$T_0(\zeta) = T_w + \left(1 + \frac{\gamma - 1}{2} M_\infty^2 - T_w\right) u_0 - \frac{\gamma - 1}{2} M_\infty^2 u_0^2 + f(\zeta) + T_\delta(x) g(\zeta)$$

where $\Delta u(\zeta)$, $f(\zeta)$, and $g(\zeta)$ represent small corrections satisfying ordinary linear, second-order inhomogeneous differential equations; these equations are now in process of being integrated. With good accuracy the actual distance normal to the surface is given by

$$\frac{y^*}{x^*}(Re_{x^*})^{1/4} = \frac{4}{3} C^{1/4} M_\infty^{1/2} \frac{\gamma - 1}{\sqrt{\gamma(\gamma + 1)}} \times \frac{1}{\delta_0} \int_0^{\eta_i} u_0(1 - u_0)\, d\eta_i$$

where

$$\delta_0 = \frac{2}{\sqrt{3}} \frac{\sqrt{\gamma - 1}\,\sqrt{0.664}}{[\gamma(\gamma + 1)]^{1/4}}$$

and $u_0(\eta_i)$ is the Blasius function. The approximate expression for local skin-friction coefficient is

$$c_{f_0} = \left\{\frac{\sqrt{3}}{4}[\gamma(\gamma + 1)]^{1/4} \sqrt{\gamma - 1}\,\sqrt{0.664}\right\} \chi \frac{0.664\sqrt{C}}{\sqrt{Re_{x^*}}} \qquad (10)$$

and the local heat transfer coefficient is given by

$$h_0 = q_0/\rho_\infty^* u_\infty^* c_p (T_s^* - T_w^*) = c_{f_0}/2$$

where $T_s^*/T_\infty^* = 1 + [(\gamma - 1)/2] M_\infty^2$. Here,

$$C = (T_w^*/T_\infty^*)^{m-1}$$

$$\bar{\chi} = \sqrt{C}\,(M_\infty^3/\sqrt{Re_{x^*}})$$

These expressions (9) and (10) for local skin-friction and heat-transfer coefficients are expected to be good approximations for $\bar{\chi} > 15$ (approximately); presumably these solutions can be improved by calculating the $1/\bar{\chi}$ term in the asymptotic series. If the *upper* limit of applicability is taken roughly as $(\delta/x^*)^2 = 0.10$, then the *minimum* value of local Reynolds Number at which these solutions are applicable would be about 1.6×10^4 for $M_\infty = 25$, for example, for the case $\gamma = 1.40$, $T_w^*/T_\infty^* = 5$, and $m = 0.76$. However, the slip-flow corrections are no longer negligible when $M_\infty/\sqrt{Re_{x^*}} > 0.10$ (see reference 7), or for $Re_{x^*} < 10^4$ at $M_\infty =$

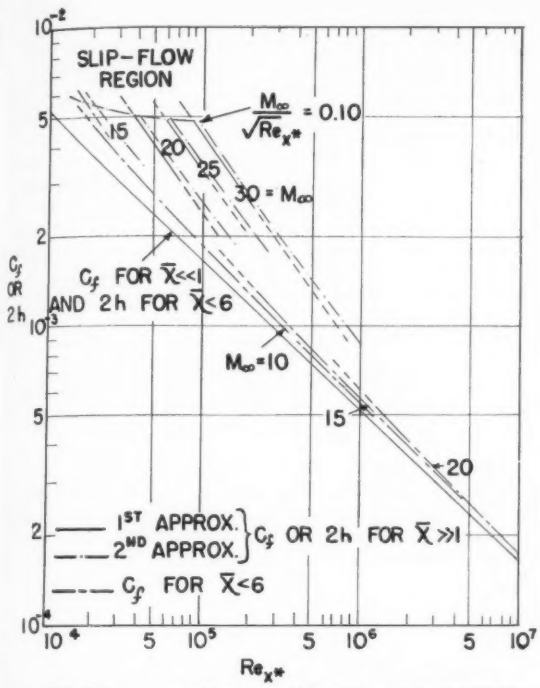

FIGURE-1. LOCAL LAMINAR SKIN-FRICTION AND HEAT TRANSFER COEFFICIENTS FOR FLAT PLATE IN HYPERSONIC FLOW. RATIO OF SURFACE TO FREE-STREAM TEMPERATURE =5.0 γ=1.4, $\mu \sim T^m$, m=0.76

10, for $Re_{x^*} < 4 \times 10^4$ at $M_\infty = 20$, and for $Re_{x^*} < 9 \times 10^4$ at $M_\infty = 30$.

All of the above results can be extended to the case of arbitrary Prandtl Number, to the case of the flow over a wedge, and probably also to the flow over slender bodies of revolution.

Solutions of the boundary-layer equations for small values of $\bar{X}(\bar{X} < 6$, approximately) have already been obtained as asymptotic series in ascending powers of $\bar{X}$.[8] Except for a region in the immediate vicinity of the leading edge where slip-flow exists, a large portion of the range of practical interest is now covered. In Fig. 1 the local skin-friction and heat-transfer coefficients are plotted as functions of Re_{x^*} for several Mach Numbers, for the case $\gamma = 1.40$, $T_w^*/T_\infty^* = 5$, and $m = 0.76$. The first approximation to the skin-friction and heat-transfer coefficients for $\bar{X} >> 1$ is given by Eq. (10), while the second approximation includes a term in $1/\bar{X}$. As the Mach Number increases and the interaction region spreads downstream over the plate, c_f increases rapidly over its conventional value. The local heat-transfer coefficient at first remains practically unaffected[8] but then also begins to increase with M_∞ for large $\bar{X}$. More extensive results and discussion will be presented in a forthcoming report.

References

[1] Shen, S. F., *On the Boundary Layer Equations in Hypersonic Flow*, Readers' Forum, Journal of the Aeronautical Sciences, Vol. 19, No. 7, pp. 500–501, July, 1952.

[2] Shen, S. F., *Hypersonic Flow Over an Insulated Wedge with Viscosity Effects*. Part I of an Sc.D. Thesis, Department of Aeronautical Engineering, Massachusetts Institute of Technology, 1949.

[3] Li, Ting-Yi, and Nagamatsu, H. T., *Shock Wave Effects on the Laminar Skin Friction of an Insulated Flat Plate at Hypersonic Speeds*, Contract No. DA-04-495-Ord-19, Memorandum No. 9 (GALCIT), July 1, 1952.

[4] Falkner, V. M., and Skan, S. W., *Some Approximate Solutions of the Boundary Layer Equations*, British A.R.C., R. & M. No. 1314, 1930.

[5] Pretsch, J., *Die Anfachung instabiler Störungen in einer laminaren Reibungsschicht*, Jahrbuch 1942 der deutschen Luftfahrtforschung, pp. I 54–I 71.

[6] Stewartson, K., *Correlated Incompressible and Compressible Boundary Layers*, Proc. Roy. Soc. (A), Vol. 200, No. 1060, pp. 84–100, December 22, 1949.

[7] Mirels, H., *Estimate of Slip Effect on Compressible Laminar-Boundary-Layer Skin Friction*, N.A.C.A. T.N. No. 2609, January, 1952.

[8] Lees, L., and Probstein, R. F., *Hypersonic Viscous Flow over a Flat Plate*, Princeton University Aeronautical Engineering Laboratory Report No. 195, April 20, 1952.

On the Use of the Neutral Point as a Stability Parameter

Judson R. Baron

Naval Supersonic Laboratory, Massachusetts Institute of Technology, Cambridge, Mass.

September 22, 1952

THE LONGITUDINAL STATIC STABILITY of an aircraft is given by the rate of change of the pitching moment coefficient with respect to the lift coefficient. Considering conventional subsonic aircraft, the well-known result follows: The above derivative is equal to the (nondimensional) distance (the "static margin") between the center of gravity and neutral point locations, the latter being aft of the former for a stable configuration. The neutral point is defined as usual as that point at which both the moment and the rate of change of moment with angle of attack vanish.

The simplicity of the result has made it extremely useful. However, it should be noted that the above is based upon an assumption of constant elevator effectiveness (rate of change of moment, or force, with control deflection). When considering supersonic missiles, the presence of nonlinear downwash effects preclude this assumption. The consequences are outlined below.

Assume only that the elevator effectiveness is independent of the control deflection for a fixed angle of attack. The moment about a point b in terms of information applicable at point a is (Fig. 1)

$$(C_M)_b = (C_M)_a - C_N X^* + \left[\left(\frac{\partial C_M}{\partial \delta}\right)_a - \left(\frac{\partial C_N}{\partial \delta}\right) X^*\right] \delta \quad (1)$$

where C_M, C_N are the moment and normal force coefficients, δ is the control deflection, and X^* is the nondimensional transfer distance from a to b, positive forward. Differentiating Eq. (1) with respect to angle of attack α with δ constant yields

$$\left(\frac{dC_M}{d\alpha}\right)_b = \left(\frac{dC_M}{d\alpha}\right)_a - \left(\frac{dC_N}{d\alpha}\right) X^* + \frac{d}{d\alpha}\left[\left(\frac{\partial C_M}{\partial \delta}\right)_a - \left(\frac{\partial C_N}{\partial \delta}\right) X^*\right] \delta \quad (2)$$

Momentarily considering point b as the neutral point, it is required that the left-hand sides of Eqs. (1) and (2) vanish. The resulting relations may be used to rewrite Eq. (2) in the form

$$\left(\frac{dC_M}{d\alpha}\right)_b = -\left[(X^* - X_N^*)\frac{dC_N}{d\alpha} + (X^*\delta - X_N^*\delta_N)\frac{d}{d\alpha}\left(\frac{\partial C_N}{\partial \delta}\right) - (\delta - \delta_N)\frac{d}{d\alpha}\left(\frac{\partial C_M}{\partial \delta}\right)_a\right] \quad (3)$$

where b is again a general point. The subscript N refers to the neutral point. Of interest is dC_M/dC_N evaluated at the center of gravity. Letting a and b coincide at the center of gravity, Eq. (3) gives the in-trim stability as

$$\left(\frac{dC_M}{dC_N}\right)_{c.g.,\,T} = -\left\{(X_{c.g.}^* - X_N^*)\left[1 + \delta_N \frac{d}{dC_N}\left(\frac{\partial C_N}{\partial \delta}\right)\right] - (\delta_T - \delta_N)\frac{d}{dC_N}\left(\frac{\partial C_M}{\partial \delta}\right)_{c.g.}\right\} \quad (4)$$

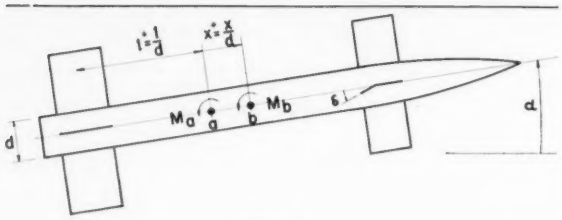

FIG. 1.

where the subscript T refers to the trim condition. In addition, since nonlinearities are due to downwash effects, it may be shown that

$$\frac{d}{dC_N}\left(\frac{\partial C_M}{\partial \delta}\right) = -\frac{d}{dC_N}\left(\frac{\partial C_N}{\partial \delta}\right) l^* \tag{5}$$

where l^* is the nondimensional tail length from the moment center to the aft surface center of pressure. Thus, from Eqs. (4) and (5),

$$\left(\frac{dC_M}{dC_N}\right)_{c.g.,\,T} = -\left\{(X_{c.g.}{}^* - X_N{}^*) - \left[\left(\frac{X_{c.g.}{}^* - X_N{}^*}{l^*}\right)\delta_N + (\delta_T - \delta_N)\right]\frac{d}{dC_N}\left(\frac{\partial C_M}{\partial \delta}\right)_{c.g.}\right\} \tag{6}$$

from which the classic result is obtained when the elevator effectiveness is constant. It is apparent that in the case considered here the stability is no longer a simple function of the center of gravity and neutral point locations.

The criterion for a stable attitude is that the quantity within the braces of Eq. (6) be positive. When $\delta_T = 0$, the bracket vanishes in Eq. (6), since then $\alpha = \delta_N = 0$ for a symmetric missile. The familiar form results and the c.g. must be forward of the neutral point for a stable configuration. Remembering that $(X_{c.g.}{}^* - X_N{}^*) \gtrless 0$ when $(\delta_T - \delta_N) \gtrless 0$ if a positive deflection increment produces a positive moment, it follows that for $\delta_T \neq 0$ a stable attitude results when

$$(d/dC_N)\,(\partial C_M/\partial \delta)_{c.g.} \lesssim A \tag{7}$$

where

$$A = \frac{X_{c.g.}{}^* - X_N{}^*}{[(X_{c.g.}{}^* - X_N{}^*)/l^*]\delta_N + (\delta_T - \delta_N)} \tag{8}$$

The "less than" sign applies to the c.g. forward of the neutral point, and vice versa. Writing

$$(d/dC_N)\,(\partial C_M/\partial \delta)_{c.g.} = kA$$

where $k = k(C_N)$, simplifies Eq. (6) to

$$(dC_M/dC_N)_{c.g.,\,T} = -(X_{c.g.}{}^* - X_N{}^*)\,(1 - k) \tag{9}$$

from which it is more easily seen that $k \lesssim 1$, in addition to the relative positions of the c.g. and neutral points, determines a stable attitude.

A graphical interpretation follows by noting that in a practical case

$$[(X_{c.g.}{}^* - X_N{}^*)/l^*]\delta_N \approx 0 \tag{10}$$

From Eqs. (7) and (8) then

$$\frac{d}{dC_N}\left(\frac{\partial C_M}{\partial \delta}\right)_{c.g.} \lesssim A \approx \frac{X_{c.g.}{}^* - X_N{}^*}{\delta_T - \delta_N} = \frac{-\{(C_M)_N/(C_N)_0\}}{-\{(C_M)_N/(\partial C_M/\partial \delta)_{c.g.}\}} = \frac{(\partial C_M/\partial \delta)_{c.g.}}{C_{N_0}} \tag{11}$$

at a specific $C_N = C_{N_0}$. Therefore, on a plot of moment effectiveness as a function of normal force (Fig. 2), one may determine the required fore and aft position of the c.g. with respect to the neutral point by comparing the slope of the curve at C_{N_0} with the slope of the line passing through both $(\partial C_M/\partial \delta)_{c.g.}$, C_{N_0} and the origin.

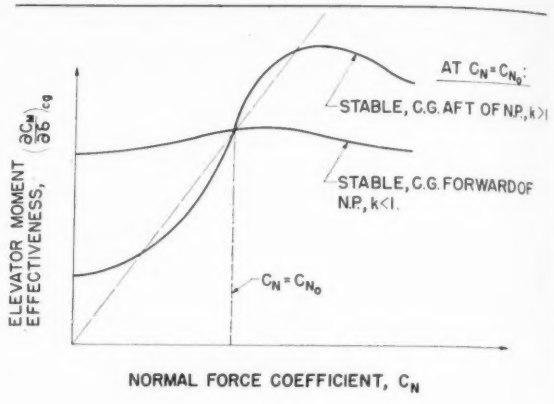
AT $C_N = C_{N_0}$:
STABLE, C.G. AFT OF N.P., k>1
STABLE, C.G. FORWARD OF N.P., k<1
$C_N = C_{N_0}$
ELEVATOR MOMENT EFFECTIVENESS, $\left(\frac{\partial C_M}{\partial \delta}\right)_{c.g.}$
NORMAL FORCE COEFFICIENT, C_N

FIG. 2.

In the vicinity of $C_N = 0$, in all cases $k < 1$ and the c.g. must be forward of the neutral point for a stable attitude. If the effectiveness variation is such that $k > 1$ for some $C_N = C_{N_0}$, then at an intermediate value, $0 < C_N < C_{N_0}$, neutral stability ($k = 1$) is implied irrespective of the c.g. location [within the validity of Eq. (10)].

On Asymptotic Solutions for the Heat Transfer at Varying Wall Temperatures in a Laminar Boundary Layer with Hartree's Velocity Profiles

H. Schuh
Royal Institute of Technology, Division of Aeronautics, Stockholm, Sweden
October 23, 1952

VARIOUS AUTHORS[1–5] HAVE MADE ALLOWANCES for a variation of the wall temperature in thermal boundary layers in laminar flow. The problem was simplified by assuming constant fluid properties and neglecting heat produced by friction and compression. Despite the variation of the wall temperature, the partial differential equations for the temperature field can be reduced to an ordinary differential equation, provided the temperature difference between wall and free stream is proportional to a power of x.[1–5]

$$t_w - t_1 = \text{const.}\; x^n \tag{1}$$

where t_w = wall temperature (= variable), t_1 = temperature outside boundary layer (= constant), n = an exponent. The ordinary differential equation so obtained reads

$$\frac{d^2\theta}{d\eta^2} + \sigma f \frac{d\theta}{d\eta} - n\sigma(2 - \beta)\frac{df}{d\eta}\theta = 0 \tag{2}$$

where the following quantities have been introduced: a dimensionless wall distance $\eta = (y/\sqrt{2 - \beta})\sqrt{u_1/\nu x}$ (y = distance normal to wall, x = distance parallel to wall, $u_1 = x^m$ = speed outside boundary layer, ν = kinematic viscosity, and $\beta = 2m \div (m + 1)$, parameter introduced by Hartree[6]); the function f defined by $\psi = \sqrt{2 - \beta}\sqrt{\nu x u_1} f(\eta)$ (ψ = stream function) and calculated by Hartree;[6] a dimensionless temperature $\theta = (t - t_1) \div (t_w - t_1)$; and $\sigma = c_p\mu/k$ = Prandtl Number (c_p = specific heat, μ = dynamic viscosity, and k = thermal conductivity). The boundary conditions for Eq. (2) are

$$\eta = 0,\ \theta = 1; \qquad \eta \to \infty,\ \theta = 0 \tag{3}$$

Eq. (2) can only be solved numerically. With three parameters β, n, and σ, the amount of labor for fairly general solutions

is considerable. It is interesting to consider whether asymptotic solutions of Eq. (2) are not easier to obtain for large or small values of the parameters or a combination of parameters, especially since these solutions are often good approximations over a wide range of the parameter.

On inspection of some solutions of Eq. (2), the thickness of the thermal boundary layer is found to become small compared to the velocity boundary layer if either n or σ becomes large. Then it is sufficient to replace the velocity profile by its tangent at the wall, since, for calculating the temperature field, only that part of the velocity profile is of influence which lies within the thermal boundary layer. With the exception of the separation point and its immediate surroundings, where the velocity gradient at the wall vanishes, we put

$$df/d\eta = b\eta \tag{4}$$

where b = constant $= df/d\eta$ at $\eta = 0$. Now Eq. (2) becomes

$$\frac{d^2\theta}{d\eta^2} + \sigma\frac{b}{2}\eta^2\frac{d\theta}{d\eta} - n\sigma b(2-\beta)\eta\theta = 0 \tag{5}$$

The first asymptotic solution is obtained by introducing a new independent variable

$$\zeta = n^{1/3}\eta \tag{6}$$

in Eq. (5),

$$\frac{d^2\theta}{d\zeta^2} + \frac{\sigma}{n}\frac{b}{2}\zeta^2\frac{d\theta}{d\zeta} - \sigma b(2-\beta)\zeta\theta = 0 \tag{7}$$

For values of $\sigma/n \to 0$, the middle term in Eq. (7) can be omitted; then we obtain

$$(d^2\theta/d\zeta^2) - \sigma b(2-\beta)\zeta\theta = 0 \tag{8}$$

this differential equation can be solved in a closed form; a solution, which fulfills the boundary conditions (3), is

$$\theta = 2^{-1/3}\,\Gamma\left(\frac{2}{3}\right)\tau[I_{-1/3}(\tau^3) - I_{1/3}(\tau^3)] \tag{9}$$

where

$$\tau = (2^{1/3}/3^{1/3})\,[\sigma b(2-\beta)]^{1/6}\,\zeta^{1/2}$$

and I_ν the modified Bessel function (Bessel function with purely imaginary argument) of the first kind and order ν as defined for instance in reference 7 and Γ the Gamma function.[8]

If q is the heat flow per unit surface area, the heat-transfer coefficient h becomes

$$h = \frac{q}{t_w - t_1} = \frac{\Gamma(2/3)}{3^{2/3}\Gamma(4/3)}\frac{(\sigma b n)^{1/2}}{(2-\beta)^{1/6}}k\sqrt{\frac{u_1}{\nu x}} \tag{10}$$

For convenience we note that

$$\Gamma(2/3)/3^{2/3}\Gamma(4/3) = 0.72895$$

For a flat plate and σ near 1, the asymptotic solution approximates the accurate solution (see Table 1) by about 1 to 2 per cent at $n = 4$ and less for $n > 4$, if allowance is made for a systematic small error of 2 per cent in reference 3; for the same case, at $\sigma = 20$, the error at $n = 4$ is slightly bigger. This is consistent with our theory, since the accuracy of the asymptotic solution depends on the quantity n/σ. For the stagnation flow, the approximation deviates by about 3 to 5 per cent at $n = 4$. The good agreement for higher σ-values even at lower values of n if fortuitous since the two influences cancel each other: (a) replacing the velocity profile by its tangent at the wall increases h for $\beta > 0$; (b) neglecting the middle term in Eq. (7) reduces h.

A second asymptotic solution can be found which is valid for $\sigma \to \infty$ with no restriction on n. We introduce a new variable

$$\xi = \sigma^{1/3}b^{1/3}\eta \tag{11}$$

in Eq. (5) and obtain

TABLE 1

$h/k\sqrt{\nu x/u_1}$

Flat Plate ($\beta = 0$, $b = 0.4696$)

	$\sigma = 0.72$			$\sigma = 0.7$		
	Ref. 3	Ref. 5	Asympt.	Ref. 5	Ref. 9	Asympt.
n						
1	0.489	0.4813	0.4524	0.4770	0.480	0.448
2	0.597	0.5863	0.5700	0.5811	0.588	0.565
3	0.684	0.6633	0.6525	0.6573	...	0.646
4	0.744	0.7255	0.7182	0.7193	0.723	0.711
5	0.799	....	0.7737	....	...	...
10	1.006	....	0.9747	....	...	...

	$\sigma = 2$		$\sigma = 10$		$\sigma = 20$	
	Ref. 5	Asympt.	Ref. 5	Asympt.	Ref. 5	Asympt.
n						
1	0.6783	0.6359	1.149	1.087	1.431	1.370
2	0.8238	0.8012	1.389	1.370	1.729	1.726
3	0.9306	0.9172	1.563	1.568	1.938	1.971
4	1.0161	1.0096	1.701	1.726	2.103	2.175

Stagnation Flow ($\beta = 1.0$, $b = 1.2326$)

	$\sigma = 0.7$		$\sigma = 5$		$\sigma = 10$	
	Ref. 5	Asympt.	Ref. 5	Asympt.	Ref. 5	Asympt.
n						
1	0.703	0.694	1.432	1.336	1.818	1.684
2	0.846	0.874	....	1.683	2.159	2.121
3	0.957	1.001	1.914	1.927	2.418	2.428
4	1.048	1.101	2.086	2.121	2.630	2.672

$$\frac{d^2\theta}{d\xi^2} + \frac{\xi^2}{2}\frac{d\theta}{d\xi} - \epsilon\xi\theta = 0 \tag{12}$$

with $\epsilon = n(2-\beta)$. This is a differential equation with only one parameter instead of three as in Eq. (2). The author found no solution of Eq. (12) in a closed form and made no attempt to solve it numerically. It should, however, be useful for supplementing the known solutions of reference 5 for values of σ above 20 and any value of n.

REFERENCES

[1] Fage, A., and Falkner, V. M., *Relation between Heat Transfer and Surface Friction for Laminar Flow*, A.R.C. R.&M. No. 1408, London, 1931.

[2] Schuh, H., *Laminarer Wärmeübergang in Grenzschichten bei hohen Geschwindigkeiten*, ZWB Forschungsbericht, 2019.

[3] Chapman, D. R., and Rubesin, M. W., *Temperature and Velocity Profiles in the Compressible Laminar Boundary Layer with Arbitrary Distribution of Surface Temperature*, Journal of the Aeronautical Sciences, Vol. 16, No. 19, pp. 547–565, September, 1949.

[4] Schlichting, H., *Der Wärmeübergang an einer längsangeströmten Platte mit veränderlicher Wandtemperatur*, Forsch. Ing. Wes., Vol. 17, No. 1, 1951.

[5] Levy, S., *Heat Transfer to Constant-Property Laminar Boundary-Layer Flows with Power-Function Free-Stream Velocity and Wall-Temperature Variation*, Journal of the Aeronautical Sciences, Vol. 19, No. 5, pp. 341–348, May, 1952.

[6] Hartree, D. R., *On an Equation Occurring in Falkner and Skans Approximate Treatment of the Equations of the Boundary Layer*, Proc. Cambr. Phil. Soc., Vol. 33, pt. II, p. 223, 1937.

[7] McLachlan, N. W., *Bessel Function for Engineers*, 1st ed.; Oxford University Press, 1934.

[8] Jahnke, E., and Ende, F., *Funktionentafeln*, 2nd Ed.; Teubner, Leipzig, 1933.

[9] Unpublished new calculations of solutions of Eq. (2) by the author.

Graphical Solution for "Turbulent Boundary Layer in Compressible Fluids"

John Joseph Martin

Research Engineer, Aerophysics Laboratory, North American Aviation, Inc., Downey, Calif.

October 24, 1952

VAN DRIEST, IN A RECENT PAPER,[1] derived equations for local and mean coefficients of friction and local coefficients of heat transfer. These equations are applicable to a flat plate with the

restrictions noted by their author and generally involve trial-and-error solutions. It is the purpose of this note to show a means by which they may be solved directly by graphical means; these solutions were made at Dr. Van Driest's suggestion.

The equation derived for the local coefficient of friction $c_{f\infty}$ is

$$\frac{0.242}{A\,(c_{f\infty})^{1/2}\,(T_w/T_\infty)^{1/2}} \cdot (\sin^{-1}\alpha + \sin^{-1}\beta) = 0.41 + \log_{10} R_\infty\, c_{f\infty} - \frac{1+2\omega}{2}\log_{10}\frac{T_w}{T_\infty} \quad (66)$$

and for the mean coefficient of friction $C_{f\infty}$

$$\frac{0.242}{A\,(C_{f\infty})^{1/2}(T_w/T_\infty)^{1/2}} \cdot (\sin^{-1}\alpha + \sin^{-1}\beta) = \log_{10} R_\infty C_{f\infty} - \frac{1+2\omega}{2}\log_{10}\frac{T_w}{T_\infty} \quad (71)$$

Using the definition, $A = [(1/2)(\gamma - 1)M_\infty^2]^{1/2}/(T_w/T_\infty)^{1/2}$, one may write, for $c_{f\infty}$,

$$\frac{0.242}{[(1/2)(\gamma-1)]^{1/2}M_\infty}(\sin^{-1}\alpha + \sin^{-1}\beta) = (c_{f\infty})^{1/2}\left[\log_{10}\frac{2.57\,R_\infty}{(T_w/T_\infty)^{(1+2\omega)/2}} + \log_{10} c_{f\infty}\right] \quad (66a)$$

and for $C_{f\infty}$

$$\frac{0.242}{[(1/2)(\gamma-1)]^{1/2}M_\infty}(\sin^{-1}\alpha + \sin^{-1}\beta) = (C_{f\infty})^{1/2}\left[\log_{10}\frac{R_\infty}{(T_w/T_\infty)^{(1+2\omega)/2}} + \log_{10} C_{f\infty}\right] \quad (71a)$$

Now the left-hand sides of Eqs. (66a) and (71a) are identical and may be called by ψ, which is a function of M_∞ and T_w/T_∞. Consequently, a family of curves as in Fig. 1 may be computed for ψ. The right-hand sides of Eqs. (66a) and (71a) as written are subject to graphical representation as in Fig. 2.

Hence, to find a value of $c_{f\infty}$ or $C_{f\infty}$, the value of ψ_1 corresponding to $(M_\infty)_1$ and $(T_w/T_\infty)_1$ is found in Fig. 1. In Fig. 2 a line is drawn through $(T_w/T_\infty)_1$ and $(R_\infty)_1$ (on the scale corresponding to $c_{f\infty}$ or $C_{f\infty}$, as marked) and intersecting the reference line. The point on the reference line is then joined with the value of ψ_1 and the value of $(c_{f\infty})_1$ or $(C_{f\infty})_1$ read on the curve.

Values for $C_{H\infty} = h/\rho_\infty u_\infty c_p$ may be found from the tentative equation $C_{H\infty} = (1/2)c_{f\infty}$ given in the reference or from more accurate relations of the form $C_{H\infty} = (1/2)c_{f\infty}\cdot F(Pr)$.

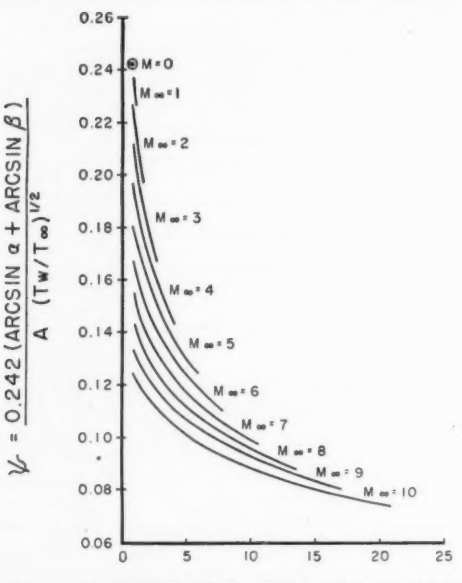

FIG. 1. Variation of $\psi\,(M_\infty, T_w/T_\infty)$ with M_∞ and T_w/T_∞.

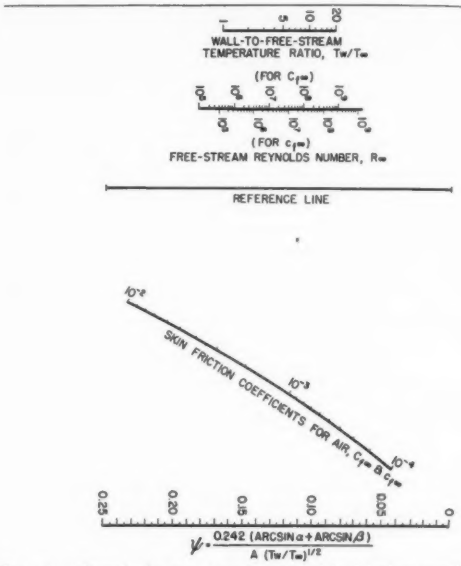

FIG. 2. Graph for local and mean skin-friction coefficients, $c_{f\infty}$ and $C_{f\infty}$.

REFERENCE

[1] Van Driest, E. R., *Turbulent Boundary Layer in Compressible Fluids*, Journal of the Aeronautical Sciences, Vol. 18, No. 3, pp. 145–161, March, 1951.

Additional Values of C(k)

W. B. Brower and R. H. Lassen
Aerophysics Laboratory, North American Aviation, Inc., Downey, Calif.

October 11, 1952

IN A RECENT WORK, Luke and Dengler[1] published, among others, a table of the Theodorsen circulation function, $C(k)$ for real arguments. It was found that this table, while the most complete known to the author, does not cover the range $k > 1.0$ with sufficiently small increments.

Additional values of $C(k)$ were computed from the following formulas:

$$C(k) = F + iG$$

$$F = \frac{J_1(J_1 + Y_0) + Y_1(Y_1 - J_0)}{(J_1 + Y_0)^2 + (Y_1 - J_0)^2}$$

$$G = -\frac{Y_1 Y_0 + J_1 J_0}{(J_1 + Y_0)^2 + (Y_1 - J_0)^2}$$

using the tables of Bessel functions given by Watson.[2] The computations were performed on IBM punched-card machines. Eight decimals were carried, seven decimals being shown in the result; no "round-off" was made. Table 1 is thought to have the

TABLE 1

k	$F(k)$	$-G(k)$
1.000	0.539 4348	0.100 2729
1.020	0.538 3005	0.098 8716
1.040	0.537 2139	0.097 5055
1.060	0.536 1723	0.096 1733
1.080	0.535 1733	0.094 8739
1.100	0.534 2148	0.093 6062
1.120	0.533 2943	0.092 3693
1.140	0.532 4099	0.091 1620
1.160	0.531 5599	0.089 9835
1.180	0.530 7425	0.088 8328
1.200	0.529 9560	0.087 7089
1.220	0.529 1989	0.086 6111
1.240	0.528 4697	0.085 5386
1.260	0.527 7672	0.084 4904
1.280	0.527 0899	0.083 4660
1.300	0.526 4367	0.082 4643
1.320	0.525 8066	0.081 4849
1.340	0.525 1984	0.080 5270
1.360	0.525 6112	0.079 5900
1.380	0.524 0439	0.078 6732
1.400	0.523 4957	0.077 7759
1.420	0.522 9658	0.076 8977
1.440	0.522 4533	0.076 0380
1.460	0.521 9574	0.075 1961
1.480	0.521 4777	0.074 3717
1.500	0.521 0132	0.073 5641
1.520	0.520 5634	0.072 7730
1.540	0.520 1277	0.071 9976
1.560	0.519 7054	0.071 2378
1.580	0.519 2961	0.070 4936
1.600	0.518 8992	0.069 7629
1.620	0.518 5143	0.069 0469
1.640	0.518 1407	0.068 3447
1.660	0.517 7782	0.067 6560
1.680	0.517 4263	0.066 9803
1.700	0.517 0845	0.066 3174
1.720	0.516 7525	0.065 6667
1.740	0.516 4300	0.065 0282
1.760	0.516 1165	0.064 4013
1.780	0.515 8118	0.063 7860
1.800	0.515 5157	0.063 1817
1.820	0.515 2274	0.062 5882
1.840	0.514 9471	0.062 0053
1.860	0.514 6743	0.061 4326
1.880	0.514 4087	0.060 8701
1.900	0.514 1502	0.060 3172
1.920	0.513 8984	0.059 7739
1.940	0.513 6533	0.059 2399
1.960	0.513 4143	0.058 7149
1.980	0.513 1818	0.058 1988
2.000	0.512 9547	0.057 6913
2.020	0.512 7337	0.057 1922
2.040	0.512 5181	0.056 7013
2.060	0.512 3077	0.056 2185
2.080	0.512 1027	0.055 7435
2.100	0.511 9026	0.055 2762
2.120	0.511 7073	0.054 8164
2.140	0.511 5168	0.054 3638
2.160	0.511 3308	0.053 9184
2.180	0.511 1490	0.053 4799
2.200	0.510 9717	0.053 0483
2.220	0.510 7985	0.053 6234
2.240	0.510 6293	0.052 2048
2.260	0.510 4639	0.051 7927
2.280	0.510 3023	0.051 3868
2.300	0.510 1443	0.050 9871
2.320	0.509 9900	0.050 5932
2.340	0.509 8391	0.050 2053
2.360	0.509 6914	0.049 8229
2.380	0.509 5471	0.049 4463
2.400	0.509 4059	0.049 0750
2.420	0.509 2678	0.048 7091
2.440	0.509 1326	0.048 3485
2.460	0.509 0002	0.047 9930
2.480	0.508 8707	0.476 6425
2.500	0.508 7441	0.047 2969
2.520	0.508 6200	0.046 9561
2.540	0.508 4985	0.046 6201
2.560	0.508 3794	0.046 2888
2.580	0.508 2628	0.045 9619
2.600	0.508 1487	0.045 6393
2.620	0.508 0369	0.045 3213
2.640	0.507 9271	0.045 0075
2.660	0.507 8199	0.044 6980
2.680	0.507 7145	0.044 3925
2.700	0.507 6114	0.044 0909
2.720	0.507 5101	0.043 7935
2.740	0.507 4110	0.043 4999
2.760	0.507 3136	0.043 2100
2.780	0.507 2182	0.042 9239
2.800	0.507 1247	0.042 6415
2.820	0.507 0328	0.042 3626
2.840	0.506 9429	0.042 0873
2.860	0.506 8544	0.041 8154
2.880	0.506 7678	0.041 5468
2.900	0.506 6826	0.041 2818
2.920	0.506 5992	0.041 0199
2.940	0.506 5170	0.040 7612
2.960	0.506 4366	0.040 5057
2.980	0.506 3576	0.040 2533
3.000	0.506 2799	0.040 0038
3.020	0.506 2037	0.039 7575
3.040	0.506 1288	0.039 5142
3.060	0.506 0553	0.039 2736
3.080	0.505 9832	0.039 0359
3.100	0.505 9122	0.038 8011
3.120	0.505 8424	0.038 5689
3.140	0.505 7738	0.038 3395
3.160	0.505 7065	0.038 1126
3.180	0.505 6401	0.037 8884
3.200	0.505 5753	0.037 6668
3.220	0.505 5114	0.037 4477
3.240	0.505 4485	0.037 2310
3.260	0.505 3867	0.037 0168
3.280	0.505 3258	0.036 8049
3.300	0.505 2660	0.036 5954
3.320	0.505 2072	0.036 3883
3.340	0.505 1492	0.036 1834
3.360	0.505 0925	0.035 9809
3.380	0.505 0366	0.035 7803
3.400	0.504 9815	0.035 5820
3.420	0.504 9273	0.035 3860
3.440	0.504 8742	0.035 1919
3.460	0.504 8216	0.035 0001
3.480	0.504 7701	0.034 8101
3.500	0.504 7192	0.034 6223
3.520	0.504 6693	0.034 4363
3.540	0.504 6200	0.034 2524
3.560	0.504 5716	0.034 0703
3.580	0.504 5237	0.033 8901
3.600	0.504 4768	0.033 7119
3.620	0.504 4306	0.033 5353
3.640	0.504 3851	0.033 3608
3.660	0.504 3402	0.033 1879
3.680	0.504 2960	0.033 0167
3.700	0.504 2525	0.032 8470
3.720	0.504 2096	0.032 6793
3.740	0.504 1672	0.032 5133
3.760	0.504 1257	0.032 3490
3.780	0.504 0845	0.032 1860
3.800	0.504 0443	0.032 0248
3.820	0.504 0044	0.031 8653
3.840	0.503 9652	0.031 7072
3.860	0.503 9264	0.031 5507
3.880	0.503 8886	0.031 3957
3.900	0.503 8509	0.031 2421
3.920	0.503 8140	0.031 0901
3.940	0.503 7774	0.030 9394
3.960	0.503 7413	0.030 7901
3.980	0.503 7059	0.030 6424
4.000	0.503 6708	0.030 4961
4.020	0.503 6364	0.030 3509
4.040	0.503 6023	0.030 2074
4.060	0.503 5688	0.030 0650
4.080	0.503 5359	0.029 9239
4.100	0.503 5029	0.029 7843
4.120	0.503 4708	0.029 6459
4.140	0.503 4391	0.029 5084
4.160	0.503 4078	0.029 3725
4.180	0.503 3770	0.029 2377

(*Concluded on page 150*)

TABLE 1 (*Continued*)

k	$F(k)$	$-G(k)$	k	$F(k)$	$-G(k)$
4.200	0.503 3465	0.029 1044	6.000	0.501 6845	0.020 5954
4.220	0.503 3164	0.028 9719	6.100	0.501 6312	0.020 2651
4.240	0.503 2867	0.028 8408	6.200	0.501 5808	0.019 9448
4.260	0.503 2574	0.028 7108	6.300	0.501 5320	0.019 6349
4.280	0.503 2284	0.028 5819	6.400	0.501 4854	0.019 3339
4.300	0.503 2000	0.028 4543	6.500	0.501 4415	0.019 0420
4.320	0.503 1718	0.028 3276	6.600	0.501 3994	0.018 7589
4.340	0.503 1438	0.028 2022	6.700	0.501 3583	0.018 4840
4.360	0.503 1166	0.028 0778	6.800	0.501 3199	0.018 2169
4.380	0.503 0895	0.027 9545	6.900	0.501 2824	0.017 9572
4.400	0.503 0627	0.027 8322	7.000	0.501 2468	0.017 7050
4.420	0.503 0362	0.027 7110	7.100	0.501 2130	0.017 4595
4.440	0.503 0104	0.027 5908	7.200	0.501 1800	0.017 2209
4.460	0.502 9845	0.027 4717	7.300	0.501 1486	0.016 9887
4.480	0.502 9592	0.027 3534	7.400	0.501 1186	0.016 7625
4.500	0.502 9340	0.027 2363	7.500	0.501 0894	0.016 5423
4.520	0.502 9093	0.027 1200	7.600	0.501 0613	0.016 3278
4.540	0.502 8848	0.027 0048	7.700	0.501 0343	0.016 1184
4.560	0.502 8609	0.026 8906	7.800	0.501 0089	0.015 9147
4.580	0.502 8369	0.027 7775	7.900	0.500 9837	0.15 7160
4.600	0.502 8131	0.026 6651	8.000	0.500 9598	0.015 5220
4.620	0.502 7901	0.026 5537	8.100	0.500 9364	0.015 3329
4.640	0.502 7670	0.026 4431	8.200	0.500 9142	0.015 1484
4.660	0.502 7443	0.026 3336	8.300	0.500 8923	0.014 9677
4.680	0.502 7222	0.026 2250	8.400	0.500 8718	0.014 7918
4.700	0.502 7000	0.026 1170	8.500	0.500 8518	0.014 6197
4.720	0.502 6781	0.026 0100	8.600	0.500 8323	0.014 4518
4.740	0.502 6564	0.025 9040	8.700	0.500 8136	0.014 2873
4.760	0.502 6350	0.025 7987	8.800	0.500 7954	0.014 1269
4.780	0.502 6137	0.025 6943	8.900	0.500 7779	0.013 9695
4.800	0.502 5930	0.025 5907	9.000	0.500 7607	0.013 8159
4.820	0.502 5722	0.025 4877	9.100	0.500 7443	0.013 6658
4.840	0.502 5519	0.025 3861	9.200	0.500 7288	0.013 5187
4.860	0.502 5318	0.025 2848	9.300	0.500 7133	0.013 3746
4.880	0.502 5119	0.025 1846	9.400	0.500 6981	0.013 2339
4.900	0.502 4923	0.025 0849	9.500	0.500 6842	0.013 0960
4.920	0.502 4729	0.024 9862	9.600	0.500 6698	0.012 9605
4.940	0.502 4536	0.024 8880	9.700	0.500 6563	0.012 8285
4.960	0.502 4348	0.024 7909	9.800	0.500 6430	0.012 6986
4.980	0.502 4158	0.024 6941	9.900	0.500 6301	0.012 5711
5.000	0.502 3974	0.024 5985	10.000	0.500 6180	0.012 4467
5.100	0.502 3076	0.024 1303	10.500	0.500 5611	0.011 8586
5.200	0.502 2228	0.023 6794	11.000	0.500 5121	0.011 3234
5.300	0.502 1426	0.023 2451	11.500	0.500 4684	0.010 8343
5.400	0.502 0663	0.022 8259	12.000	0.500 4304	0.010 3859
5.500	0.501 9946	0.022 4216	12.500	0.500 3972	0.009 9725
5.600	0.501 9260	0.022 0311	13.000	0.500 3673	0.009 5905
5.700	0.501 8609	0.021 6541	13.500	0.500 3410	0.009 2373
5.800	0.501 7992	0.021 2895	14.000	0.500 3170	0.008 9091
5.900	0.501 7404	0.020 9369	14.500	0.500 2952	0.008 6030
			15.000	0.500 2766	0.008 3174
			15.500	0.500 2589	0.008 0502
			16.000	0.500 2433	0.007 7993

same estimated accuracy as those of Luke and Dengler—i.e., the error is $\leq 3 \times 10^{-7}$.

With this table supplementing those of Luke and Dengler and using the three-point Lagrangian interpolation table,[3] it is possible to interpolate for k given to six decimals with an estimated error $\leq 5 \times 10^{-6}$.

REFERENCES

[1] Luke, Y. L., and Dengler, M. A., *Tables of the Theodorsen Circulation Function for Generalized Motion*, Journal of the Aeronautical Sciences, Vol. 18, No. 7, p. 481, July, 1951.

[2] Watson, G. N., *A Treatise on the Theory of Bessel Functions*, 2nd Ed., p. 666; Cambridge University Press, London, 1945.

[3] *Tables of Lagrangian Interpolation Coefficients;* Columbia University Press, 1944.

Comments on "Two-Dimensional Airfoils at Moderate Hypersonic Velocities"

L. E. Flanagan, Jr.

Research Engineer, Aerophysics Laboratory, North American Aviation, Inc., Downey, Calif.

October 27, 1952

IN HIS RECENT PAPER ON HYPERSONIC AIRFOILS, Dorrance[1] has developed power series for pressure coefficients for an expansion and a nonisentropic compression. For an expansion,

$$\frac{C_{pe}}{\delta^2} = \frac{2}{K} f + \frac{\gamma+1}{2} f^2 + \frac{\gamma+1}{6} K f^3 + \frac{(\gamma+1)(3-\gamma)}{48} K^2 f^4 + \ldots \quad (1a)$$

For a compression,

$$\frac{C_{pc}}{\delta^2} = \frac{2}{K} f + \frac{\gamma+1}{2} f^2 + \frac{(\gamma+1)^2}{16} K f^3 + \frac{(\gamma+1)^4}{1{,}024} K^2 f^4 + \ldots \quad (1b)$$

Substituting the relations $K = M\delta$ and $f = \theta/\delta$, where δ = airfoil thickness ratio and θ = angle of surface inclination relative to stream, in Eqs. (1a) and (1b) gives

$$\left.\begin{aligned} C_{p_a} &= \frac{2}{M}\theta + \frac{\gamma+1}{2}\theta^2 + \frac{\gamma+1}{6}M\theta^3 + \\ &\qquad \frac{(\gamma+1)(3-\gamma)}{48}M^2\theta^4 + \ldots \\ &= \frac{2}{M}\theta + 1.2\,\theta^2 + 0.40\,M\theta^3 - O[10^{-1}M^2]\theta^4 \end{aligned}\right\} \quad (2a)$$

for $\gamma = 1.4$, and

$$\left.\begin{aligned} C_{p_c} &= \frac{2}{M}\theta + \frac{\gamma+1}{2}\theta^2 + \frac{(\gamma+1)^2}{16}M\theta^3 + \\ &\qquad \frac{(\gamma+1)^4}{1{,}024}M^2\theta^5 + \ldots \\ &= \frac{2}{M}\theta + 1.2\theta^2 + 0.36M\theta^3 + O[10^{-2}M^2]\theta^5 \end{aligned}\right\} \quad (2b)$$

for $\gamma = 1.4$.

It is the purpose of this note to compare these equations with the expressions developed by Busemann[2] and Miles[3] under the condition that $\sqrt{M^2-1}/M \cong 1$. The lower limit of Mach Number for which Dorrance's equations apply is 3.19. At this value of M, $\sqrt{M^2-1}/M = 0.95$.

The expressions for pressure coefficients as developed by Busemann and corrected by others are

$$C_{p_a} = C_1\theta + C_2\theta^2 + C_3\theta^3 + \ldots$$
$$C_{p_c} = C_1\theta + C_2\theta^2 + (C_3 - D)\theta^3 + \ldots$$

where

$$C_1 = 2/\sqrt{M^2-1}$$
$$C_2 = [\gamma M^4 + (M^2-2)^2]/2(M^2-1)^2$$
$$C_3 = \frac{1}{(M^2-1)^{\gamma/(\gamma-1)}}\left[\frac{\gamma+1}{6}M^8 + \frac{2\gamma^2-7\gamma-5}{6}M^6 + \frac{5(\gamma+1)}{3}M^4 - 2M^2 + \frac{4}{3}\right]$$
$$D = \frac{1}{(M^2-1)^{\gamma/(\gamma-1)}}\left(\frac{\gamma+1}{12}\right)M^4 \times \left[\frac{5-3\gamma}{4}M^4 + (\gamma-3)M^2 + 2\right]$$

For hypersonic flow,

$$\sqrt{M^2-1} \cong M; \quad (M^2-2)^2 \cong M^4; \quad (M^2-1)^{\gamma/(\gamma-1)} \cong M^7 \quad (3)$$

for $\gamma = 1.4$.

Therefore,

$$C_1 \cong 2/M$$
$$C_2 \cong (\gamma+1)/2$$
$$C_3 \cong \frac{\gamma+1}{6}M + \frac{2\gamma^2-7\gamma-5}{6}M^{-1} + O[M^{-3}]$$
$$(C_3 - D) \cong \frac{(\gamma+1)^2}{16}M + \frac{5\gamma^2-16\gamma-13}{12}M^{-1} + O[M^{-3}]$$

The pressure coefficients then become

$$\left.\begin{aligned} C_{p_a} &\cong \frac{2}{M}\theta + \frac{\gamma+1}{2}\theta^2 + \frac{\gamma+1}{6}M\theta^3 + \\ &\qquad \frac{2\gamma^2-7\gamma-5}{6}M^{-1}\theta^3 \\ &\cong \frac{2}{M}\theta + 1.2\theta^2 + 0.40M\theta^3 - O[M^{-1}]\theta^3 \end{aligned}\right\} \quad (4a)$$

for $\gamma = 1.4$, and

$$\left.\begin{aligned} C_{p_c} &\cong \frac{2}{M}\theta + \frac{\gamma+1}{2}\theta^2 + \frac{(\gamma+1)^2}{16}M\theta^3 + \\ &\qquad \frac{5\gamma^2-16\gamma-13}{12}M^{-1}\theta^3 \\ &\cong \frac{2}{M}\theta + 1.2\theta^2 + 0.36\,M\theta^3 - O[M^{-1}]\theta^3 \end{aligned}\right\} \quad (4b)$$

for $\gamma = 1.4$.

These equations agree with those of Dorrance for the first three terms.

Miles has developed the following expressions for the pressure coefficients, for $\gamma = 1.4$:

$$C_{p_a} = \frac{2}{\sqrt{M^2-1}}\theta + \frac{10(3M^4-5M^2+5)}{25(M^2-1)^2}\theta^2 + \frac{10(15M^8-68M^6+150M^4-75M^2+50)}{375(M^2-1)^{7/2}}\theta^3 + \ldots$$
$$C_{p_c} = \frac{2}{\sqrt{M^2-1}}\theta + \frac{2(3M^4-5M^2+5)}{5(M^2-1)^2}\theta^2 + \frac{27M^8-112M^6+270M^4-150M^2+100}{75(M^2-1)^{7/2}}\theta^3 + \ldots$$

Applying the conditions of Eqs. (3) gives

$$C_{p_a} \cong (2/M)\theta + 1.2\theta^2 - O[M^{-2}]\theta^2 + 0.40M\theta^3 - O[M^{-1}]\theta^3 \quad (5a)$$
$$C_{p_c} \cong (2/M)\theta + 1.2\theta^2 - O[M^{-2}]\theta^2 + 0.36M\theta^3 - O[M^{-1}]\theta^3 \quad (5b)$$

The effect of the terms of the order of $M^{-2}\theta^2$ may be determined readily. For hypersonic flow, $M\delta$ is of the order of 1, and δ is of the order of θ. Therefore, θ is of the order of M^{-1}, so that $M^{-2}\theta^2$ is of the order of $M^{-1}\theta^3$. Thus, Eqs. (5a) and (5b) become

$$C_{p_a} \cong (2/M)\theta + 1.2\theta^2 + 0.40M\theta^3 - O[M^{-1}]\theta^3$$
$$C_{p_c} \cong (2/M)\theta + 1.2\theta^2 + 0.36M\theta^3 - O[M^{-1}]\theta^3$$

It is apparent that the first three terms of Miles' equations agree with the corresponding terms of Busemann and of Dorrance and that the remaining terms are of the same orders in θ and M as are those of Busemann.

It should be pointed out that the fourth terms of Eqs. (2a) and (2b), being of the order of $10^{-1}M^2\theta^4$ and $10^{-2}M^2\theta^5$, are, under the condition that $M\theta$ is of the order of 1, of the second order in θ. All subsequent terms of these series developed by Dorrance are also of the order of θ^2, but, since the series converge rapidly, it is practical, as Dorrance points out, to neglect all terms beyond the third in the expressions for C_{p_a} and C_{p_c}.

References

[1] Dorrance, W. H., *Two-Dimensional Airfoils at Moderate Hypersonic Velocities*, Journal of the Aeronautical Sciences, Vol. 19, No. 9, p. 593, September, 1952.

[2] Busemann, A., *Aerodynamischer Auftrieb bei Uberschallgeschwindigkeit*, Luftfahrforschung, Band 12, Nr. 6, 1935.

[3] Miles, E. R. C., *Supersonic Aerodynamics*, p. 235; McGraw-Hill Book Company, Inc., New York, 1950.

On the Transition Through a Weak Shock Front*

Paul Mandl

Institute of Aerophysics, University of Toronto, Toronto, Canada

September 29, 1952

THE TRANSITION OF THE one-dimensional steady flow of real fluids through shock fronts has received much attention re-

* The complete report is available at the Institute of Aerophysics, University of Toronto, Toronto (U.T.I.A. Report No. 14).

cently. Becker's exact solution for a Prandtl Number of $^3/_4$,[1] has been extended by several authors;[2, 3] approximate solutions have been derived for other Prandtl Numbers.[4]

This investigation deals rigorously with the shock transition of a perfect gas passing through a weak shock front for arbitrary values of the Prandtl Number. The mathematical analysis is based on the differential equation describing the transition of velocity which can be deduced readily from the general equations of motion of a continuous fluid. If the coefficients of viscosity and heat conduction are assumed constant, then the basic equation for the velocity can be expressed as

$$U\frac{d^2U}{dR^2} + \left(\frac{dU}{dR}\right)^2 + (A - BU)\frac{dU}{dR} + C(U-1)(U-U_2) = 0 \quad (1)$$

where U is a velocity ratio equal to unity at the initial state and U_2 at the final state; R is a shock-wave Reynolds Number proportional to the distance normal to the shock front; and A, B, C are constants depending on the free-stream Mach Number M_1, the ratio of specific heats of the gas γ and the Prandtl Number σ.

The condition of uniform flow both ahead of, and behind, the shock front requires that the solution of Eq. (1) satisfy the following boundary conditions:

$$\text{as } R \to -\infty, \quad U \to 1$$
$$\text{as } R \to +\infty, \quad U \to U_2$$

The additional condition that $d^2U/dR^2 = 0$ when $R = 0$ determines the position of the centre of the shock front.

If, and only if, the constants of the gas satisfy the relation

$$(\sigma - {}^3/_4)(\gamma - 1) = 0 \quad (2)$$

Eq. (1) can be factorized into the differential operators

$$\left[\frac{d}{dR} + \left(\frac{2A}{1+U_2} - B\right)\right] \times \left[U\frac{dU}{dR} - \frac{A}{1+U_2}(U-1)(U-U_2)\right] = 0 \quad (3)$$

Eq. (3) is satisfied if the second factor equals zero. This equation can be integrated at once, yielding a solution in a closed form that satisfies the above boundary conditions—viz.,

$$R = \frac{1}{A}\frac{1+U_2}{1-U_2}\left[\log\left(\frac{1-U}{1-\sqrt{U_2}}\right) - U_2\log\left(\frac{U-U_2}{\sqrt{U_2}-U_2}\right)\right] \quad (4)$$

Hence, the basic equation for the velocity degenerates to a first order equation if $\sigma = {}^3/_4$ [cf. Eq. (2); the value $\gamma = 1$ must be rejected for a real gas]. This result coincides with the solution Becker obtained by entirely different reasoning.[1]

To solve Eq. (1) for arbitrary values of σ, the substitution $dU/dR = \eta$ transforms it into an equation of the hodograph type

$$U\eta\frac{d\eta}{dU} + \eta^2 + (A - BU)\eta + C(U-1)(U-U_2) = 0 \quad (5)$$

The corresponding boundary conditions become

$$\eta(1) = \eta(U_2) = 0$$

The initial state is a nodal point and the final state a saddle point of Eq. (5). An infinite number of integral curves passes through the node but only two through the saddle. The problem is, therefore, to find a curve connecting the neighborhoods of these two singular points.

If calculations are started from the initial state, an integral of Eq. (5) can be expressed in terms of the following series:

$$\eta = \sum_{m=1}^{\infty} c_{m0}\,\xi^m + \sum_{m=1}^{\infty}\sum_{n=1}^{\infty} c_{mn}\,\xi^m\,(\bar{C}\,\xi^b)^n \quad (6)$$

where $\xi = (1-U)/(1-U_2)$; b is a constant that depends on the physical quantities γ, σ, M_1 and is generally irrational; and $\bar{C}$ is an arbitrary constant characterizing the single infinity of solutions through the node.

The coefficients c_{m_n} are determined from the differential equation but are of such a form that the solution of Eq. (6) breaks down for a discrete set of Mach Numbers; the series must then be modified by including logarithmic terms.

Because of the presence of the arbitrary constant $\bar{C}$, the series solution (6) is not, in general, suitable for numerical calculations. However, for infinitely weak shock fronts ($|\bar{C}| \to 0$), Eq. (6) reduces to an ordinary power series which converges slowly. (If only the first two terms are retained, the solution is identical with Taylor's approximate formula.)[5]

Since the final state is a saddle point of the differential equation, a "backwards" solution should yield a more satisfactory result. In fact the solution can always be expressed in terms of an ordinary power series, which converges rapidly. (The rate of convergence increases as $M_1 \to 1$.)

This power series was used to calculate the variation of velocity through the shock front for various values of M_1 and σ. The following results were obtained:

(1) Increasing the Prandtl Number at a constant Mach Number steepens the local velocity gradients and, hence, shortens the transition zone.

(2) In the neighborhood of $\sigma = {}^3/_4$, the results are relatively insensitive to small deviations in σ, particularly at Mach Numbers near 1. Therefore, Becker's results can be applied in this range, though caution should be used at higher Mach Numbers.

(3) Taylor's solution[5] predicts slightly high values for the dimensions of the transition zone.

(4) The present results agree with Mises' approximate values for the thickness of the shock front.[4]

References

[1] Becker, R., *Stosswelle und Detonation*, Zeitschrift für Physik., Vol. 8, pp. 321–362, 1922.

[2] Thomas, L. H., *Note on Becker's Theory of the Shock Front*, Journal of Chemical Physics, Vol. 12, No. 11, pp. 449–453, 1944.

[3] Morduchow, M., and Libby, P. A., *On a Complete Solution of the One-Dimensional Flow Equations of a Viscous, Heat-Conducting, Compressible Gas*, Journal of the Aeronautical Sciences, Vol. 16, No. 11, p. 674, November, 1949.

[4] Mises, R., *On the Thickness of a Steady Shock Wave*, Journal of the Aeronautical Sciences, Vol. 17, No. 9, pp. 551–554, 1950.

[5] Taylor, G. I., *The Conditions Necessary for Discontinuous Motion in Gases*, Proceedings of The Royal Society, Vol. A84, pp. 371–377, 1910.